Investigation of Peptidic Templates for Bioorthogonal Ligations

Dissertation

for the award of the degree

“Doctor rerum naturalium” (Dr. rer. nat.)

of the Georg-August-Universität Göttingen

within the doctoral program chemistry

of the Georg-August University School of Science (GAUSS)

submitted by

Benedikt Kugler

from Neu-Ulm

Göttingen, 2021

Thesis Committee

Prof. Dr. Ulf Diederichsen
Institute of Organic and Biomolecular Chemistry, University of Göttingen

Prof. Dr. Manuel Alcarazo
Institute of Organic and Biomolecular Chemistry, University of Göttingen

Members of the Examination Board

Reviewer:
Prof. Dr. Ulf Diederichsen
Institute of Organic and Biomolecular Chemistry, University of Göttingen

Second Reviewer:
Prof. Dr. Manuel Alcarazo
Institute of Organic and Biomolecular Chemistry, University of Göttingen

Further members of the Examination Board

Prof. Dr. Marina Bennati
Max Planck Institute for Biophysical Chemistry, Göttingen

Prof. Dr. Kai Tittmann
Department of Molecular Enzymology, University of Göttingen

Dr. Holm Frauendorf
Institute of Organic and Biomolecular Chemistry, University of Göttingen

Dr. Michael John
Institute of Inorganic Chemistry, University of Göttingen

Date of the oral examination: April 13, 2021

The work described in this thesis was carried out under the supervision of Prof. Dr. Ulf Diederichsen at the Institute of Organic and Biomolecular Chemistry of the Georg-August University of Göttingen between March 2017 and February 2021.
It was supported in part by the *Deutsche Forschungsgemeinschaft* within the priority program 1623 (SPP 1623) *Chemoselective reactions for the synthesis and application of functional proteins*.

Declaration of authorship

I hereby declare that I prepared the doctoral thesis entitled *Investigation of Peptidic Templates for Bioorthogonal Ligations* on my own and with no other sources and aids than quoted.

Göttingen,

(Benedikt Kugler)

Table of contents

1 Introduction

One of the biggest challenges for biochemical researchers in the postgenomic era remains the elucidation of structure-activity relationships in proteins. While many proteins can be routinely produced by recombinant protein expression and studied in a controlled environment, post-translational modifications (PTMs), such as acylation, methylation, phosphorylation, lipidation, prenylation, ubiquitination, or glycosylation are additionally required to reproduce the diversity found in nature.[1,2] Traditionally, these modifications have been carried out by targeting nucleophilic amino acid (AA) side chains, often by enzymatic means. This process frequently results in a heterogeneous product distribution. Furthermore, this approach is inherently limited to the chemistry encoded in the 20 common proteinogenic amino acids and while efforts have been made to incorporate unnatural AAs by expansion of the genetic code, this process is often labor-intensive.[3–5] Of special interest is the introduction of non-natural modifications, such as fluorescent labels, to proteins of interest. Fluorescence assays in their simplest form allow the visualization of the protein in its environment, whereas more advanced methods can reveal details about protein-protein interactions or conformational changes.[6] While the discovery of the genetically encoded green fluorescent protein (GFP) and its application as a protein tag first bypassed the need for site-selective targeting and has thus led to an increase in the understanding of protein interactions, disadvantages still remain. Usage of GFP is limited to biomolecules accessible by protein expression and its large size presents an additional drawback, since this may directly influence the structure of the studied molecule.[7,8] These restrictions can be circumvented by applying a two-step tag-and-modify approach. First, a chemical tag with unique reactivity is installed genetically or *via* the cell's biosynthetic pathway and subsequently targeted by a reporter group with complementary functionality. Ideally, the reaction proceeds fast and selectively in a minimally invasive manner.[9]
The scope of these methods can be transferred to the field of peptide therapeutics, where control over drug loading - and therefore product homogeneity - is an important objective. Similarly, this approach can be used for the creation of uniform biomaterials, where site-selective modifications allow control over material structure and function.[10,11] The discovery of additional methods for the chemoselective modification of proteins, as well as the scope expansion of currently existing methodology is therefore worth investigating.

Within the scope of this thesis, fundamental research on the application and effect of templates for protein labeling is conducted. A long-term research goal in our workgroup is the development of a method to simultaneously introduce two protein modifications, while

maintaining site selectivity. Our approach in reaching this goal is based on the use of peptide templates to facilitate the labeling reaction at low concentrations by increasing the effective molarity of the reactants. The sequence specificity of the template is furthermore responsible for ensuring site-selectivity. Introduction of photocleavable linkers (PCL) between the template strands and tags aid in the (partial) removal of the reaction scaffold after transfer of the label to the target protein. Based on previous work in our group by Middel *et al*.,[12] photocleavable peptide nucleic acid (PNA) templates are investigated with respect to their orthogonality. To extend the scope of this method, the template's ability to enhance a cross-coupling reaction is explored. Finally, coiled-coil peptides are investigated as templates because of the additional layer of orthogonality they provide in terms of recognition and site-selectivity and their standalone ability to serve as a platform for stoichiometric bioconjugations at low concentrations.

2 State of the art

2.1 Classic methods for chemical protein modification

Classic methods for protein bioconjugation make use of the chemical diversity embedded in the side chains of the canonical amino acids. Of these, nucleophilic amino acids, such as cysteine and lysine are most often targeted. The thiol group of cysteine can undergo disulfide exchange to form mixed disulfides,[13] alkylation with α-halocarbonyls[13] or Michael addition with α,β-unsaturated carbonyls (*e.g.* maleimides[13,14] or vinyl sulfones[15]). The ε-amino group of lysine can be favored over the *N*-terminus by pH control. It primarily undergoes reactions with electrophiles, such as activated acids to form amides,[16] iso(thio)cyanates to form urea and thiourea compounds,[17] as well as reductive amination with aldehydes.[18] An overview of these methods is presented in Figure 1.

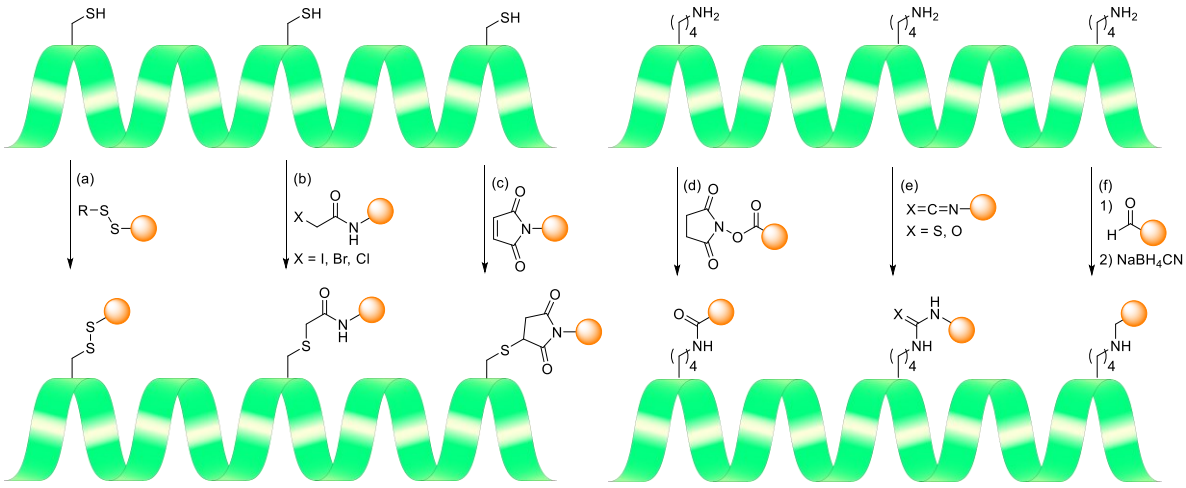

Figure 1: Classic methods of protein modification on cysteine (left) and lysine (right) through (a) disulfide exchange, (b) alkylation, (c) Michael addition, (d) amide formation, (e) urea or thiourea formation and (f) reductive amination.

A major drawback of these reactions is the selectivity. While other nucleophiles can lead to side reactions, the simple presence of more than one target amino acid in the protein sequence will lead to a statistical product distribution. This can be partly circumvented by different accessibility of the target residue (*i.e.* surface-exposed *versus* hydrophobically shielded) and substoichiometric addition of the reagent.[16] However, none of these methods have prevailed for single site-selective labeling.

A major exception is the ligation of thioesters with an *N*-terminal cysteine to give a native peptide bond. The reaction, termed native chemical ligation (NCL), was first reported by Kent and co-workers.[19] It allows the condensation of unprotected peptide fragments under physiological conditions by transthioesterification of an *N*-terminal cysteine with a

C-terminal thioester, followed by an irreversible intramolecular *S,N*-acyl shift that proceeds through a 5-membered transition state, to yield an amide bond between the two fragments (see Figure 2). While non-terminal cysteines can also react with the thioester, the *S*,*N*-acyl shift cannot occur, thus leading to a reversion to the starting materials. Due to its high chemoselectivity, NCL has become a staple in protein (semi)synthesis and modification. With the help of NCL, proteins larger than the limitation of conventional solid phase peptide synthesis (SPPS) have been accessed and studied, most impressively demonstrated in the synthesis of a 203-residue HIV-1 protease dimer.[20,21] While the requirement of a cysteine residue in the peptide sequence poses some limitations due to its low abundance,[22] introduction of desulfurization protocols, coupled with the use of other cysteine surrogates has expanded the scope of the reaction,[23–25] which also includes the use of fluorescent thioesters as chemical probes.[26]

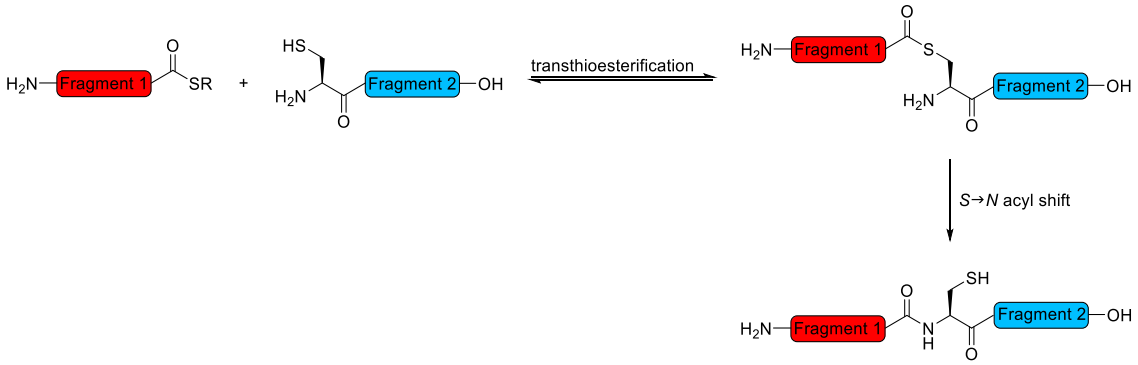

Figure 2: Mechanism of the native chemical ligation (NCL). An *N*-terminal cysteine and a *C*-terminal thioester undergo reversible transthioesterification, followed by an intramolecular, irreversible *S*-to-*N* acyl shift.

2.2 Bioorthogonal reactions

To overcome the limitations in control over extent and location of the modification associated with classic methodology, new functional groups with unique reactivity are introduced to the target protein. This can either be achieved by metabolic labeling of natural biomolecules with modified metabolic precursors[27] or by synthetic incorporation of an unnatural moiety.[28] After incorporation, this tag can be subsequently targeted by a probe molecule equipped with a complimentary functionality. The participating functional groups should be inert to biological moieties, stable under physiological conditions, not interact with a biological system and ideally be small in size as to not perturb the protein. The conjugation reaction should proceed fast and selectively at low concentrations and under biocompatible conditions without the production of toxic side products (for *in vivo* applications). This concept of “bioorthogonal” reactions was introduced by Bertozzi and

co-workers.[29,30] As of today, a conjugation reaction fulfilling every criterion remains an ideal, however some of the reactions discussed in this chapter have come close.

2.2.1 Oxime and hydrazone ligation

The keto group, while omnipresent in organic chemistry, is absent from the side chains of the canonical amino acids. Due to its unique reactivity, it presents a target for the selective modification with hydroxylamine or hydrazine derivatives (see Figure 3). While keto groups can be present in cofactors and metabolites, oxime and hydrazine forming ligations are compatible in a variety of biological systems lacking these functionalities.[31] The oxime bond is stable under physiological conditions, whereas hydrazones are often reduced to form a more stable linkage. Oxime ligations tend to have moderate reaction rates at acidic pH, but perform sluggish at neutral pH, thus often requiring millimolar concentrations of the reactants.[32]

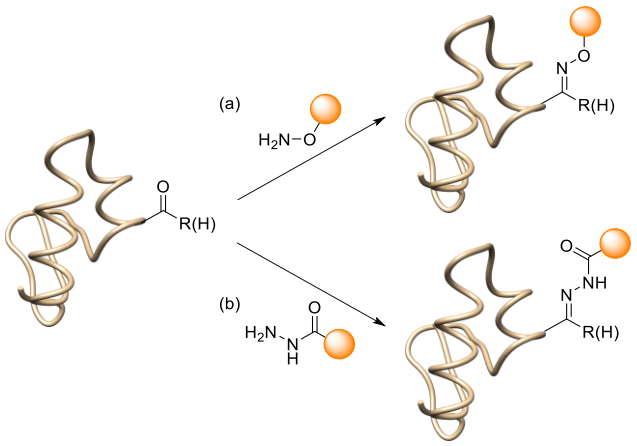

Figure 3: Condensation of an aldehyde/ketone with (a) a hydroxylamine or (b) a hydrazine derivative to form oxime or hydrazone linkages.

Schultz and co-workers reported the site-selective, genetic incorporation of *p*-acetylphenylalanine into anti-Her2 antibody Fab fragments, as well as full-length IgG in *E. coli* and mammalian cells, respectively. The amino acid was targeted with a hydroxylamine modified variant of the antineoplastic agent auristatin F to create a homogenous antibody-drug conjugate (ADC) with precise control over stoichiometry. While the ADC showed excellent pharmacokinetics and a high cytotoxic activity against $Her2^+$ cancer cells, both *in vitro* and in mouse xenograft treatment models, the rate constant of the oxime ligation was far from optimal. Despite being performed at pH 4.5, reaction times

of one to four days and a twenty to thirty-fold reagent excess of the drug were required (see Figure 4a).[33]

To overcome this problem, Dawson and co-workers disclosed the role of aniline as a nucleophilic catalyst that undergoes a transamination with the carbonyl compound, thereby increasing the reaction rate by a factor of 400 at pH 4.5 and a factor of 40 at pH 7.0.[32] This principle was utilized in the rapid labeling of model peptide substrates and human serum albumin *via* oxime or hydrazone ligation, demonstrating rate constants of 10^1-10^3 M^{-1} s^{-1}at low micromolar concentrations and neutral pH.[34] The broad applicability was further demonstrated by Zeng *et al*. in the labeling of cell-surface sialylated glycoproteins by aniline-catalyzed oxime ligation at micromolar concentrations at moderate speed (see Figure 4b).[35]

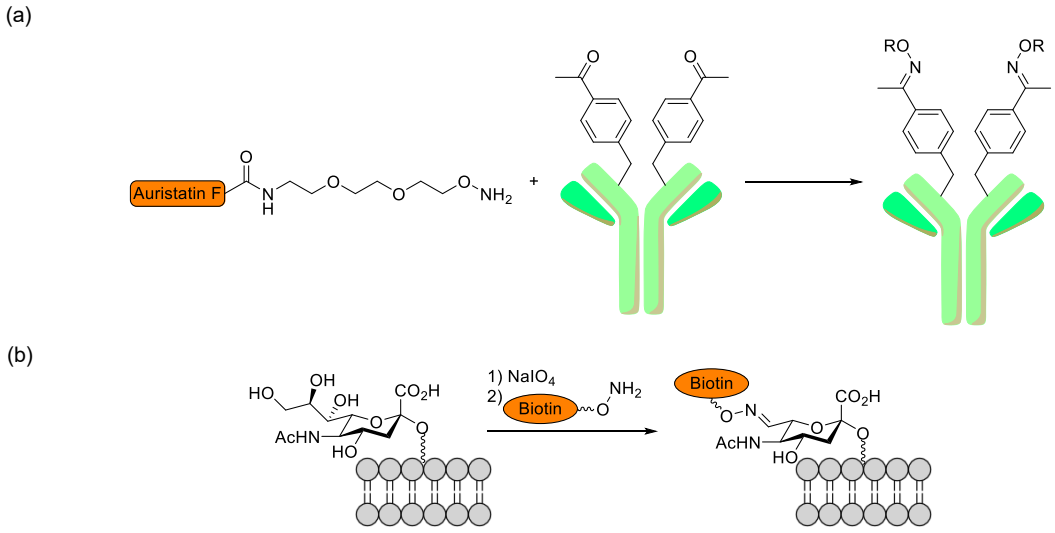

Figure 4: (a) Synthesis of an ADC *via* oxime ligation and (b) labeling of cell-surface sialylated glycoproteins by aniline-catalyzed oxime ligation. Figure based on [33,35].

Further studies by Proulx and co-workers showed that incorporation of electron rich *N*-aryl groups to peptides leads to coupling with alkoxyamines to yield ketoximes, with O_2 being the only additive. Mechanistically, the ligation involves the *in situ* generation of a protonated aniline Schiff base that reacts with the alkoxyamine while expelling aniline.[36,37] In addition, Xu *et al*. reported the use of easy to modify electron deficient chloro-benzaldehyde reagents to increase the reactivity of the keto compound in the imine formation to provide a fast, catalyst free hydrazone ligation. The diversity of the scope was demonstrated by modifying ubiquitin with fluorescent labels, a drug, or polyethylene glycol (PEG), the latter showing 96% conversion at micromolar concentrations at pH 7 after 30 min.[38,39]

2.2.2 Ketoacid-hydroxylamine (KAHA) and potassium acyltrifluoroborate (KAT) ligations

Another reaction between a keto compound and a nucleophile enhanced by the α-effect was disclosed by Bode and co-workers with the KAHA ligation. It describes the decarboxylative condensation of α-ketoacids with *N*-alkylhydroxylamines to form a native amide bond (see Figure 5). The reaction proceeds without additives or formation of byproducts, despite using unprotected functional groups and can be carried out in polar protic and aprotic solvents.[40] Further mechanistic studies revealed that the reaction with *O*-unsubstituted hydroxylamines proceeds *via* formation of nitrone and oxaziridine intermediates, whereas the reaction with unsubstituted oxaproline forms an ester under acidic conditions that undergoes an *O*,*N* acyl shift to yield the native amide bond at basic pH.[40–42]

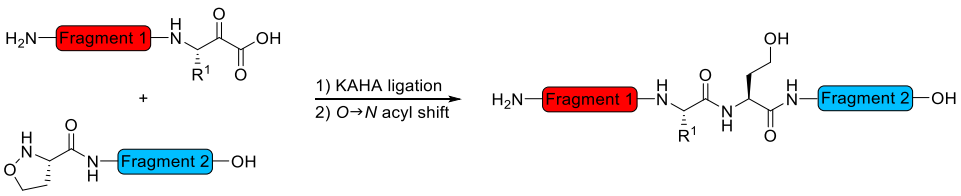

Figure 5: Amide bond forming ligation between unprotected ketoacid peptide fragment 1 and hydroxylamine (oxaproline) peptide fragment 2.

The ligation strategy was further optimized by the synthesis of SPPS-compatible resins that form enantiopure α-ketoacids upon cleavage,[43–45] the synthesis of oxaproline and oxazetidine derivatives that lead to different amino acid side chains at the ligation site[44,46–48] and the introduction of (photocleavable) protecting groups for the hydroxylamine and ketoacid functionalities.[49,50] Despite being limited to a lower pH and possessing a slower reaction rate than NCL, the KAHA ligation is broadly applicable in the synthesis of proteins by utilizing aqueous acidic NMP or DMSO, allowing various ligation sites that are more common than cysteine (the ligation site of NCL), utilizing easily protected functional groups, while being tolerant to all canonical amino acids. These advancements have culminated in the total chemical synthesis of the 20 kDa heme protein nitrophorin 4 by sequential ligation.[51] The requirement of strong acidic conditions can also be turned into an advantage by allowing the synthesis of difficult peptides with highly hydrophobic sequences (the low pH prevents aggregation). This was demonstrated in the synthesis of a cyclic, antibacterial peptide with a large hydrophobic segment. HFIP was used as a co-solvent in the ligation of two sub-fragments, whereas the following cyclization occurred spontaneously in a mixture of water and DMSO. Of note, both ligation and cyclization were

carried out as KAHA ligations, with photocleavable protecting groups (PPGs) allowing site-selectivity.[50]

In an effort to find a chemoselective reaction that proceeds with a faster reaction rate under dilute concentrations, Bode and co-workers further identified potassium acyltrifluoroborates (KATs) as ligation partners for hydroxylamines. The reaction proceeds fast and selectively on unprotected peptides under acidic conditions in aqueous media at room temperature to yield an amide bond (see Figure 6).[52,53]

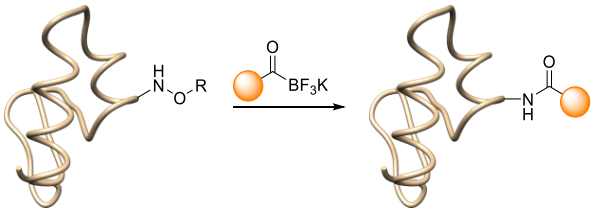

Figure 6: Amide bond forming ligation between an unprotected hydroxylamine and a potassium acytrifluoroborate.

Biotinylation, PEGylation, palmitoylation, and introduction of a dye molecule were successfully demonstrated on a 31mer GLP1-analogue. The reaction proceeded within minutes at a 1 mM concentration.[53] In a study comparing reaction rates of chemoselective ligations, an influence of the pH value on the rate constant was revealed. A second-order rate constant of 0.39 $M^{-1}s^{-1}$ was determined for the reaction between a hydroxylamine containing model peptide and a KAT dye in ammonium acetate buffer (pH 5.1, 200 µM reagent concentration). The same reaction was carried out in presence of oxalic acid in H_2O/*t*BuOH to reveal a rate constant of 22.4 $M^{-1}s^{-1}$ (25 µM substrate concentration).[54] The ligation was furthermore demonstrated to be orthogonal to the Cu(I)-catalyzed azide-alkyne cycloaddition (CuAAC), thiol-Michael addition and strain-promoted azide-alkyne cycloaddition (SPAAC).[55,56] This versatility was impressively demonstrated by Mazunin *et al*. with the stepwise immobilization of multiple bovine serum albumin (BSA) derivatives on a PEG hydrogel scaffold. The hydrogel was synthesized by a Michael-type reaction of a thiol and a vinyl sulfone. The resulting gel was doped with an azide for targeting *via* SPAAC and either a hydroxylamine or potassium acyltrifluoroborate for targeting *via* KAT ligation. Staining occurred by exposure to fluorescent BSA derivatives bearing a complementary moiety (cyclooctyne for SPAAC and a potassium acyltrifluoroborate or a hydroxylamine for KAT ligation). The order in which the staining was carried out proved to be inconsequential, resulting in dual immobilization of the proteins (see Figure 7).[56]

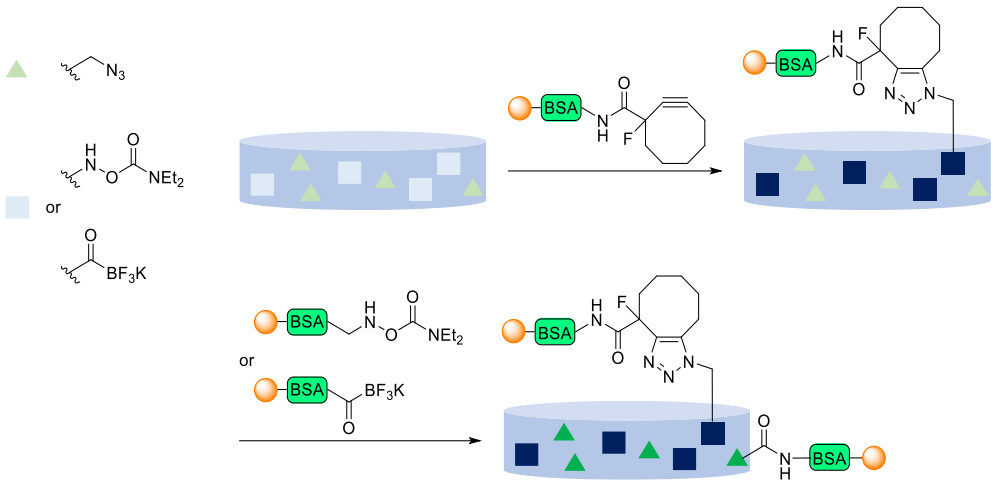

Figure 7: Dual independent immobilization of BSA derivatives onto hydrogels. Depicted is the 1st staining *via* SPAAC ligation of a fluorescein containing, cyclooctyne modified BSA and 2nd staining *via* KAT ligation of a hydroxylamine modified, rhodamine containing BSA variant. Figure based on [56].

2.2.3 Staudinger ligation

The Staudinger ligation was developed by the Bertozzi group as a modification to the Staudinger reduction. Herein, azides are treated with triphenylphosphine to give aza-ylides that are subsequently hydrolyzed to yield primary amines.[57] The mild conditions, tolerance of water and abiotic nature of both participating functional groups would make this reaction a prime candidate for biological applications. Alas, the initially formed covalent bond between the substrates is later hydrolyzed. To address this issue, an ester group was introduced in *ortho* position to the phosphorus atom at one of the aryl rings to act as an electrophilic trap. Formation of the aza-ylide intermediate occurs according to the known mechanism, however a nucleophilic attack of the nitrogen atom on the electrophilic trap yields a cyclic intermediate that forms a stable amide-linked product upon hydrolysis (see Figure 8a).[58]

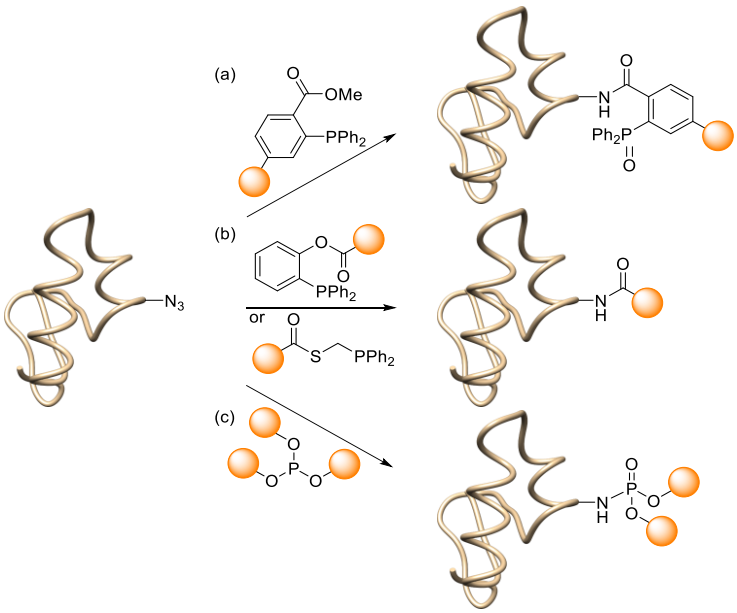

Figure 8: Schematic representation of (a) the Staudinger ligation, (b) traceless variants and (c) the Staudinger-phosphite reaction.

This method was successfully employed in the labeling of live cells. Azides were incorporated within the cell surface by metabolization of a synthetic azidosugar (metabolic labeling). Subsequently, these moieties were addressed by a number of phosphine probes to form covalent linkages (tagging).[58] Biotinylation,[58] dual incorporation of fluorophores with an orthogonal hydrazone ligation,[59] FRET-based turn-on fluorescence,[60] and real-time bioluminescence imaging[61] have been demonstrated. The general concept of this so-called metabolic labeling approach is illustrated in Figure 9.

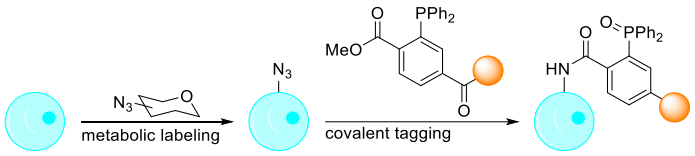

Figure 9: Depiction of the metabolic labeling approach. Azides are delivered to the cell surface by unnatural sialic acid biosynthesis and addressed by a variety of phosphine probes in a Staudinger ligation. Figure based on [59].

In addition, “traceless” approaches have been reported independently by the groups of Raines and Bertozzi (see Figure 8b). Here, the phosphine starting material was modified to expel the phosphine oxide in a manner similar to NCL to yield an unaltered amide bond between the ligation partners.[62,63] This technique has been successfully employed on the solid phase in tandem with NCL to synthesize the functional protein ribonuclease A.[64]

The Staudinger ligation proceeds with high selectivity, however, slow kinetics are an obstacle for *in vivo* applications.[30] Attempts to increase the electron density of the

phosphine substituents, and therefore the reaction rate, were partly successful since phosphine oxidation by air was observed as a side reaction.[65] To address the latter issue, Hackenberger and co-workers applied air-stable phosphites as ligation partners to yield phosphoramidate linkages after hydrolysis (see Figure 8c).[66] With this approach, up to two functional groups can be introduced to the target molecule, including biotin[67] and PEG.[68] Addition of a PPG to the phosphite allows the generation of charged phosphoramidates that are of interest as biologically relevant phosphate ester mimics.[66]

2.2.4 Copper(I)-catalyzed azide alkyne cycloaddition (CuAAC)

The proposal of azide and alkyne reacting in a concerted [3+2] cycloaddition was first made by Huisgen. However, the studied 1,3-dipolar additions exhibited slow reaction kinetics, making elevated temperatures or pressures necessary.[69] The groups of Fokin/Sharpless[70] and Meldal[71] independently reported the catalytic effect of Cu(I) on the 1,3-dipolar cycloaddition of azides and terminal alkynes to produce 1,4-disubstituted 1,2,3-triazoles. The formation of copper acetylides activates the terminal alkyne towards reactions with azides. The reaction proceeds fast and selectively in high yields at room temperature in aqueous systems, needing only the addition of a reducing agent for the use of more cost-efficient Cu(II) salts. This reaction therefore signifies the first click reaction[a][72] with the additional potential to be bioorthogonal.[70] The reaction rate can be further increased by using ligands that stabilize the Cu(I) oxidation state in water.[73,74]

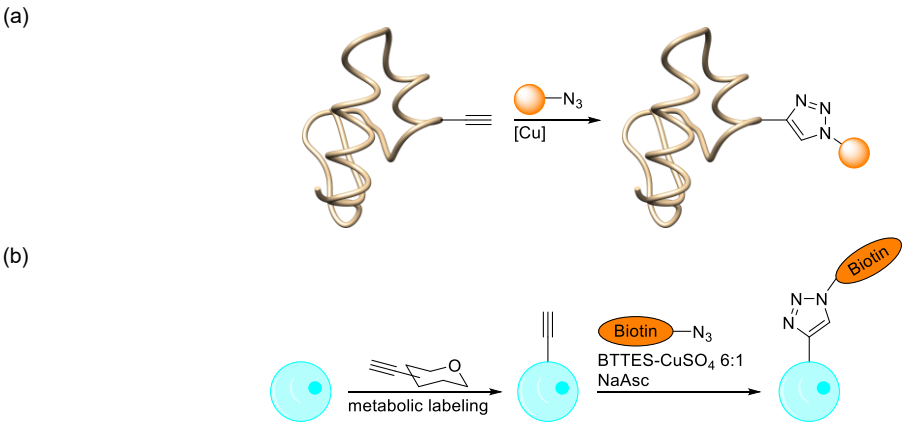

Figure 10: (a) Schematic representation of the CuAAC and (b) biocompatible version applied to the labeling of cell-surface sialic acids. Figure based on [75].

[a] Click reactions comprise a family of reactions that are defined by their high thermodynamic driving force, thereby enabling rapid and selective heteroatom linkage. Reactions of this type are modular, wide in scope, have a high yield and proceed under simple reaction conditions from readily available starting materials without the need for chromatographic purification of the products.[72]

Wang *et al*. applied the ligation method to a more complex biological system. Cowpea mosaic virus (CPMV) was decorated with azide or alkyne handles at surface exposed lysine residues or with an alkyne functionality at exposed cysteine residues. The virus was visualized with fluorescein dyes bearing compatible functional groups. Tris((1-benzyl-4-triazolyl)methyl)amine (TBTA) was used as a ligand to stabilize Cu(I) and to protect the protein from potentially harmful soluble copper species. Labeling was performed with a large dye excess in slightly basic phosphate buffer (pH 8.0) containing 5% *t*BuOH and a metal to ligand ratio of 1:2 at 4 °C for 16 h (see Figure 10a).[76] Chang *et al*. reported a similar approach for the labeling of alkynylated sialic acids in the organs of mice. After metabolic incorporation of the sialic acid analogue in live mice, the organs were harvested and the metabolized sugars visualized by biotin azide. A large excess of $CuSO_4$ and sodium ascorbate (NaAsc) was used in addition to TBTA to drive the labeling reaction to completion at room temperature within 1 h.[77] One of the biggest challenges to apply CuAAC ligation in living systems is the toxicity associated with the $CuSO_4$/CuBr, NaAsc and TBTA catalytic system. Due to the low water solubility of the TBTA ligand, high copper loading becomes necessary, thereby increasing the risk of free Cu(I) ions that escape the coordination sphere of the ligand and form reactive oxygen species that are detrimental to the cell metabolism. *E. coli* cells were observed to survive treatment with 100 µM CuBr for up to 16 h, however, they were unable to divide. Most mammalian cells underwent apoptosis and cell lysis within 20 minutes upon treatment with 1 mM Cu(I); similar effects were observed for zebrafish embryos. Soriano del Amo *et al*. therefore screened a library of TBTA analogues. A bis(*tert*-butyltriazolyl) ligand (BTTES) was identified as a compromise between reaction rate and water solubility. A metal to ligand ratio of 1:6 was observed to completely suppress apoptosis. Live cell labeling was performed on functionalized cell-surface glycoconjugates within 14 min, utilizing 75 µM Cu(I) (see Figure 10b). No long-term effect on cell growth was observed. The authors therefore applied the ligand to the labeling of fucosylated glycans in zebrafish embryos, only observing minor defects.[75] An alternative approach was disclosed by Uttamapinant *et al*., utilizing picolyl azides as internal chelators for Cu(I). Due to the increase of the effective concentration at the ligation site, the copper concentration could be lowered to a level of minimal toxicity. The resulting increase in reaction rate was also observed to offset the lowering of the copper concentration and showed a rate increase similar to a conventional system with the water-soluble THPTA ligand. The viability of this approach was demonstrated by *in cellulo* labeling of lipoic acid ligase bearing a picolyl azide moiety, as well as in rat neuron cultures.[78]

In another display of the versatility of CuAAC, Kofoed *et al*. reported the synthesis of an active enzyme by Cu(I)-catalyzed ligation. Two inactive halves of the tobacco etch virus

(TEV) protease bearing an azide and alkyne moiety respectively, were ligated. The created triazole bridge was observed to mimic the natural protein loop and the semi-synthetic protein exhibited the same activity as the wild type (WT). These findings demonstrate the isosteric nature of the triazole bond and provide a tool for the semisynthesis of difficult to express proteins.[79]

2.2.5 Strain-promoted azide alkyne cycloaddition (SPAAC)

In an effort to completely circumvent the need for a catalyst, Bertozzi and co-workers reported the reaction of an azide with a strained alkyne, cyclooctyne (see Figure 11). Driving force of the reaction is the bond angle deformation (163°) of cyclooctyne, resulting in close to 18 kcal/mol of ring strain. The energetic difference of the strained ground state to the transition state accelerates the reaction in comparison to the reaction with unstrained alkynes. The strain-promoted [3+2] cycloaddition is well tolerant of physiological conditions and was therefore applied by the authors in *in cellulo* labeling experiments. Metabolic labeling of cell surface glycans in Jurkat cells with azidosialic acid, followed by labeling with biotinylated cyclooctyne for 1.5 h showed robust labeling without evident cell toxicity.[80] The rate constant of the reaction was later reported to be $2.4 \cdot 10^{-3}$ $M^{-1}s^{-1}$, which is comparable to the Staudinger ligation, but slower than most CuAAC reactions.[65]

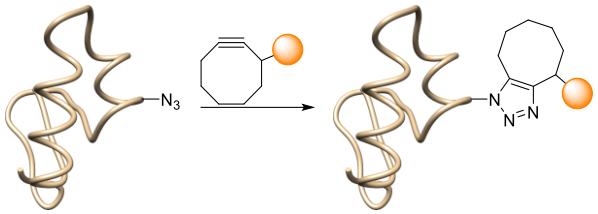

Figure 11: General representation of the SPAAC between an azide and a cyclooctyne derivative.

To further enhance the reaction rate, different cyclooctyne derivatives were investigated. Baskin *et al*. reported the introduction of an electron withdrawing difluoromethylene moiety (DIFO), resulting in a second-order rate constant of 0.076 $M^{-1}s^{-1}$ in acetonitrile.[81] Ning *et al*. fused two aryl rings to the cyclooctyne core (DIBO), imposing additional ring strain and a conjugated system with the alkyne, resulting in a second-order rate constant of 0.17 $M^{-1}s^{-1}$ in methanol.[82] Introduction of an additional sp^2-like center within the cyclooctyne ring in the form of an amide bond and retaining the two aryl substituents (BARAC) resulted in a second-order rate constant of 0.96 $M^{-1}s^{-1}$ in acetonitrile.[83] In addition, each cyclooctyne derivative was successfully used in the live cell labeling of azide surface glycans.

Showing promising results in live cells, SPAAC was applied to small model organisms. Laughlin *et al*. used DIFO-fluorophore conjugates for the imaging of azide-modified cell-surface glycans in developing zebrafish. Within a minute of exposure to DIFO-647, fluorescence was observed without background noise, increasing in a time-dependant manner. In order to achieve distinction between temporally different glycan populations, a two-color imaging strategy was developed. Cell-surface glycans were visualized with DIFO-647 (red) at 60 h post fertilization (hpf). Newly secreted glycans were visualized in a second step by treatment with DIFO-488 (green). This method gave insight into the cell-surface expression, intracellular trafficking and tissue distribution of glycans during embryonic development of zebrafish.[84] The strategy was refined in the dual-color imaging of developing *C. elegans*. Here, an azide-modified glycan population was first visualized with DIFO-488, followed by additional incubation with the azido-sugar (metabolic precursor). The resulting nascent glycans were visualized with DIFO-566 (red).[85] For visualization in the early stages of embryogenesis in zebrafish, a different approach was chosen. Azidosugars were directly administered *via* microinjection at the one-cell stage and labeled with DIFO-488 to visualize mucin-type *O*-glycans within 9 hpf, followed by a second labeling step with DIFO-555 (red) 2 h or 12 h later, revealing differences in the distribution of both glycan populations. In addition, sialylated glycans were imaged utilizing a nonmetabolic approach. Selective oxidation was performed with $NaIO_4$, followed by targeting of the aldehyde with an Alexa Fluor 488 reagent bearing an aminooxy moiety (AO-488). Labeling was observed starting at 7 hpf. Since both oxime ligation and SPAAC are orthogonal, dual labeling was carried out simultaneously in the same embryo. They were microinjected with the azidosugar, followed by incubation with $NaIO_4$ to produce an azide and aldehyde moiety at the cell surface, respectively. The functionalities were targeted with DIFO-555 in a SPAAC and AO-488 in an oxime ligation. Time-lapse imaging visualized differences between *O*-glycans and sialylated glycans in the enveloping layer during different stages of embryogenesis, as well as a rapid reorganization of cell surface glycans during mitosis.[86]

Following these results, labeling was studied in live animals. Metabolic precursors of sialic acid were administered to mice to produce cell-surface glycans bearing an azide functionality. Different cyclooctyne-FLAG conjugates, as well as Phos-FLAG, bearing a triarylphosphine handle for Staudinger ligation, were examined. DIMAC, a water-soluble dimethoxy azacyclooctyne, and DIFO showed the most promise in preliminary tests. Administration of Phos-FLAG, DIMAC-FLAG and DIFO-FLAG showed labeling in all harvested organs (most dominantly intestine, heart and liver). However, despite the comparable kinetics between Phos-FLAG and DIMAC-FLAG and the 10-fold faster kinetics of DIFO-FLAG *ex vivo*, the triarylphosphine probe produced more reaction products on the

same timeframe and administered concentration. Further studies revealed that the hydrophobic DIFO-FLAG and to an extent DIMAC-FLAG bind to mouse serum albumin, resulting in imperfect agents for *in vivo* applications.[87]

2.2.6 Inverse electron demand Diels-Alder reactions (IEDDA)

Sauer and co-workers first reported on the kinetics of the reaction between electron-deficient 1,2,4,5-tetrazines (Tz) and olefins, observing that strained dienophiles react extraordinarily fast. *trans*-Cyclooctene (TCO) was reported to be the most reactive substrate.[88] The groups of Fox[89] and Hildebrand[90] independently reported the application of IEDDA reactions for bioconjugation. Since the conditions reported by Sauer were not biocompatible, as the tetrazines were observed to react with water,[91] different substrates had to be identified. Fox and co-workers therefore reported the reaction of 3,6-di(2-pyridyl)-*s*-tetrazine with TCO. The reaction displayed very fast kinetics (k_2 = 2000 $M^{-1}s^{-1}$) and tolerance to more complex solvent systems, such as cell medium and cell lysate, with dinitrogen being the only byproduct. The reaction was applied to the labeling of the 11.7 kDa protein thioredoxin (Trx), modified with a TCO derivative. In acetate buffer (pH 6.0), the reaction between 15 µM Trx-TCO and 30 µM of the aforementioned Tz was complete within 5 min, thereby demonstrating the ability to label biomolecules rapidly at low concentrations and near equistoichiometric substrate ratios (see Figure 12a).[89]

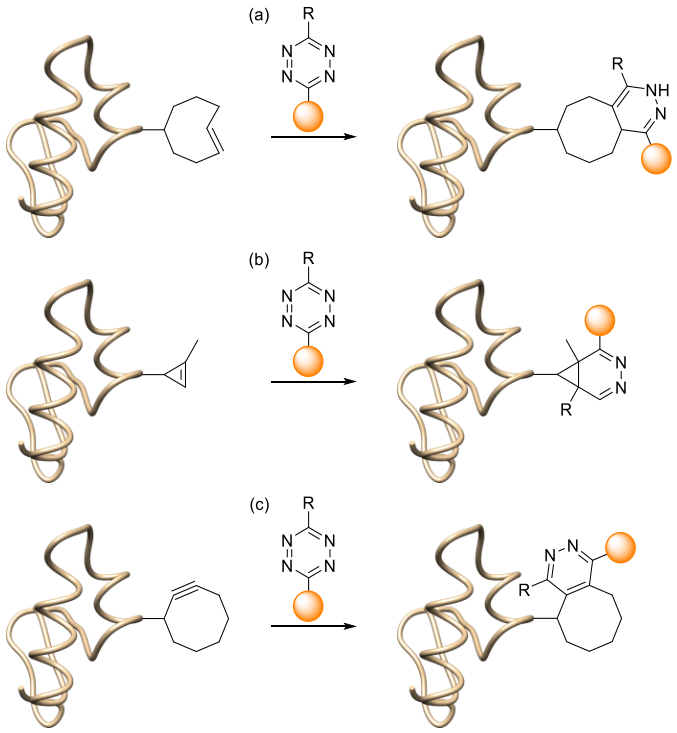

Figure 12: Schematic representation of IEDDA reactions with substituted *s*-tetrazines, targeting (a) *trans*-cyclooctene, (b) methylcyclopropene and (c) cyclooctyne.

In contrast, Hildebrand and co-workers utilized a norbornene derivative as a reaction partner for 3-(4-benzylamino)-*s*-tetrazine. The reaction displayed kinetics of 1.9 $M^{-1}s^{-1}$ in aqueous buffer and 1.6 $M^{-1}s^{-1}$ in fetal bovine serum (FBS). Labeling in a biological context was carried out in live SKBR3 human breast cancer cells after treatment with trastuzumab antibodies conjugated with norbornene and tetramethylrhodamine (for visualization). IEDDA conjugation was carried out using 200 nM of antibody and 50 µM of a near-infrared (NIR) fluorophore tetrazine conjugate (Tz-VT680) in 10% FBS/HBSS solution at 37 °C for 30 min, thereby providing dual-channel labeling.[90]

Rossin *et al*. applied the IEDDA ligation for pretargeted tumor imaging in live mice. Animals bearing colon carcinoma xenografts were targeted with TCO-modified antibodies, followed by reaction with a 3,6-diaryl-*s*-Tz radiolabeling probe (^{111}In-DOTA). A rate constant of 13090 $M^{-1}s^{-1}$ was observed at a concentration of 1.67 µM in PBS at 37 °C, resulting in complete conversion after 3 min. Labeling in living animals was performed with 3.4 eq. of the [^{111}In]-Tz derivative for 1 h, after which single photon emission computed tomography (SPECT) was performed. Despite the observation of a high amount of free mAb-TCO circulating in blood, a 52% reaction yield in tumor was observed. This report demonstrates the high selectivity and reaction rate of IEDDA in complex reaction environments, making it a prime target for applications limited by degradation of one of the starting materials, in this work the circulation half-life of the [^{111}In]-Tz conjugate, which is 9.8 min (see Figure 13).[92]

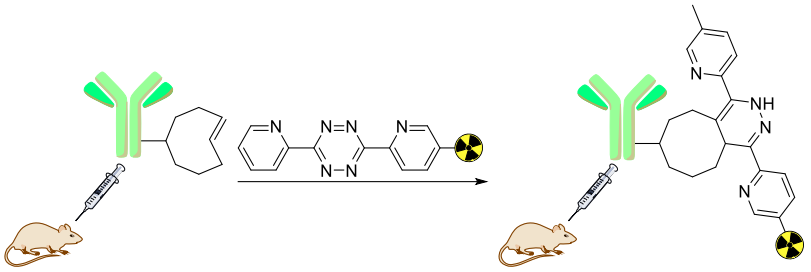

Figure 13: Schematic representation of tumor targeting using the IEDDA reaction. Mice bearing colon cancer xenografts were injected with a TCO-mAb conjugate, followed by [^{111}In]-Tz. Figure based on [92].

In an effort to create a minimally invasive tag, Yang and co-workers studied the reaction of substituted methylcyclopropenes with tetrazines (see Figure 12b). A rate constant of 13 $M^{-1}s^{-1}$ was observed for the reaction of a methylcyclopropene equipped with a carbamate handle and benzylalcohol tetrazine in 12% DMSO/H_2O at 37 °C. Application in a biological context was demonstrated by incubating SKBR3 breast cancer cells with cyclopropane phospholipids and subsequent imaging with a Tz-BODIPY fluorophore within an hour.[93] Patterson *et al*. used methylcyclopropane and azido sialic acid conjugates for metabolic incorporation into cell surface glycans. Simultaneous labeling was performed for 1 h in Jurkat cells with a Tz-biotin and a DBCO-rhodamine derivative (100 µM each), respectively, thereby illustrating the orthogonality of IEDDA and SPAAC ligations.[94] In addition to the aforementioned orthogonality, Nikić and co-workers reported a pair of IEDDA reactions selective among themselves. The strategy is based on the fact that tetrazines can react with strained alkenes, as well as strained alkynes. A cyclooctynyl (SCO)-lysine derivative was shown to react with H-Tz with a rate two times higher than the corresponding SPAAC with an azide (see Figure 12c). It did however not show significant reactivity towards Me-Tz under the reported conditions. Therefore, an isomerism stable variant of TCO, termed TCO* was used to target said moiety. Since TCO* exhibits reactivity towards both tetrazine derivatives, it had to be consumed first in labeling experiments. The authors therefore set up a scheme for dual-color labeling using super-resolution microscopy. Lysine-derived unnatural amino acids (UAAs) bearing SCO or TCO* moieties were genetically encoded into insulin receptors and virus-like particles. Dual-color imaging occurred by treatment with the dye conjugates Me-Tz-Cy5, followed by H-Tz-Atto532 for 10 min.[95]

2.2.7 Transition metal mediated ligations

With the very notable exception of the CuAAC ligation, transition metals have not found widespread application in bioorthogonal reactions. Here, the restrictions imposed by biological systems weigh heaviest. Challenges include the solubility and activity of the catalyst in buffered systems and the possibility of protein-as-ligand interactions. The latter might lead to catalyst poisoning or sequestration and degradation of the protein. These problems can be partly circumvented by applying the labeling reagent and the catalyst in superstoichiometric amounts.[96] An overview of current transition metal mediated ligation methods is presented in Figure 14.

In one of the earliest examples of transition metal mediated bond formation in proteins, Kodama *et al*. targeted a variant of the Ras protein that was genetically engineered to contain *p*-iodophenylalanine (*p*IPhe), with a Mizoroki-Heck reaction. Coupling was performed between the unnatural amino acid and a vinylated biotin in the presence of water-soluble Pd-TPPTS catalyst. Slightly basic conditions (pH 8.3) were applied, while a percentage of organic solvent and reaction times of 50 h were still needed to achieve a yield for the biotinylation of 2%.[97]

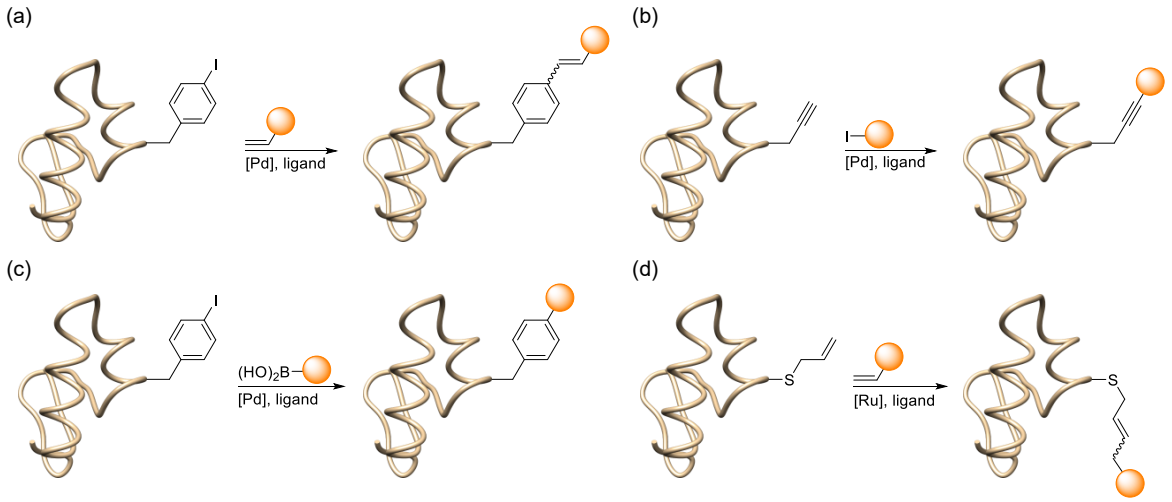

Figure 14: Schematic representation of transition metal mediated ligations: (a) Mizoroki-Heck, (b) Sonogashira, (c) Suzuki-Miyaura, and (d) olefin cross metathesis.

Developments in this field gathered speed when Chalker *et al*. reported an inexpensive, water-soluble Pd-pyrimidine catalyst for Suzuki-Miyaura protein functionalization. Chemically installed *p*-iodobenzyl cysteine (PIC) was targeted in a mutant of subtilisin *Bacillus lentus* (SBL) with a variety of boronic acid derivatives and a glucose boronic ester. Reactions proceeded within 30 min for the acids and 60 min for the ester under mild conditions (37 °C, phosphate buffer pH 8.0). However, both the catalyst (50 eq.) and the

reagent (500 eq.) were employed in superstoichiometric amounts.[98] The same catalyst was employed in the labeling of cell-surface channels at genetically encoded *p*IPhe in the OmpC protein with a fluorescein derived boronic acid (see Figure 15). Further investigations showed that the concentration of both Pd-catalyst and boronic acid can be lowered to a level, where they only exhibit low toxicity.[99] The same strategy and protein was used in the labeling with novel carbohydrate based boronic acids. The resulting cell surface glycans were visualized *via* the selective binding to fluorescein-lectin conjugates.[100] Bilyard *et al*. used the aforementioned carbohydrate based boronic acids for a mechanistical study of the glycosyltransferase enzyme glycogenin (GYG) that is responsible for the initiation of glycogenesis. The enzyme catalyzes its own autoglucosylation at the Tyr 195 residue. The authors mutated the residue to *p*IPhe which lacks the native glycosyl acceptor and therefore cannot undergo glucosylation. Pd-mediated Suzuki-Miyaura cross-coupling with a variety of boronic acid sugar templates led to active species mimicking defined GYG glycoforms, representative of different intermediates of the enzyme's catalytic cycle. Indeed, three distinct phases, prime, extend, and refine, were identified by this approach, thereby demonstrating how uniquely powerful transition metal based ligations can be if applied in the right context.[101]

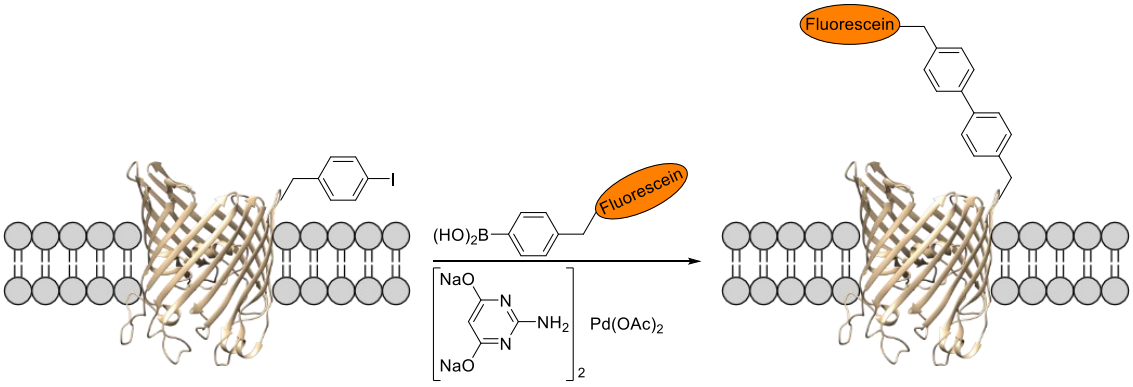

Figure 15: Suzuki-Miyaura labeling of the transmembrane protein OmpC (PDB ID: 2J1N) at a genetically encoded *p*IPhe residue, using the water-soluble $(ADHP)_2{\cdot}Pd(OAc)_2$ catalyst. Figure based on [99].

Water-soluble Pd-pyrimidine catalysts are not only limited to facilitating the Suzuki-Miyaura cross-coupling. Indeed, Li *et al*. reported the functionalization of a homopropargylglycine (HPG)-encoded ubiquitin (Ub) protein *via* Sonogashira cross-coupling. Modifications with a fluorophore, as well as PEGylation were achieved under mild conditions within 30 min in good to excellent yields. Similar to the previously reported Suzuki-Miyaura functionalizations, superstoichiometric amounts of catalyst and reagent (50 eq. each) were used. Utility of this method was furthermore demonstrated by fluorescence labeling of HPG-Ub in *E. coli* cells within 4 h.[102]

Recent advances have further demonstrated that both reactions can be carried out in a ligand-free manner. Dumas *et al*. reported the PEGylation of proteins *via* Suzuki-Miyaura cross-coupling catalyzed by K_2PdCl_4,[103] whereas Li *et al*. used ligand-free Sonogashira coupling for *in vivo* protein labeling. Here, an alkyne analogue of pyrrolysine was encoded into a type III secretion toxin, OspF, and visualized in *Shigella* cells with a iodophenyl-bearing fluorophore.[104] Furthermore, Ma *et al*. reported an *N*-heterocyclic carbene (NHC) stabilized palladium complex as an alternative catalyst for aqueous Suzuki-Miyaura cross-coupling. Applicability was demonstrated by labeling of membrane proteins in HeLa cells with biotin. Comparable to the Pd-pyrimidine catalyst, labeling proceeded within 1 h at 37 °C in PBS buffer (pH 8.0).[105]

Recently, Bhushan *et al*. reported olefin cross-methasesis (CM) on a variety of proteins, as well as in human cells. *S*-Allylhomocysteine (Ahc) was introduced to the target protein as a priviledged substrate *via* Met codon reassignment. Allylic reaction partners were coupled using Hoveyda-Grubbs II catalyst in buffered systems containing significant amounts of organic solvent. Nonetheless, the Fc region of immunoglobulin G (IgG-Fc) was labelled with an olefin-biotin derivative in human cells, within 3 h. Recurrently, superstoichiometric amounts of catalyst (100 eq.) and olefin (5000 eq.) were required.[106]

2.2.8 Summary and conclusion

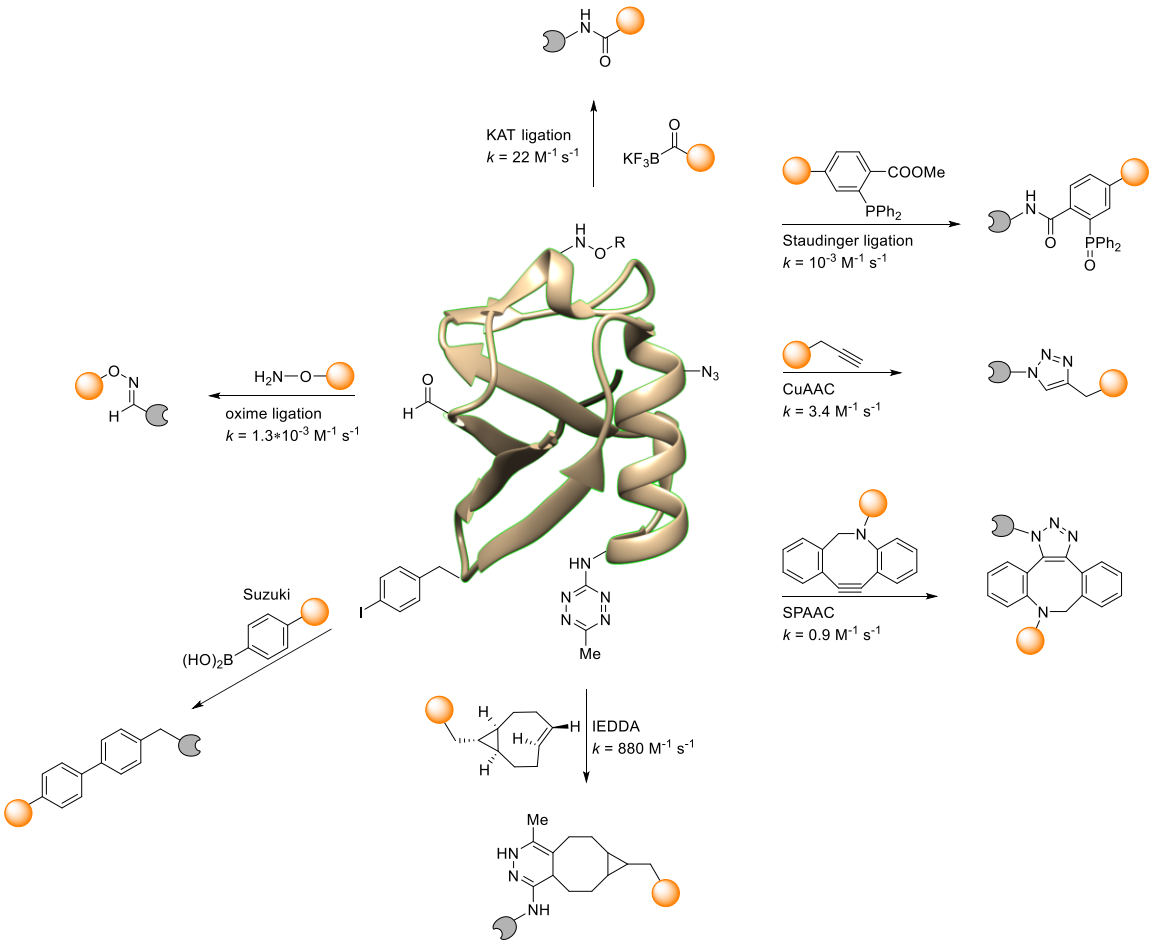

Figure 16: Overview of the previously discussed prevalent bioorthogonal reactions in the context of protein modification and their respective rate constants. Rate constants were taken from [54,107]. The protein structure is part of FAAP20-UBZ (PDB ID: 3WWQ) and was used as a dummy protein for illustrative purposes.

The reactions discussed in chapter 2.2 helped to provide detailed insight into protein structures, their dynamics and functions, both *in vitro* and in live organisms. Areas of application include the modification of protein functions, visualization of protein-protein interactions and protein trafficking up to super-resolution imaging, as well as the generation of protein-based pharmaceuticals. However, challenges still remain for the field of bioorthogonal chemistry. Figure 16 summarizes the previously discussed, prevalent methods of bioorthogonal labeling. Since rate constants greatly differ depending on environmental factors (pH value, temperature, solvent) and chemical surroundings, the specified second-order rate constants refer to a unifying study by Saito and co-workers. Here, chemoselective ligation reactions were evaluated for systems consisting of an unprotected peptide, equipped with a unique *N*-terminal functional group and an organic dye molecule bearing the complementary functionality. The reaction partners were supplied

in equimolar ratio, using optimized conditions for aqueous systems.[54] For the IEDDA reaction, the rate constant was determined for the reaction between a tetrazine modified GFP derivative and sTCO under pseudo-first-order conditions and the second-order rate constant was derived from the measurements.[107] Taking into account that for stoichiometric reactions at a 100 µM reactant concentration, a rate constant of 1 $M^{-1}s^{-1}$ would correspond to reaction times of over one day to achieve >90% conversion,[34] it becomes evident that most reactions to date do not yet meet this criterion for bioorthogonal ligations. Furthermore, the stability of hydroxylamines, phosphines and tetrazines poses problems for applications were longer incubation times are required. In addition, some of the presented reactions are not truly bioorthogonal: aldehydes and ketones are present in many metabolites in living systems, strained alkynes may react with free thiols and the Staudinger ligation, CuAAC and SPAAC target the same residue, while the presence of transition metals and the hydrophobicity of cyclooctyne and cyclooctene derivatives may still cause concerns for *in vivo* applications.[108]

2.3 Templated ligations

While the concept of bioorthogonal reactions can be seen as an expansion of conventional laboratory synthesis by offering uniquely selective functionalities with ideally high reaction rates, nature relies on a different approach to control reactivity. Here, a plethora of reactants are present in a system at concentrations too low (nM-µM) to enable spontaneous intermolecular reactions. Instead, selectivity and rate control are achieved by macromolecular templates. These molecules recognize reagents, bind them non-covalently and bring their reactive centers into proximity, thereby increasing the effective molarity, while also providing catalytic functionality.[109] This concept is illustrated in Figure 17 for the biosynthesis of isopenicillin N.

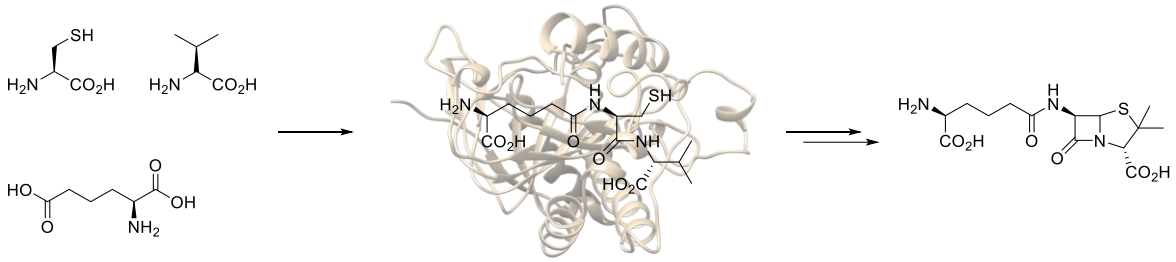

Figure 17: Biosynthesis of isopenicillin N. The starting materials are selectively recognized and undergo enzyme-catalyzed peptide bond formation to give a tripeptide, which undergoes thiazolidine formation, catalyzed by IPN synthase (PDB ID: 1BK0).[110] Figure inspired by [109].

Exploitation of this strategy would offer interesting opportunities for protein labeling. Indeed, high selectivity has been achieved by utilizing proteins that undergo self-modification reactions, such as the SNAP,[111] CLIP,[112] Halo[113] or TMP[114] tag and fusing them to proteins of interest. However, the size of these tags (ca. 18-33 kDa) are of major concern. Another approach is to use enzymes that selectively promote reactivity between functional groups or short peptide recognition sequences and reactive probes, such as sortase A,[115] biotin ligase[116] or transglutaminase.[117] In these cases, high substrate concentrations or long incubation times may be required. The development of methods that focus solely on the concept of effective molarity, *i.e.* a reaction template is therefore of prime interest for biochemical researchers with the goal to create minimally invasive tags that facilitate specific labeling under dilute conditions.

2.3.1 Nucleic acid templates

Nucleic acids present an obvious choice as a template. Due to their natural occurrence they are already compatible with *in vivo* applications, while the Watson-Crick base pairing between two complementary nucleobases offers a high degree of selectivity and preorganization between the reaction partners. Liu and co-workers exploited these characteristics to develop the field of DNA-templated organic synthesis (DTS). Here, complementary DNA strands are utilized to enable reactions between organic molecules attached to opposing ends. This principle was successfully applied to the templated reaction of a thiol and a maleimide. The reaction proceeded at 25 °C and pH 7.5 with a reagent (strand) concentration of 60 nM and a rate constant of k_{app} = 10^5 $M^{-1}s^{-1}$. Under these heavily dilute reaction conditions, little to no product formation was observed for the nontemplated approach, as well as for mismatched template strands.[118] The same approach has been applied to a variety of organic reactions, such as reductive amination, Heck coupling, Wittig olefination, nitro-aldol and Huisgen cycloaddition.[119,120] Impressively,

DTS was also applied to selectively form reaction products in a one-pot experiment of competing functional groups. Selectivity was installed by the choice of individual annealing sequences and template length, thus generating mismatches and suppressing the formation of undesired reaction products (see Figure 18).[121]

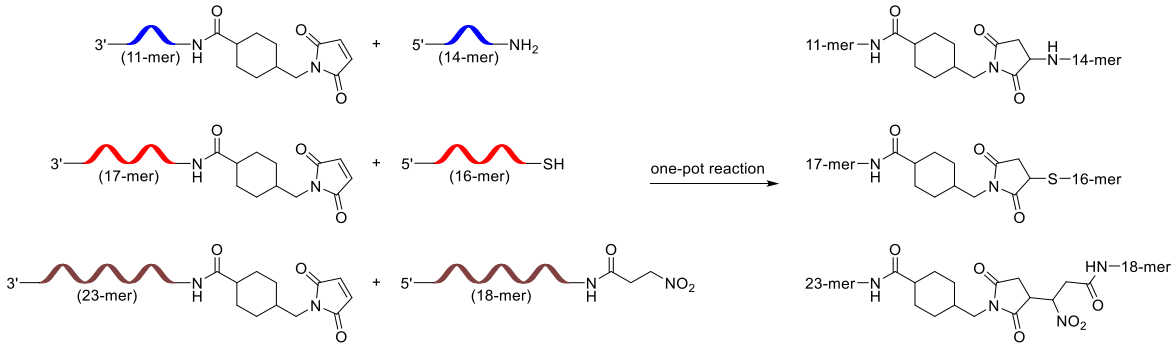

Figure 18: Selective targeting of maleimide moieties with competing functional groups. Selectivity is achieved by incorporating templates with different annealing sequences and strand lengths. Figure based on [121].

Seitz and co-workers demonstrated that nucleic acid templates can also be used for the generation of native peptide bonds. Peptide nucleic acid (PNA) strands were chosen as reactive strands due to their compatibility with peptide chemistry. PNA is a non-ionic DNA analogue, based on an *N*-2-(aminoethyl)-glycine (aeg) backbone, to which the nucleobases are attached *via* carboxymethylene linkages. The molecule exhibits high affinity to complementary DNA or RNA templates and a low mismatch tolerance. Two short PNA fragments bearing either their native termini or a *C*-terminal glycine thioester on one strand and an *N*-terminal cysteine residue on the other were selected. The fragments were annealed to a complementary DNA strand in such a fashion that the reactive termini were facing each other. Formation of the peptide bond was achieved by addition of a carbodiimide reagent to the native termini or by native chemical ligation. Probe concentrations of 1 µM with respect to 500 nM template enabled successful ligation within 120 min at 25 °C (see Figure 19).[122] Installation of an abasic site was found to further increase the initial reaction rate by 10^3 over the non-templated ligation and introduction of a single nucleobase mismatch led to a 10^3 fold increase in reaction rate.[123]

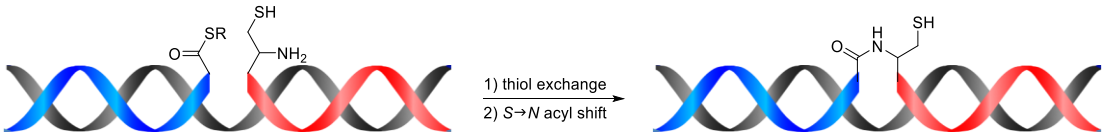

Figure 19: DNA-templated formation of a native peptide bond. The DNA strand (grey) serves as a template for two complementary fragments of PNA, equipped with a *C*-terminal thioester (blue) or an *N*-terminal cysteine (red). The reaction proceeds *via* formation of a thioester which prompts an intramolecular nucleophilic attack by the α-amino group of the *N*-terminal cysteine to establish the amide bond. Figure based on [122].

Research in our group has focused on one of the limitations of DNA templated ligation. While one of the templating scaffolds is removed upon product formation, previous designs had the second strand permanently attached to the distal site of the other reagent. Middel *et al*. introduced a photocleavable linker (PCL) between the guiding PNA strands and reactive peptide fragments that allowed traceless liberation of the ligated peptide upon irradiation (see Figure 20).[12] Recently, a similar approach has been reported by Hayashi *et al*. Introduction of photocleavable DNA templates to the side chains of peptide fragments allowed the simultaneous templated ligation of several peptide fragments.[124]

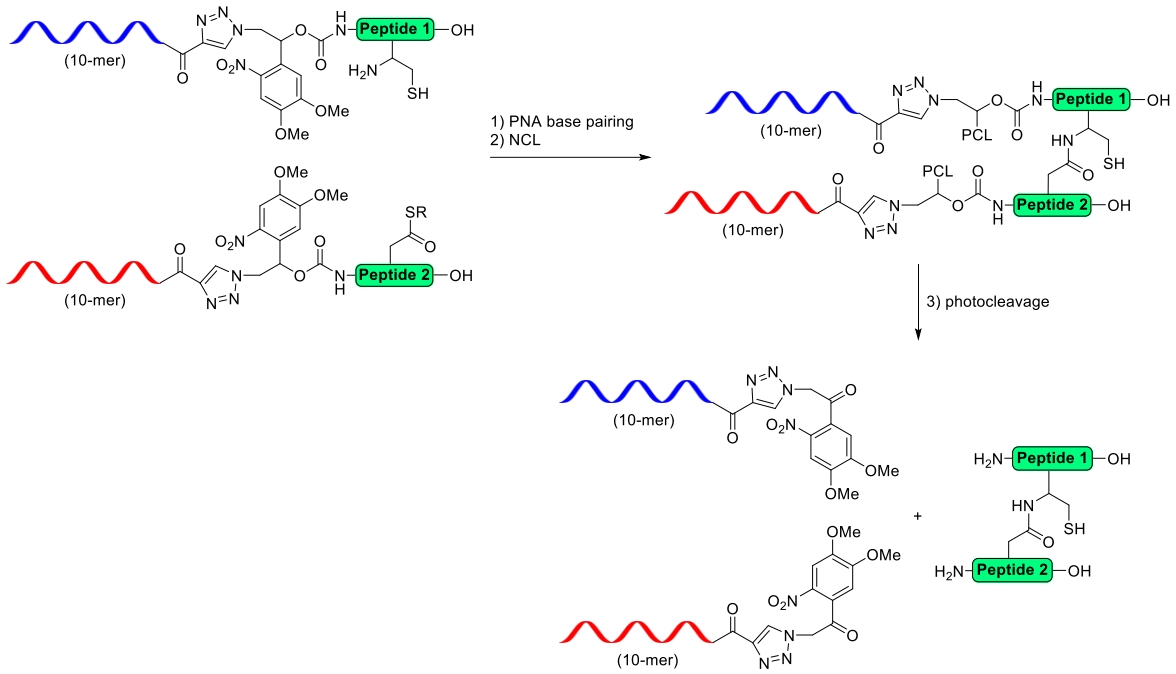

Figure 20*:* Overview of the photocleavable, PNA mediated NCL. Base pairing of the PNA nucleobases brings the reactant peptides into proximity to enable NCL between a cysteine and a side chain bound thioester. After completion of the reaction, the ligation product is released by photolysis of an *o*-nitrobenzyl derived linker. Figure based on [12].

Furthermore, Gothelf and co-workers developed a strategy, which applies DNA templates in the labeling of proteins. This approach, referred to as DNA-templated protein conjugation (DTPC) relies on pretargeting of proteins with a guiding DNA strand, followed by annealing of a reactive strand to form a covalent bond with the target protein. In preliminary work, pretargeting of His_6-tagged or WT-metal binding proteins (GFP-His_6, serotransferrin) was carried out with a guiding strand, equipped with a metal binding moiety. A complimentary oligonucleotide (ON) strand modified with an NHS ester was added and underwent selective conjugation to the ε-amino group of a proximal lysine residue, located near the metal binding site on the protein. The conjugation was selective under dilute conditions (0.25 µM), displaying a conversion of 61% after 3 h. Product and guiding strand were

separated by toe-hold-mediated strand displacement (see Figure 21).[125] The scope of this technique was broadened by utilizing reductive amination as the DTPC reaction on GFP-His_6. Additionally, installation of an oxidation labile linker between the aldehyde moiety and the reaction template gave access to a second reaction handle. A 1,2-diol linker was used to install an aldehyde moiety upon oxidative cleavage that was subsequently targeted by alkoxyamine-PEG 5000.[126] DTPC was furthermore used in the synthesis of an ADC. A guiding strand equipped with a Ni^{2+} chelating ligand was used to target a cluster of three histidine residues in the Fc domain of the antibody cetuximab. Annealing of the complementary reactive strand bearing an aldehyde moiety, followed by reductive amination targeting a proximal lysine residue yielded a covalent linkage between DNA duplex and mAb. As cargo, the hydrophobic anticancer drug doxorubicin was selected. The drug intercalates non-covalently into ds-DNA. While normally suffering from poor selectivity due to lack of active targeting capability, using the antibody as a delivering system negated this effect. Additionally, the selectivity of DTPC yielded homogeneous ADCs and therefore control of loading capacity. The construct was shown to exhibit highly selective cell toxicity against $EGFR^+$ cancer cells, allowing the release of the non-covalently bound drug after internalization of the ADC.[127] Other methods of pretargeting have been explored in the form of protein-binding cyclic peptides.[128]

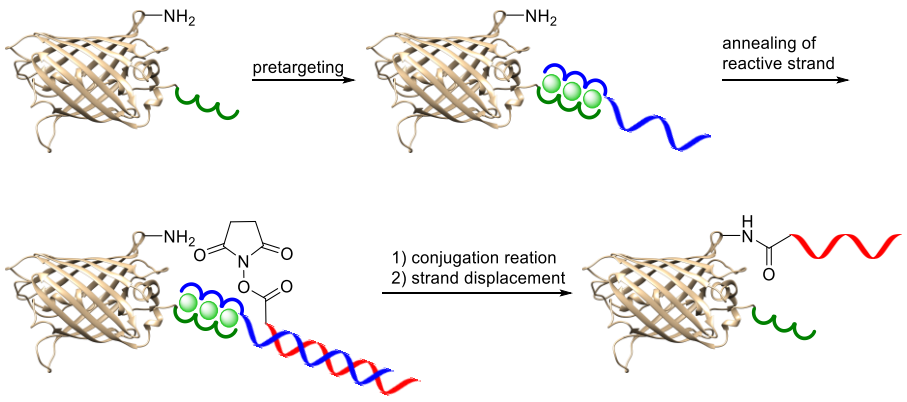

Figure 21: Illustration of DNA-templated protein conjugation on GFP-His_6 (PDB ID for GFP: 1GFL). The histidine-tag (green semicircles) of the protein is pretargeted by the guiding DNA strand (blue) bearing a Ni^{2+} (lime green) chelating ligand (blue semicircles). The reactive DNA strand bearing an NHS ester (red) is annealed, followed by covalent linkage to an ε-amino residue proximal to the His-tag. The guiding DNA strand is removed by strand displacement. Figure based on [125].

2.3.2 Peptide templates

While nucleobases offer a defined scaffold to form complementary interactions, transfer of this information in peptides is more intricate. Since a uniquely defined and predictable protein tertiary structure is required to perform this task, it necessitates intimate knowledge of the relationship between peptide sequence and protein structure. Lee *et al*. disclosed that a 32-residue α-helical peptide based on the leucine zipper homodimerization domain of yeast transcription factor GCN4 was able to template its own self-replication. Recognition in the leucine zipper is based on the structural motif of an α-helical coiled-coil peptide. It is defined by an amphiphilic primary sequence consisting of a series of heptad repeats $(abcdefg)_n$, where the amino acids at positions *a* and *d* define a hydrophobic core that serves as a continuous recognition surface throughout the protein. Native chemical ligation on the solvent-exposed surface was performed between a 17-residue thioester fragment and a 15-residue fragment bearing an *N*-terminal cysteine, each identical in sequence to their complementary part on the template chain. An autocatalytic efficiency of approximately 500 was achieved for the ternary reaction.[129] Introduction of charged residues flanking the hydrophobic core led to a higher degree of selectivity through salt-bridge formation for matching pairs and electrostatic repulsion for mismatched pairs. To achieve this effect, Kennan *et al*. introduced charged residues (lysine or glutamic acid) *i* at heptad positions *e* and *g* that would form salt-bridges with amino acids of opposite charges at position *i'*+5 or *i'*-5, respectively, on the complementary strand. The resulting entropic gain from binding the substrate led to a 4100-fold increase in initial reaction rate of the autocatalytic reaction over the non-templated ligation.[130]

Tamamura and co-workers used an antiparallel coiled-coil trimer of a GCN4 mutant to develop a tool for the fluorescent imaging of proteins. A dimeric coil-loop-coil motif was established as a tag motif, wherein the loop contained a cysteine residue for crosslinking and two leucine residues had been substituted for alanine to provide a hydrophobic pocket for an environmentally sensitive dye. The dye was introduced to the side chain of the complementary third α-helical peptide, which was further modified *N*-terminally with chloroacetic acid. Upon addition of the probe peptide to the tag, a covalent link between the two fragments was established and the fluorescence of the dye increased due to the hydrophobic environment. Proximity induced crosslinking was performed in a one-to-one ratio of substrates at a concentration of 1 μM for 20-30 min (see Figure 22).[131]

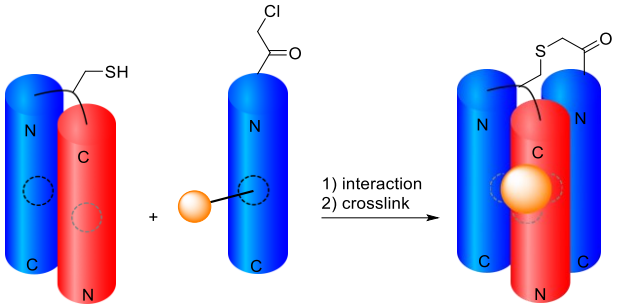

Figure 22: Fluorophore labeling by proximity induced crosslinking. An antiparallel coiled-coil dimer serves as a reaction scaffold for a probe strand bearing an environmentally sensitive dye. Upon recognition, the trimer is established by formation of a covalent bond between linker region of the dimer and *N*-terminus of the probe. Binding of the dye inside the hydrophobic cavity greatly increases fluorescence. Figure based on [131].

Further studies on the coiled-coil motif have revealed a basic set of characteristics that define the sequence-to-structure relationship. The term defines two or more α-helical peptides with a 3.5-residue repeat that wrap around each other, forming a left-handed supercoiled quaternary structure. Following the aforementioned general heptad repeat pattern of $(abcdefg)_n$, where *a* and *d* are hydrophobic amino acids, interactions between helices are mainly controlled by these two positions. The side chains of amino acids *a* and *d* (knobs) thereby insert into diamond-shaped regions, formed by the side chains of the recipient helix (holes). These interactions lead to the formation of a hydrophobic core along the continuous heptad pattern. The steric demand of the amino acid side chains placed at positions *a* and *d* (Ile or Leu) furthermore controls the oligomer state of the coiled coils, owing to the fit into the resulting holes. A rationally designed toolkit for *de novo* design additionally requires glutamic acid and lysine at positions *g* and *e* to establish intermolecular salt bridges, while alanine at positions *b* and *c* promotes helicity. Introduction of glutamic acid or lysine at position *f* increases the water solubility of the coiled-coil system.[132]

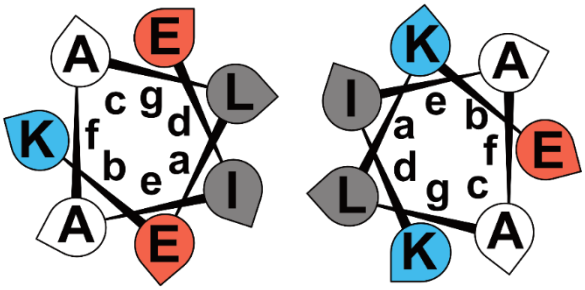

Figure 23: Helical-wheel representation of a coiled-coil heptad unit. Small letters represent the heptad position, whereas the capitalized letters represent the corresponding amino acid. The hydrophobic core is highlighted by amino acids on grey background, salt bridges are established between glutamic acid and lysine at positions *e* and *g*. Figure based on [133].

Litowski *et al*. used these general design principles to design a heterodimeric parallel coiled-coil, termed E3/K3, in which dimer formation is specified by having all glutamic acid residues at positions *e* and *g* of one strand (E3), and lysines on the opposing strand (K3). Charged residues at position *f* were opposite to those at positions *e* and *g* to decrease the net charge. The dimer, comprised of three heptad repeats per coil, showed a dissociation constant of 70 nM (see Figure 23).[133] In a series of publications, the groups of Seitz and Beck-Sickinger applied this system for the covalent labeling of membrane proteins. In their seminal work, the E3/K3 coiled-coil served as a tag/probe pair to transfer a fluorescent label from the K3-donor strand to the target protein-fused E3-acceptor strand *via* templated NCL. Therefor, the E3-peptide bearing an *N*-terminal cysteine was fused to the WW2 protein domain (5.8 kDa total). The K3 peptide, bearing a thioester-linked fluorophore (TAMRA) was added and transfer of the probe (1.0 µM) to the WW2 domain (0.5 µM) occurred in 58% yield after 10 min in neutral buffer. General applicability of the method in a complex environment was demonstrated for the labeling of the Cys-E3-tagged human neuropeptide Y_2 receptor (hY_2R(1-46)), *C*-terminally fused to the autofluorescent eYFP (37.5 kDa total). Addition of the TAMRA-K3 tag provided labeling within two minutes at a probe concentration of 20 µM or 100 nM for the labeling of cells expressing Cys-E3-hY_2R-eYFP. These finding demonstrated a minimally invasive tag/probe system, applicable for rapid *in cellulo* fluorescent imaging at low concentrations of the labeling agent (see Figure 24).[134] The scope of this method was further broadened by introducing a variety of fluorescent dyes (TAMRA, AF350 or ATTO488) and labeling of different membrane proteins of the family of G protein-coupled receptors (GPCR), such as hY_1R, hY_2R, hY_4R, hY_5R, human neuropeptide FF receptors 1 ($hNPFF_1R$) and 2 ($hNPFF_2R$) and the human dopamine receptor 1 (hD_1R). The authors further observed different yields for the transfer of the fluorescent label. While AF350-equipped K3 showed 58% yield after 2 min, ATTO488 transfer reached 50% after 10 min and transfer of TAMRA plateaued at 41% after 5 min. The latter effect was attributed to competing hydrolysis of the TAMRA-thioester, while the general discrepancy in reaction rate was attributed to the difference in fluorophore structure. It was furthermore observed that the K3-donor peptide does not penetrate the cell membrane, which limits the application of this method to the labeling of extracellular proteins.[135] In addition, the templated acyl transfer was used to investigate the internalization of GPCRs. A two-color pulse-chase experiment was designed to visualize the internalization pathway of two separately labeled and stimulated populations of hY_2R. For this, unstimulated, Cys-E3-tagged GPCRs were labeled with TAMRA-K3. Stimulation (*i.e.* internalization) of the receptor was induced by addition of the exogeneous ligand porcine neuropeptide Y (pNPY). After 30 min, ATTO488-K3 was used to label the remaining hY_2R at the cell surface. Again, the receptors were internalized and the two

populations were tracked by fluorescence microscopy. The experiment revealed the fusion of both subsets within the early endosome 10 min after the second stimulation.[136]

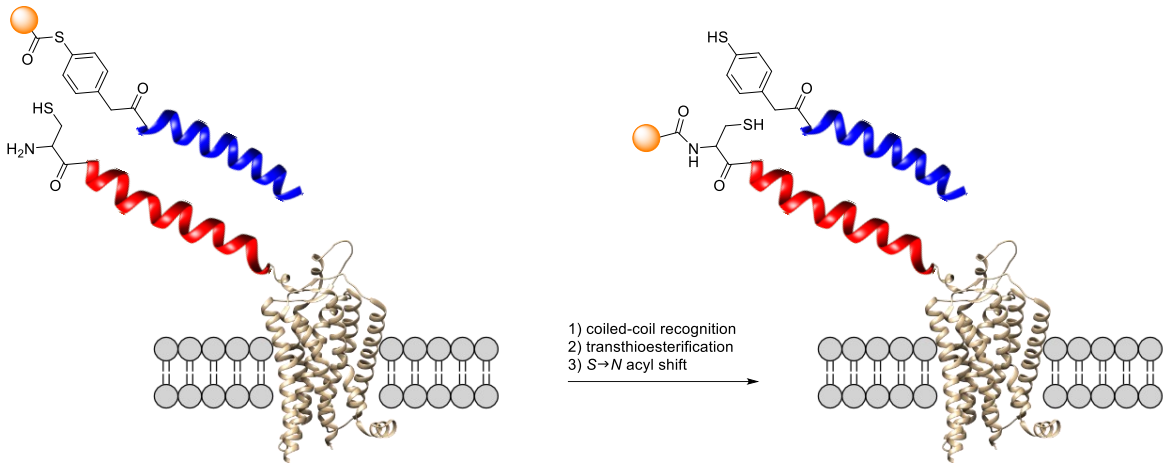

Figure 24: Schematic representation of coiled-coil mediated membrane protein labeling by acyl transfer. The acceptor strand (red) is fused to the protein of interest. Upon addition of the donor strand (blue) and coiled-coil recognition, NCL transfers the thioester-linked fluorophore from the donor to the acceptor strand. Figure based on [136].

Wang *et al*. used a similar system for protein labeling by covalently linking two coiled-coil strands. The utilized CCE3/CCK3 pair is similar to the previously described E3/K3 motif, but isoleucine residues in the hydrophobic core were replaced by valine. Furthermore, a pair of opposite amino acids in the hydrophobic core (*a*-*a'* or *d*-*d'*) were replaced by cysteine and an α-chloroacetyl functionalized amino acid. Formation of the heterodimer was followed by an S_N2 reaction to establish a thioether bond with the same length as the natural distance between the two strands. The authors found a preference for substitution of terminal amino acids, observing 50% conversion after 13.8 min when replacing the first *a* position in both strands. This effect was explained by a lower disturbance of the overall peptide structure and its stability, a higher flexibility of the functional groups at the strands termini and a better hydration of the leaving group (chloride ion). It was also shown that the use of coiled-coil tectons, *i.e.* peptides with maximum specificity to their binding partner, provided orthogonality for the covalent ligation of three coiled-coil pairs. Application of the covalent dimer formation for labeling purposes was shown by labeling a modified epidermal growth factor receptor (EGFR) on the surface of mammalian cells. Prior experiments had shown that labeling was more efficient when employing the CCK3 strand as a dimer, which resulted in labeling of the receptor within 20 min at a probe concentration of 0.2 µM or 1.0 µM.[137]

Similarly, Yano *et al*. used an in cell-crosslinking approach based on a sulfosuccinimide ester to covalently label membrane proteins. A heterodimeric parallel coiled-coil pair was

selected, and lysine residues were substituted for arginine to avoid side reactions. The fluorescent dye was attached to the *N*-terminus of the probe, $(RIAALRE)_3GC$, while the *C*-terminal amide was labelled with a sulfosuccinimide ester. The probe sequence, $(EIAALER)_3$, was fused to the target protein *via* a lysine containing linker peptide. The method was used to label the β_2-adrenergic receptor in CHO-K1 cells, as well as to analyze the oligomer states of glycoprotein A by FRET measurements. In both cases, labeling was carried out with a probe concentration of 150 nM for 20 min.[138]

Ball and co-workers demonstrated additional applications of a coiled-coil template by using a dirhodium metallopeptide catalyst for the covalent modification of a variety of amino acid side chains. The system used a heterodimeric coiled-coil based on Hodges' E/K peptides. The metallopeptide catalyst was generated by attaching $Rh_2(OAc)_4$ through glutamate side chains at heptad positions *a* and *e* of the K3 strand. On the acceptor strand (E3), tryptophan was introduced at the heptad position *g* opposite the catalytically active site. The catalyst was utilized for the covalent modification of Trp with a styryl-diazo reagent. 74% conversion was achieved within 2 h, a catalyst loading of 2 mol%, a substrate concentration of 50 µM and 70 eq. of the diazo compound at pH 6.2. It was further demonstrated that the modification of Tyr and Phe was likewise possible, albeit at a lower reaction rate, reaching 50% conversion after 5 h with a catalyst loading of 20 mol%.[139] The scope was further expanded to include amino acids Cys, Gln, Asn, Glu, Asp, Arg, Ser, His and Lys as possible targets for the diazo reagent. In addition, modification was carried out utilizing a naturally occurring coiled-coil pair. A glutamine residue in the leucine zipper (bZip domain) of the oncogene c-Fos was selected and targeted by an affinity-optimized variant of its natural binding partner c-Jun, with glutamate residues at heptad positions *a* and *g* binding $Rh_2(OAc)_4$. Modification of c-Fos (100 µM) was carried out using two equivalents of the peptide catalyst and an excess (10 mM) of the diazo reagent. Higher yields were observed at lower temperatures (17% at room temperature compared to 52% at -15 °C after 24 h), which was justified by a higher stability of the coiled-coil at lower temperatures.[140] Chen *et al*. demonstrated the applicability of this method for the labeling of proteins under biological conditions. The proximity induced ligation proved to be efficient enough to overcome the preferred pH range of the catalyst of ≤ 6.2, as demonstrated by an 80% conversion after 45 min in PBS buffer at pH 7.4. In addition, a biotin-diazo compound was synthesized and applied to the labeling of maltose binding protein (MBP). The tryptophan modified E3 peptide was fused to the *C*-terminal end of the protein (1 µM) and reacted with diazo-biotin (100 µM) upon addition of the $K3(Rh)_2$ catalyst (5 µM) in physiological buffer. 70% conversion was observed after a reaction time of 16 h at 4 °C (see Figure 25).[141] Interestingly, the repetitive nature of the heptad motif allows for the design of orthogonal acceptor/metallopeptide pairs. It was demonstrated that varying the position of the Trp

residue on the acceptor strand (*e* or *g*) or within the sequence (2nd or 3rd heptad) created facial or axial mismatches that led to stark discrepancies in selectivity (~ 9:1) when competing with the corresponding matched pair. These findings were exploited for the simultaneous labeling of MBP and glutathione *S*-transferase (GST). The proteins were expressed as a fusion with tryptophan modified E3, bearing the residue at the *g* or *e* position of the second heptad, respectively. Employing two equivalents (2 µM) of the catalyst was sufficient to selectively label both proteins simultaneously with diazo-biotin (100 µM) at 4 °C within 16 h.[142]

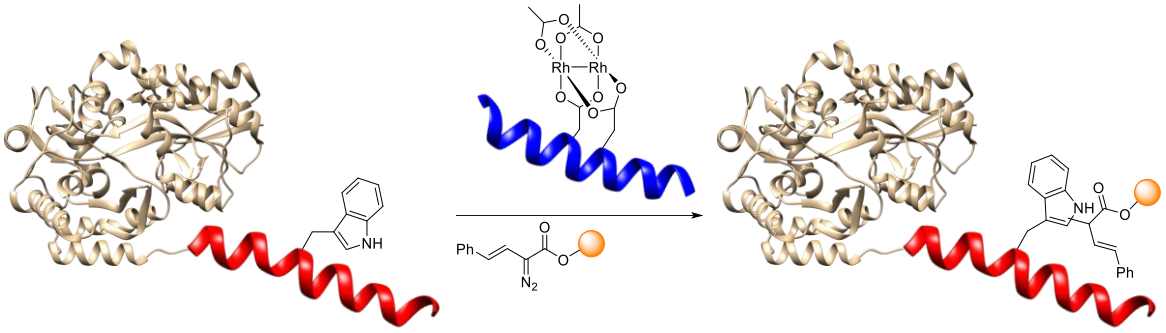

Figure 25: Proximity-induced protein labeling with a metallopeptide catalyst. Using a parallel heterodimeric coiled-coil, the dirhodium probe mediates the labeling of a tryptophan residue on the acceptor strand by catalyzing C-H activation. Figure based on [141], PDB ID for MBP: 1URD.

3 Project outline

While an ideal bioorthogonal ligation would be suitable for any number of chemoselective protein modifications, in reality, disadvantages such as substrate stability and excess reagent use might restrict applications. Templated organic synthesis has been identified as a possible solution, taking inspiration from nature. There, such reactions are widely used in biological systems to accelerate or enable covalent bond formation by bringing reactants into proximity, thereby increasing their effective molarity. More widespread use of this approach has been limited by the fact that at least one part of the templating scaffold is retained on the target protein after the ligation. To address this limitation, Middel *et al*. disclosed a PNA templated NCL that allows the removal of the template strands from the ligation product *via* photolysis of a photocleavable linker. Here, the two *N*-terminally activated peptides, a thiol and a thioester, are attached *via* CuAAC between the azide moiety of a nitrobenzene linker and the directing PNA strands. PNA base pairing brings the reactive groups into proximity, thereby enabling ligation. Photocleavage of the PNA auxiliary groups leaves the ligation product, a side chain-to-side chain linked isopeptide.[12] To fully capitalize on the advantages of templated ligation, the long-term goal in our workgroup is to use this approach for the mediation of two simultaneous ligation events (see Figure 26). The orthogonality encoded within the sequence of the template (red or blue strands) would provide chemoselectivity for both reactions, even when employing functional groups with competing reactivity (moieties A and B). The purpose of this thesis is the development of methods necessary to achieve this goal. Therefore, orthogonal templates have to be identified and tested in a one-pot reaction that performs a parallel ligation. Orthogonality of the templates is achieved, if there is a significant energy gap between least favorable desirable and most favorable undesirable template interaction, *i.e.* between matched and mismatched pairs. This can be achieved in two ways. First, due to selectivity installed in the sequence of the template's building blocks and second due to the use of two templates that utilize different modes of recognition.

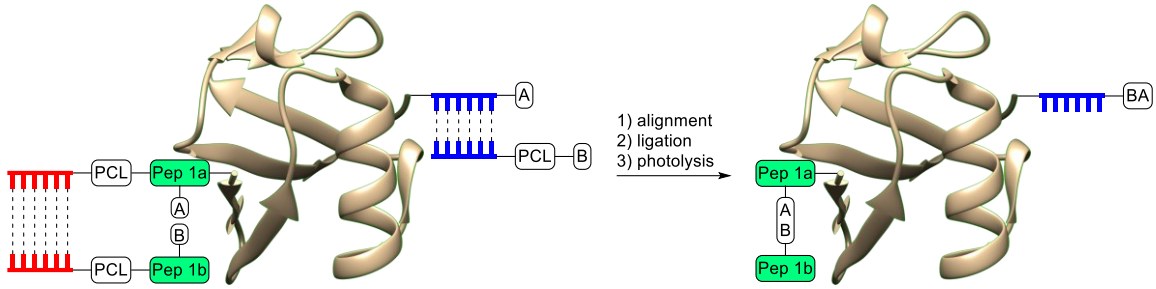

Figure 26: Schematic representation of the parallel functionalization of a protein employing two orthogonal templates (red and blue). Depicted are two reaction architectures leading to full (left) and partial (right) removal of the scaffold after successful ligation.

Sequence-programmed control over product formation in a multicomponent ligation system

The first project assesses the sequence selectivity and viability of PNA as an orthogonal template. Based on the findings by Middel *et al.*,[12] two independently complementary sets of parallel PNA strands (cPNA) are used as templates in a one-pot reaction between peptides with competing functionalities (see Figure 27). Annealing of the template strands is based on the self-recognition of complementary Watson-Crick base pairs.[143] PNA has been shown to exhibit a higher thermal stability and lower mismatch tolerance than its natural counterparts, DNA and RNA.[144] Therefore, two distinct duplexes are expected to show strong strand discrimination based on the energy penalty associated with a mismatched base pair. In addition, PNA oligomer synthesis is fully compatible with standard SPPS procedures, making it an ideal candidate for the identification of orthogonal template pairs. A series of oligomers with positional or size mismatches are synthesized, and their selectivity is determined by UV-Vis melting curve measurements. To facilitate this undertaking, a method for the automated solid phase synthesis of PNA oligomers is developed.

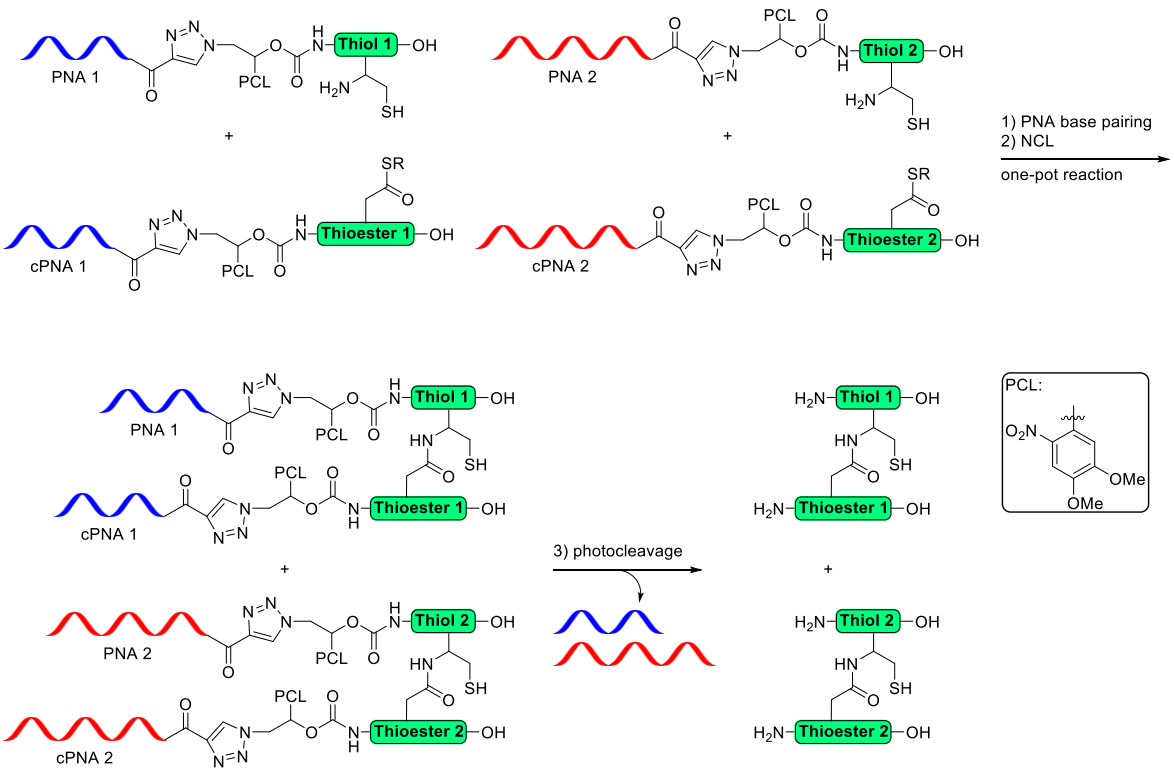

Figure 27: Schematic representation of the PNA mediated one-pot reaction between peptide fragments with competing functionalities. Orthogonality is installed by selection of independently complementary oligomer sequences.

Development of a PNA mediated Suzuki cross-coupling ligation

The second project focuses on expanding the scope and optimization of the photocleavable template. Our goal is to promote a reaction between two latent halves of a fluorophore whose functionality is restored upon ligation. We chose the Suzuki coupling, since it has been well established for the work on peptides and proteins and is compatible to the required mild conditions.[96] Furthermore, access to halogenated tryptophan derivatives enables linear synthesis of the two ligation partners that would form a Trp-Phe fluorophore.[145,146] As a proof of concept, the ligation is demonstrated between two peptide strands and subsequently the influence of the template is investigated (see Figure 28). One of the drawbacks of Middel's original system is the prolonged irradiation at low wavelengths necessary to cleave the guiding strands, thereby increasing the potential phototoxicity in biological systems. Coumarin derived photocages have been extensively studied[147] and display high quantum yields and ultrafast release.[148–151] A 7-diethylamino-4-methylcoumarin (DEACM) derivative, based on the work of Seyfried *et al.*[152], is therefore pursued as a viable alternative to the 4,5-dimethoxy-2-nitrobenzyl (DMNB) linker.

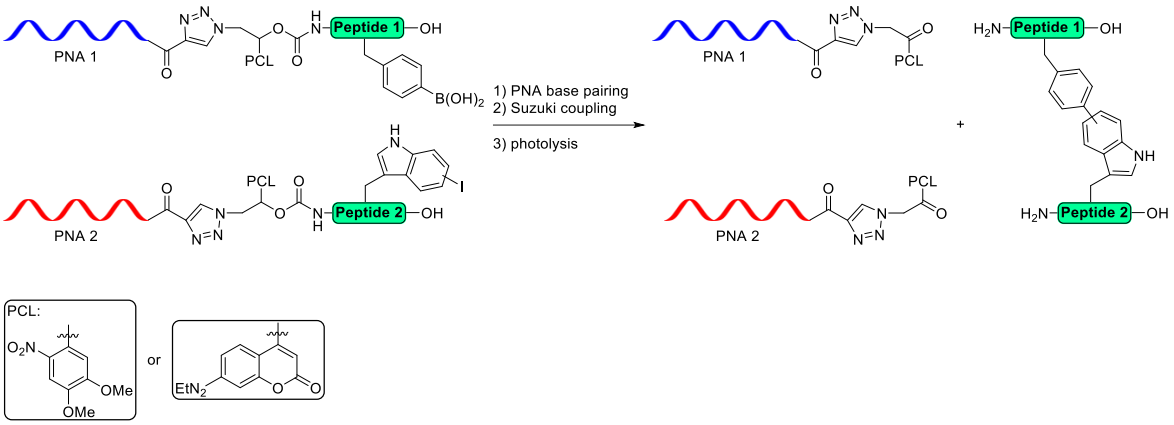

Figure 28: Schematic representation of the novel Suzuki coupling ligation strategy using photocleavable PNA strands as the directing scaffold.

Evaluation of coiled-coil peptides as a platform for templated reactions

Since most templated ligations rely on NCL or other ligations targeting canonical amino acids, we sought to find a platform that would support a variety of bioorthogonal ligation methods. Coiled coils were chosen as the templating motif, because of their facile synthesis, well understood association mechanism and previous application as a reaction scaffold.[132,153] They would furthermore provide an orthogonal template to PNA, since their association is mainly based on the interaction of hydrophobic residues, resulting in the formation of a hydrophobic core. Inspired by the work of Reinhardt *et al.*,[134] the aim of the third project is to attach different functional groups for bioorthogonal ligations to the *N*-termini of a parallel heterodimeric coiled-coil, thus achieving proximity induced covalent bond formation between the strands. Introduction of a photocleavable linker on the donor strand minimizes the tag size, ultimately resulting in a functional group transfer. The implementation of a variety of ligation reactions offers a modulable platform for an application-tailored approach (see Figure 29).

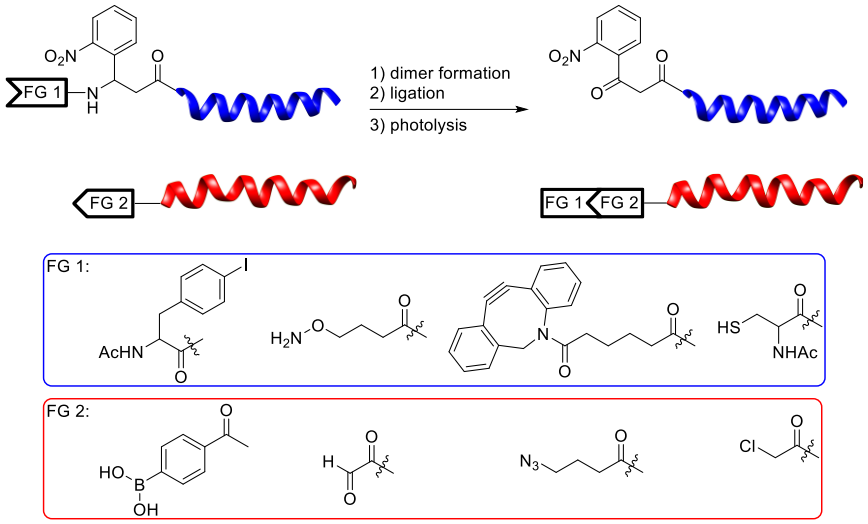

Figure 29: Schematic representation of a novel coiled-coil templated tag-and-modify approach utilizing a variety of ligation reactions.

4 Results and discussion

4.1 Sequence-programmed control over product formation in a multicomponent ligation system

In this chapter, the ability of PNA templates to mediate multiple reactions simultaneously based on their sequence selectivity is evaluated. The system is based on complementary PNA/peptide hybrids that have been developed previously.[154] They consist of PNA decamers as recognition units and utilize Melnyk's SEA native peptide ligation.[155] Hybrids are generated by conjugation with a photocleavable linker. This chapter introduces the general properties of PNA oligomers and their duplex formation (chapter 4.1.1), as well as the design of the system (chapter 4.1.2). Identification and selection of duplexes with sequence orthogonality is discussed based on UV-Vis melting curve measurements, while an emphasis is placed on the optimization of the PNA oligomer synthesis (chapter 4.1.3). The following subsections describe the buildup of the PNA/peptide hybrids consisting of the thioester surrogate for native peptide ligation (chapter 4.1.4), synthesis of the photocleavable linker and incorporation into peptides (chapter 4.1.5), as well as the conjugation to the PNA templates *via* CuAAC (chapter 4.1.6). The last section evaluates the selectivity of the templates in a competitive one-pot experiment (chapter 4.1.7).

4.1.1 Properties of PNA oligomers and their duplex formation

PNA is a fully synthetic DNA analogue in which the backbone consists of pseudopeptidic *N*-(2-aminoethyl)glycine (aeg) units that are structurally homomorphous to the deoxyribose phosphate backbone. The natural DNA nucleobases are retained and attached to the glycine nitrogen *via* a methylene carbonyl linker. Although originally designed as a DNA major groove binding ligand, PNA displays sequence-specific Watson-Crick binding to complementary nucleotides.[156] PNA hybridizes with both naturally occurring oligonucleotides, forming right-handed, antiparallel helices resembling B-DNA (PNA-DNA) or the A-form of RNA duplexes (PNA-RNA). The formed dimers exhibit thermal stabilities well above those of their corresponding natural counterparts, likely owing to the lack of repulsion between the backbones.[157–159] Two complementary PNA strands also form a duplex, with the antiparallel strand orientation being preferred. The antiparallel conformation of a 10-mer is approximately 20 °C more stable than the parallel version, which is comparable to complexes formed between DNA strands. The helices are wide and shallow with a large pitch (18 bp), with base pair stacking similar to the canonical A-form.

Because the monomers contain no asymmetric centers, helices are stacked alternating between right- and left-handed forms. Chiral information, and therefore control of the helix-handedness, can be introduced by addition of enantiomerically pure amino acids into the sequence or by binding to a chiral oligomer. Antiparallel PNA exhibits a low mismatch tolerance, with a single mismatch resulting in a drop of the melting temperature by approximately 20 °C.[143,160]

4.1.2 System design and synthesis strategy

The chimeric character of PNA between nucleic acids and peptides and the accompanying accessibility by SPPS,[157] as well as the stability in a cellular environment, *i.e.* towards nucleases and proteases, have made PNA the template of choice for the system described by Middel *et al*. Briefly, a parallel PNA duplex was used to align two reactive peptide fragments (thiol and thioester) to undergo NCL. Introduction of a photocleavable linker between the peptide and the PNA scaffold allowed traceless removal of the latter by irradiation.[12] After successful demonstration of this concept, a possible application lies in the dual functionalization of a protein with two imaging or bioactive moieties. This approach requires the identification of two orthogonal templates, in this case PNA duplexes. Selectivity is encoded within the nucleobase sequence. Even when employing competing functional groups in the ligation, strand displacement of the lower energy complex would leave only the groups attached to the matched strands with a sufficiently high effective molarity for a reaction to proceed. The feasibility of this strategy is evaluated in this chapter. The ligation approach has not been changed in comparison to the original approach and the most successful conditions have been selected. Its modular synthesis is presented in Figure 30. Synthesis of SPPS applicable building blocks of the DMNB-based PCL and the thioester precursor was required for the generation of the reactive peptide fragments. Conjugation to alkynylated PNA strands by on-resin CuAAC yielded the corresponding PNA/peptide hybrids, which after activation of the thioester and deprotection of the thiol fragment underwent templated NCL. Capping of the resulting free thiol and photocleavage of the templating strands yielded the side chain linked ligation product. Reaction procedures were duplicated from the PhD thesis of Stephen Middel or marginally improved upon, while emphasis was placed on the optimization of PNA coupling conditions and automatization.[154]

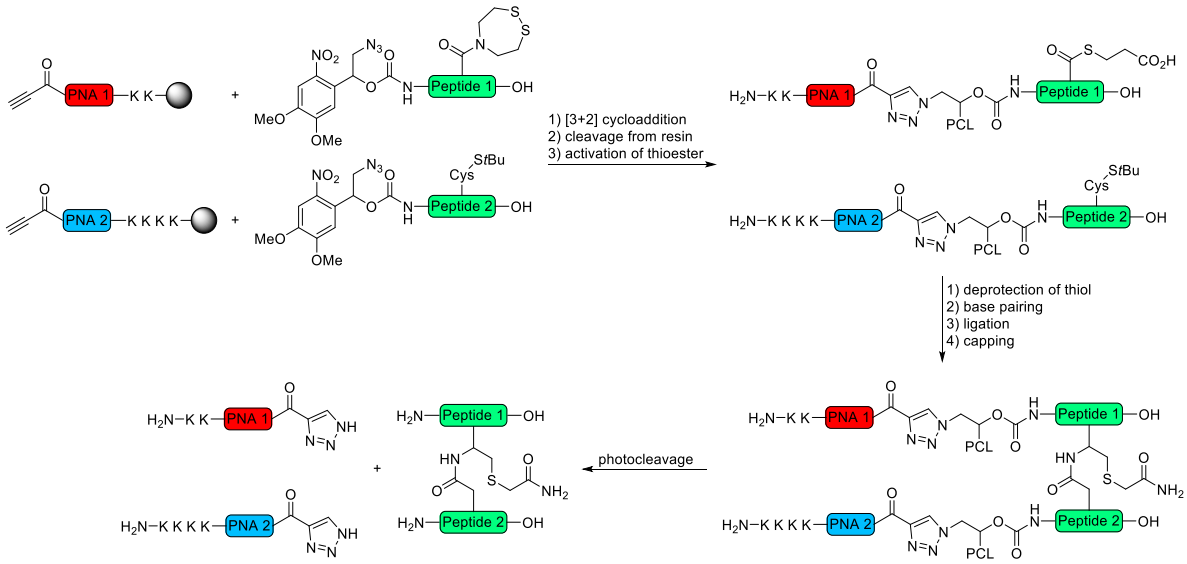

Figure 30: Schematic representation of the photocleavable PNA-templated NCL approach. Figure inspired by [154].

4.1.3 Identification of complementary PNA duplexes with sequence orthogonality

The influence of mismatched nucleobases on the thermal stability of oligomers containing at least one PNA strand has been best studied for antiparallel PNA-DNA duplexes. Kilså Jensen *et al*. conducted a study on the stability of antiparallel duplexes between 15-mer mixed sequence PNA and complementary DNA and RNA strands. Mismatches were introduced in one of the four center base positions and each possible mismatch (12 variants total) was investigated. Depending on the position and chemical nature of the mismatch, a drop in melting temperature of 8-19.5 °C was observed for the DNA-PNA complexes. Similar results were observed for the RNA-PNA complexes, where the destabilization ranged from 9.8-20.6 °C. The most stable mismatches occurred for the G·T wobble base pairing, which still retains two hydrogen bonds.[161] A study by Igloi on the stability of single base mismatched 11-mer PNA-DNA 17-mer duplexes (5bp overhang on the 5'-end) affirmed the importance of mismatch position and chemical nature. Melting point differences of as low as 0.4 °C for a G·T mismatch at the 3'-end were observed, contrasted by a drop in stability of 24.6 °C for a G·G mismatch four base pairs from the 5'-end. The study revealed the G·T and T·T pairs to be most stable among the mismatches, while A·A and G·G contributed the most destabilization. Maximal destabilization occurred at positions four base pairs from either end.[162] Ratileinen *et al*. studied the effect of mismatches at the central position of 9-mer PNA-DNA and 12-mer PNA-DNA duplexes. While introduction of the mismatch on the DNA strand mirrored the aforementioned results, with drops in melting

temperature of 13-17 °C for the 9-mer and 15-21 °C for the 12-mer, introduction of the mismatched base pair on the PNA strand (only 9-mer series) resulted in a deviation from the trend. Stark drops in melting temperature were observed for C·T and T·T mismatches (32 °C and 29 °C), resulting in melting temperatures for the duplexes around 10 °C. On the contrary, the G·T mismatch only displayed an 8 °C drop.[144] Studies on the destabilizing effect of purely PNA containing duplexes are scarce. Wittung *et al*. found that T·T and C·C mismatches in an antiparallel 10-mer decreased the melting temperature by 16 °C and 20.5 °C, respectively. Introduction of two C·C mismatches led to a destabilization of over 25 °C.[143] Similarly, Sacui *et al*. determined drops in melting temperature of -20 °C and -27 °C when introducing a G·T or T·T mismatch on antiparallel, left handed γ-methyl PNA (γPNA). No hybridization was observed for the C·T mismatch.[163]

In order to conduct this study, it is important to have fast and reliable access to PNA oligomers of high quality. While PNA is fully compatible with solid phase synthesis, prolonged coupling times complicate the process. Coupling times of 45 min are required, which, in addition to deprotection (10 min) and capping (5 min), leads to a coupling cycle of 2 h per monomer since every step is performed in duplicate to guarantee maximum coupling efficiency. Furthermore, several washing steps are required that add to the total time. For a single 10-mer the coupling time therefore exceeds 20 h.[154] Taking inspiration from the current state of the art in SPPS, it seemed reasonable to assume that PNA synthesis could be carried out assisted by microwave irradiation and possibly also in an automated fashion on a peptide synthesizer. Based on previous work in our group by Geralin Höger on the synthesis of β-PNA,[164] a microwave assisted synthesis protocol was developed. Deprotection of the *N*-terminal Fmoc-protecting group was carried out with 20% piperidine in DMF at 40 °C for 1 min, followed by a second deprotection step at 50 °C for 5 min. Coupling of the building blocks was performed after preactivation with HATU, HOAt, DIPEA and 2,6-lutidine at 50 °C for 2 x 20 min. The capping step remained unchanged, applying a mixture of 10% acetic anhydride and 5% 2,6-lutidine in DMF for 2 x 5 min at room temperature. These changes already resulted in a reduced coupling time by more than half compared to the manual room temperature approach. Next, a possible automatization of the coupling cycle was investigated. The development of the methodology described hereafter was carried out in collaboration with Denis Pahlke and Patrick Menzel. Since coupling protocols for automated microwave assisted SPPS differ from the manual approach and are dependent on the device manufacturer, we first tested a protocol developed by the *CEM Corporation* (Mathews, NC, United States)[165] on a *Liberty Blue* automated microwave peptide synthesizer. Here, coupling was performed on a PEG-PS resin (0.23 mmol/g) at a 50 µmol scale. Deprotection of the Fmoc-protecting

group was carried out for 5 min at room temperature, followed by a second step for 10 min. Coupling was performed at 50 °C for monomers A, T and G and at 75 °C for 60 min for monomer C, using DIC and HOBt as activators. Surprisingly, when we translated this method to our 10-mer sequence (see Table 1, entry 1), only exchanging the resin for a NovaPEG Rink amide resin (0.17 mmol/g), we did not observe product formation. Instead, a peak corresponding to a truncation after the first coupling was identified in mass spectrometry. We decided to directly adapt our room temperature coupling method, since it includes additional washing steps, a capping step and less harsh coupling conditions. We also decided to test the standard activators DIC and Oxyma and to employ 2% piperazine (2 x 15 min) as the deprotection solution, since it is recommended by the manufacturer for small scale synthesis (here: 10 µmol).[166] In our hands, this strategy proved more successful, yielding the desired 10-mer in acceptable purity. Next, we tested the influence of microwave irradiation. We found that deprotection at 40 °C for 1 min, followed by 5 min at 40 °C and coupling times of 2 x 30 min at 50 °C proved ideal (see Figure 31). Oligomers synthesized in this way provided an optimal compromise between time saved and product purity. Decreasing the coupling time to 20 min led to an increased formation of deletion sequences, while the effect was more pronounced when increasing the coupling temperature. Manual microwave assisted synthesis seems to hold a slight edge over the automated version, since it employs more efficient coupling reagents and is better compatible with larger synthesis scales. Both methods are however viable and were employed in the identification of orthogonal PNA pairs.

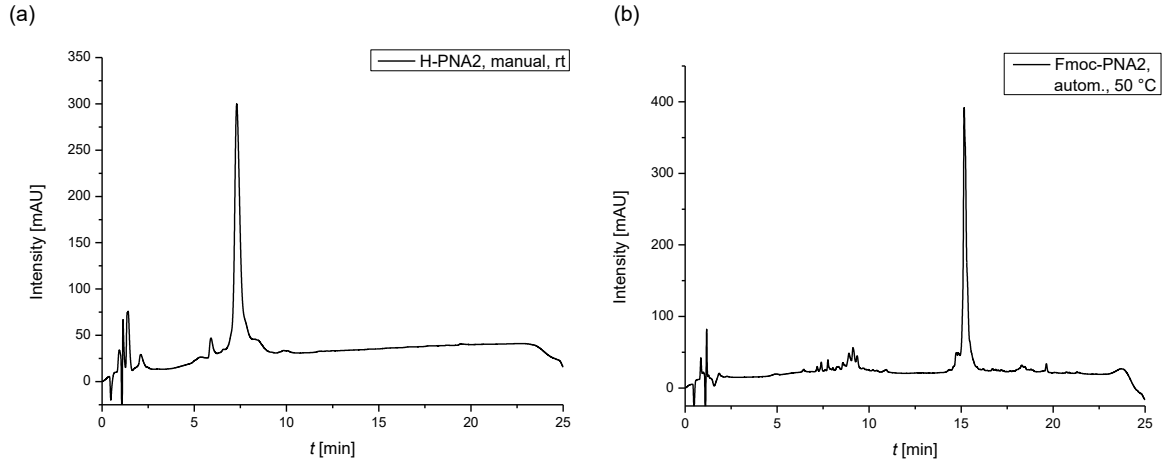

Figure 31: HPLC chromatograms (215 nm) of (a) crude PNA 2, obtained by manual coupling at room temperature and (b) crude Fmoc-PNA 2, obtained by automated microwave supported coupling. The difference in retention times can be attributed to the absence or presence of an *N*-terminal Fmoc protecting group.

To the best of our knowledge, studies on the destabilizing effect of mismatched base pairs in parallel PNA-PNA duplexes have not been published. While it seems reasonable to

assume similar destabilizing effects in the range of 15-20 °C, experiments have to be carried out to verify this hypothesis.

Table 1: PNA sequences employed in this thesis. Mismatch positions of entries 1-3 in regard to duplex formation with entry 4 are indicated in red.

Entry	Number	Mismatch	Sequence (*N* to *C*)				Lys
1	**1** (PNA 1)	none	g	tag	atc	act	K_2
2	**2** (PNA 1')	C·C, G·G	g	tac	atc	agt	K_2
3	**3** (PNA 1'')	A·A, C·C, G·G	g	aac	atc	agt	K_2
4	**4** (PNA 2)		c	atc	tag	tga	K_4
5	**5** (PNA 3)		acg	tca	caa	cta	K_2
6	**6** (PNA 4)		tgc	agt	gtt	gat	K_4

Based on the original parallel duplex introduced by Wittung *et al*.[143] (see Table 1, entries 1 and 4), two (C·C and G·G, entry 2) and three (A·A, C·C and G·G, entry 3) mismatches were introduced. While a difference in melting temperature was observed for the mismatched complexes the differences were only subtle, with a decrease of 5 °C (PNA 1') and 4.6 °C (PNA 1'') when compared to the fully matched duplex (T_m = 46.3 °C). Furthermore, introduction of the third mismatch inexplicably led to no further destabilization (see Figure 32a). While these results starkly contrast the aforementioned trends,[143] an unintentional selection of a mismatch position with little contribution to the thermal stability[162] might offer an explanation. This seems however unlikely, since introduction of central mismatches supposedly result in the weakest binding interaction, possibly due to the remaining short specific regions on either side of the mismatch on the complementary strand. Another possible explanation is the coincidental design of unsurprisingly strong complexes, despite the introduced mismatches. A hybridization study of DNA to PNA oligomer arrays by Weiler *et al*. revealed few strong hybridization events with PNA oligomers containing up to three continuous mismatches in the center of the sequence.[167] No explanation of this phenomenon could be identified and therefore seems more like a chance encounter, unlikely to be replicated. Instead, it seems more probable that parallel PNA duplexes behave differently to their antiparallel counterparts. Therefore, a length mismatch was investigated. The 12-mer duplex of PNA 3·PNA 4 (see Table 1, entries 5 and 6) showed a melting temperature of 57.5 °C, which equals ΔT = 11.4 °C compared to the 10-mer (see Figure 32b). Although not an ideal value, this represented a good starting point. Mix-and-match experiments with the 10-mer strands however revealed a different picture (see Figure 32c). The mismatched 10-mer·12-mer complexes were close in melting temperatures to the matched 10-mer duplex, with values ranging from 39.1 °C

(PNA 2·PNA 4) to 46.7 °C (PNA 1·PNA 3). Nonetheless, it was decided to test a one-pot parallel ligation approach, hoping for sequence selectivity to prevail and applying the 10-mer and 12-mer parallel duplexes as templates.

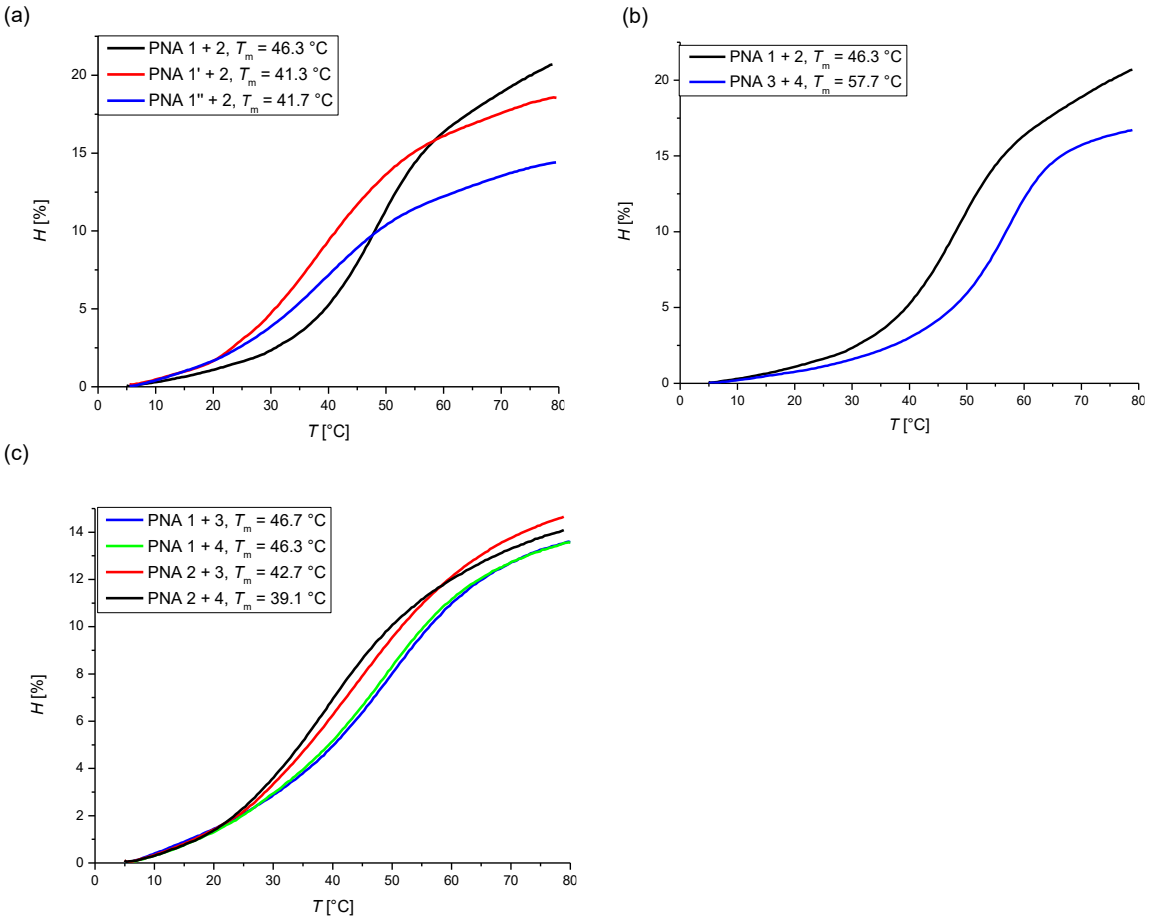

Figure 32: UV-Vis melting curve measurements of (a) parallel PNA 10-mers with base pair mismatches, (b) comparison of 10-mer and 12-mer duplexes and (c) size mismatch between 10-mer and 12-mer strands. Measurements were carried out with a strand concentration of 5 µM in TBS buffer (50 mM Tris-Cl, 150 mM NaCl) at pH 7.5.

4.1.4 Synthesis of the thioester surrogate

Central to the success of the presented ligation system was the incorporation of a thioester precursor that would tolerate the basic conditions necessary during the deprotection step of SPPS. The employed thioester was based on the bis(2-sulfanylethyl)amido (SEA) peptide ligation developed by Melnyk and co-workers (see Figure 33).[155,168] Activation of thioester surrogate **I** (SEA^{off}) takes place under reductive conditions, due to formation of dithiol **II** (SEA^{on}) from a disulfide. *In-situ* formation of intermediate **III** via *N*,*S*-acyl shift yields a thioester applicable in NCL. The equilibrium of its formation however lies on the side of

the dithiol. It can be shifted, for example by removing the product *via* transthioesterification (*e.g.* with 3-mercaptopropionic acid (MPA)), to afford the final thioester (**IV**).

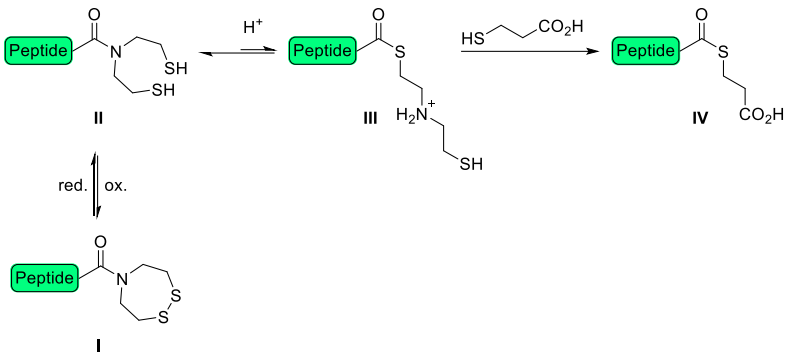

Figure 33: Overview of the SEA native peptide ligation. Figure inspired by [154,155].

Unless otherwise stated, synthetic procedures in this part of the thesis were replicated from the PhD thesis of Stephen Middel[154] and are therefore presented in an abbreviated, summarizing form. For application in SPPS, the side chain of glutamic acid was modified with the SEA^{off} building block (see Figure 34). Therefore, bis([2-{triphenylmethyl} sulfanyl]ethyl)amine (**8**) was synthesized by reacting bis(2-chloroethyl)amine (**7**) with triphenylmethanethiol and DBU in an S_N2 reaction in 48% yield. **8** was coupled to the side chain of *N*-Boc-protected glutamic acid, using PyBrOP as the coupling reagent. A moderate yield of 51% was achieved, followed by oxidative cleavage of the trityl protecting group (Trt) with iodine in 78% yield to afford **10**. Boc deprotection and Fmoc protection of the amino group afforded the final SPPS building block (**11**) in 37% yield.

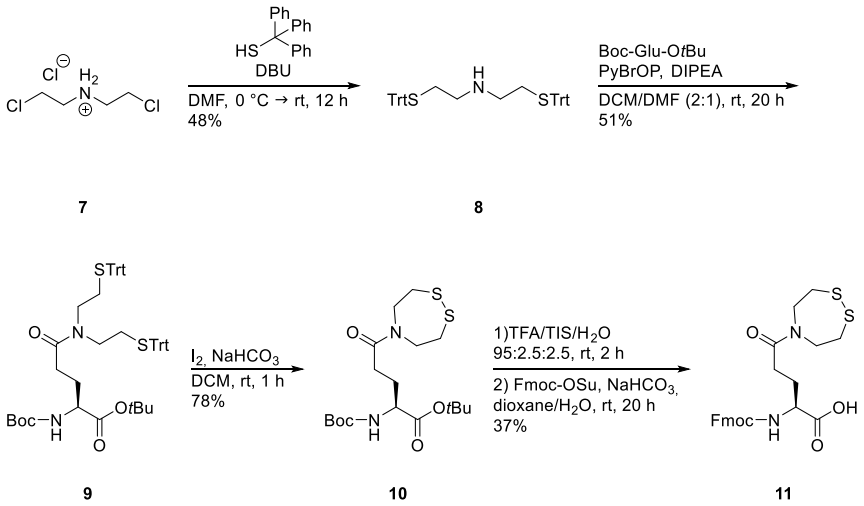

Figure 34: Synthesis of Fmoc-Glu(SEA^{off})-OH.

4.1.5 Synthesis of the photocleavable linker and incorporation into peptides

Another key part of the designed system is the photocleavable linker (see PCL in Figure 30), which allowed the removal of the templating strands upon ligation. The synthetic approach slightly deviates from the established procedure, since a Corey-Chaykovsky epoxidation was selected to synthesize **13**, starting from commercially available 6-nitroveratraldehyde (**12**). This stroke saves one synthetic step, since the original procedure was designed to transform the aldehyde into an alkene *via* a Wittig type reaction, followed by epoxidation with *m*CPBA. Since the Corey-Chaykovsky approach yielded a moderate 49% of the product, the overall yield of both strategies was similar. Nucleophilic ring opening of epoxide **13** with sodium azide provided intermediate **14** in 52% yield. Activation of the hydroxy group with *N,N'*-disuccinimidyl carbonate (DSC) yielded 82% of the PCL (**15**, see Figure 35), which was now directly applicable for peptide synthesis.

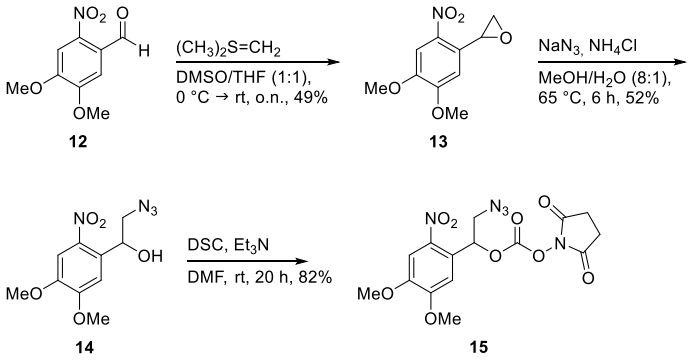

Figure 35: Synthesis of the DMNB-derived photocleavable linker **15**.

Building block **11** was directly incorporated into the thioester peptide fragment following standard SPPS procedure, while PCL **15** was attached on resin employing the conditions outlined in Figure 36.

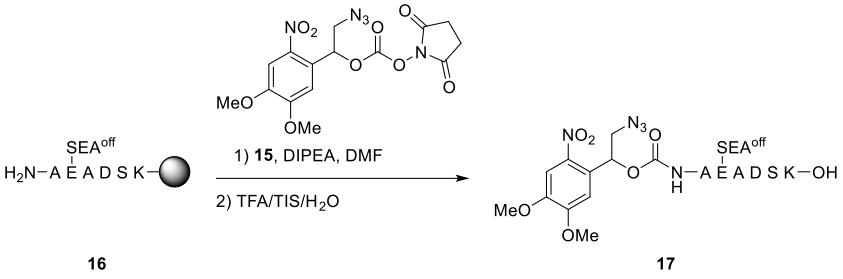

Figure 36: On-resin coupling of the PCL to the corresponding peptide.

Coupling of the thiol fragment and conjugation of the PCL was achieved in a similar fashion, after introduction of a *tert*-butyl thiol protected cysteine to the side chain of the penultimate amino acid.

4.1.6 Synthesis of PNA/peptide hybrids

PNA strands 1-4 were synthesized using the newly developed protocols and prepared for on-resin CuAAC by introduction of an alkyne moiety. The coupling conditions are exemplary presented for PNA 2 in Figure 37.

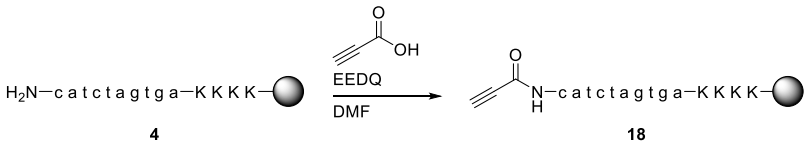

Figure 37: On-resin alkyne functionalization of PNA strands by coupling of propiolic acid.

On-resin azide-alkyne cycloaddition between alkynylated PNA and PCL-peptide fragments was carried out using copper(I) iodide and sodium ascorbate. Subsequent cleavage from resin and purification by HPLC yielded the desired PNA/peptide hybrids (see Figure 38).

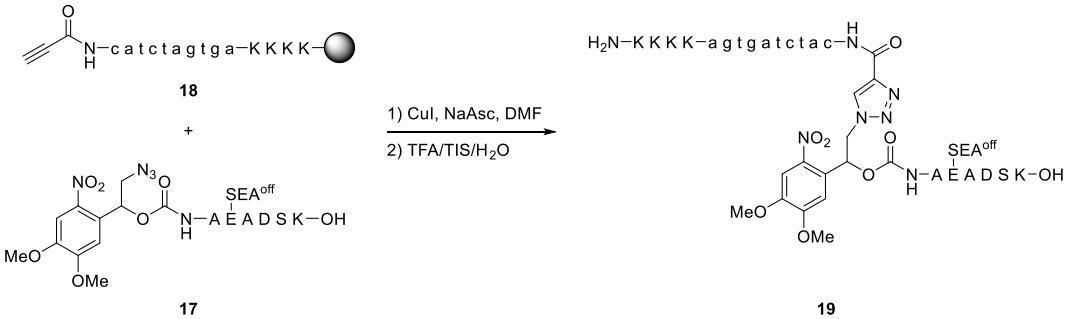

Figure 38: Formation of PNA/peptide hybrids by on-resin CuAAC.

In the case of the SEA^{off} peptide hybrids, transformation into the active species was achieved by dissolving the peptide in TCEP containing phosphate buffer at pH 3 and addition of MPA (see Figure 39). The individual PNA/peptide hybrids, as well as their respective chromatograms are presented in Figure 40.

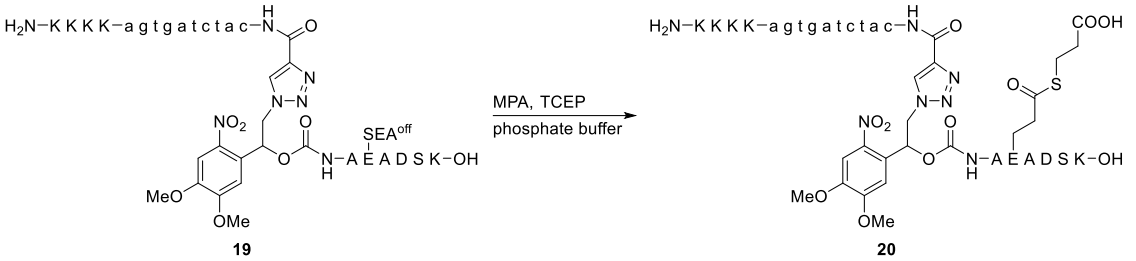

Figure 39: Transformation of the thioester precursor into the active species.

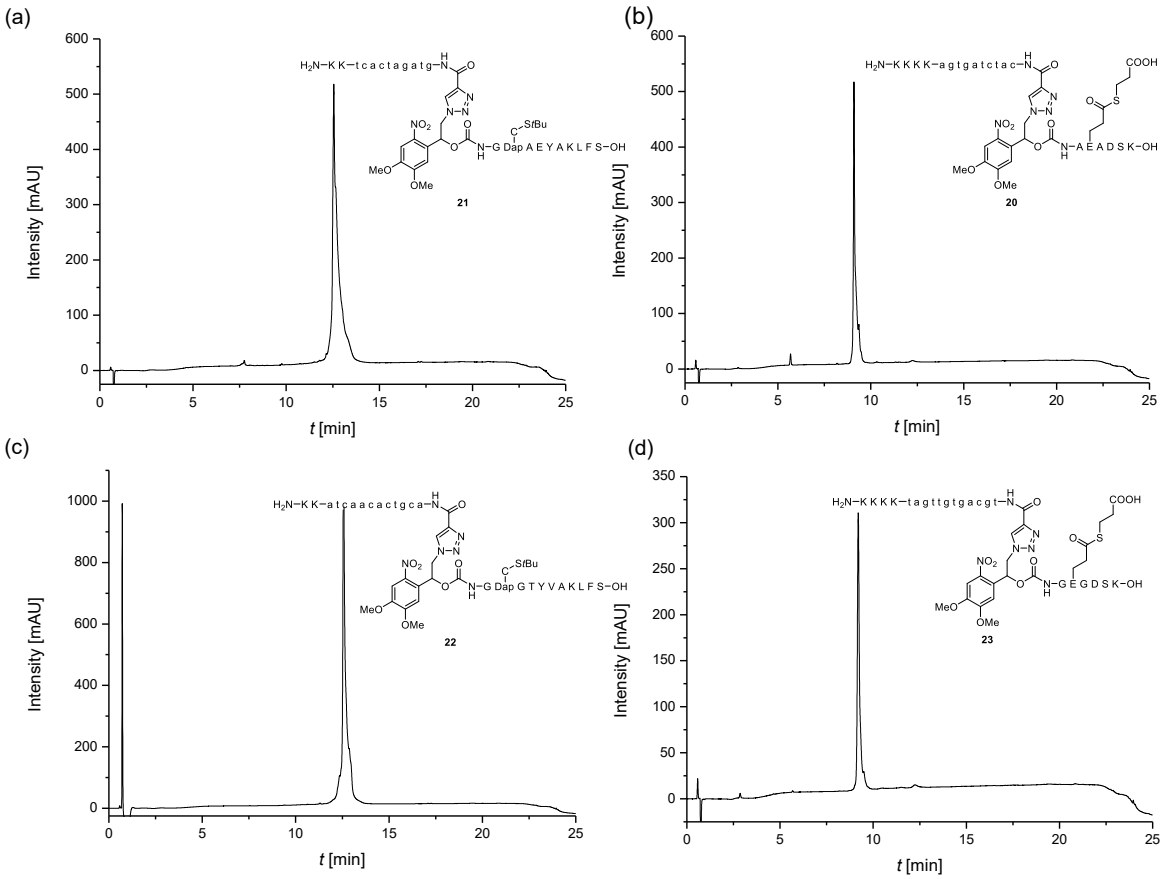

Figure 40: HPLC chromatograms (215 nm) of the purified PNA/peptide hybrids: (a) 10-mer thiol (**21**), (b) 10-mer thioester (**20**), (c) 12-mer thiol (**22**) and (d) 12-mer thioester (**23**).

4.1.7 Competitive PNA mediated NCL

Following the successful synthesis of the two complementary PNA/peptide hybrid pairs, their reactivity was studied in a one-pot reaction (see Figure 41). Despite the high purity of starting materials, no product formation was observed upon addition of ligation buffer after 24 h. Neither starting material, nor a (cross) reaction product was identified by UHPLC or LC-MS analysis. Instead, a reaction mixture without distinctly separated peaks was observed. This could be either the result of retention times of the reactants being too similar, or due to the fact that the nucleobase recognition was not selective enough,

therefore forming mixed products, effectively lowering the concentrations under the detection limit. A combination of both factors seems likely, thereby disproving the applicability of parallel PNA duplexes for simultaneous ligation events.

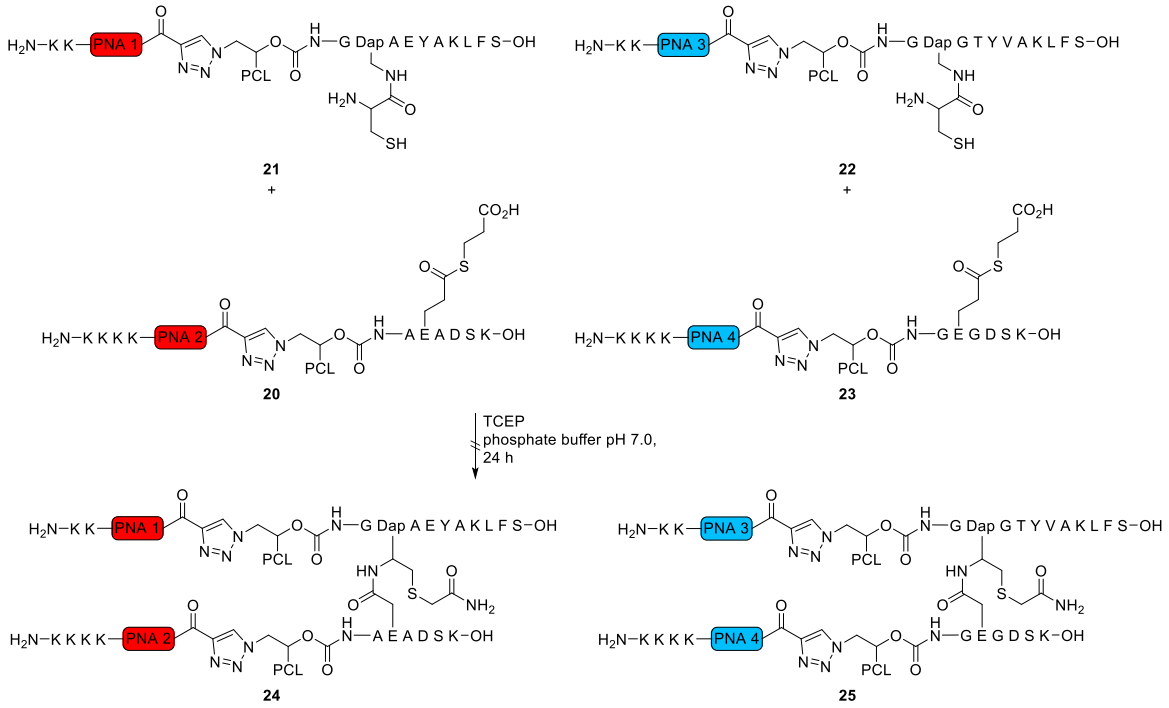

Figure 41: PNA mediated competitive NCL experiment utilizing length- and sequence mismatched templates.

4.1.7 Conclusion

In this chapter it was evaluated whether orthogonal photocleavable PNA templates can mediate two ligation events with competing functional groups. To this end, a new method for the automated solid phase synthesis of PNA was developed. Strands of a variety of individual annealing sequences and lengths were synthesized to investigate their sequence selectivity *via* UV-Vis melting curve measurements. Surprisingly, individual base pair mismatches did not lead to a pronounced change in the melting temperature. Instead, a pair of length and sequence mismatched duplexes (PNA 1·PNA 2 and PNA 3·PNA 4) were suitable for an orthogonal ligation approach. They were therefore modified with a photocleavable linker and a thiol or thioester to undergo a competitive ligation experiment. Neither (cross) reaction products nor retained starting materials were identified. Instead, a mixture without distinct HPLC peaks was observed, presumably due to a lack of template selectivity. The approach was therefore not pursued further and instead focus was shifted to the ligation method and identification of a different template.

4.2 Development of a PNA mediated Suzuki cross-coupling ligation

This chapter evaluates an additional ligation reaction for use with the PNA template. The method is based on the biocompatible Suzuki cross-coupling.[98] An introduction to this method is given and conditions for the stoichiometric conjugation of peptides are established (chapter 4.2.1). For the hybridization of peptides and PNA, a photocleavable linker with improved properties is designed. The synthesis and evaluation of its photolysis are discussed (chapter 4.2.2). The following subsection describes the synthesis of the PNA/peptide hybrids for Suzuki cross-coupling. Complications following the previously established strategy are discussed and an alternative approach, based on the synthesis of an unnatural borylated amino acid, is presented (chapter 4.2.3). The final chapter investigates the PNA templated Suzuki cross-coupling reaction and addresses possible interactions of the transition metal catalyst with the template nucleobases (chapter 4.2.4).

4.2.1 Establishing conditions for Suzuki cross-coupling between peptide fragments

We decided to investigate a different ligation method to broaden the scope of the templated ligation strategy. A conjugation method that would generate a fluorophore upon covalent linkage of the peptide fragments is highly desirable. It would offer the possibility to track the target protein *via* fluorescence microscopy, as well as give a live readout of the ligation progress. Previous research in our group by Swantje Nawratil already investigated the possibility to introduce a tetrazole-alkene “photoclick” or fluorescence-generating CuAAC reaction.[169] Since both attempts did not yield the desired templated peptide ligation with fluorophore generation, a third approach was explored.

A possible cause for the reaction deficiency is the high steric demand of the modified peptide side chains. Therefore, a geometry agreeing with a natural, linear peptide structure was preferable. As previously discussed (see chapter 2.2.7), Suzuki coupling provides compatibility with biological systems and access to a fluorophore *via* cross-coupling of modified phenylalanine and tryptophan residues.[146,170] The required halogenated derivatives of tryptophan are accessible from the corresponding haloindole *via* tryptophan synthase catalyzed biotransformation.[145] The most prominent drawback of applying a transition metal mediated strategy, namely excess of catalyst and reaction partner, should be negated by application of the template. Since generation of an SPPS applicable halogenated tryptophan derivative is labor-intensive, it was decided to first optimize the

coupling conditions on a non-fluorescent system with easier accessible building blocks. Therefore, the viability of the coupling conditions had to be established. Chalker *et al*. had already demonstrated the applicability of the pyrimidine derived catalyst $(ADHP)_2 \cdot Pd(OAc)_2$ for the modification of Boc-*p*IPhe-OH with phenylboronic acid under biocompatible conditions.[98] Therefore, similar conditions were applied for the modification of test peptide **26**, bearing a iodophenylalanine residue. The reaction progress was monitored over 36 h by UHPLC measurements. Conversion of the reactants was observed forming the desired product, with 43% conversion after 12 h and 93% after 24 h. (see Figure 42).

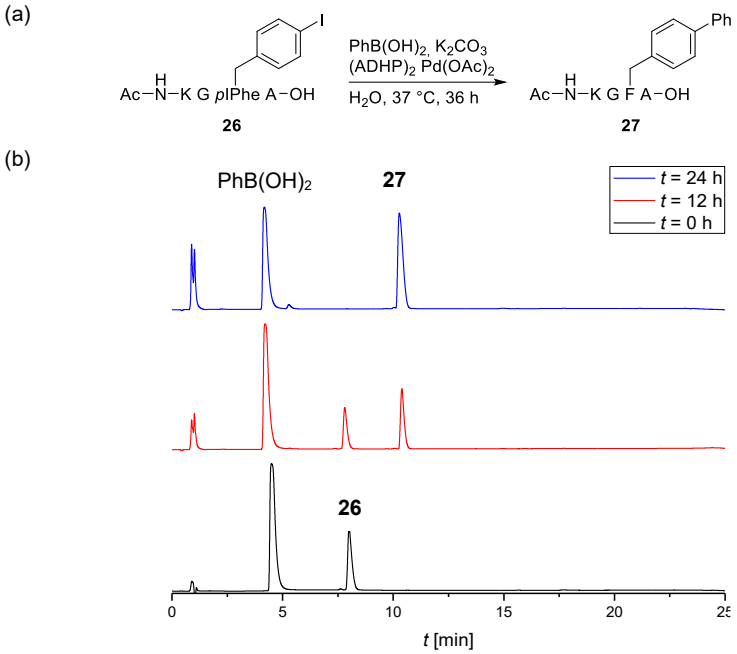

Figure 42: (a) Suzuki coupling on a short peptide with phenylboronic acid and (b) reaction monitoring by UHPLC (215 nm).

While the reaction proceeded sluggishly, especially in comparison with the lone halogenated amino acid, the method was further pursued for the coupling of two peptide fragments and eventually templated ligation. To obtain the borylated counterpart (**28**), a method for on-resin Miyaura borylation, developed by Afonso *et al*. was employed (see Figure 43).[171]

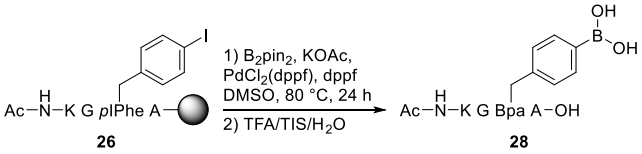

Figure 43: On-resin Miyaura borylation of a *p*IPhe containing test peptide.

The reaction yielded the desired product under loss of the pinacol ester protecting group, which was presumably hydrolyzed during HPLC purification.[172] Nonetheless, **28** was used in a cross-coupling reaction with **26** employing the previously established conditions. Once again, product formation was observed, however, conversion proceeded even slower than for the coupling of **26** with phenylboronic acid. Product formation of 23% was observed after 36 h, while only 42% conversion was detected after 84 h. (see Figure 44).

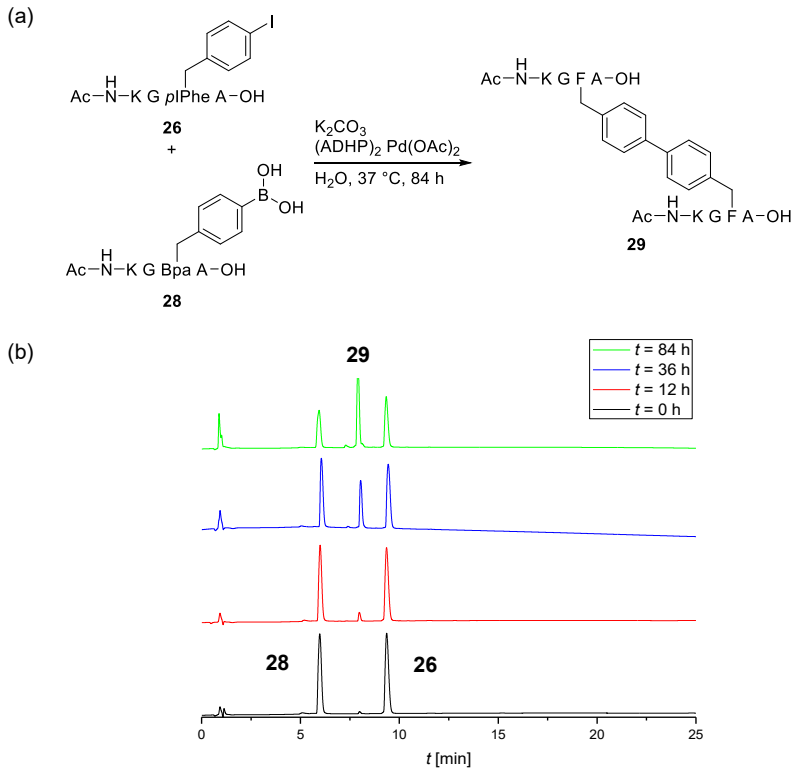

Figure 44: (a) Suzuki cross-coupling between two peptide fragments under biocompatible conditions and (b) reaction monitoring by UHPLC (215 nm).

Judging from the decrease in reaction rates from the cross-coupling of amino acid and phenylboronic acid (fast) to peptide and phenylboronic acid (slow) to the coupling of two peptide fragments (very slow), a correlation to the steric hinderance in accessing the reaction partners seems apparent. These results explain the superstoichiometric use of reagents in Suzuki cross-coupling on proteins. A preorganization of the reaction partners by a template might mitigate this effect to some extent.

4.2.2 Development of a coumarin based photocleavable linker

Before incorporation of the peptide fragments into PNA/peptide hybrids, the viability of a new photocleavable linker was assessed. One of the drawbacks of the previously utilized DMNB linker is its low quantum yield and excitation wavelength. This results in the use of high energy irradiation over a prolonged time. Furthermore, the release mechanism discussed below reveals the formation of a potentially toxic byproduct. Those factors suggested the necessity of a novel photocleavable linker with improved photophysical properties. Herein, nitroveratryl and coumarin based linkers are compared, starting with their photolysis mechanism and release in a test experiment. Some of the following experiments are part of the bachelor thesis of Ivana Gavrilova.[173]

4,5-Dimethoxy-2-nitrobenzol (DMNB, or 6-nitroveratryl, NV) is a derivative of *o*-nitrobenzol and was first introduced as a photocleavable protecting group in 1970.[174] Introduction of the two methoxy groups increases the absorbance at higher wavelengths, enabling cleavage at 365 nm. Yet shorter wavelengths ($\lambda_{abs} \approx 345$ nm) are more effective.[175]

The photorelease mechanism of *o*-nitrobenzyl protected compounds (see Figure 45) comprises of three critical steps. First, the caged compound **I** undergoes a photoinduced *H*-atom transfer (HAT*), resulting in *aci*-nitro intermediate **II**. Ground state cyclization leads to the isoxazolidin-1-ol intermediate III, whose formation competes with the reverse HAT to reform the starting material. Under basic conditions, **III** is deprotonated giving intermediate **IV**, which cleaves irreversibly by release of the leaving group X and formation of *o*-nitrosobenzaldehyde derivative **V**.[176] *O*-nitrosobenzaldehydes are potentially toxic to surrounding bioprocesses.[147] Due to the low quantum yield and absorbance maxima of *o*-nitrobenzyl protecting groups, as well as the improved DMNB protecting group (Φ = 0.006, 365 nm, λ_{abs} = 345 nm), low wavelengths, combined with powerful irradiation over a long period of time had to be applied in previous experiments.[154,175]

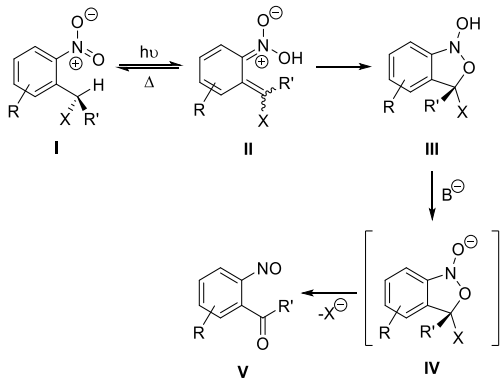

Figure 45: Simplified mechanism of the photolysis of *o*-nitrobenzyl compounds. Figure based on [176].

In contrast, coumarin derived photoremovable protecting groups (PPGs) have been extensively studied[147] and found application in caging a number of functionalities, including phosphates,[148,177,178] carboxylic acids,[179,180] amines,[181–183] alcohols[184] and thiols.[185] Deiters and co-workers furthermore demonstrated *in vivo* applications of protein activation.[186–188] Coumarin presents itself as a versatile platform, allowing for the caging of different functional groups *via* the alcohol moiety of a 4-hydroxycoumarin scaffold. Changing of the residues at positions six, seven or even two, alters the photochemical properties enabling a shift to higher wavelengths or two-photon uncaging.[175]

7-Diethylamino-4-methylcoumarin (DEACM) was selected as a basis for the photocleavable linker due to the bathochromic shift introduced by the electron donating groups at the *C*-7 position, resulting in an absorption maximum around 390 nm. In addition, the molecule displays a high quantum yield (DEACM-puromycin, Φ = 0.47, 380 nm) and ultrafast release.[148–151] Once again, the uncaging mechanism offers insight about the advantages of this linker (see Figure 46). First, excitation of (coumarin-4-yl)methyl (CM) ester **I** by a photon takes place, followed by relaxation to the lowest singlet state **II**. This step competes with the deactivation by fluorescence and nonradiative processes. However, the rate constants of these processes are low, leading to a long lifetime of the excited state. Heterolytic ester cleavage leads to the formation of the singlet ion pair **III**, which can recombine to form the starting material. Again, due to the high stability of the coumarinylmethyl cation and the anionic product the ion formation successfully competes with the deactivation pathway. Following, the ion pair escapes from its solvent cage, leading to the solvent separated ions displayed in **IV**. A crucial part of the photolysis pathway is the reaction of the cation with water yielding the CM alcohol (**V**). Since the presence of water is not only tolerated, but necessary for the uncaging, this makes CM derivatives ideal candidates for biological applications. Decarboxylation of the carbamate yields the free amine and CM-OH (**VI**).[151,189,190]

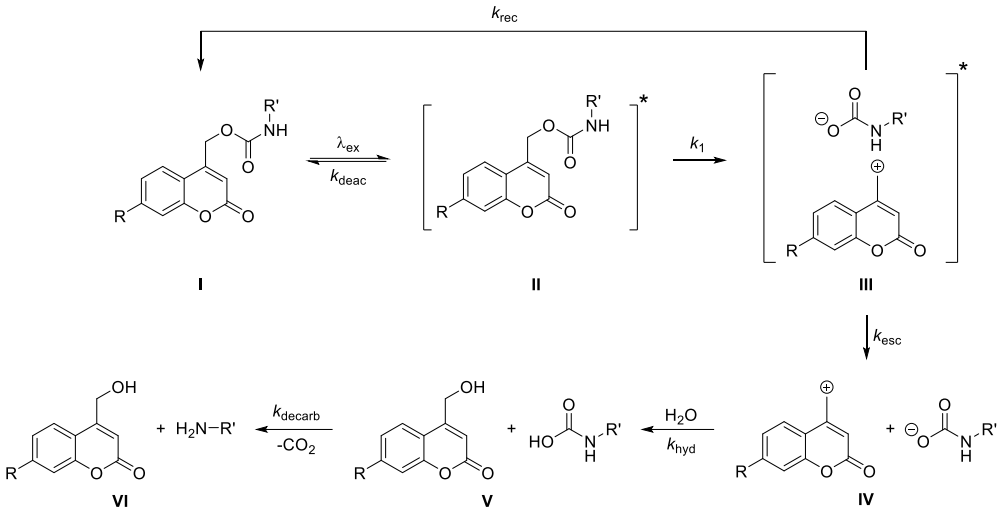

Figure 46: Photolytic cleavage pathway of a DEACM caged amine. Figure based on [151].

Following the design strategy presented by Seyfried *et al.*,[152] a DEACM-derived photolinker suitable for CuAAC derivatization was devised (see Figure 47). Briefly, aldehyde **31** was generated in a Riley oxidation in moderate yield, starting from commercially available 7-diethylamino-4-methylcoumarin (**30**). The alkyne functionality necessary for attachment of the PNA template was introduced in a zinc mediated Barbier reaction with propargyl bromide to give **32**. Activation of the alcohol moiety with DSC yielded PCL **33** in acceptable yield, ready for direct peptide conjugation.

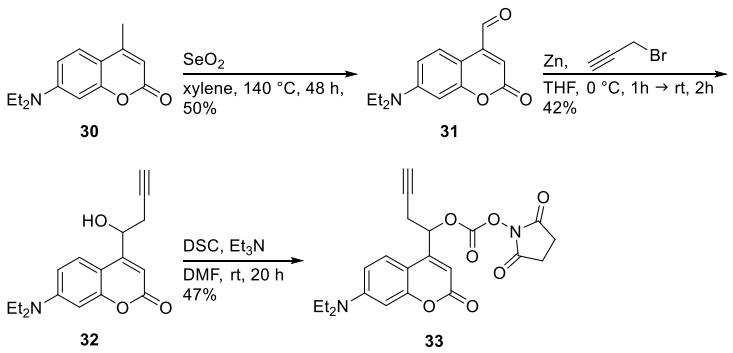

Figure 47: Synthesis of the novel DEACM-derived photocleavable linker **33**.

In order to test the effectiveness of PCL photolysis, DEACM-derived **33** and DMNB-derived PCL **15** were attached to a test peptide and conjugated to a small organic molecule as cargo *via* CuAAC (see Figure 48).

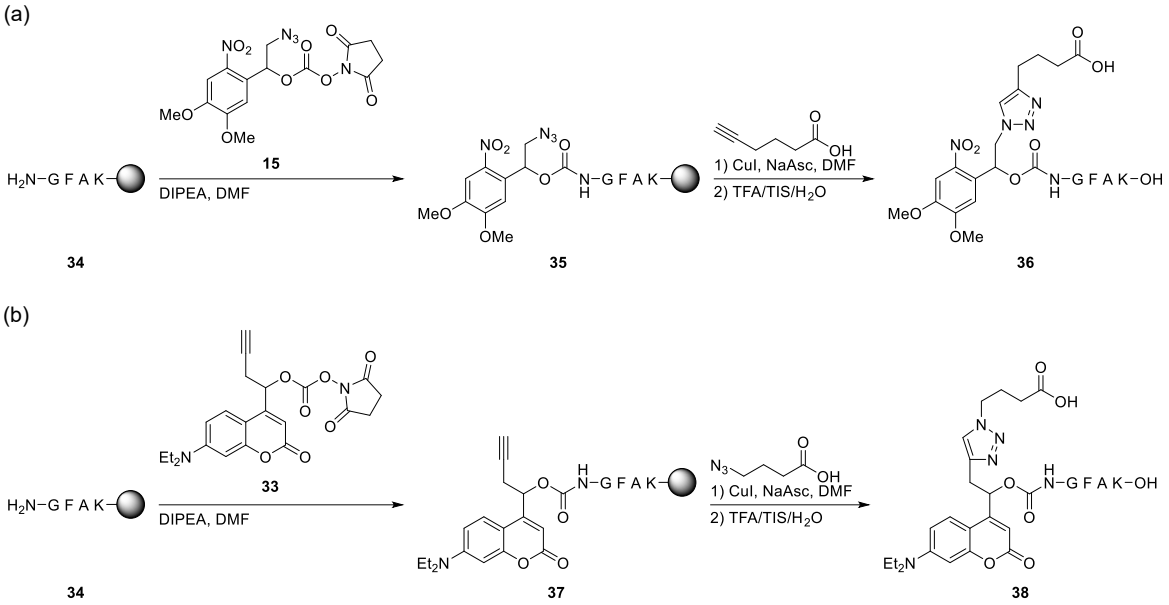

Figure 48: Test peptides bearing (a) DMNB and (b) DEACM derived PCLs, loaded with test cargo.

Then, solutions of both derivatives were prepared for irradiation and the process followed by UHPLC. While the times necessary to reach full deprotection are somewhat comparable, the employed conditions for DMNB and DEACM differ significantly (see Figure 49). **36** was irradiated at 347 nm (1000 W) for 10 min, while **38** was irradiated at 405 nm (100 mW) for 5 min. The photodeprotection assay proved **38** to be a successful PCL that fulfils the intended properties of a higher absorption maximum, combined with a faster release of the cargo. Since the geometries of the linker molecules differs in the steric bulk provided by the DEACM moiety, as well as by attachment of the cargo to the linker (1,4-regioisomerism), **15** was first evaluated as a linker for the templated Suzuki coupling and upon success would be compared to **38**.

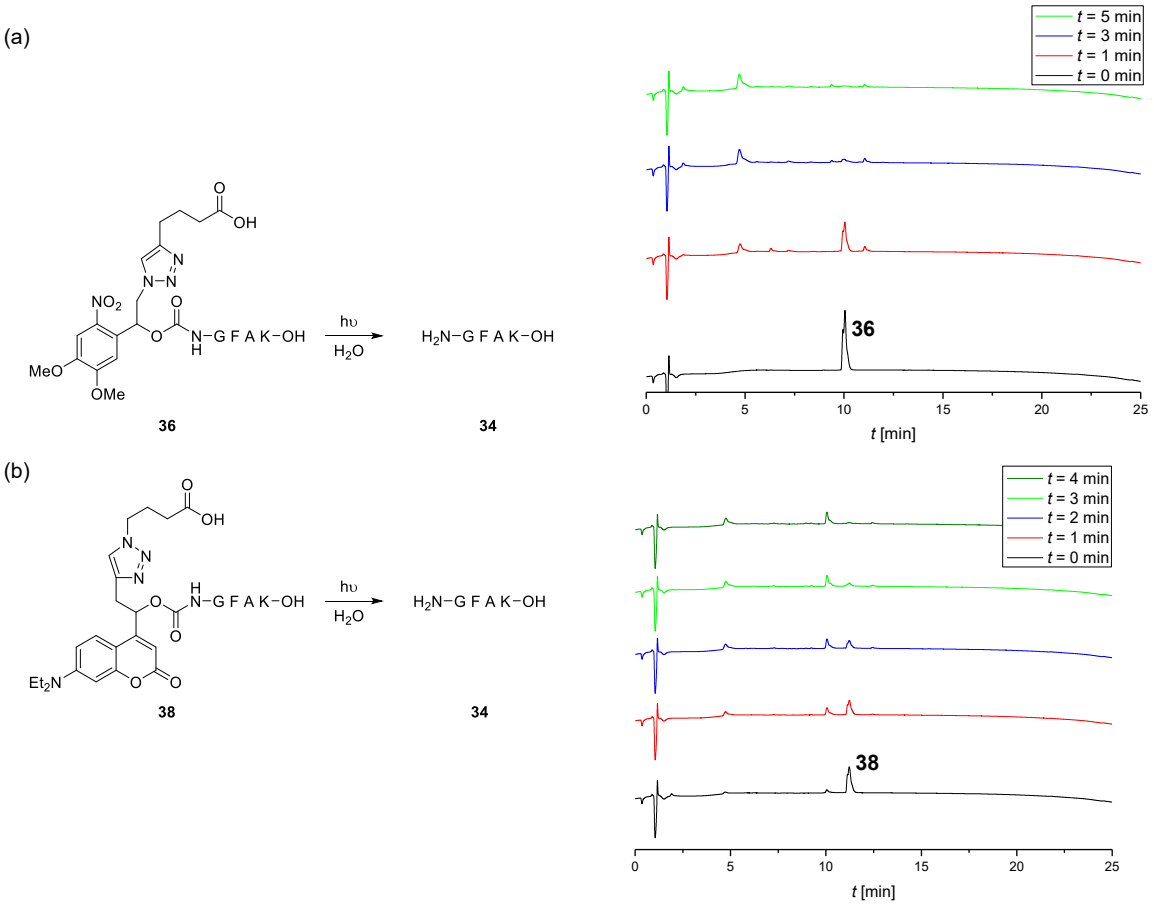

Figure 49: Photolysis of (a) **36** and (b) **38** and their respective UHPLC chromatograms (215 nm). A 50 µM solution of the respective compound was irradiated at 347 nm (1000 W) for 10 min (**36**) or at 405 nm (100 mW) for 5 min (**38**).

4.2.3 Synthesis of PNA/peptide hybrids for templated Suzuki coupling

Having established the ligation conditions and photophysical properties of the PCL, conjugation of PCL **15** to the iodinated peptide **39** followed the procedure described in the previous section (see Figure 50a). For the synthesis of the borylated peptide and attachment of the PCL, a slight adjustment was necessary. Since a glycine residue had to be introduced as a spacer between linker and ligation site, a different protecting group strategy had to be utilized. A protecting group on the *N*-terminus was found to be crucial for product formation during on-resin Miyaura borylation and since the Fmoc protecting group does not tolerate the combination of basic conditions and elevated temperatures of the Miyaura borylation, an alternative had to be identified. The Boc protecting group employed in the original method was unusable, since its deprotection conditions are the same as for the removal of the side chain protecting groups and cleavage of the peptide from the solid support. In order to selectively install the PCL, trityl (Trt) was therefore utilized

as the *N*-terminal protecting group. Selective removal of the highly acid labile group was achieved by treatment of the resin with 0.2% TFA in DCM, which did not affect the side chain protecting groups or the linkage to the resin. This strategy yielded the borylated peptide **42**, to which **15** could be attached following the established pathway (see Figure 50b).

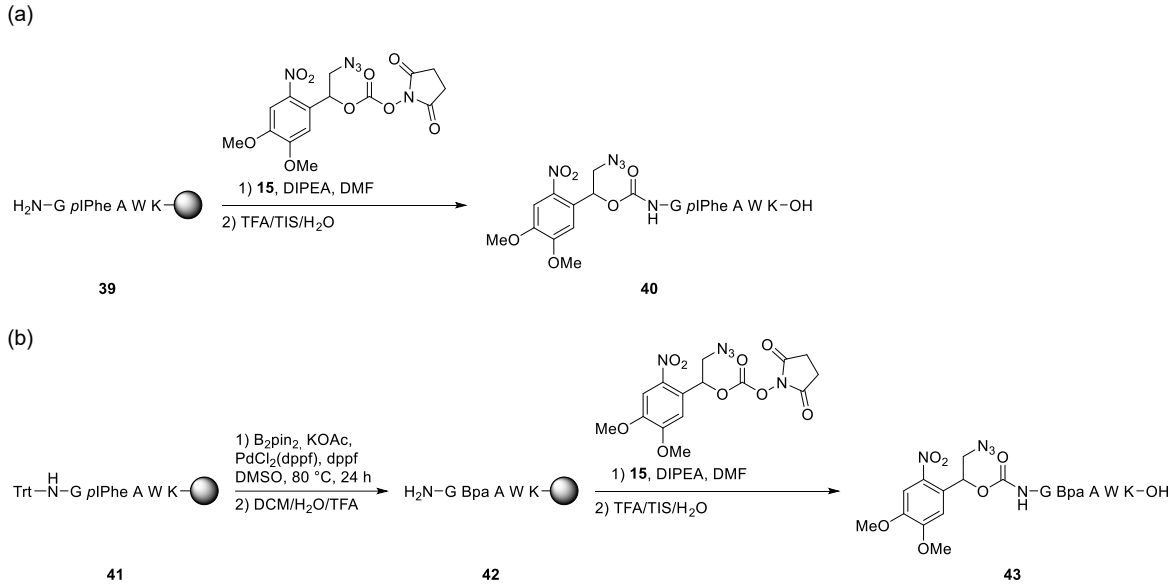

Figure 50: Attachment of PCL to (a) the iodinated and (b) to the borylated peptide.

With the PCL attached to the peptide fragments, hybridization to the alkynylated PNA sequences was performed by on-resin CuAAC (see Figure 51). However, contrary to the reactions described in chapter 4.1 (see Figure 38), no product formation could be observed by UHPLC or mass spectrometry. Instead, a complex reaction mixture was observed in the chromatograms that corresponded to neither starting material or product. Due to the only significant change in peptide sequence being the addition of iodinated and borylated amino acids, it seems likely that they interfered with the copper catalyst.

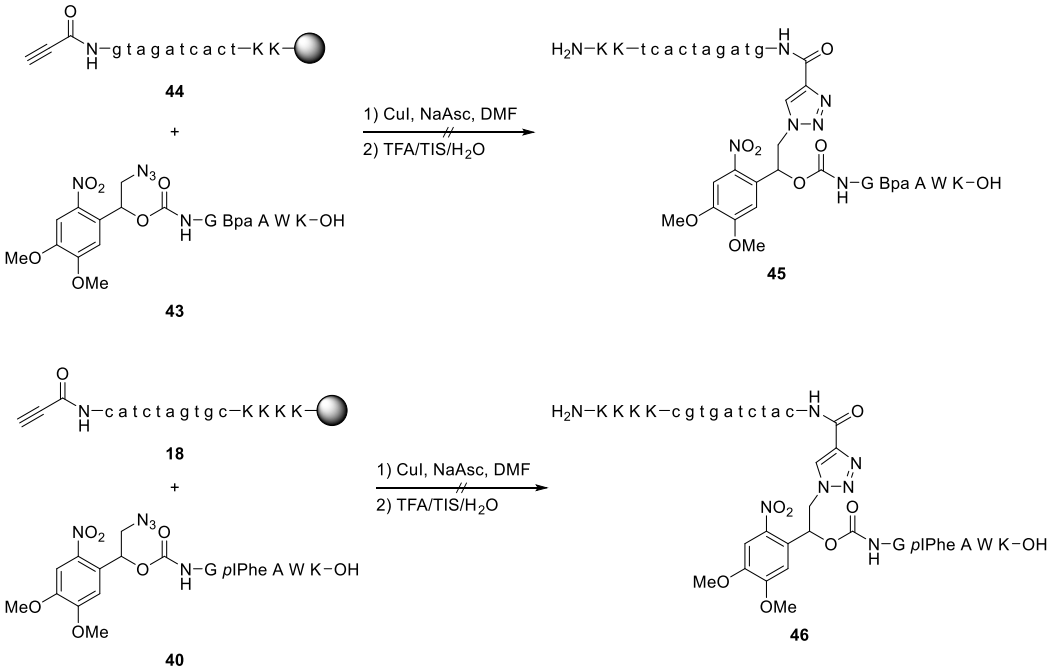

Figure 51: Generation of the PNA/peptide hydrids necessary for templated Suzuki ligation.

With the previously established pathway not being viable for the generation of PNA/peptide hybrids for templated Suzuki coupling, a new approach to acquire the ligation partners had to be identified. Since one of the drawbacks of the previous approach was the additional synthetic effort and purification step necessary in order to attach the PCL bearing peptide, a strategy for the linear build up of the hybrids was devised. An amino acid derived PCL was necessary for this undertaking and commercially available Fmoc-D-β-Phe(2-NO_2)-OH was deemed suitable. While not ideal as a photolinker due to the disadvantages previously described for *o*-nitrobenzyl derived compounds, it could be employed in a proof of concept reaction. Therefore, iodinated PNA/peptide hybrids **47** and **49** were synthesized in one continuous SPPS cycle. On-resin Miyaura borylation of **47** proved unsuccessful, with only trace amounts of the product species identifiable by mass spectrometry (see Figure 52).

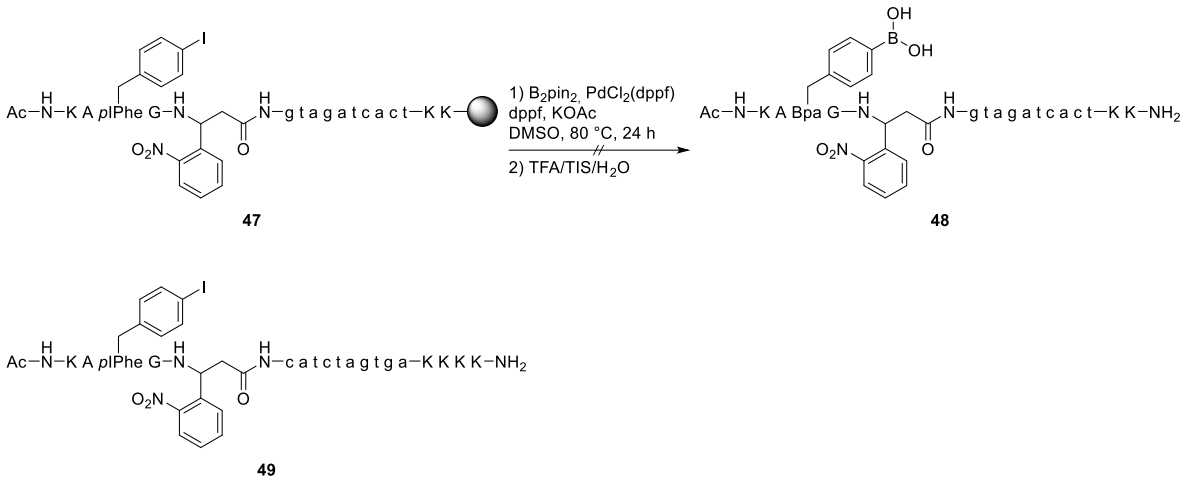

Figure 52: Linear synthesis of iodinated PNA/peptide hybrids and on-resin Miyaura borylation of **47**.

An alternative pathway for the introduction of the boronic acid had to be found. Direct synthesis of SPPS building block Fmoc-Bpa-OH was the obvious approach (see Figure 53). Following procedures by Malan[191] and Raines,[192] Boc-4-iodophenylalanine (**50**) underwent Miyaura borylation to give Boc-4-pinacolborane-phenylalanine (**51**) in good yield. *N*-terminal deprotection with HCl yielded the free amine (**52**) in quantitative yield, followed by Fmoc protection with Fmoc-OSu under basic conditions to yield the desired building block **53**. Although product formation was observed, purification proved to be difficult, since the crude mixture began to oligomerize. A small sample was purified by HPLC, which probably led to the hydrolysis of the pinacol ester protecting group. **53** was directly applicable for SPPS and employed using standard coupling procedures at 50 °C. This resulted in the direct synthesis of **48**.

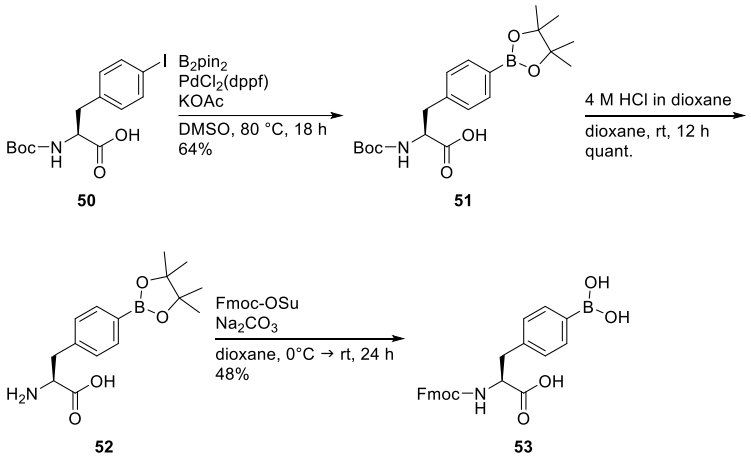

Figure 53: Synthesis of Fmoc-Bpa-OH (**53**).

4.2.4 PNA mediated Suzuki cross-coupling

Having obtained both PNA/peptide hybrids necessary to perform template mediated Suzuki cross-coupling, the ligation was carried out in pH 8 phosphate buffer and its progress monitored by UHPLC. However, no conversion of the starting materials was observed after 48 h, even after increasing the amount of catalyst to up to 10 eq. over time (see Figure 54).

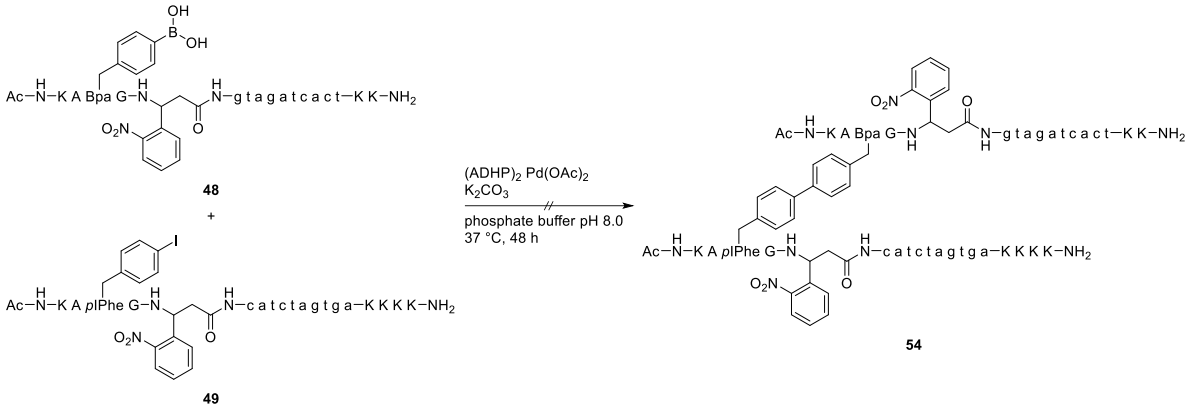

Figure 54: Templated Suzuki cross-coupling of PNA/peptide hybrids **48** and **49**.

Various explanations can be used to describe the absent reactivity of the hybrids. Improper horizontal positioning of the residues along the peptide sequence or incorrect vertical spacing may have led to a loss of reactivity. Furthermore, following the observations from the initial ligation test, more complex environments led to slower reaction rates. Should the templating effect be lacking to contribute, the reaction rate may have been to slow to observe. In addition, interference of the template with the catalyst is possible, either due to preorganization of the reactive moieties into an unsuitable geometry or by interaction of the palladium catalyst with the nucleobases.

First, screening of different palladium complexes was performed to identify the most efficient catalyst. In a study on the Suzuki cross-coupling of halogenated phenylalanines and tryptophans, Willemse *et al*. had identified $PdCl_2$(dppf) as a viable alternative to the Pd-pyrimidine catalyst $(ADHP)_2 \cdot Pd(OAc)_2$. However, temperatures of 80 °C and 50% *i*PrOH as a cosolvent were applied, both of which exceeds biocompatibility.[193] Davis and co-workers furthermore disclosed that water-soluble palladium complexes with guanidine ligands may surpass the catalytic efficiency of the respective pyrimidine system, depending on the substrates.[194] Furthermore, they described a ligandless system based on K_2PdCl_4.[103] In addition, a catalyst described by Ma *et al*.,[105] based on an *N*-heterocyclic carbene (NHC) ligand was tested because of its presumed higher complex stability. To replicate these conditions as best as possible under unifying aqueous conditions at 37 °C,

screening on Boc-*p*IPhe-OH as a model substrate in the cross-coupling reaction with phenylboronic acid was performed (see Table 2).

Table 2: Screening of Boc-*p*IPhe-OH as a substrate in a cross-coupling reaction with phenylboronic acid.

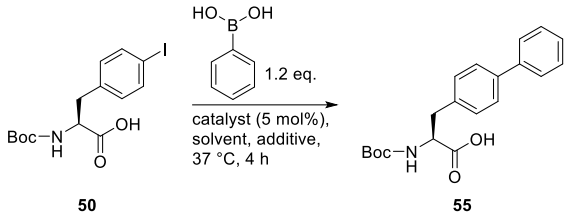

50 **55**

Entry	Catalyst	Solvent	Additive	Conversion[c]
1	$Pd(OAc)_2$	phosphate buffer pH 8	-	97%
2	$(ADHP)_2{\cdot}Pd(OAc)_2$	phosphate buffer pH 8	-	97%
3	$Pd(dppf)Cl_2$	phosphate buffer pH 8	10% *i*PrOH	30%
4	$(TMG)_2{\cdot}Pd(OAc)_2$	phosphate buffer pH 8	-	97%
5	$(NHC)_2{\cdot}Pd(OAc)_2$	phosphate buffer pH 8	-	95%
6	$Pd(OAc)_2$	phosphate buffer pH 8	Ac-PNA 2[a]	0%
7	$(ADHP)_2{\cdot}Pd(OAc)_2$	phosphate buffer pH 8	Ac-PNA 2[a]	0%
8	$(NHC)_2{\cdot}Pd(OAc)_2$	phosphate buffer pH 8	Ac-PNA 2[a]	0%
9	$(ADHP)_2{\cdot}Pd(OAc)_2$ (1.0 eq.)	H_2O	K_2CO_3, Ac-PNA 2[b]	3% - 96% (26.5 h)

[a]: Ac-PNA 2 (6 mol%), [b]: K_2CO_3 (5.0 eq), Ac-PNA 2 (1 mol%), [c]: determined by UHPLC peak integration (215 nm, uncorrected).

The ligandless catalyst $Pd(OAc)_2$ (see Table 2, entry 1), as well as the water-soluble catalysts based on pyrimidine (entry 2), guanidine (entry 4) and NHC ligands (entry 5) performed exceptionally well with conversions of ≥ 95%. A more detailed look at the UHPLC reaction monitoring performed at 0.5, 1, 2, 3 and 4 hours however revealed that while the end results were similar, $(ADHP)_2{\cdot}Pd(OAc)_2$ had distinctly slower initial kinetics, only reaching 11% conversion after 0.5 h and 39% after 1 h. The ligandless system had already reached 94% conversion after 0.5 h, while the guanidine and NHC based systems had a more gradual rise (68% and 74% conversion after 0.5 h, respectively). Unsurprisingly, ferrocene-based catalyst $Pd(dppf)Cl_2$ (entry 3) did not offer sufficient conversion, most likely due to the low amount of organic solvent and low temperature. To ascertain whether the presence of PNA would influence the reaction, 6 mol% of acetylated PNA 2 was added to the substrates. As the most efficient catalyst in the screening, $Pd(OAc)_2$ was selected, in addition to $(ADHP)_2{\cdot}Pd(OAc)_2$ as the standard and $(NHC)_2{\cdot}Pd(OAc)_2$ due to its complex stability. In all cases (entries 6-8), no conversion was observed after 4 h and the same held

true after increasing the reaction time to 20 h. When the same experiment was performed with an excess of Pd-catalyst, slow conversion was observed (entry 9). After 4 h, 3% product formation was observed that rose to 19% after 8 h. 97% conversion was observed after 26.5 h, clearly indicating that the presence of PNA severely dampens the catalyst's efficiency.

To gain further insight into this issue, UV-Vis measurements were performed. Two modes of interaction of the catalyst with PNA seem feasible. First, direct binding of the metal to the nucleobases through the *N*-7 position of the purine bases or the *N*-3 position of the pyrimidine bases. This mechanism is believed to be the predominant target of metal-based anticancer complexes. While other modes of binding to the nucleobases have been observed, the *N*-7 position of guanine seems to be the most likely target.[195] Eichhorn *et al*. investigated the influence of metal ions Mg(II), Co (II), Ni(II), Mn(II), Zn(II), Cd(II) and Cu(II) on DNA structure and stability. They found that the melting temperature increased with higher concentration of Mg(II), Co(II) and Ni(II), owing to the sole (Mg(II)) or predominant binding to the phosphates. Whereas the increase in Cd(II) or Cu(II) concentration over 0.5 eq. resulted in a decrease in melting temperature, associated with binding to the nucleobases. The authors argued that the latter metals held the bases of unwound DNA in register and continued to do so upon cooling, thereby preventing rewinding of the duplex. Metal ions in the middle of the series showed the highest T_m at intermediate metal concentrations, where the stabilization of the charged backbone outweighed the destabilization due to binding to the nucleobases.[196] Since PNA possesses a neutral backbone, either no effect or a destabilizing effect would be expected.

Second, intercalative binding of aromatic heterocycles through π-stacking is possible. While usually observed in fused aromatic systems, the employed pyrimidine based ligand ADHP partly fulfills the criteria. This mode of interaction usually results in hypochromism and a bathochromic shift in the observed band.[197]

Two experiments were performed to differentiate between both scenarios. Melting curve measurements on the duplex PNA 1·PNA 2 (for the sequences, see Table 1) were performed in the presence (0.05 or 2.5 eq.) or absence of $(ADHP)_2 \cdot Pd(OAc)_2$ (see, Figure 55a). While the melting curve corresponding to the addition of 0.05 eq Pd(II) was almost identical to the native one, a strong deviation was observed at the higher metal ion concentration. The corresponding melting curve showed a decreased hyperchromic effect and significantly lower melting temperature. Based on the previously discussed study by Eichhorn *et al*., [196] this seems to be indicative of metal ions binding to the nucleobases at higher concentrations.

Furthermore, a titration experiment with increasing Pd(II) amounts was performed on the same double stranded PNA while monitoring the nucleobase absorbance (see Figure 55b).

While a general trend could not be established, an interaction of catalyst and PNA seems to be evident, nonetheless.

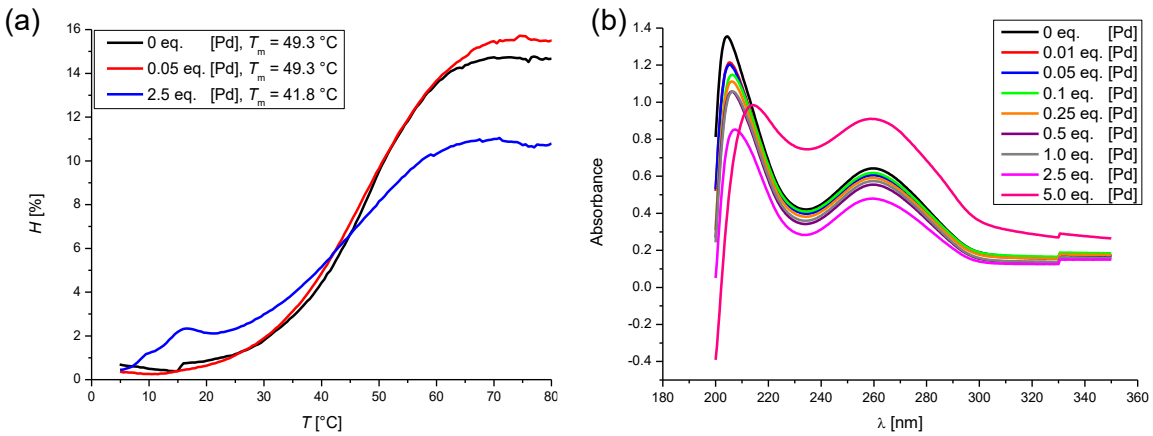

Figure 55: (a) UV-Vis melting curve measurements of acetylated parallel PNA (PNA 1+2) upon addition of Pd(II). (b) Absorbance measurements under titration of various amounts Pd(II) (b). Measurements were carried out with a strand concentration of 5 µM in phosphate buffer (50 mM, pH 8.0).

While not all of the previously discussed factors of the templated Suzuki cross-coupling can be dismissed, it seems likely that interaction of the PNA nucleobases with the palladium catalyst contribute most to the failed attempt. Based on the UV-Vis studies, binding of the catalyst to the nucleobases seems likely. Though the amount utilized in the ligation experiments proved insufficient to destabilize the duplex structure, binding of the palladium ions would still render the catalyst useless. Simply increasing the amount of catalyst could lead to a slow conversion, albeit at a loss of the templating effect due to unwinding of the helix. For a precise assertion of the positions and distances of the reactive sites, as well as the binding of the catalyst, X-ray crystallography could be performed, while NMR spectroscopy would provide an additional method to determine if palladium binds to the PNA nucleobases.

4.2.5 Conclusion

In this section, the ability of a PNA template to mediate a biocompatible Suzuki cross-coupling reaction was assessed. The catalytic system was based on Davis' water-soluble Pd-pyrimidine catalyst. Its efficiency was demonstrated in the modification of an iodinated small test peptide with phenylboronic acid or its borylated counterpart. Impressively, the reaction was performed without reagent excess and the catalyst was employed in a small percentage. However, an increase in the steric demand of the reactants was shown to slow the reaction considerably, possibly due to difficult accessibility of the functional groups by the palladium catalyst.

Installation of the PNA template proved to be challenging, since the functional groups of the peptides interfered with the CuAAC used for conjugation. This problem was overcome by utilizing an amino acid derived PCL and linear incorporation of iodo-phenylalanine and a newly synthesized borono-phenylalanine building block (**53**). The obtained PNA/peptide hybrids **48** and **49** were employed in a cross-coupling experiment. Presence of the template showed clear inhibition of the reaction. A catalyst screening in the presence of PNA, as well as UV-Vis titration and melting curve measurements with various amounts of Pd(II) suggest binding of the metal ions to the template's nucleobases.

Furthermore, a novel DEACM-based PCL (**33**) was synthesized and directly compared to the previously employed DMNB linker (**15**). Linkers were applied to a test setting and their photolysis was studied. The DEACM-based PCL proved to cleave marginally faster and under less harsh conditions. However, the attachment of both linkers *via* CuAAC and incompatibility with iodo- or borono-moieties prevented further studies with the PNA template. Its success does however provide a second-generation PCL as well as a starting point for the development of an amino acid-based linker with improved photophysical properties.

Since PNA proved to be an unsuitable template for the mediation of a Suzuki cross-coupling reaction, a different template architecture will be investigated in the next chapter.

4.3 Evaluation of coiled-coil peptides as a platform for templated reactions

This chapter examines the use of coiled-coil peptides as reaction templates for biocompatible ligations. The strategy is based on a previously reported template mediated acyl transfer system.[134] A parallel heterodimeric coiled-coil dimer is used as a recognition unit to align *N*-terminal functional groups for covalent linkage. Herein, a variety of ligation methods are studied. The subchapters are categorized by reaction type. Chapter 4.3.1 illustrates the design of the system and investigates the Suzuki cross-coupling reaction. Oxime ligation (chapter 4.3.2), cysteine alkylation (chapter 4.3.3) and SPAAC (chapter 4.3.4) are discussed in the following sections. Finally, a photocleavable linker is used to perform a templated functional group transfer with partial scaffold release *via* oxime ligation (chapter 4.3.5).

4.3.1 Coiled-coil templated Suzuki cross-coupling

Because the experiments described in the previous chapter revealed a possible interaction of the palladium catalyst with the nucleobases of the PNA template and a reaction between the cross-coupling partners was not observed, a different reaction template had to be investigated. The coiled-coil motif was selected, since its rules for structure, oligomerization state and partner specificity are among the most well-understood for protein folding motifs.[132,198,199] In addition, the system provides easy access *via* SPPS at a lower time and monetary cost. Furthermore, despite offering limited modularity in its sequence, the design of orthogonal pairs based on hydrophobic and electrostatic mismatches is possible.[200–202] Thus, coiled coils offer the potential to mediate multiple simultaneous ligation events. The aim of this project is to design a platform to mediate functional group transfer from a donor to an acceptor strand, similar to the system proposed by Reinhardt *et al*.[134] In order to circumvent the restriction of using NCL to lead to cleavage of the donor strand, a photocleavable linker will be installed. This opens up the possibility of using faster, more selective ligation reactions in line with the previously established principles of bioorthogonality. Ideally, this system could be used to study the influence of the template on reaction kinetics, as well as to establish parameters for the distance between functional group and template at which preorganization is replaced by diffusion. Hodges' parallel, heterodimeric IAAL E3/K3 coiled-coil[133] was selected as a starting template to re-evaluate the templated Suzuki cross-coupling. The original sequence was altered to include

tryptophan as a UV chromophore for concentration determination and reaction monitoring and the *C*-terminus was capped with glycine (see Table 3).

Table 3: Sequence and heptad register of the coiled-coil strands based on Hodges' E/K peptides. Peptides were synthesized as *C*-terminal amides.

		Sequence and heptad register			
Entry	Name	gabcdef	gabcdef	gabcdef	*C*-term.
1	CC-E3 (**56**)	EIAALEK	EIAALEK	EIAALEW	G
2	CC-K3 (**57**)	KIAALKE	KIAALKE	KIAALKW	G

Phenylboronic acid and *p*-iodophenylalanine were introduced as ligation partners to the E3 and K3 strand, respectively. Conditions for the aqueous Suzuki coupling of peptides, previously established in chapter 4.2, were applied (see Figure 56). However, no product formation was observed after 24 h.

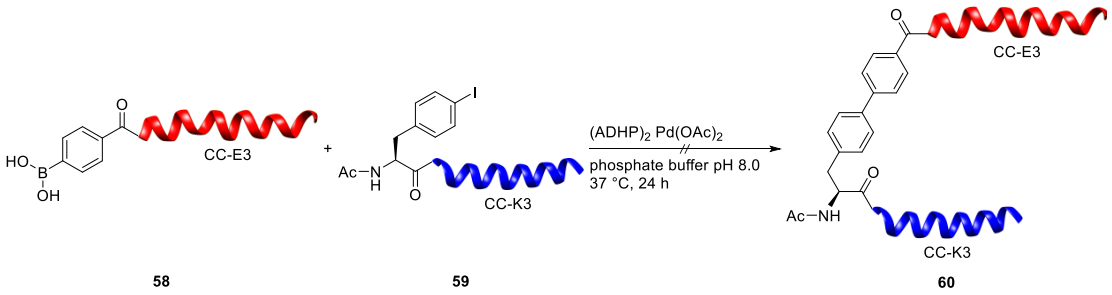

Figure 56: Suzuki coupling between modified coiled-coil strands.

In order to exclude interference from the catalyst with the template formation, circular dichroism (CD) spectroscopy was performed. CD spectroscopy is an established technique for determining the structure of proteins in solution and has been commonly used to analyze coiled-coil interactions. Briefly, left-handed and right-handed circularly polarized light will be absorbed to different extents by asymmetric molecules, resulting in an elliptic polarization after passing through the sample. The ellipticity can be measured as the CD signal. A change in polarization will occur for a chromophore that is chiral, covalently bond to a chiral center or placed within an asymmetric environment of a three-dimensional structure. Different structural elements in proteins produce distinct CD spectra that can be used to characterize their secondary structure.[203,204] At pH 7 the IAAL E3/K3 coiled-coil exhibits the characteristics of an α-helix, with nearly equally intensive minima at 208 and 222 nm and a maximum at 193 nm. However, under the same conditions, the individual strands show spectra of random coils with a minimum around 200 nm.[204–206] A shift in these parameters is indicative of a structural change. Apostolovic *et al*. discovered that the

aforementioned E3/K3 coiled-coil becomes unstable at pH 5, resulting in its unfolding and the formation of E3 homotrimers that coexist with K3 unimers and a small amount of K3 homodimers.[206] Similar observations were made by Yang *et al*. when investigating the antiparallel heterodimer formed by oppositely charged CCE and CCK peptides. When the pK_a value of the charged side chain (Glu or Lys) was reached, the heterodimer unfolded and homodimers of one strand formed that coexisted with unimers of the other strand. Unfolding was already observed at a pH value as low as 9.[207] Thus, the stability of the employed E3/K3 coiled-coil was probed for acetylated species of **56** and **57** at pH 7 (see Figure 57a) and under catalytic conditions (see Figure 57b). However, both experiments were found to comply to coiled-coil parameters. Therefore, it can be concluded that the reaction did not falter due to unfolding of the template.

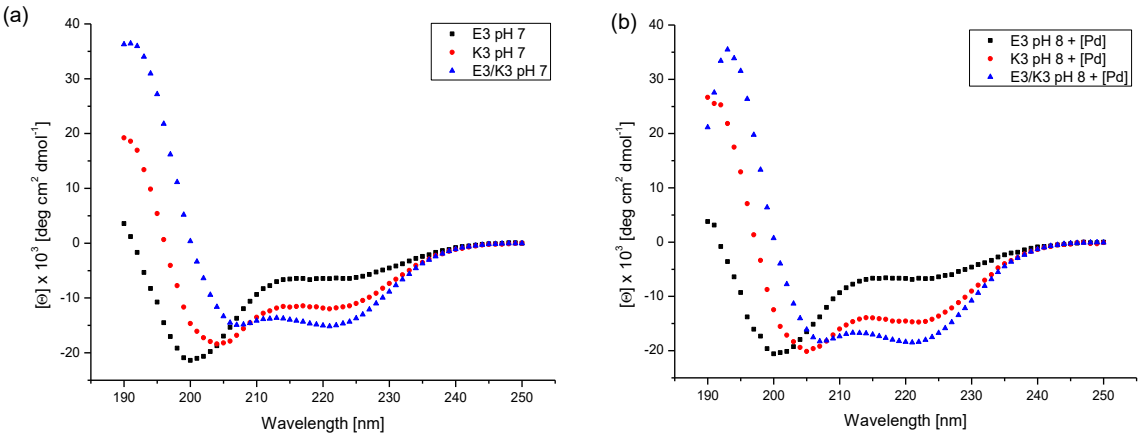

Figure 57: CD Spectra of acetylated peptides E3 (black), K3 (red), and their equimolar mixture (blue) in (a) pH 7 phosphate buffer and (b) pH 8 phosphate buffer upon addition of 1 µL 0.01 M $(ADHP)_2{\cdot}Pd(OAc)_2$ solution.

Instead, a focus was placed on increasing the distance between the functional groups and the template, thereby offering less steric constraint and easier access for the catalyst. Accordingly, peptides **56** and **57** were elongated with a glycine spacer and different variants of the K3 peptide were synthesized, containing an additional glycine (**63**), β-alanine (**64**) or γ-aminobutyric acid residue (**65**). The resulting four K3 peptides were modified with *p*-iodobenzoic acid and combined with phenylboronic acid modified peptide **61** under cross-coupling conditions. No reaction was observed for any of the derivatives (see Figure 58).

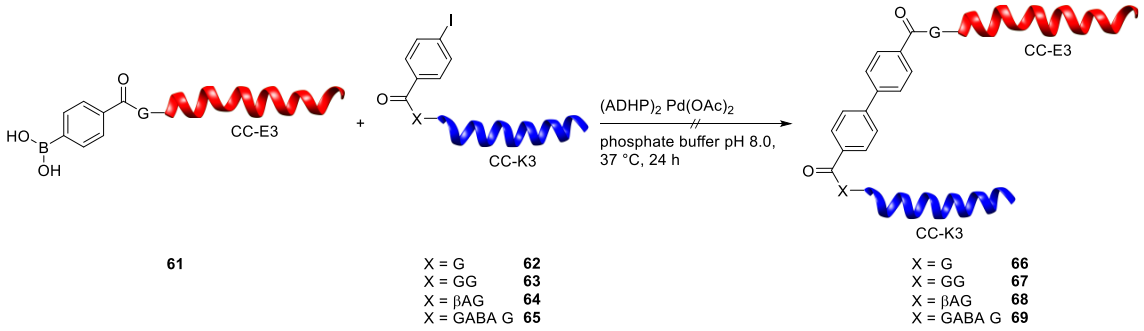

61

X = G **62**
X = GG **63**
X = βAG **64**
X = GABA G **65**

X = G **66**
X = GG **67**
X = βAG **68**
X = GABA G **69**

Figure 58: Coiled-coil templated Suzuki coupling utilizing different amino acid spacers on the K3 peptide.

Next, changes in the template structure were investigated. Thomas *et al*. reported a version of the E3/K3 coiled-coil that includes asparagine at position *a* of the central heptad. While this change was found to overall destabilize the hydrophobic core, it also showed an improved specificity for dimer formation, presumably due to formation of a hydrogen bond between asparagine residues. Said change was also found to prevent slippage of the helices relative to each other because of a greater destabilization from unpaired asparagine residues. Therefore, the authors theorized that upon dimer formation, the peptides should be brought together in register. Furthermore, glutamine, lysine, and one of the chromophores tyrosine or tryptophan were introduced at the *f* positions and the sequences were capped by glycine residues. In addition, the authors found that elongating one or both helices by an additional half or full heptad further stabilized the helix.[208] Implication of these modifications were thought to be beneficial for templated ligation. First, introduction of arginine would ensure the alignment of the functional groups. Secondly, the higher K_D value would result in a greater flexibility of the template, which might negate sterically constrained reaction geometries to some extent. These changes were applied to peptides **70** and **71**. Furthermore, the crystal structure of IAAL E3/K3 (PDB ID: 1U0I) shows the *N*-termini of both peptides averted from one another. To prevent this from interfering in a successful reaction, peptide K3 was elongated by up to half a heptad to find a suitable geometry. The heptad register of the new sequences is shown in Table 4. Figure 59 shows the helical-wheel diagram of the coiled-coil heptad repeat and a one-heptad slice through the X-ray crystal structure of the asparagine containing heptad of GCN4 leucine zipper.

Table 4: Sequence and heptad register of the asparagine containing coiled coils and *N*-terminal elongation of the K-strand by one to three residues. Peptides were synthesized as *C*-terminal amides.

		Sequence and heptad register				
Entry	Name	gabcdef	gabcdef	gabcdef	gabcdef	*C*-term.
1	CC-E3$_{N1}$ (**70**)		EIAALEK	ENAALEW	EIAALEQ	GG
2	CC-K3$_{N1}$ (**71**)		KIAALKW	KNAALKK	KIAALKQ	GG
3	CC-K3$_{N1}$+1 (**72**)	Q	KIAALKW	KNAALKK	KIAALKQ	GG
4	CC-K3$_{N1}$+2 (**73**)	KQ	KIAALKW	KNAALKK	KIAALKQ	GG
5	CC-K3$_{N1}$+3 (**74**)	LKQ	KIAALKW	KNAALKK	KIAALKQ	GG

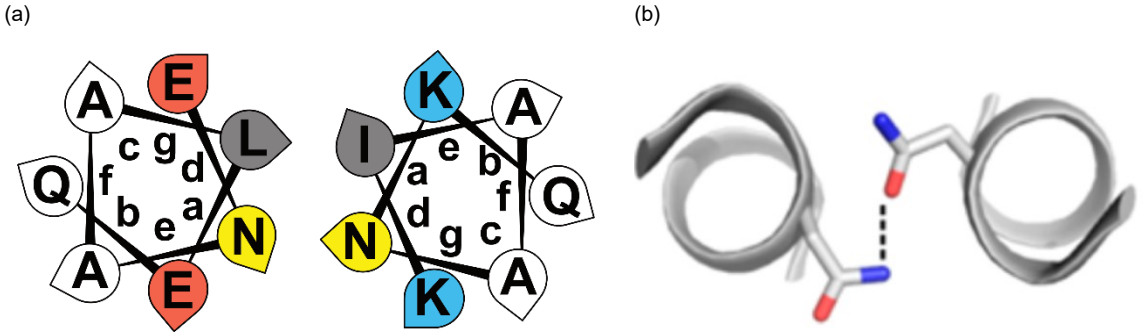

Figure 59: (a) Helical-wheel diagram depicting asparagine (yellow) in the hydrophobic core of a heptad. (b) One-heptad slice through the X-ray crystal structure of the asparagine containing heptad of GCN4 leucine zipper (PDB ID: 2ZTA), showing the hydrogen bond between Asn residues (dotted line). Figure 59a was based on [208] and figure 59b was reprinted with permission from Thomas *et al.*, *J. Am. Chem. Soc.* **2013**, *135*, 5161. Copyright 2013 American Chemical Society.

Asparagine containing E3 (**70**) was modified with phenylboronic acid and combined under ligation conditions with asparagine containing K3 (**71**), elongated by zero to three heptad residues and modified with acetylated *p*-IPhe. No cross-coupling reaction between the peptides was observed after 24 h (see Figure 60).

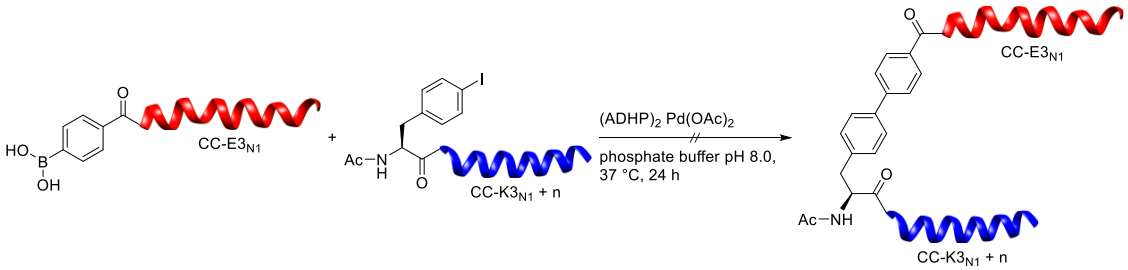

75

n = 0 **76**
n = 1 **77**
n = 2 **78**
n = 3 **79**

n = 0 **80**
n = 1 **81**
n = 2 **82**
n = 3 **83**

Figure 60*:* Coiled-coil templated Suzuki coupling utilizing Asn modified peptides and an *N*-terminal overhang of zero to three amino acid residues.

Following the observations laid out in this chapter and the previous one, the ensuing conclusion can be offered. Through a number of changes in the geometry of the functional groups, as well as in the reaction template, either by introduction of spacers, overhang or by virtue of an altogether different template, template mediated Suzuki coupling was not observed. Possible reasons include (i) steric constraint as a result of the reaction template, (ii) preorganization of the functional groups into unsuitable geometries by dimer formation of the template, (iii) interaction of the catalyst with the template and (iv) low nucleophilicity of the employed boronic acid. While interaction of the catalyst with the template seems to be more prevalent for the nucleobase template, steric constraint, preorganization, and low reactivity of the nucleophile all seem to be valid reasons, possibly pointing to a combination of all factors.

4.3.2 Coiled-coil templated oxime ligation

Due to the complications associated with the Suzuki cross-coupling approach, a different type of ligation reaction had to be identified. Staying within the principles of bioorthogonal reactions, oxime ligation was selected as a suitable candidate due to its simple reaction mechanism and low steric demand of the employed functional groups. While this reaction proceeds slowly under standard reaction conditions without the use of a nucleophilic catalyst,[32] increasing the effective concentration of the reagents by employing a reaction template might increase the reaction rate.

In order to introduce a hydroxylamine functionality to one of the coiled-coil strands, Boc-protected 4-(aminooxy)butanoic acid (**86**) was synthesized according to a procedure by Saito *et al*.[54] Briefly, *N*-Boc hydroxylamine (**84**) and ethyl 4-bromobutyrate (**85**) underwent Williamson ether synthesis, followed by basic hydrolysis of the ethyl ester protecting group. The product was obtained in moderate yield (see Figure 61).

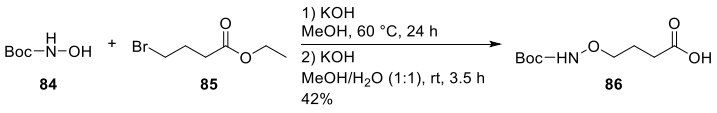

Figure 61: Synthesis of *N*-Boc-protected 4-(aminooxy)butanoic acid.

Insertion of the building block to E3 peptide **70** under standard coupling conditions proved to be successful (see Figure 62).

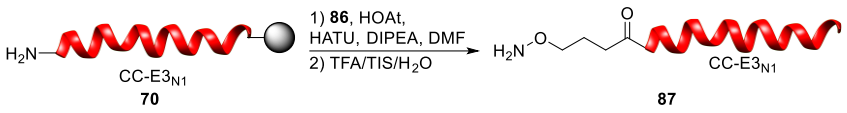

Figure 62: Introduction of a hydroxylamine moiety to the E3 peptide.

For the introduction of an aldehyde moiety, oxidation of *N*-terminal serine with sodium periodate was chosen (see Figure 63 for the general approach).

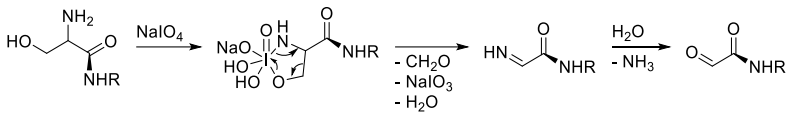

Figure 63: Schematic representation of the oxidation of an *N*-terminal serine with sodium periodate. Figure based on [209].

However, when this approach was applied to serine modified **71**, no product formation was detected. Instead, side products with mass differences of +14 Da, +30 Da, +32 Da and -2 Da were observed in different fractions after HPLC purification. The most apparent explanation would be additional oxidation of peptide side chains. Commonly, oxidation is found in peptides containing methionine, cysteine or tryptophan. While oxidation of tryptophan proceeds slowest, it is the only amino acid on this list to be present in the sequence of **71**. Indeed, a mass difference of +32 Da could be explained by double hydroxylation of the tryptophan residue.[210] Data obtained by HR-MS did not support this theory.

Due to the aforementioned difficulties, a different approach for the introduction of the aldehyde moiety was pursued. Duflocq *et al*. introduced thiazolidine as an aldehyde precursor, which would undergo deprotection under Pd(II) or Ag(I) mediation and acidic conditions.[211] *N*-Boc-protected 2-carboxy thiazolidine was synthesized according to a literature known procedure.[212] Condensation of 2-aminoethane thiol (**88**) with glyoxylic acid (**89**) led to thiazolidine 2-carboxylic acid (**90**) in good yields, followed by Boc protection with di-*tert*-butyl dicarbonate in excellent yields, to give the desired SPPS applicable product (**91**, see Figure 64).

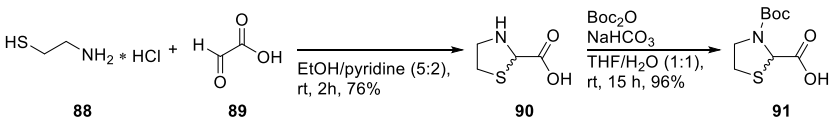

Figure 64: Synthesis of Boc-protected aldehyde precursor 2-carboxy thiazolidine (Thz, **91**).

Introduction of the building block to peptide **71** was successful under standard coupling conditions. However, formation of the aldehyde after treatment with $PdCl_2$ was not observed (see Figure 65).

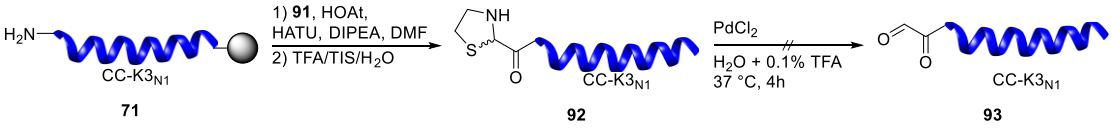

Figure 65: Introduction of an aldehyde moiety by Pd(II) mediated cleavage of a thiazolidine precursor.

Since a chromatogram similar to the oxidation approach was obtained, oxidation of the tryptophan residue seems unlikely. Instead, a different side reaction might be the root problem. A nucleophilic attack of the ε-amino group of a lysine residue would be the next explanation, due to its positioning as the second to last amino acid on the *N*-terminal end. It would furthermore explain the presence of multiple, near inseparable peaks in the HPLC chromatogram due to different resulting stereoisomers.

Based on this assumption, functional groups on the E3 and K3 strand were interchanged. Attachment of the hydroxylamine moiety to K3 and of the thiazolidine precursor to E3 was successful applying standard coupling conditions. Removal of the protecting group was achieved by $PdCl_2$ under acidic conditions. The resulting purified peptides were suspended in phosphate buffer (pH 7.0) and agitated for 7 h at 37 °C. After lyophilization and purification by HPLC, the ligation product was obtained under loss of water (see Figure 66).

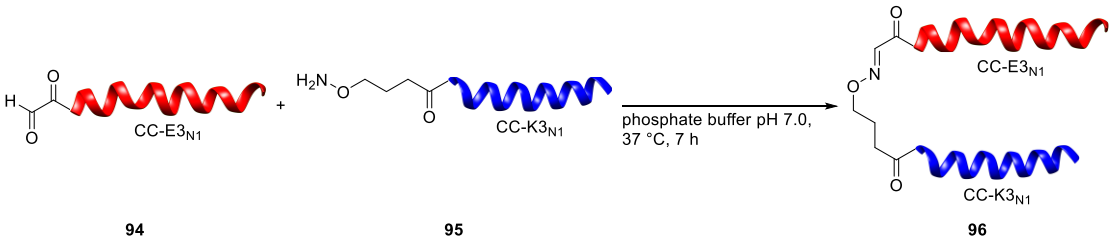

Figure 66: Oxime ligation between aldehyde modified **94** and hydroxylamine bearing **95**.

To obtain more insight into the reaction progress, a new set of coiled-coil peptides was synthesized, equipped with an additional *N*-terminal glycine cap, as well as an optional alloc-protected lysine residue at the *C*-terminus. Due to the additional layer of orthogonality introduced by the alloc protecting group, this residue can be used to introduce a fluorescent label for quantification of the conversion *via* peak integration in the UHPLC chromatogram. Furthermore, a reference peptide was synthesized to serve as comparison for the non-templated reaction (see Table 5).

Table 5: Sequence and heptad register of the arginine containing coiled-coil strands based on [208] and additional sets bearing an attachment point for a fluorophore. Sequence of the reference peptide **101**, based on [213]. Peptides were synthesized as *C*-terminal amides and **99** and **100** were synthesized as Fmoc-protected species for further derivatization.

			Sequence and heptad register			
Entry	Name	*N*-term.	gabcdef	gabcdef	gabcdef	*C*-term.
1	CC-E3$_{N2}$ (**97**)	G	EIAALEK	ENAALEW	EIAALEQ	GG
2	CC-K3$_{N2}$ (**98**)	G	KIAALKY	KNAALKK	KIAALKQ	GG
3	*CC-E3$_{N2}$ (**99**)	G	EIAALEK	ENAALEW	EIAALEQ	GGK(alloc)
4	*CC-K3$_{N2}$ (**100**)	G	KIAALKY	KNAALKK	KIAALKQ	GGK(alloc)
5	**101**	EWAETAAAKFLAAHA				

With these peptides in hand, aldehyde containing peptides **102** and **105** were synthesized, in addition to hydroxylamine modified **100**, to which fluorescein isothiocyanate (FITC) isomer I was attached (**103**). Both aldehydes were combined with the hydroxylamine under oxime ligation conditions (see Figure 67) and their reaction progress was monitored over the course of 20 and 8 h, respectively (see Figure 68a,b). Afterwards, the successfully ligated products were purified by analytical HPLC and **104** was subjected to CD-spectroscopic analysis to verify its α-helical structure (see Figure 68d).

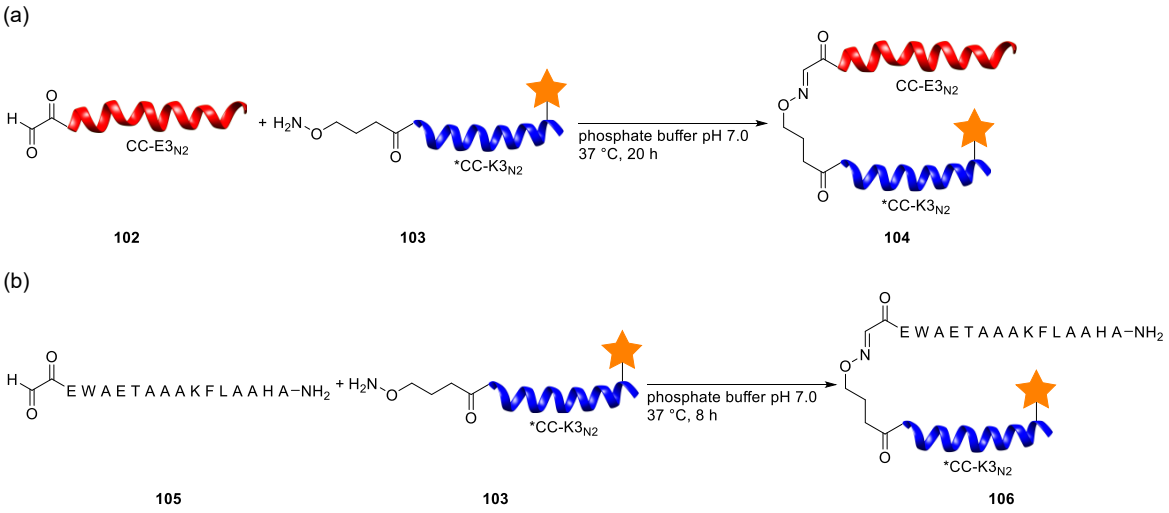

Figure 67: (a) Coiled-coil mediated oxime ligation and (b) non-templated reference. The star represents FITC.

Although product formation and the structural integrity of the coiled-coil were confirmed, reaction monitoring showed several discrepancies. First, the aliquot analyzed after 5 min shows a high conversion (31% for **104**, 70% for **106**) for both reactions. While this reaction behavior might be explained by the template effect, it does not fit the kinetic profile for the non-templated oxime ligation at pH 7.0.[32,54] Secondly, product formation for the templated reaction did not follow a linear pathway. While the intensity of the product peak was strong in the *t* = 5 min chromatogram, it was almost non-existent after *t* = 20 min. This behavior

was accompanied by an increase in the aldehyde signal intensity and almost complete disappearance of the hydroxylamine. Following this point in time, the product signal increased steadily in line with a decrease of the aldehyde signal to reach 61% conversion after 4 h and 71% after 6 h. Two possible explanations come to mind. First, the aldehyde exists in equilibrium with its diol form, being shifted towards the latter.[214] However, this phenomenon is not in agreement with the observed chromatograms. Second, dynamic covalent chemistry between the aldehyde moiety and the ε-amino groups of the K3 strand are plausible. Since this reaction behavior would also be accompanied by consumption of the aldehyde this explanation is also not plausible. In comparison to these observations, the non-templated ligation proceeded in a more linear fashion. Therefore, an unidentified interaction with the coiled-coil template seems likely, it does however not appear to influence formation of the desired product. Owing to these effects, a ligation with a positive templating effect could not be observed. Instead a faster, more steady conversion was observed for the non-templated approach.

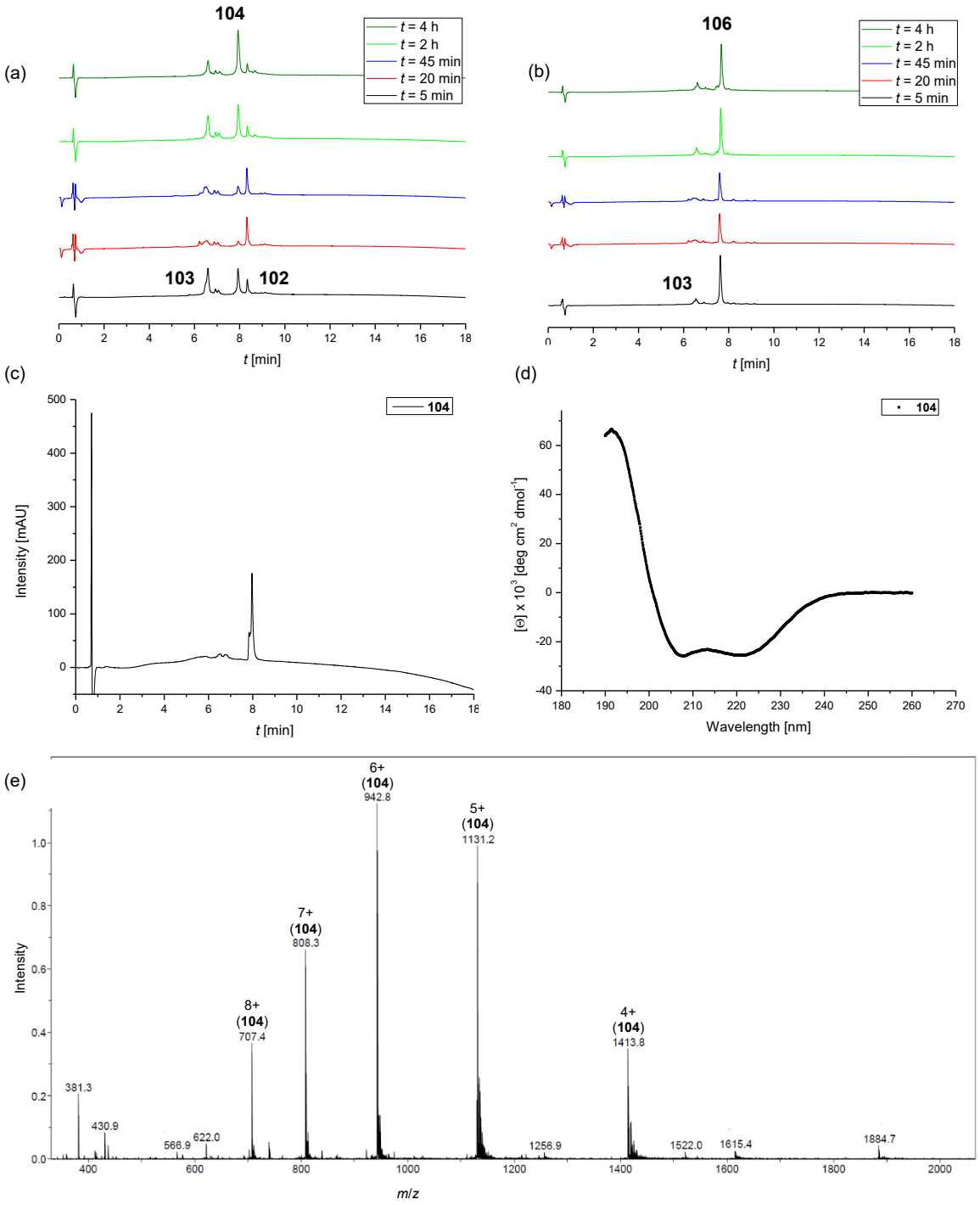

Figure 68: UHPLC reaction monitoring (215 nm) of (a) the coiled-coil mediated oxime ligation (**104**) and (b) of the non-templated reference (**106**). (c) Chromatogram (215 nm) of the purified ligation product **104** and (d) CD spectrum of the purified ligation product **104**. CD spectra were recorded at a concentration of 25 µM in phosphate buffer (50 mM, pH 7.0) at 20 °C. (e) ESI-MS spectrum of purified **104**.

4.3.3 Coiled-coil templated alkylation of cysteine with chloroacetamide

Having established the successful product formation *via* oxime ligation, a reaction with a similar geometry was investigated. The choice fell on the alkylation of an *N*-terminal cysteine residue with chloroacetamide. While this reaction does not conform to the principles of bioorthogonal chemistry, it follows a similar reaction pathway in the form of a nucleophilic substitution. Furthermore, there is no reversibility of the reaction equilibrium and possible side reactions are excluded for the presented experimental setup, since only one cysteine residue is present. In addition, this ligation approach was already demonstrated to be successful in linking coiled-coil strands, albeit with different geometries by placing the reactive moieties in the hydrophobic core[137] or by introduction of a peptidic spacer.[215]

Nonetheless, chloroacetic acid was introduced to E3 strand **97** by standard coupling procedures to yield **107**. Similarly, cysteine was introduced to K3 strand **100**, labeled with FITC and acetylated at the *N*-terminus. Chloroacetic acid was also attached to the reference peptide **101** to yield **110**. Both chloroacetamide bearing peptides were combined with the cysteine containing peptide in a reducing buffer for 6 h (see Figure 69.)

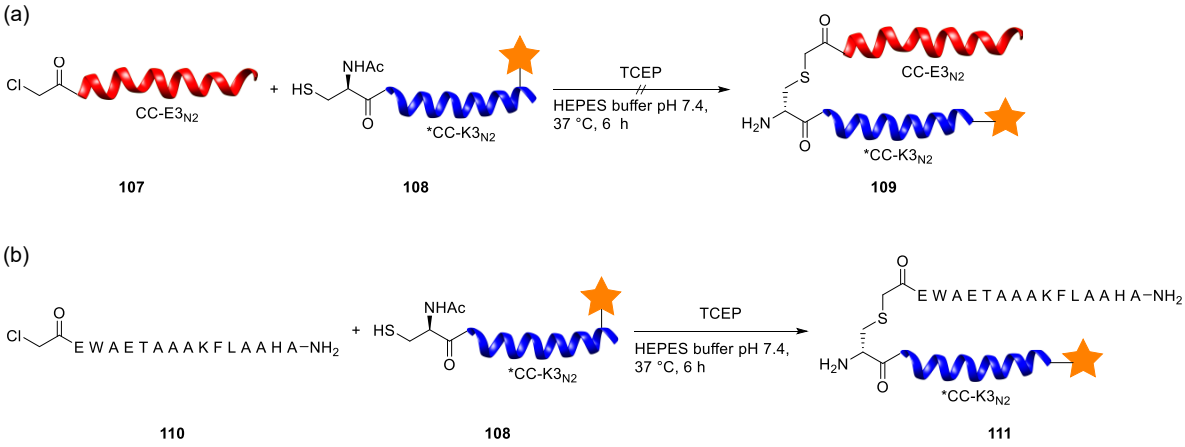

Figure 69*:* (a) Coiled-coil mediated cysteine alkylation and (b) non-templated reference. The star represents FITC.

Surprisingly, only the non-templated approach led to product formation, while the starting materials were retained in the templated approach. This seems to indicate the necessity of a linker of at least moderate length between template and reactive centers. The hypothesis could however not be tested, since incorporation of a PEG(3) linker between **97** and chloroacetic acid failed. Of note, the non-templated cysteine alkylation proceeded much slower than the non-templated oxime ligation (see Figure 70).

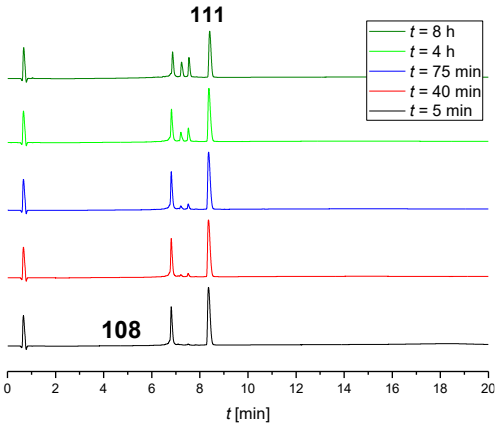

Figure 70: UHPLC reaction monitoring (215 nm) of the non-templated cysteine alkylation.

4.3.4 Coiled-coil templated SPAAC ligation

To complete the assessment of coiled-coil peptides as a reaction template, the SPAAC ligation was investigated. While its kinetics are inherently faster than that of oxime ligation, introduction of the sterically demanding cyclooctyne might offer additional insight into the compatibility of reaction templates and bulky functional groups.

In line with the experiments described in the previous sections, 4-azidobutyric acid was introduced to FITC labeled **99**. The building block (**113**) was synthesized according to a procedure by Maltzahn *et al*.[216] *via* nucleophilic substitution of ethyl 4-bromobutyrate (**112**) with sodium azide, followed by basic hydrolysis of the ethyl ester protecting group. The product was obtained in excellent yields (see Figure 71). Subsequent attachment to the peptide was performed following standard coupling protocols to yield **114**.

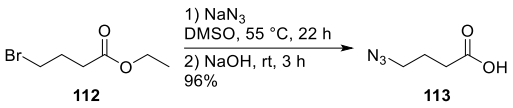

Figure 71: Synthesis of 4-azidobutyric acid.

Commercially available DBCO-acid was attached to K3 peptide **98** and reference peptide **101** to yield **115** and **117**, respectively. Both peptides were combined with azide-modified **114** in PBS buffer at 37 °C for 24 and 4 h, however no reaction was observed (see Figure 72).

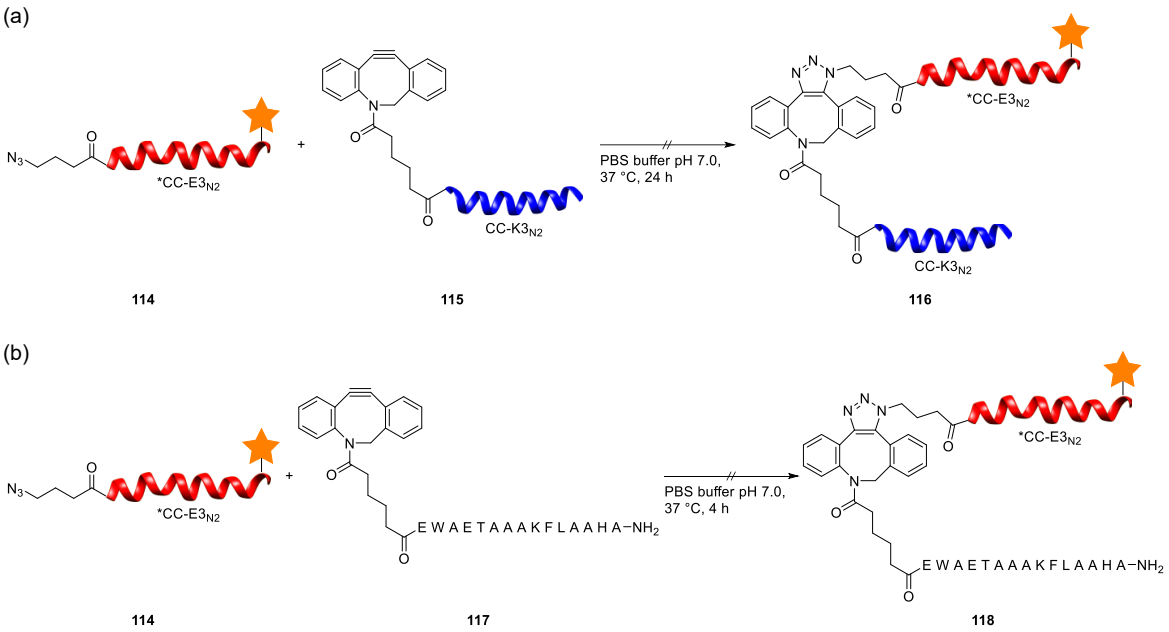

Figure 72: (a) Coiled-coil mediated SPAAC ligation and (b) non-templated reference. The star represents FITC.

This result seems to be indicative for high steric constraint between the peptide and the attached functional groups. Surprisingly, for this approach even the non-templated geometry seems to be unfitting. To further investigate this phenomenon, a PEG(3) linker was introduced as an additional spacer between the CC-K3$_{N2}$ peptide and DBCO-acid to yield **119**. However, no reaction was observed after 6 h when combined with **114** (see Figure 73), suggesting a crowding of the functional groups that cannot be easily overcome.

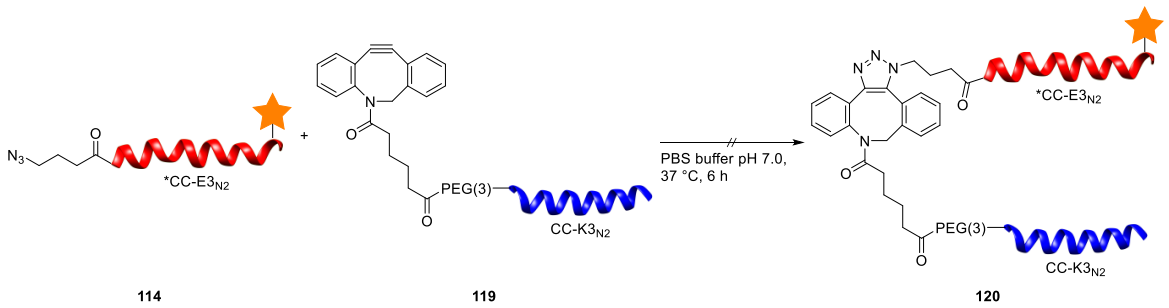

Figure 73*:* Coiled-coil mediated SPAAC ligation with an additional spacer. The star represents FITC.

4.3.5 Coiled-coil mediated functional group transfer with partial scaffold release

Of the investigated reactions, oxime ligation was the only approach to yield the covalently cross-linked coiled-coil dimer. Monitoring of the reaction progress did show reaction kinetics that do not conform to a second-order rate. The observed deviations in combination with no apparently observed template effect could complicate future applications in protein labeling. Nonetheless, a proof of concept experiment was designed to demonstrate the functional group transfer with subsequent removal of the donor strand. For this, commercially available Fmoc-D-β-Phe(2-NO_2)-OH was introduced as a PCL between the CC-$K3_{N2}$ donor strand and the hydroxylamine to give **121**. It was combined with aldehyde modified **102** under ligation conditions, to yield the cross-linked species **122** (see Figure 74a). Due to the long irradiation times associated with the PCL, use of a fluorophore was foregone, since bleaching and possible degradation were suspected, which would result in a more complex analysis.

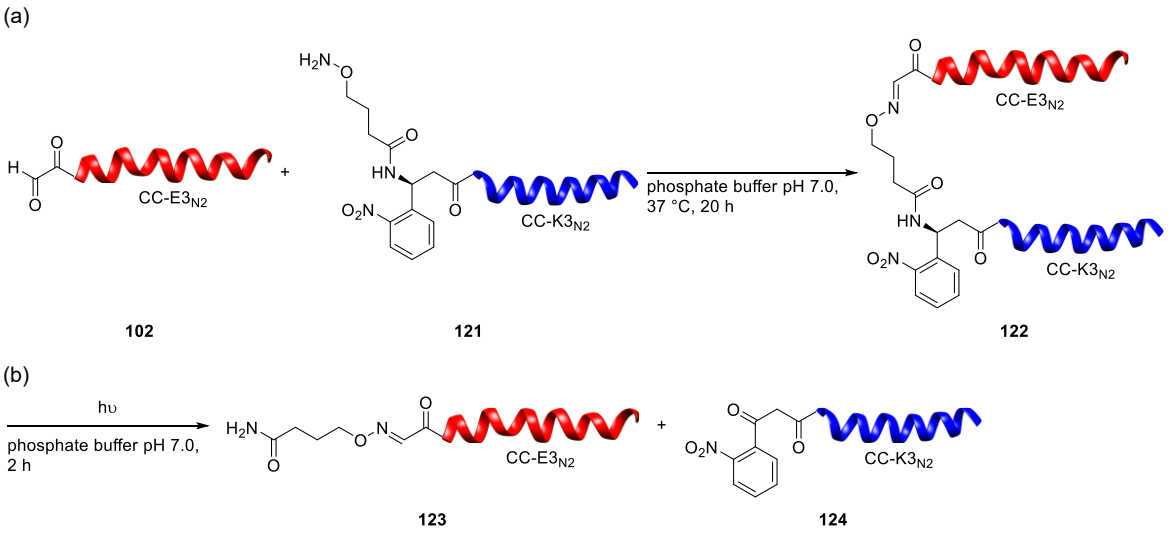

Figure 74: (a) Oxime ligation between aldehyde modified **102** and hydroxylamine bearing **121**. (b) Removal of the donor strand by irradiation at 347 nm (600 W).

The identity of **122** was confirmed by HR-MS after purification by HPLC and a solution of the pure peptide was irradiated in phosphate buffer at 347 nm and 600 W (see Figure 74b). The photolysis was followed by high-resolution LC-MS. The first aliquot was analyzed after 45 min, which revealed an incomplete cleavage, but still identified the species **123** and **124** (see Figure 75). These results are in line with the generally accepted photolysis mechanism of *o*-nitrobenzyl compounds (see Figure 45, chapter 4.2.2). Photocleavage was found to be complete after 2 h, owing to the poor photophysical properties of the linker. Despite the

expected slow removal of the helper strand, the proof of concept experiment was successful, yielding the functionalized peptide **124**, as well as the removed helper fragment **123**. Photocleavage could be optimized by utilizing a linker with more beneficial properties, such as a bifunctional coumarin linker based on the work of Yamazoe *et al*.[187]

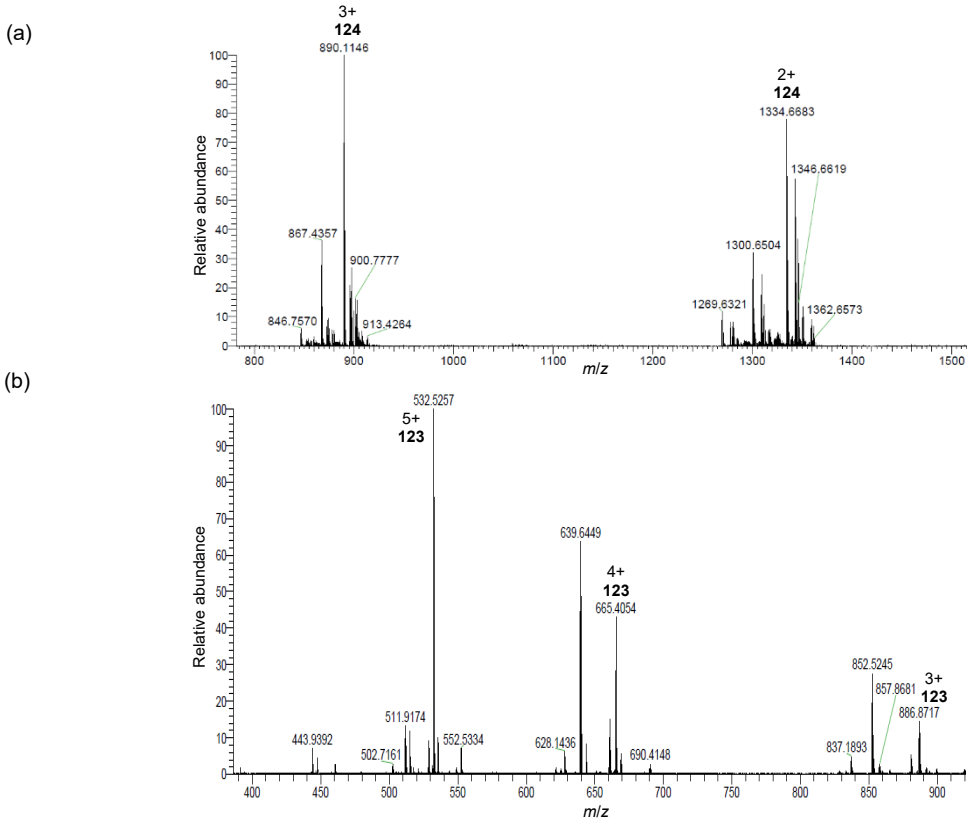

Figure 75*:* ESI-MS spectra of the photolysis of **122**, showing (a) **124** and (b) **123**.

4.3.6. Conclusion

In this chapter the viability of coiled-coil peptides as templates for a variety of biocompatible reactions was investigated. Contrary to the previously described approach utilizing PNA, an architecture leading to the transfer of a functional group from a donor to an acceptor strand, with release of the former, was pursued. Tying in with the findings of the previous chapter, the Suzuki cross-coupling was first investigated. Starting from Hodges' parallel heterodimeric IAAL E3/K3 peptides, templates with different flexibility, length, and linker region were investigated without success. Since CD spectroscopy revealed an intact template and binding of the catalyst to the amino acids is highly unlikely, a more reasonable explanation is the preorganization of the functional groups by the template into an unsuitable geometry or a low reactivity of the employed reagents. Therefore, a number of reactions with defined parameters were screened. In a reference study without a template,

only oxime ligation and cysteine alkylation showed product formation. Application of the template only led to success of the former. Surprisingly, no increase in reaction rate was measured compared to the non-templated approach. Instead, a non-linear reaction behavior was observed that could not be explained based on experimental data. Nonetheless, a proof of concept experiment was designed, ligating hydroxylamine equipped coiled-coil **121** and aldehyde modified coiled-coil **102**. Irradiation of an *o*-nitrobenzyl derived PCL completed the functional group transfer by releasing the donor strand.

5 Summary and outlook

Site-selective protein modification is an important tool to study and influence the function of proteins. The use of template assisted ligation allows for substrate selectivity and an enhanced reaction rate due to an increase of the reactant's effective molarity. Employing more than one template in a series of parallel ligation events would provide selectivity, while the concentration of a non-templated reaction should be too low to form a significant amount of product, even if competing functional groups are involved. In this work, a peptide nucleic acid template was investigated towards this goal, utilizing NCL as the ligation reaction. To further broaden the scope of the template and improve its photolytic release, a Suzuki cross-coupling reaction with the potential for fluorescence generation upon ligation was studied. In addition, a different template architecture, based on a heterodimeric parallel coiled-coil was explored to facilitate functional group transfer *via* a variety of biocompatible ligations. Common to all approaches was the use of a photocleavable linker that led to (partial) scaffold release after the ligation.

Based on previous work in our group by Middel *et al*.,[12,154] a template directed NCL strategy applying photocleavable PNA strands was selected to be studied in the parallel mediation of two ligation events. PNA associates *via* Watson-Crick base pairing and strands with a non-complementary sequence should be discriminated based on the energy penalty associated with a mismatched base pair. In order to identify orthogonal templates, an automated protocol for the synthesis of PNA strands was developed in collaboration with Denis Pahlke and Patrick Menzel that has recently found application in the synthesis of PNA-peptide conjugates as functional SNARE protein mimetics.[217] To this end, three PNA duplexes containing zero, two or three mismatched base pairs, as well as two duplexes of different length and sequence (10-mer, 12-mer) were synthesized. The stability of matched and mismatched pairs was studied by UV-Vis melting curve measurements. While positional mismatches did not show the expected difference in melting temperature, a difference of 11.4 °C was observed between length mismatched complexes PNA 1·PNA 2 and PNA 3·PNA 4. However, a discrepancy between length and sequence mismatched pairs (combinations of PNA 1 or PNA 2 with PNA 3 or PNA 4) was almost nonexistent. This behavior seems to differ from antiparallel PNA duplexes or PNA·DNA or PNA·RNA duplexes, although the studied sample size was small.[144,161,162] Nonetheless, the corresponding building blocks for a parallel ligation approach were synthesized (**20-23**) and their selective native chemical ligation studied. Neither starting material nor a (cross) reaction product was identified. This may have been the result of the nucleobase

recognition not being sufficiently selective, therefore forming mixed products, effectively lowering the concentrations under the detection limit. While the absent selectivity of the PNA duplexes prevents their use in a simultaneous ligation, they could still find application in combination with a structurally different template.

In order to expand the scope of reactions templated by photocleavable PNA strands, a method with fluorescence generation upon ligation was investigated. A second reaction type would furthermore bypass the use of competing functional groups. Suzuki cross-coupling was selected, since a reaction of halogenated tryptophan and phenylboronic acid would result in a fluorophore to monitor the reaction progress and track a protein of interest with different microscopy techniques. Initial tests verified the established methods for cross-coupling of a peptide and a small organic substrate and were expanded to show application in the coupling of two small peptide fragments. Reaction times increased substantially for the more complex reaction architectures, suggesting steric inhibition.
Implementation of the guiding PNA strands to increase the reaction rate of the cross-coupling reaction however revealed problems. No reactivity was observed for a templated cross-coupling approach and screening of various catalyst systems revealed inhibition by PNA. UV-Vis measurements observing the change in melting temperature and absorbance of dsPNA at various Pd(II) concentrations suggested direct binding of the palladium ion to the PNA nucleobases, thereby stalling the reaction. While an increase in catalyst concentration might lead to a successful cross-coupling reaction, it would also most likely result in the unwinding of the template.

Coiled-coil peptides were investigated as an alternative reaction template since the different dimer recognition mode would result in orthogonality to PNA templates. Their facile synthesis would also provide a toolbox approach for a variety of bioorthogonal ligations. The employed architecture provides a functional group transfer, while a PCL releases the donor strand. Initially, Suzuki cross-coupling was tested and while the template remained intact, no reaction was observed. This led to the assumption that the template might pre-organize the functional groups into an undesirable reaction geometry. In this light, biocompatible reactions with different steric demands were screened. Oxime ligation, cysteine alkylation and SPAAC were studied under influence and absence of a coiled-coil template. Of the templated reactions, only oxime ligation led to product formation, while cysteine alkylation additionally led to the reaction product without use of a template. Notably, both reactions possess simple reaction architectures and have a low steric demand. Absence of a reaction for the templated cysteine alkylation approach seems to suggest a specific distance of the functional group from the template and orientation are

necessary for a successful ligation. Reaction monitoring of the templated oxime ligation further revealed a non-linear conversion that proved to be slower than the non-templated approach. Nonetheless, oxime ligation was successfully applied in a proof of concept experiment that resulted in the transfer of the functional group from the donor to the acceptor strand and a successful release of the former by photolysis. The general approach is outlined in Figure 76.

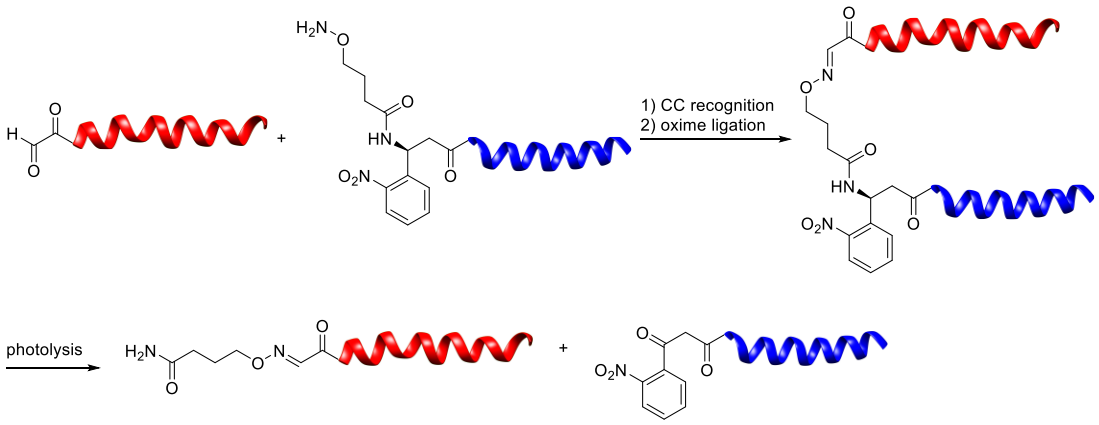

Figure 76: Concept of the coiled-coil mediated functional group transfer. The strategy allowed oxime ligation between donor (blue) and acceptor strand (red) with removal of the former by photolysis.

For the future of the project, different reactions should be studied in combination with the coiled-coil template. An inverse electron demand Diels-Alder reaction between methylcyclopropene and *s*-tetrazine might offer a compromise between low steric demand and fast reaction kinetics. Furthermore, a detailed study into the geometry necessary to provide a positive templating effect should be conducted. The already established coiled-coil templated NCL could be studied regarding linker length, reaction kinetics and possibly X-ray crystal-structures to determine suitable alignments and distances between the functional groups. Another possibility is the investigation of orthogonal peptide tectons to facilitate simultaneous reactions. Furthermore, the applied PCL lacks desirable photophysical properties. Within this thesis, an improved PCL based on DEACM has been synthesized for conjugation of the PNA template. A bifunctional variant suitable for direct incorporation into peptides *via* automated SPPS is imaginable based on the studies by Yamazoe *et al.*[187] Since the coiled-coil templated oxime ligation was successful, a combination with the PNA mediated NCL might be conceivable for an application where site-selectivity and parallel labelling would compensate slow reaction times. This combination of PNA and coiled-coil template might offer the best results towards facilitating parallel ligation events. However, for ease of synthesis and higher selectivity, the PNA sequence should be changed to accommodate antiparallel alignment. Different linkers

based on an orthogonal release mechanism, such as higher wavelength, change in pH value or susceptibility to proteases might complement this approach.

6 Experimental section

6.1 Materials and methods

6.1.1 Reagents and solvents

Fmoc-protected amino acids and PNA monomers were purchased from *Carbolution Chemicals GmbH* (St. Ingbert, Germany), *Iris Biotech GmbH* (Marktredwitz, Germany), *GL Biochem Ltd.* (Shanghai, China), *Sigma-Aldrich* (*Merck KGaA*, Darmstadt, Germany) *ChemPUR* (Karlsruhe, Germany), *BLD Pharmatech Ltd.* (Shanghai, China), *Chem-Impex International, Inc.* (Wood Dale, IL, USA) and *ASM Research Chemicals GmbH* (Hannover, Germany). Oxyma Pure and HATU were obtained from *Carl Roth GmbH & Co. KG* (Karlsruhe, Germany), DIC was supplied by *Iris Biotech GmbH* and HOAt by *GL Biochem Ltd.* H-Rink amide ChemMatrix® resin was purchased from *Sigma-Aldrich*, Wang resins and NovaPEG Rink amide resins were obtained from *VWR International GmbH* (Darmstadt, Germany). DMF used for peptide synthesis was obtained from *Thermo Fisher Scientific GmbH* (Schwerte, Germany) in laboratory reagent quality. Piperidine and piperazine in peptide synthesis quality was acquired from *Carl Roth GmbH & Co. KG* and *abcr GmbH* (Karlsruhe, Germany), respectively. 2,6-Lutidine for PNA synthesis was purchased from *Thermo Fisher Scientific GmbH*. Acetonitrile and methanol used for HPLC were supplied by *Thermo Fisher Scientific GmbH* in HPLC grade quality. Water used for HPLC was obtained by purifying deionized water with an arium® mini lab water system from *Sartorius* (Göttingen, Germany). All other reagents were supplied by *abcr GmbH*, *Alfa Aesar* (*Thermo Fisher GmbH*, Kandel, Germany), *Carl Roth GmbH & Co. KG*, *ChemPUR*, *Fluorochem* (Hadfield, United Kingdom), *J&K Scientific bvba* (Lommel, Belgium), *Merck KGaA*, *Sigma-Aldrich*, *TCI Deutschland GmbH* (Eschborn, Germany), *Thermo Fisher Scientific GmbH* and *Th. Geyer GmbH & Co.KG*. All reagents were of synthesis grade quality and were used as supplied.

6.1.2 Thin-layer chromatography (TLC) and column chromatography

TLC analysis was performed on aluminum TLC plates with silica gel 60 F_{254} from *Merck KGaA*. Compounds were detected by fluorescence quenching with UV-light (λ = 254 or 366 nm). Column chromatography was performed on Geduran® silica gel 60 (40-63 µm), supplied by *Merck KGaA*.

6.1.3 High Performance Liquid Chromatography (HPLC)

HPLC purification was mainly carried out on three devices from *JASCO* Deutschland GmbH (Pfungstadt, Germany). For sample purification on a preparative scale, a device equipped with *PU-4086* pumps, a *UV-4075* detector and a *CO-4060* column oven was used at flow rates of 10 mL/min. Semi-preparative purification was performed on a system with *PU-2080plus* pumps and a *MD-2010* detector at flow rates of 3 mL/min. A system with identical pumps and a *MD-4015* detector was used for purification on an analytical scale at flow rates of 1 mL/min.

Peptide samples were detected at 215, 254 and 280 nm. PNA samples were detected at 215, 265 and 280 nm. Samples containing coumarin derived building blocks were detected at 215, 280 and 380 nm. Samples containing nitroveratryloxycarbonyl derived building blocks were detected at 215, 280 and 350 nm. Samples containing fluorescein isothiocyanate were detected at 215, 280 and 440 nm. For preparative HPLC, only the signal at 215 and 280 nm was followed.

The solvents used for purification are listed below. Linear gradients of solvent B and C were used.

Solvent A	H_2O + 0.1% TFA
Solvent B	MeCN + 0.1% TFA
Solvent C	MeOH + 0.1%TFA

The employed columns were purchased from *MACHEREY-NAGEL GmbH & Co. KG* (Düren, Germany) *Advanced Chromatography Technologies Ltd.* (Aberdeen, Scotland) and *KNAUER Wissenschaftliche Geräte GmbH* (Berlin, Germany) and are specified below.

Column 1	MN Nucleodur, 100-5 C18ec, 250 x 21 mm, 5 µm
Column 2	MN Nucleodur, 100-5 C18ec, 250 x 10 mm, 5 µm
Column 3	MN Nucleodur, 100-5 C18ec, 250 x 4.6 mm, 5 µm
Column 4	MN Nucleodur Sphinx RP, 250 x 10 mm, 5 µm
Column 5	Ace® 5 C18-100, 150 x 10 mm, 5 µm
Column 6	Knauer Eurosil Bioselect 300-5 C18, 250 x 4.6 mm, 5 µm

The gradient composition is indicated in the respective experimental procedures.

6.1.4 Ultra High Performance Liquid Chromatography (UHPLC)

Reaction monitoring and analysis of sample quality by UHPLC was performed on an *UltiMate 3000* system from *Thermo Fisher Scientific GmbH*, using an ACE® Excel® 2 C18-100 (100 x 2.1 mm, 2 µM) column at a flow rate of 0.45 mL/min at 50 °C. Linear gradients of A (water + 0.1% TFA) and B (MeCN + 0.1% TFA) were applied as stated in the respective experimental procedures.

6.1.5 Nuclear Magnetic Resonance (NMR) Spectroscopy

^{1}H-NMR spectra were recorded on Avance III HD (300 or 500 Mhz) and Avance Neo (400 or 600 MHz) devices from *Bruker BioSpin GmbH* (Rheinstetten, Germany) at 25 °C. ^{13}C-NMR spectra were recorded on the same devices at the corresponding frequencies of 75, 100, 125 and 150 MHz at 25 °C. The utilized deuterated solvents are indicated for each compound individually. The residual proton signal of the solvent served as an internal standard and was referenced according to Gottlieb *et al*. (see table below).[218] Chemical shifts δ are given in ppm and coupling constants *J* are given in Hertz (Hz). For peak assignment, the following abbreviations for multiplicities and descriptors were used: s = singlet, d = doublet, t = triplet, q = quartet, quint = quintet, m = multiplet, dd = doublet of doublets, dt = doublet of triplets, td = triplet of doublets and br = broad signal.

	$CDCl_3$	$(CD_3)_2SO$	CD_3OD	D_2O
solvent residual peak (^{1}H-NMR)	7.26 ppm	2.50 ppm	3.31 ppm	4.79 ppm
solvent residual peak (^{13}C-NMR)	77.16 ppm	39.52 ppm	49.00 ppm	

6.1.6 Mass spectrometry (MS)

Peptides were characterized by high-resolution mass spectrometry (HR-MS). Electrospray ionization (ESI-HRMS) spectra were recorded on a *maXis* (ESI-QTOF-MS) or a *micrOTOF* (ESI-TOF-MS) device from *Bruker Daltonik GmbH* (Bremen, Germany). The detected ion masses are reported in *m/z* (mass-to-charge ratio).

6.1.7 Liquid chromatography-mass spectrometry (LC-MS)

Chromatographic analysis was performed on an *Accela*™ system from *Thermo Fisher Scientific GmbH*, using a Kinetex® C18-100 (150 x 2.1 mm, 5 µM) column from

Phenomenex Ltd. Deutschland (Aschaffenburg, Germany) at a flow rate of 0.2 mL/min. Linear gradients of A (water + 0.05% FA) and B (MeOH + 0.05% FA) were applied as stated in the respective experimental procedures. Mass spectra were recorded on a coupled LTQ Orbitrap XL™ spectrometer from *Thermo Fisher Scientific GmbH*.

6.1.8 Concentration determination

Peptide concentrations were determined by UV-absorbance using a *NanoDrop™2000c* or *NanoDrop™One^C* spectrophotometer from *Thermo Fisher Scientific GmbH*. The following tabulated wavelengths and extinction coefficients were used for calculation according to the Beer-Lambert law.

Compound	λ [nm]	ε_λ [M^{-1} cm^{-1}]	Reference
Trp	280	5690	[219]
Tyr	280	1280	[219]
PNA-A	260	13700	[220]
PNA-C	260	6600	[220]
PNA-G	260	11700	[220]
PNA-T	260	8600	[220]
Nvoc	350	5485	[221]
DEACM-OH	385	16000	[177]
FITC	494	77000	[215]

6.1.9 UV-Vis spectroscopy

UV-Vis measurements were carried out on a *Jasco V-650* spectrophotometer equipped with a *Jasco ETCS-761* temperature controller. Suitable cuvettes from *Hellma GmbH & Co. KG* (Müllheim, Germany) with a path length of 1 cm were employed.
PNA melting curves were recorded from 5 µM duplex solutions in TBS buffer (50 mM Tris-Cl, 150 mM NaCl, pH 7.5). The *time course measurement* program was chosen, and the wavelength set to 260 nm. Spectra were recorded in the range of 5-80 °C, where each measurement consisted of a heating (5→80 °C) and a cooling (80→5 °C) cycle. Three accumulations were measured for every duplex pair. The UV-Vis bandwidth was set to 2.0 nm with a fast response time. The acquired data was interpreted according to the following equation for the hyperchromicity *H*:

$$H(\%) = \frac{A(T) - A_0}{A_0} \cdot 100\%$$

with $A(T)$ (absorbance at a given temperature) and A_0 (minimum absorbance). The melting temperature T_m is the maximum of the first derivative of the resulting curve.

PNA titration experiments in the presence of Pd-catalyst were carried out using a total strand concentration of 5 µM in phosphate buffer (50 mM, pH 8.0). *Spectra measurement* was performed in the range of 200-350 nm in intervals of 0.5 nm at 20 °C. A scanning speed of 100 nm/min with a fast response time and a bandwidth of 1.0 nm was selected. Three accumulations were recorded for every experiment. Every measurement was corrected for a blank containing the buffer and the titrated amount of catalyst.

6.1.10 Circular dichroism (CD) spectroscopy

CD spectra were recorded on a *Jasco J1500* CD spectrometer equipped with a *Julabo* (Seelbach, Germany) *F250* cooler. Suitable cuvettes from *Hellma GmbH & Co. KG* with a path length of 0.1 cm were employed.

CD measurements were recorded from 80 µM coiled-coil solutions in phosphate buffer (50 mM, pH 7.0 or 8.0). *Spectra measurement* was performed in the range of 190-250 nm in intervals of 1.0 nm at 20 °C. A scanning speed of 100 nm/min was selected, the CD scale was set to 2000 mdeg/1.0 dOD and the bandwidth to 1.0 nm. Ten accumulations were recorded for every experiment. Alternatively, for a coiled-coil concentration of 25 µM intervals of 0.1 nm were chosen with a scanning speed of 50 nm/min.

Raw data was corrected by subtracting a blank containing the buffer and then interpreted according to the following equation[206] for the molar ellipticity [Θ]:

$$[\Theta]\ (\mathrm{deg} \cdot \mathrm{cm}^2 \cdot \mathrm{dmol}^{-1}) = \frac{\Theta_{\mathrm{obs}} \cdot MRW}{10 \cdot d \cdot c}$$

where Θ_{obs} is the measured ellipticity (mdeg), *MRW* is the mean residue molecular weight (g · dmol^{-1}), *d* is the path length (cm) and *c* is the concentration (g · dm^{-3}).

6.1.11 Photolysis

Photolytic cleavage was performed in a UV cuvette (1 cm) from *Hellma GmbH & Co. KG* using an Ark Lamp Source (66924) from *Newport Spectra-Physics GmbH* (Darmstadt, Germany), consisting of a 1000 W Arc Housing-IGN F/1.0 (66921), a 1000 W Hg-Xe lamp (6295NS), power supply (69920), dichroic mirror (280-400 nm, 66226) and optionally a 347 nm longwave cut-on filter (20CGA-345, setup a). Alternatively, an *Osela inc.* (Lachine,

QC, Canada) Streamline Laser (405 nm, 100 mW, 70 mA) was used as the irradiation source (setup b).

6.1.12 Software

ChemDraw Professional 16.0 (*PerkinElmer Informatics*, Waltham, MA, United States) was used for the drawing of chemical structures and calculation of molecular masses. Figures were created with the help of Affinity Designer (*Serif (Europe) Ltd*, Nottingham, United Kingdom) and data files from the RCSB protein data bank (PDB)[222] were interpreted and modified using UCSF Chimera. The identifier of the corresponding PDB entry is indicated in the respective figure. For coiled-coil peptides and generic protein structures entries 1U0I and 4FC1 were used for illustrative purposes. Chimera is developed by the Resource for Biocomputing, Visualization, and Informatics at the University of California, San Francisco, with support from NIH P41-GM103311.[223] NMR spectra were analyzed with MestReNova 10.0 (*Mestrelab Research, S.L.*, Santiago de Compostella, Spain) and graphs were compiled using OriginPro 8.5G (*OriginLab Corporation*, Northampton, MA, United States).

6.1.13 Preparation of catalyst stock solutions

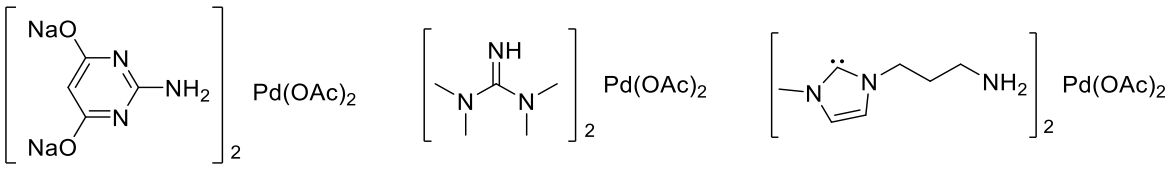

$(ADHP)_2\ Pd(OAc)_2$ $(TMG)_2\ Pd(OAc)_2$ $(NHC)_2\ Pd(OAc)_2$

2-Amino-4,6-dihydroxypyrimidine (25.4 mg, 0.2 mmol, 2.0 eq.), 1,1,3,3-tetramethyl-guanidine (23.0 mg, 0.2 mmol, 2.0 eq.) and 1-(3-(trimethylammonium)propyl)-3-methylimidazole bromide (68.6 mg, 0.2 mmol, 2.0 eq.) were each dissolved in NaOH (0.1 M, 4 mL) in a 10 mL volumetric flask at 65 °C. $Pd(OAc)_2$ (22.5 mg, 0.1 mmol, 1.0 eq.) was added and the solution was stirred at 65 °C for 2 h. The solution was allowed to cool to room temperature and diluted to 10 mL, giving a 0.01 M stock solution of the respective catalyst.

6.1.14 Catalyst screening

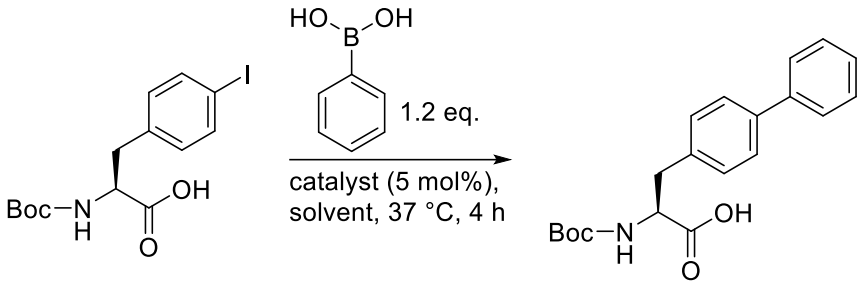

Boc-*p*IPhe-OH (1 µmol) and phenylboronic acid (1.2 µmol) were dissolved in 1000 µL of the indicated solvent. 5 mol% of the respective catalyst were added and the reaction mixture was agitated at 37 °C. 10 µL aliquots were taken after 0.5, 1, 2, 3 and 4 h, quenched by the addition of 6 mol% glutathione and diluted to 20 µL with H_2O. Samples containing PNA strands as an additive were additionally analyzed after 20 h. Conversion was determined by UHPLC (gradient: 5-90% B in 15 min).

6.2 Standard Operating Procedures (SOPs)

SOP 1: Automated Solid Phase Peptide Synthesis (SPPS)

Peptides were synthesized on a *Liberty Blue* automated microwave peptide synthesizer from *CEM GmbH* (Kamp-Lintfort, Germany). Prior to coupling, the resin was swollen in DMF for at least 30 min. Synthesis was performed according to standard Fmoc/*t*Bu-protocol using diisopropylcarbodiimide (DIC) and Oxyma as coupling reagents and a solution of piperidine in DMF (20% (v/v)) for Fmoc deprotection. Attachment of the amino acid building blocks was performed as double coupling, using a modified CarboMax method (5 eq. aa, 10 eq. DIC, 5 eq. Oxyma, 0.5 eq. DIPEA in DMF; 1: 75 °C, 170 W, 15 s; 2: 90 °C, 30 W, 110 s). Milder conditions with an elongated reaction time were applied for the coupling of His (1: 25 °C, 0 W, 120 s; 2: 50 °C, 35 W, 480 s). Removal of the temporary protecting group was carried out under standard conditions (1: 75 °C, 260 W, 15 s; 2: 90 °C, 60 W, 50 s).

After completion of the peptide synthesis, the resin was transferred to a *Discardit II*™ syringe equipped with a filter supplied by *Becton Dickinson GmbH* (*BD* syringe, Heidelberg, Germany), washed with DMF (10x5 mL) and DCM (10x5 mL) and dried *in vacuo*.

SOP 1b: Synthesis of branched peptides

Synthesis of the linear peptide was carried out according to SOP 1. The branching point was marked by Fmoc-Dap(Mmt)-OH. Following automated SPPS, the resin was transferred to a *BD* syringe. Deprotection of the side chain was performed with DCM/TIS/TFA (94:5:1, 1 mL/10 µmol) for 2 x 5 min at room temperature. Afterwards, the resin was washed with DMF, DCM and DMF (each 5 x 1 mL/10 µmol). Then, Boc-Cys(S*t*Bu)-OH (5.0 eq.) was coupled to the side chain with PyBOP (5.0 eq.) and DIPEA (10 min) for 2 x 30 min at room temperature. Further elongation of the main chain was achieved following SOP2.

SOP 2: Microwave assisted manual SPPS

Manual coupling of peptides was carried out in a *BD* syringe, according to Fmoc/Boc-strategy following the subsequent procedure. Prior to coupling the dry resin was swollen in DMF for 30 min. 5.0 eq. of the Fmoc-protected amino acid were dissolved in DMF to give a 0.05 M solution. 4.9 eq. HATU, 5.0 eq. HOAt and 10.0 eq. DIPEA were added and the solution was added to the resin, which was transferred to the reaction cavity of a *Discover*® microwave synthesizer from *CEM* and coupling was performed at 75 °C (25 W) for 5 min. Afterwards, the resin was washed five times with DMF and the coupling step was repeated. If necessary, capping was carried out by treating the resin with a solution of DMF/Ac_2O/DIPEA (17:2:1 (v/v)) for 2 x 5 min. Afterwards, the resin was washed five times with DMF. Deprotection of the Fmoc-protecting group was achieved by treatment of the resin with 20% piperidine in DMF at 40 °C (20 W) for 30 s and repeated at 75 °C (50 W) for 3 min. After each deprotection step, the resin was washed five times with DMF. After completion of the peptide synthesis, the resin was washed ten times with DMF and DCM and dried *in vacuo*.

SOP 2b: Microwave assisted manual SPPS at lower temperatures

The same procedure as for SOP2 was applied. However, deprotection was performed at 40 °C (20 W) for 1 min and repeated at 50 °C (25 W) for 5 min. Coupling of the amino acids was performed at 50 °C (25 W) for 15 min and repeated once.

SOP 2c: Manual SPPS at room temperature

Alternatively, coupling at room temperature was performed applying deprotection times of 15 min and coupling times of 1 h.

SOP 3: Manual solid phase PNA synthesis

Manual coupling of the PNA strands was carried out in a *BD* syringe according to Fmoc/Bhoc-strategy on NovaPEG Rink amide resin (0.17 mmol/g) resin following the subsequent procedure. Prior to coupling the dry resin was swollen in DMF for 30 min. 5.0 eq. of the Fmoc-protected building block were dissolved in DMF to give a 0.05 M solution. 4.9 eq. HATU, 5.0 eq. HOAt, 10.0 eq. DIPEA and 10.0 eq. 2,6-lutidine were added and the solution was transferred to the resin, which was agitated for 45 min. Afterwards, the resin was washed with DMF (5 x 2 mL/10 µmol) and the coupling step was repeated. Capping was carried out by treating the resin with a solution of DMF/Ac_2O/2,6-lutidine (17:2:1 (v/v), 2 mL/10 µmol) for 2 x 5 min. The resin was washed five times each with 5% DIPEA in DMF (2 mL/10 µmol) and DMF (2 mL/10 µmol). Deprotection of the Fmoc-protecting group was achieved by treatment of the resin with 20% piperidine in DMF (2 mL/10 µmol) for 2 x 10 min. After each deprotection step, the resin was washed with DMF (5 x 2 mL/10 µmol). After completion of the peptide synthesis, the resin was washed with DMF (10 x 2 mL/10 µmol) and DCM (10 x 2 mL/10 µmol) and dried *in vacuo*.

SOP 4: Microwave assisted manual solid phase PNA synthesis

Microwave assisted manual coupling of the PNA strands was carried out in a *BD* syringe according to Fmoc/Bhoc-strategy on NovaPEG Rink amide resin (0.17 mmol/g) following the subsequent procedure. Prior to coupling the dry resin was swollen in DMF for 30 min. 5.0 eq. of the Fmoc-protected building block were dissolved in DMF to give a 0.05 M solution. 4.9 eq. HATU, 5.0 eq. HOAt, 10.0 eq. DIPEA and 10.0 eq. 2,6-lutidine were added and the solution was transferred to the resin, which was placed in the reaction cavity of a *Discover*® microwave synthesizer from *CEM* and coupling was performed at 50 °C (25 W) for 20 min. Afterwards, the resin was washed with DMF (5 x 2 mL/10 µmol) and the coupling step was repeated. Capping was carried out by treating the resin with a solution of DMF/Ac_2O/DIPEA (17:2:1 (v/v), 2 mL/10 µmol) for 2 x 5 min. The resin was washed five times each with 5% DIPEA in DMF (2 mL/10 µmol) and DMF (2 mL/10 µmol). Deprotection of the Fmoc-protecting group was achieved by treatment of the resin with 20% piperidine in DMF at 40 °C (20 W) for 1 min and repeated at 50 °C (25 W) for 5 min. After each deprotection step, the resin was washed with DMF (5 x 2 mL/10 µmol). After completion of the peptide synthesis, the resin was washed with DMF (10 x 2 mL/10 µmol) and DCM (10 x 2 mL/10 µmol) and dried *in vacuo*.

SOP 5: Automated solid phase PNA synthesis

PNA strands were synthesized on NovaPEG Rink amide resin (0.17 mmol/g) at a 0.01 mmol scale following Fmoc/Bhoc-strategy on a *Liberty Blue* automated microwave peptide synthesizer from *CEM*. Fmoc-deprotection was achieved with a solution of 2% piperazine in DMF. Building blocks were used as 0.08 M solutions in DMF. Activation of the building blocks was accomplished with DIC (0.1 M in DMF) and Oxyma (0.1 M + 0.1 eq. DIPEA in DMF). A solution of DMF/Ac_2O/DIPEA (17:2:1 (v/v)) was used for capping *via* external positions. A 5% DIPEA solution in DMF was used as an additional wash at the end of the cycle. Prior to coupling, the dry resin was swollen in DMF for 30 min and afterwards transferred to the microwave reaction vessel. The deprotection solution (3 mL) was added and the Fmoc-protecting group was removed at elevated temperatures (40 °C, 20 W, 60 s). After washing with the main solvent (3 x 2 mL), the step was repeated for an extended time period (50 °C, 25 W, 300 s). After washing of the resin (5 x 2 mL), coupling of the building blocks (0.62 mL aa, 1.5 mL Act, 0.75 mL ActB) was performed under microwave irradiation (50 °C, 20 W, 1800 s) as a double coupling step. The resin was washed with DMF (3 x 3 mL) and capping was performed by addition of the aforementioned solution (3 mL) at room temperature for 300 s. The resin was washed with 5% DIPEA in DMF (3 x 2 mL) and DMF (4 x 2 mL). After completion of the synthesis, the resin was transferred to a *BD* syringe. The resin was washed with DMF (10 x 3 mL) and DCM (10 x 3 mL) and dried *in vacuo*.

SOP 6: Cleavage from resin and work up

Cleavage of the crude peptide from resin and global deprotection of acid labile protecting groups was performed in a *BD* syringe. The resin was suspended in the appropriate cleavage cocktail (1 mL/10 µmol) and agitated at room temperature for 2 h. Afterwards, the mixture was filtered off and concentrated under a nitrogen stream. The crude peptide was precipitated by addition of ice-cold diethyl ether, centrifuged and the supernatant discarded. This step was repeated four times, followed by drying of the crude peptide *in vacuo*.

A mixture of TFA/H_2O/TIS (95:2.5:2.5) was used as the standard cleavage cocktail, whereas a mixture of TFA/H_2O/EDT/TIS (94:2.5:2.5:1) was used for peptides containing cysteine or FITC.

SOP 7: On-resin attachment of photocleavable linker

The caging group **BK073** or **BK059** (2.0 eq.) was dissolved in DMF (0.5 mL/10 µmol) and DIPEA (5.0 eq.) was added. The solution was transferred to the resin-bound peptide

(1.0 eq.) in a *BD* syringe and shaken for 18 h at room temperature. Afterwards, the resin was washed with DMF (10 x 3 mL) and DCM (10 x 3 mL) and dried *in vacuo*.

SOP 8: On-resin alkyne modification

Propiolic acid (1.2 eq.) was dissolved in DMF (1 mL/10 µmol) and EEDQ (1.2 eq.) was added. The solution was transferred to the resin-bound peptide in a *BD* syringe and shaken for 12 h at room temperature. Afterwards, the resin was washed with DMF (10 x 2 mL) and DCM (10 x 2 mL) and dried *in vacuo*.

SOP 9: On-resin CuAAc reaction

In a *BD* syringe, resin-bound alkyne functionalized PNA (1.0 eq.), the PCL containing peptide (1.25 eq.), CuI (1.4 eq.) and NaAsc (1.5 eq.) were suspended in dry DMF (1.5 mL/10 µmol). The mixture was shaken at room temperature for 48 h. Afterwards, the resin was washed with DMF (10 x 2 mL) and DCM (10 x 2 mL) and dried *in vacuo*.

SOP 10: Template-directed NCL

The *tert*-butyl protected thiol (100 nmol, 1.0 eq) was dissolved in 1.0 mL degassed buffer (10 mM NaH_2PO_4, 100 mM NaCl, 20 mM TCEP, pH 7.0) and stirred at room temperature for 30 minutes to remove the protecting group. Then, the thioester (100 nmol, 1.0 eq) was added and the reaction mixture was stirred for 24 h. Progress of the reaction was analyzed by UHPLC.

SOP 11: On-resin Miyaura borylation

Synthesis of the iodinated precursor was carried out following SOP 2 with *p*IPhe marking the cross-coupling site.

In a Schlenk tube, the resin-bound iodinated peptide (1.0 eq.) was suspended in dry DMSO (5 mL/10 µmol). Bis(pinacolato)diboron (4.0 eq.), $PdCl_2$(dppf) (0.18 eq.), dppf (0.09 eq.) and KOAc (6.0 eq.) were added and the reaction mixture was stirred slowly at 80 °C for 24 h. Afterwards, the resin was transferred to a *BD* syringe, washed with DMSO, DCM, Et_2O and DCM (10 x 5 mL each) and dried *in vacuo*.

SOP 12: Suzuki coupling of peptides

Stock solutions of the purified peptides were prepared in H_2O/MeCN (4:1). 0.1 µmol of each peptide strand were combined in a 1.5 mL *Eppendorf AG* (Hamburg, Germany) safe-lock tube and diluted with phosphate buffer (50 mM, pH 8.0) to 1000 µL to give a 100 µM

solution. 10 mol% of $Na_2[ADHP]_2 \cdot Pd(OAc)_2$ was added and the reaction mixture was agitated at 37 °C.

Quenching of the reaction was performed by addition of 15 mol% L-glutathion (reduced) as an aqueous solution. Aliquots (20 µL) for analysis were taken at specified time points, diluted with H_2O (10 µL) and quenched with aqueous L-glutathion solution (10 µL).

SOP 13: Synthesis of peptide aldehydes by oxidation of serine

Introduction of an *N*-terminal aldehyde moiety was achieved by coupling of Fmoc-Ser(*t*Bu)-OH as the last amino acid according to SOP 2c. The *N*-terminal protecting group was removed, followed by global deprotection and cleavage from resin following SOP 6. The crude peptide was dissolved in PBS buffer (10 mM KH_2PO_4, 100 mM Na_2HPO_4, 0.137 M NaCl, 27 mM KCl, pH 7.0), 10.0 eq. $NaIO_4$ were added and the reaction mixture was agitated at 37 °C for 15 min. The reaction was stopped by freezing the solution in liquid nitrogen, followed by lyophilization. The crude peptide aldehyde was purified by HPLC as indicated in the experimental procedures.

SOP 13b: Synthesis of peptide aldehydes from thiazolidine

Introduction of an *N*-terminal aldehyde moiety was achieved by coupling of Boc-Thz-OH (**BK314**) as the last amino acid according to SOP 2c. Global deprotection and cleavage from resin was performed following SOP 6. The crude peptide was dissolved in H_2O + 0.1% TFA (1 mL), $PdCl_2$ (1.0 eq) was added and the reaction mixture agitated for 6 h at 37 °C. The mixture was filtered, lyophilized and purified by HPLC as indicated in the experimental procedure.

SOP 14: Oxime ligation of peptides

Stock solutions of the purified aldehyde- and aminooxy-containing peptides were prepared in H_2O/MeCN (7:3). Equimolar amounts were transferred into a 1.5 mL *Eppendorf* safe-lock tube and diluted with phosphate buffer (50 mM, pH 7.0) to give a 100 µM solution. The reaction mixture was agitated at 37 °C and the progress monitored by UHPLC.

SOP 15: Microwave assisted removal of the alloc protecting group

The resin-bound peptide was swollen in DCM (2 mL) for 30 min. Alloc deprotection was carried out by suspending the resin in DCM and $PhSiH_3$ (15.0 eq.), followed by addition of $Pd(PPh_3)_4$ (0.5 eq.) and heating to 38 °C (15 W) for 5 min. The resin was washed with DCM (5 x 1 mL) and the deprotection step was repeated twice, followed by washing with DCM (10 x 1.5 mL) and drying *in vacuo*.

SOP 16: SPAAC ligation of peptides

Stock solutions of the purified azide- and dibenzocyclooctyne-containing peptides were prepared in H_2O/MeCN (7:3). Equimolar amounts were transferred into a 1.5 mL *Eppendorf* safe-lock tube and diluted with PBS buffer (10 mM KH_2PO_4, 100 mM Na_2HPO_4, 0.137 M NaCl, 27 mM KCl, pH 7.0) to give a 100 µM solution. The reaction mixture was agitated at 37 °C and the progress monitored by UHPLC.

SOP 17: Ligation of peptides containing chloroacetic acid and cysteine

The cysteine containing peptide (1.0 eq) was incubated in 10 x TCEP-buffer (25 mM HEPES, 100 mM NaCl, 10 mM TCEP, pH 7.4) at 37 °C for 30 min. Then, the chloroacetic acid containing peptide (1.0 eq.) was added as a stock solution in H_2O/MeCN (7:3) and the reaction mixture was diluted with HEPES buffer (25 mM HEPES, 100 mM NaCl, pH 7.4) to give a TCEP concentration of 1 mM and a peptide concentration of 100 µM per strand. The reaction mixture was agitated at 37 °C and the progress monitored by UHPLC.

6.3 Organic synthesis

Synthesis of bis([2-{triphenylmethyl}sulfanyl]ethyl)amine (8)[168]

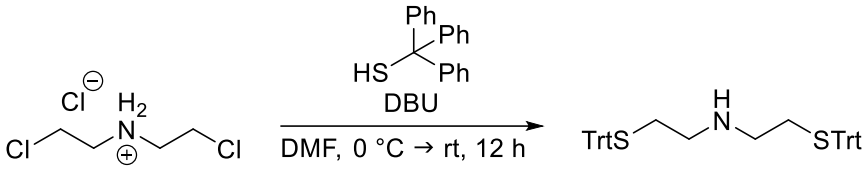

7 **8**

Bis(2-chloroethylamine) hydrochloride (5.19 g, 29.1 mmol, 1.0 eq.) and triphenylmethanethiol (16.1 g, 58.1 mmol, 2.0 eq.) were dissolved in DMF (85 mL) and the solution was cooled to 0 °C. DBU (17.9 g, 17.6 mL, 116 mmol, 4.0 eq.) was added dropwise and the reaction mixture was allowed to warm to room temperature and stirred for 12 h. The solvent was reduced under reduced pressure, the residue was dissolved in DCM (200 mL) and washed with an aqueous 5% KH_2PO_4 solution (3 x 100 mL). The organic layer was dried over $MgSO_4$ and the solvent was removed under reduced pressure. The crude product was purified by column chromatography (Hexane/EtOAc/NEt_3 8:2:0.1) to yield 8.79 g (14.1 mmol, 48%) of the title compound.

^{1}H-NMR (400 MHz, CD_2Cl_2): δ =7.42-7.39 (m, 12H, CH_{ar}), 7.31-7.19 (m, 18H, CH_{ar}), 2.37-2.20 (m, 8H, CH_2) ppm.

^{13}C-NMR (100 MHz, CD_2Cl_2): δ = 145.6 ($C_{q,ar}$), 130.1 (CH_{ar}), 128.4 (CH_{ar}), 127.2 (CH_{ar}), 67.0 (C_q),48.3 (CH_2), 32.9 (CH_2) ppm.

HR-MS (ESI+): calcd. for $[M+H]^+$: 622.2597; found: 622.2590.

Synthesis of Boc-Glu(SEA{Trt}$_2$)-O*t*Bu (9)[155]

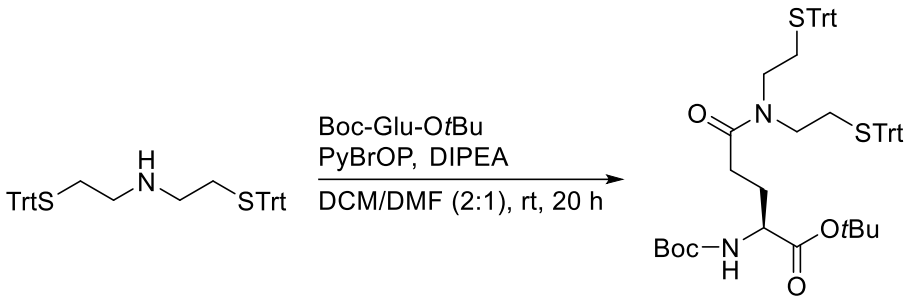

8 **9**

Boc-Glu-O*t*Bu (1.87 g, 6.15 mmol, 1.0 eq.) was dissolved in DMF (22.5 mL) and added dropwise to a solution of bis({2-[triphenylmethyl]sulfanyl}ethyl)amine (7.50 g, 12.3 mmol, 2.0 eq.) in DCM (45 mL). Then, PyBrOP (2.87 g, 6.15 mmol, 1.0 eq.) and DIPEA (2.38 g, 3.21 mL, 18.5 mmol, 3.0 eq.) were added and the resulting mixture was stirred for 20 h at room temperature. The solvent was removed under reduced pressure and the crude product was purified by column chromatography (hexane/EtOAc/NEt_3 8:2:0.1) to yield 2.87 g (3.16 mmol, 51%) of the title compound.

^{1}H-NMR (400 MHz, CD_2Cl_2): δ =7.40-7.19 (m, 30H, C*H*$_{ar}$), 5.15 (d, $^3J_{H,H}$ = 7.5 Hz, 1H, N*H*), 3.98 (m, 1H, α-C*H*), 2.78-2.70 (m, 4H, C*H*$_2$), 2.28-2.24 (m, 2H, C*H*$_2$), 2.16 (t, $^3J_{H,H}$ = 7.8 Hz 2H, C*H*$_2$), 1.99-1.90 (m, 3H, C*H*$_2$), 1.78-1.72 (m, 1H, C*H*$_2$), 1.44 (s, 9H, C*H*$_3$), 1.41 (s, 9H, C*H*$_3$) ppm.

^{13}C-NMR (100 MHz, CD_2Cl_2): δ = 172.2 (*C*O), 171.9 (*C*O), 156.0 (*C*O$_{carbamate}$), 145.4 (*C*$_{q,ar}$), 145.1 (*C*$_{q,ar}$), 130.2 (*C*H$_{ar}$), 130.1 (*C*H$_{ar}$), 128.6 (*C*H$_{ar}$), 128.5 (*C*H$_{ar}$), 127.4 (*C*H$_{ar}$), 127.3 (*C*H$_{ar}$), 82.0 (*C*$_{q,tBu}$), 79.8 (*C*$_{q,tBu}$), 67.7 (*C*$_{q,Trt}$), 67.3 (*C*$_{q,Trt}$), 60.8 (α-*C*H), 47.8 (*C*H$_2$), 45.8 (*C*H$_2$), 30.9 (*C*H$_2$), 30.0 (*C*H$_2$), 29.5 (*C*H$_2$) 28.7 (*C*H$_3$), 28.3 (*C*H$_3$), 28.0 (*C*H$_2$) ppm.

HR-MS (ESI+): calcd. for $[M+H]^+$: 907.4173; found: 907.4168.

Synthesis of Boc-Glu(SEA^{off})-O*t*Bu (10)[155]

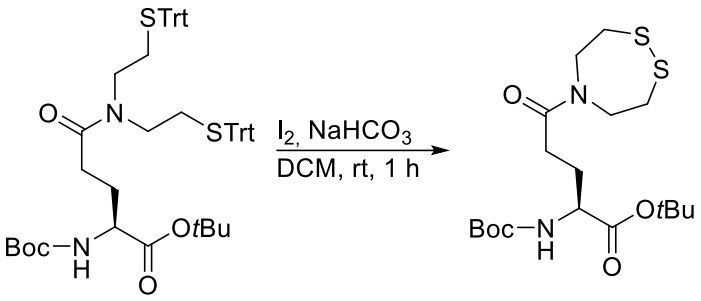

9 **10**

Boc-Glu(SEA{Trt}$_2$)-O*t*Bu (2.87 g, 3.16 mmol, 1.0 eq.) was dissolved in DCM (175 mL) and $NaHCO_3$ (0.80 g, 9.48 mmol 3.0 eq.) and I_2 (2.41 g, 9.48 mmol, 3.0 eq.) were added. The solution was stirred for 1 h at room temperature and then quenched with an aqueous 3 M $Na_2S_2O_3$ solution (100 mL). The aqueous layer was extracted with DCM (3 x 100 mL), the combined organic layers were dried over $MgSO_4$ and the solvent was removed under reduced pressure. The crude product was purified by column chromatography (hexane/EtOAc/NEt_3 1:1:0.1) to yield 1.03 g (2.45 mmol, 78%) of the title compound.

^{1}H-NMR (400 MHz, CD_2Cl_2): δ = 5.21 (d, $^3J_{H,H}$ = 7.7 Hz, 1H, N*H*), 4.15 (m, 1H, α-C*H*), 3.96-3.77 (m, 4H, C*H*$_2$), 3.07 (t, $^3J_{H,H}$ = 5.8 Hz, 2H, C*H*$_2$), 2.91 (td, $^3J_{H,H}$ = 5.7 Hz, 2.0 Hz, 2H, C*H*$_2$), 2.48-2.30 (m, 2H, C*H*$_2$), 2.25-2.16 (m, 1H, C*H*$_2$), 2.00-1.91 (m, 1H, C*H*$_2$) 2.16 (t, $^3J_{H,H}$ = 7.8 Hz, 2H, C*H*$_2$), 1.99-1.90 (m, 3H, C*H*$_2$), 1.78-1.72 (m, 1H, C*H*$_2$), 1.46 (s, 9H, C*H*$_3$), 1.43 (s, 9H, C*H*$_3$) ppm.

^{13}C-NMR (100 MHz, CD_2Cl_2): δ = 172.3 (*C*O), 171.6 (*C*O), 155.7 (*C*O$_{carbamate}$), 82.2 (*C*$_{q,tBu}$), 79.8 (*C*$_{q,tBu}$), 53.9 (α-*C*H), 52.5 (*C*H$_2$), 50.4 (*C*H$_2$), 39.6 (*C*H$_2$), 35.7 (*C*H$_2$), 29.3 (*C*H$_2$), 28.4 (*C*H$_3$), 28.1 (*C*H$_3$) ppm.

HR-MS (ESI+): calcd. for $[M+H]^+$: 421.1825; found: 421.1830.

Synthesis of Fmoc-Glu(SEA^{off})-OH (11)[155]

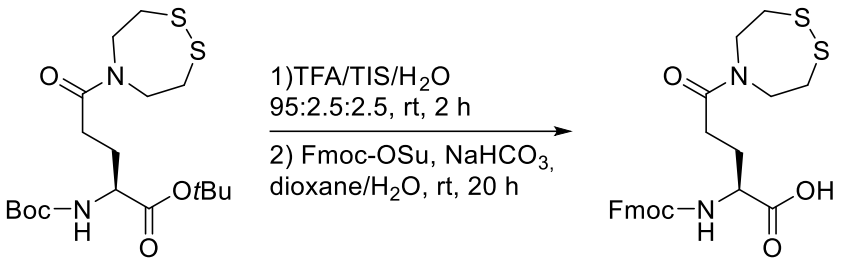

10 **11**

Boc-Glu(SEA^{off})-O*t*Bu (1.03 g, 2.46 mmol, 1.0 eq.) was dissolved in TFA/TIS/H_2O (95:2.5:2.5, 20 mL), stirred for 2 h at room temperature and the solvent was removed under a N_2-stream. The residue was dissolved in H_2O (30 mL), washed with DCM (3 x 20 mL) and the aqueous phase lyophilized. The intermediate was used without further purification. H_2N-Glu(SEA^{off})-OH · TFA (0.93 g, 2.46 mmol, 1.0 eq.) and $NaHCO_3$ (0.83 g, 9.84 mmol, 4.0 eq.) were dissolved in H_2O (30 mL) and cooled to 0 °C. Fmoc-OSu (1.24 g, 3.69 mmol, 1.5 eq.) in dioxane (50 mL) was added and the pH was adjusted to 9 with an aqueous 0.1 M $NaHCO_3$ solution. The reaction mixture was allowed to warm to room temperature and was stirred for 20 h. The solution was washed with Et_2O (2 x 75 mL), the aqueous phase was adjusted to pH 1 with 1 M HCl and extracted with DCM (3 x 100 mL). The combined organic layers were dried over $NaSO_4$, the solvent was removed under reduced pressure and the crude product was purified by preparative HPLC to yield 0.44 g (0.90 mmol, 37%) of the title compound.

HPLC (column 1, gradient: 40-90 %B in 30 min): t_R = 24.21 min.

UHPLC (gradient: 30-80% B in 20 min): t_R = 9.30 min.

^{1}H-NMR (400 MHz, $(CD_3)_2SO$): δ = 12.63 (s_{br}, 1H, CO_2H), 7.89 (d, $^3J_{H,H}$ = 7.8 Hz, 2H, CH_{ar}), 7.74-7.66 (m, 2H, CH_{ar}), 7.42 (t, $^3J_{H,H}$ = 7.3 Hz, 2H, CH_{ar}), 7.33 (t, $^3J_{H,H}$ = 7.3 Hz, 2H, CH_{ar}), 4.29-4.20 (m, 3H), 4.05-3.98 (m, 1H), 3.8-3.75 (m, 4H), 2.99-2.94 (m, 4H), 2.45-2.33 (m, 2H), 2.08-1.76 (m, 2H) ppm.

^{13}C-NMR (100 MHz, $(CD_3)_2SO$): δ = 172.9 (*C*O), 172.2 (*C*O), 156.2 ($CO_{carbamate}$), 143.9 ($C_{q,Fmoc}$), 143.7 ($C_{q,Fmoc}$), 141.1 ($C_{q,Fmoc}$), 127.5 (*C*H_{ar}), 126.9 (*C*H_{ar}), 124.9 (*C*H_{ar}), 119.8 (*C*H_{ar}), 53.3 (α-*C*H), 52.2 (*C*H_2), 50.1 (*C*H_2), 47.1 (*C*-9_{Fmoc}), 39.2 (*C*H_2), 35.3 (*C*H_2), 29.2 (*C*H_2), 27.6 (*C*H_2) ppm.

HR-MS (ESI+): calcd. for $[M+H]^+$: 487.1356, found: 487.1360.

Synthesis of 2-(4,5-dimethoxy-2-nitrophenyl)oxirane (13)

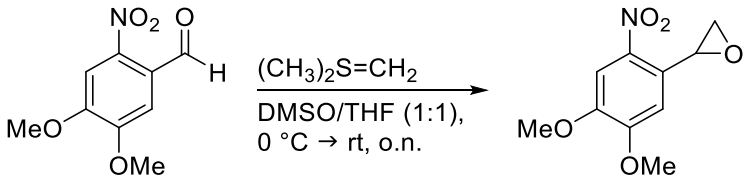

12 **13**

Synthesis was performed according to a protocol adapted from literature.[224]

NaH (1.88 g, 46.9 mmol, 2.0 eq.) was suspended in DMSO (75 mL) and stirred for 1.5 h at 60 °C. The solution was allowed to cool to room temperature and Me_3SI (9.57 g, 46.9 mmol, 2.0 eq.) was added in three portions at 0 °C and stirred for 1 h. 4,5-Dimethoxy-2-nitrobenzaldehyde (5.00 g, 23.5 mmol, 1.0 eq.) in THF (75 mL) was added dropwise at 0 °C and the reaction mixture was allowed to warm to room temperature over night. The reaction was quenched by the addition of a saturated aqueous NH_4Cl-solution (100 mL). The solvent was removed under reduced pressure and the crude product was extracted with diethyl ether (3 x 150 mL). The combined organic layers were dried over $MgSO_4$ and the solvent was removed under reduced pressure. The crude product was purified by column chromatography (pentane/EtOAc 8:1 → 4:1) to yield 2.59 g (11.5 mmol, 49%) of the title compound.

^{1}H-NMR (400 MHz, $CDCl_3$): δ = 7.73 (s, 1H, CH_{ar}), 7.04 (s, 1H, CH_{ar}), 4.54-4.52 (dd, $^3J_{H,H}$ = 4.4 Hz, 2.6 Hz, 1H, PhCH), 3.98 (s, 3H, OCH_3), 3.96 (s, 3H, OCH_3), 3.31-3.28 (dd, $^2J_{H,H}$ = 5.5 Hz, $^3J_{H,H}$ = 4.4 Hz, 1H, CHCH_2), 2.65-2.63 (dd, $^2J_{H,H}$ = 5.5 Hz, $^3J_{H,H}$ = 2.6 Hz, 1H, CHCH_2).

^{13}C-NMR (100 MHz, $CDCl_3$): δ = 154.4 ($C_{q,ar}$), 148.3 ($C_{q,ar}$), 140.3 ($C_{q,ar}$), 130.0 ($C_{q,ar}$), 108.1 (CH$_{ar}$), 107.9 (CH$_{ar}$), 56.7 (OCH$_3$), 56.6 (OCH$_3$), 51.4 ($C_{epoxide}$), 50.8 ($C_{epoxide}$) ppm.

HR-MS (ESI+): calcd. for $[M+H]^+$: 226.0710; found: 226.0714.

Synthesis of 2-azido-1-(4,5-dimethoxy-2-nitrophenyl)ethanol (14)[12]

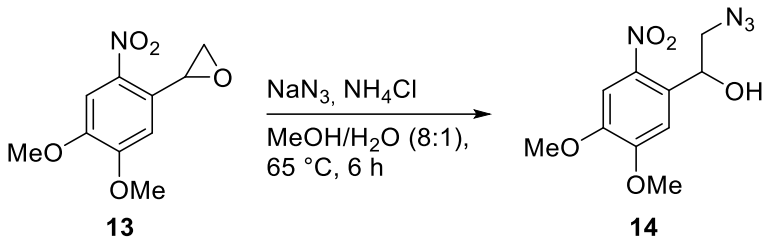

13 **14**

2-(4,5-Dimethoxy-2-nitrophenyl)oxirane (2.59 g, 11.5 mmol, 1.0 eq.) and NH_4Cl (1.23 g, 23 mmol, 2.0 eq.) were dissolved in MeOH/H_2O 8:1 (45 mL). Sodium azide (5.98 g, 91.9 mmol, 8.0 eq.) was added and the solution was stirred for 6 h at 65 °C. The solvent was removed under reduced pressure and the residue was diluted with water and extracted with Et_2O (3 x 75 mL). The combined organic layers were dried over $MgSO_4$ and the solvent was removed *in vacuo*. The crude product was purified by column chromatography (pentane/EtOAc 5:1) to yield 1.62 g (6.02 mmol, 52%) of the title compound.

^{1}H-NMR (400 MHz, $CDCl_3$): δ = 7.67 (s, 1H, C*H*$_{ar}$), 7.35 (s, 1H, C*H*$_{ar}$), 5.64-5.61 (dd, $^3J_{H,H}$ = 7.6 Hz, 2.8 Hz, 1H, PhC*H*), 4.00 (s, 3H, OC*H*$_3$), 3.94 (s, 3H, OC*H*$_3$), 3.72-3.68 (dd, $^2J_{H,H}$ = 12.6 Hz, $^3J_{H,H}$ = 2.8 Hz, 1H, C*H*$_2$N$_3$), 2.65-2.63 (dd, $^2J_{H,H}$ = 12.6 Hz, $^3J_{H,H}$ = 7.6 Hz, 1H, C*H*$_2$N$_3$) ppm.

^{13}C-NMR (100 MHz, $CDCl_3$): δ = 154.0 (*C*$_{q,ar}$), 148.4 (*C*$_{q,ar}$), 139.6 (*C*$_{q,ar}$), 131.7 (*C*$_{q,ar}$), 109.5 (*C*H$_{ar}$), 108.0 (*C*H$_{ar}$), 69.3 (Ph*C*H), 57.3 (*C*H$_2$N$_3$), 56.7 (O*C*H$_3$), 56.5 (O*C*H$_3$) ppm.

HR-MS (ESI+): calcd. for $[M+Na]^+$: 291.0700; found: 291.0702.

Synthesis of 2-azido-1-(4,5-dimethoxy-2-nitrophenyl)ethyl *N*-succinimidyl carbonate (15)

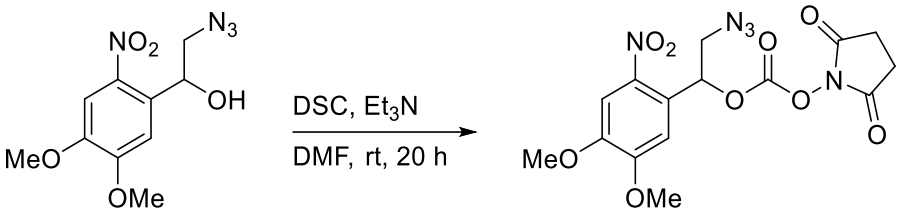

14 **15**

Synthesis was performed according to a protocol adapted from literature.[12]
2-Azido-1-(4,5-dimethoxy-2-nitrophenyl)ethanol (1.62 g, 6.02 mmol, 1.0 eq.) and *N,N'*-disuccinimidyl carbonate (2.47 g, 9.63 mmol, 1.6 eq.) were dissolved in DMF (35 mL). Et_3N (1.83 g, 18.1 mmol, 3.0 eq.) was added and the reaction mixture was stirred for 20 h at room temperature. The solvent was removed under reduced pressure and the crude product was purified by column chromatography (pentane/EtOAc 1:1) to yield 2.02 g (4.95 mmol, 82%) of the title compound.
^{1}H-NMR (400 MHz, $CDCl_3$): δ = 7.70 (s, 1H, C*H*$_{ar}$), 7.10 (s, 1H, C*H*$_{ar}$), 6.56-6.54 (dd, $^3J_{H,H}$ = 6.3 Hz, 2.7 Hz, 1H, PhC*H*), 4.09 (s, 3H, OC*H*$_3$), 3.96 (s, 3H, OC*H*$_3$), 3.96-3.92 (m, 1H, C*H*$_2$N$_3$), 2.65-2.63 (dd, $^2J_{H,H}$ = 13.6 Hz, $^3J_{H,H}$ = 6.3 Hz, 1H, C*H*$_2$N$_3$), 2.81 (s, 4H, C*H*$_2$) ppm.
^{13}C-NMR (100 MHz, $CDCl_3$): δ = 168.3 (*C*O$_{succinimide}$), 154.5 (*C*$_{q,ar}$), 150.7 (*C*O$_{carbonate}$), 149.3 (*C*$_{q,ar}$), 139.7 (*C*$_{q,ar}$), 126.0 (*C*$_{q,ar}$), 108.5 (*C*H$_{ar}$), 108.4 (*C*H$_{ar}$), 78.3 (Ph*C*H), 56.9 (*C*H$_3$), 56.6 (*C*H$_3$), 54.3 (*C*H$_2$N$_3$), 25.6 (*C*H$_2$) ppm.
HR-MS (ESI+): calcd. for $[M+Na]^+$: 432.0762; found: 432.0755.

Synthesis of 7-diethylamino-4-formylcoumarin (31)

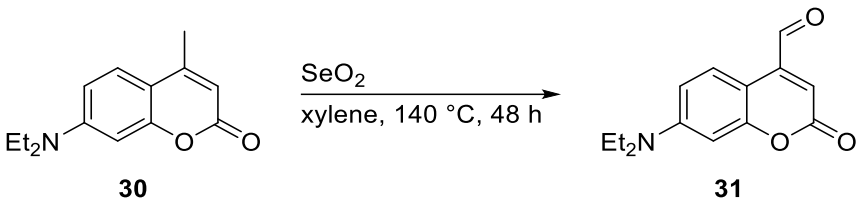

30 **31**

Synthesis was performed according to a protocol adapted from literature.[225]

7-Diethylamino-4-methylcoumarin (4.21 g, 18.2 mmol, 1.0 eq.) and selenium dioxide (2.10 g, 18.9 mmol, 1.04 eq.) were dissolved in xylene (350 mL). The reaction mixture was refluxed for 48 h, allowed to cool to room temperature and filtered. The solvent was removed under reduced pressure and the crude product was purified by column chromatography (DCM/acetone 95:5) to yield 2.23 g (9.10 mmol, 50%) of the title compound.

^{1}H-NMR (300 MHz, $CDCl_3$): δ = 10.00 (s, 1H, C*H*O), 8.27 (d, $^{3}J_{HH}$ = 9.2 Hz, 1H, *H*-5), 6.63-6.59 (dd, $^{3}J_{HH}$ = 9.2 Hz, $^{4}J_{HH}$ = 2.7 Hz, 1H, *H*-6), 6.50 (d, $^{4}J_{HH}$ = 2.7 Hz, 1H, *H*-8), 6.42 (s, 1H, *H*-3), 3.42 (q, $^{3}J_{HH}$ = 7.1 Hz, 4H, C*H*$_2$CH$_3$), 1.20 (t, $^{3}J_{HH}$ = 7.1 Hz, 6H, CH$_2$C*H*$_3$) ppm.

^{13}C-NMR (75 MHz, $CDCl_3$): δ = 192.4 (*C*HO), 161.7 (*C*-2), 157.3 (*C*-8'), 151.0 (*C*-4), 143.9 (*C*-7), 127.0 (*C*-5), 117.3 (*C*-4'), 109.6 (*C*-6), 103.8 (*C*-3), 97.7 (*C*-8), 45.0 (*C*H$_2$CH$_3$), 12.6 (CH$_2$*C*H$_3$) ppm.

HR-MS (ESI+): calcd. for $[M+H]^+$: 246.1125, found: 246.1123.

Synthesis of 7-diethylamino-4-(1-hydroxy-3-butyn-1-yl)-coumarin (32)

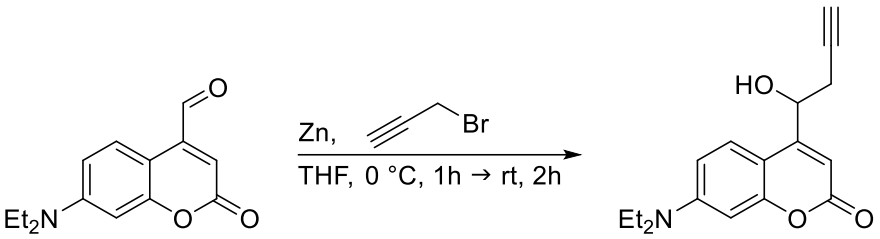

31 **32**

Synthesis was performed according to a protocol adapted from literature.[152]

Propargyl bromide (80 wt.% in toluene, 2.37 mL, 21.3 mmol, 2.5 eq.) was added to a mixture of zinc (3.34 g, 51.1 mmol, 6.0 eq.) in THF (25 mL) at 0 °C. The solution was stirred for 1 h. 7-Diethylamino-4-formylcoumarin (2.09 g, 8.52 mmol, 1.0 eq.) was dissolved in THF (8 mL) and added to the reaction mixture. The mixture was allowed to warm to room temperature, stirred for 2 h and quenched by the slow addition of an aqueous saturated NH_4Cl solution (35 mL). The reaction mixture was filtered, treated with an aqueous 10% HCl solution (100 mL) and extracted with EtOAc (3 x 75 mL). The combined organic layers were dried over $MgSO_4$ and the solvent was removed under reduced pressure. The crude product was purified by column chromatography (DCM/acetone 95:5) to yield 1.02 g (3.57 mmol, 42%) of the title compound.

^{1}H-NMR (300 MHz, $CDCl_3$): δ = 7.38 (d, $^3J_{HH}$ = 9.0 Hz, 1H, *H*-5), 6.53-6.51 (dd, $^3J_{HH}$ = 9.0 Hz, $^4J_{HH}$ = 2.6 Hz, 1H, *H*-6), 6.41 (d, $^4J_{HH}$ = 2.6 Hz, 1H, *H*-8), 6.25 (d, $^5J_{HH}$ = 0.9 Hz, 1H, *H*-3), 5.11-5.09 (m, 1H, C*H*OH), 3.65 (d, $^3J_{HH}$ = 4.2 Hz, 1H, O*H*), 3.35 (q, $^3J_{HH}$ = 7.1 Hz, 4H, CH_2CH$_3$), 2.78-2.74 (ddd, $^2J_{HH}$ = 17.0 Hz, $^3J_{HH}$ = 7.4 Hz, $^4J_{HH}$ = 2.6 Hz, 1H, CHCH_2), 2.62-2.57 (ddd, $^2J_{HH}$ = 17.0 Hz, $^3J_{HH}$ = 4.7 Hz, $^4J_{HH}$= 2.7 Hz, 1H, CHCH_2), 2.08 (t, $^4J_{HH}$ = 2.6 Hz, 1H, CC*H*), 1.14 (t, $^3J_{HH}$ = 7.1 Hz, 6H, CH$_2$CH_3) ppm.

^{13}C-NMR (75 MHz, $CDCl_3$): δ = 162.2 (*C*-2), 156.6 (*C*-8'), 155.2 (*C*-4), 150.4 (*C*-7), 124.7 (*C*-5), 108.8 (*C*-6), 106.1 (*C*-3), 98.3 (*C*-8), 79.4 (C*C*H), 68.2 (C*H*OH), 45.0 (*C*H$_2$CH$_3$), 28.0 (CH*C*H$_2$), 12.7 (CH$_2$*C*H$_3$) ppm.

HR-MS (ESI+): calcd. for $[M+H]^+$: 286.1438; found: 286.1440.

Synthesis of 1-(7-diethylamino-coumarinyl)-3-butynyl *N*-succinimidyl carbonate (33)

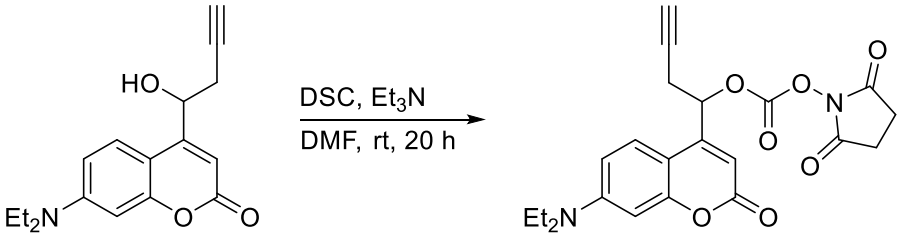

32 **33**

N,N'-Disuccinimidyl carbonate (0.47 g, 1.84 mmol, 1.60 eq.) and **32** (0.32 g, 1.15 mmol, 1.00 eq.) were dissolved in 7 ml DMF. NEt_3 (0.16 ml, 1.15 mmol, 1.00 eq.) was slowly added and the reaction was stirred for 20 h at room temperature. The solvent was removed under reduced pressure and the crude product was purified by column chromatography (DCM → DCM/acetone 19:1) to yield 0.23 g (0.54 mmol, 47%) of the title compound.

^{1}H-NMR (300 MHz, $CDCl_3$): δ = 7.35 (d, $^3J_{HH}$ = 9.0 Hz, 1H, *H*-5), 6.62-6.58 (dd, $^3J_{HH}$ = 9.0 Hz, $^4J_{HH}$ = 2.6 Hz, 1H, *H*-6), 6.53 (d, $^4J_{HH}$ = 2.6 Hz, 1H, *H*-8), 6.23 (d, $^5J_{HH}$ = 0.8 Hz, 1H, *H*-3), 6.05-6.00 (m, 1H, α-C*H*), 3.42 (q, $^3J_{HH}$ = 7.1 Hz, 4H, CH_2CH_3), 2.97-2.92 (m, 2H, β-CH_2), 2.84 (s, 4H, $CH_{2,succin.}$), 2.15 (t, $^4J_{HH}$ = 2.6 Hz, 1H, CC*H*), 1.21 (t, $^3J_{HH}$ = 7.1 Hz, 6H, CH_2CH_3) ppm.

^{13}C-NMR (75 MHz, $CDCl_3$): δ = 168.1 ($CO_{succin.}$), 161.3 ($CO_{coum.}$), 156.7 (*C*-8'), 151.0 ($CO_{carbonate}$), 150.8 (*C*-7), 149.4 (*C*-4), 124.5 (*C*-5), 109.0 (*C*-6), 107.1 (*C*-3), 105.2 (*C*-4'), 98.4 (*C*-8), 76.9 (*C*CH), 76.7 (α-*C*H), 73.3 (C*C*H) 45.0 (CH_2CH_3), 25.7 ($CH_{2,succin.}$), 25.4 (β-*C*H), 12.7 (CH_2CH_3) ppm.

HR-MS (ESI+): calcd. for $[M+H]^+$: 427.1500; found: 427.1487.

Synthesis of Boc-4-pinacolborane-phenylalanine (51)

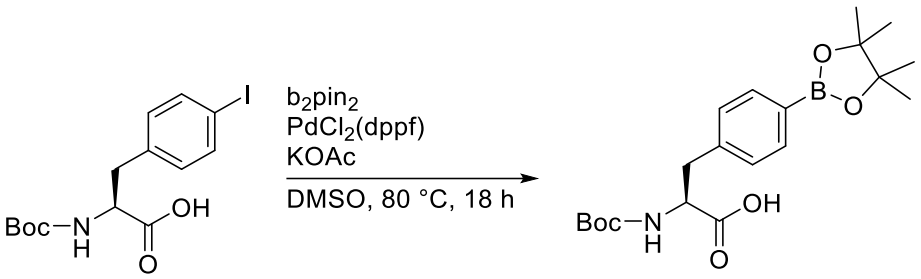

50 **51**

Synthesis was carried out according to a protocol adapted from literature.[192]

Boc-*p*IPhe-OH (3.00 g, 7.67 mmol, 1.0 eq.), B_2pin_2 (3.89 g, 15.3 mmol, 2.0 eq.), $PdCl_2$(dppf) (0.56 g, 0.77 mmol, 0.1 eq.), dppf (0.43 g, 0.77 mmol, 0.1 eq.) and KOAc (3.01 g, 30.7 mmol, 4.0 eq.) were suspended in dry DMSO (50 mL). The reaction mixture was stirred overnight at 80 °C. The reaction mixture was allowed to cool to room temperature and then diluted with a saturated aqueous NaCl solution (250 mL). The aqueous phase was extracted with EtOAc (3 x 150 mL), the combined organic phases were dried over $MgSO_4$ and the solvent was removed under reduced pressure. The crude product was purified by column chromatography (hexane/EtOAc 3:2 → EtOAc + 0.1% HOAc) and lyophilized from dioxane/H_2O to yield 1.91 g (4.89 mmol, 64%) of the title compound.

^{1}H-NMR (500 MHz, $CDCl_3$): δ = 7.75 (d, $^3J_{H,H}$ = 7.9 Hz, 2H, CH_{ar}), 7.19 (d, $^3J_{H,H}$ = 7.9 Hz, 2H, CH_{ar}), 4.95 (d, $^3J_{H,H}$ = 7.8 Hz, 1H, N*H*), 4.60 (m, 1H, α-C*H*), 3.21 (dd, $^3J_{H,H}$ = 14.0 Hz, $^2J_{H,H}$ = 5.8 Hz, 1H, β-CH_2), 3.10 (dd, $^3J_{H,H}$ = 14.0 Hz, $^2J_{H,H}$ = 5.8 Hz, 1H, β-CH_2), 1.41 (s, 9H, $CH_{3,bpin}$), 1.33 (s, 12H, $CH_{3,tBu}$) ppm.

^{13}C-NMR (125 MHz, $CDCl_3$): δ = 175.6 (*C*O_2H), 155.5 (*C*$O_{carbamate}$), 139.3 ($C_{ar,bpin}$), 135.2 (C_{ar}), 129.0 (C_{ar}), 84.0 ($C_{q,bpin}$), 80.4 ($C_{q,tBu}$), 54.3 (α-*C*H), 37.9 (β-*C*H_2), 28.4 (*C*$H_{3,tBu}$), 25.0 (*C*$H_{3,bpin}$) ppm.

HR-MS (ESI+): calcd. for $[M+H]^+$: 392.2243; found: 392.2225.

Synthesis of 4-pinacolborane-phenylalanine (52)

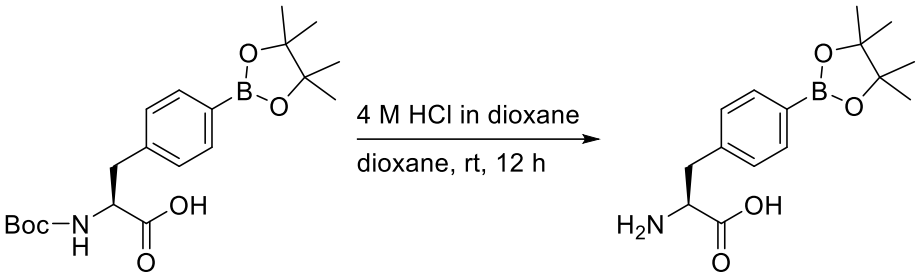

51 **52**

Synthesis was carried out according to a protocol adapted from literature.[192]

51 (1.90 g, 4.86 mmol) was dissolved in dioxane (2 mL) and 4 M HCl in dioxane (6 mL) were added. The reaction mixture was stirred over night and purged with N_2 gas for 20 min to remove the HCl gas. The residue was taken up in H_2O (20 mL) and lyophilized to yield 1.41 g (4.84 mmol, quant.) of the title compound.

^{1}H-NMR (500 MHz, CD_3OD): δ = 7.75 (d, $^3J_{H,H}$ = 8.1 Hz, 2H, CH_{ar}), 7.32 (d, $^3J_{H,H}$ = 8.1 Hz, 2H, CH_{ar}), 4.28 (dd, $^3J_{H,H}$ = 7.8 Hz, 5.5 Hz, 1H, α-CH), 3.34 (dd, $^3J_{H,H}$ = 5.5 Hz, $^2J_{H,H}$ = 14.8 Hz, 1H, β-CH_2), 3.19 (dd, $^3J_{HH}$ = 7.8 Hz, $^2J_{HH}$ = 14.8 Hz, 1H, β-CH_2), 1.34 (s, 12H, C$H_{3,bpin}$) ppm.

^{13}C-NMR (125 MHz, CD_3OD): δ = 171.1 (CO_2H), 138.9 ($C_{ar,bpin}$), 136.4 (C_{ar}), 129.9 (C_{ar}), 85.2 ($C_{q,bpin}$), 54.9 (α-CH), 37.5 (β-C2), 25.2 (CH$_{3,bpin}$) ppm.

HR-MS (ESI+): calcd. for $[M+H]^+$: 292.1728; found: 292.1726.

Synthesis of Fmoc-4-borono-phenylalanine (53, Fmoc-Bpa)

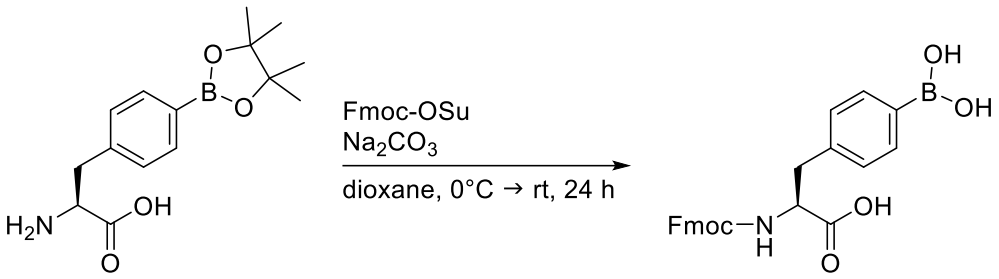

52 **53**

Synthesis was carried out according to a protocol adapted from literature.[192]

52 (0.30 g, 1.03 mmol, 1.0 eq.) was dissolved in a 10% aqueous Na_2CO_3 solution (25 mL) and cooled to 0 °C. Fmoc-Osu (0.42 g, 1.24 mmol, 1.2 eq.) was dissolved in dioxane (10 mL) and slowly added. The reaction mixture was allowed to warm to room temperature and stirred over night, after which time H_2O/dioxane (1:1, 30 mL) was added and the reaction mixture was stirred for another 8 h. 1 M aqueous HCl (100 mL) was added and the aqueous phase was extracted with EtOAc (3 x 150 mL). The combined organic layers were washed with brine (100 mL), dried over $MgSO_4$ and the solvent was removed under reduced pressure. The crude product was dissolved in MeOH (2 mL) and purified by preparative HPLC to yield 0.21 g (0.49 mmol, 48%) of the title compound.

HPLC (column 1, gradient: 50-99% C in 30 min): t_R =27.64 min.

UHPLC (gradient: 50-90% C in 20 min): t_R = 8.14 min.

^{1}H-NMR (300 MHz, $(CD_3)_3SO$): δ = 7.97 (s_{br}, 2H, B(O*H*)$_2$), 7.88 (d, $^3J_{H,H}$ = 7.6 Hz, 2H, C*H*$_{ar}$), 7.74-7.70 (m, 2H, C*H*$_{ar}$), 7.64 (t, $^3J_{H,H}$ = 7.6 Hz, 2H, C*H*$_{ar}$), 7.43-7.37 (m, 2H, C*H*$_{ar}$), 7.34-7.20 (m, 4H, C*H*$_{ar}$), 4.22-4.15 (m, 4H, α-C*H*$_{Fmoc}$, β-C*H*$_{Fmoc}$, α-C*H*), 3.08 (dd, $^2J_{HH}$ = 13.5 Hz, $^3J_{HH}$ = 4.2 Hz, 1H, β-C*H*$_2$), 2.87 (dd, $^2J_{HH}$ = 13.5 Hz, $^3J_{HH}$ = 10.4 Hz, 1H, β-C*H*$_2$) ppm.

^{13}C-NMR (75 MHz, $(CD_3)_3SO$): δ = 173.4 (*C*O$_2$H), 156.0 (*C*O$_{carbamate}$), 143.9 (*C*$_q$), 140.7 (*C*$_q$), 139.9 (C$_q$) 134.1 (*C*H$_{ar}$), 128.2 (*C*H$_{ar}$), 127.7 (*C*H$_{ar}$), 127.1 (*C*H$_{ar}$), 125.3 (*C*H$_{ar}$), 120.1 (*C*H$_{ar}$), 65.7 (β-*C*H$_{2,Fmoc}$), 55.4 (α-*C*H), 46.6 (α-*C*H), 36.5 (β-*C*H$_2$) ppm.

HR-MS (ESI+): calcd. for $[M+CH_2-H]^-$: 444.1628; found: 444.1624 (corresponds to methyl ester of the boronic acid)

Synthesis of *N*-Boc-4-(aminooxy)butanoic acid (86)[54]

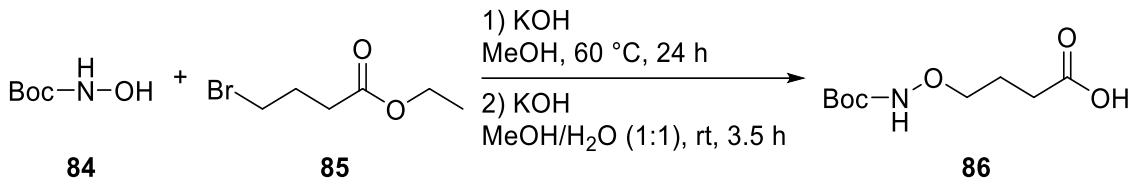

84 **85** **86**

N-Boc-hydroxylamine (5.00 g, 37.6 mmol, 1.0 eq.) and KOH (2.11 g, 37.6 mmol, 1.0 eq.) were dissolved in MeOH (55 mL) and stirred at 60 °C for 30 min. Then, ethyl 4-bromobutyrate (7.33 g, 5.28 mL, 37.6 mmol, 1.0 eq.) was added and the resulting mixture was stirred at 60 °C for 24 h. The solvent was removed under reduced pressure and H_2O (100 mL) was added to the residue before extraction with EtOAc (3 x 75 mL). The combined organic phases were dried over Na_2SO_4, filtered and the solvent was removed under reduced pressure. The crude product was purified by column chromatography (hexane/ethyl acetate 9:1 → 4:1) to yield the intermediate as a colorless oil. The oil was dissolved in MeOH/H_2O (1:1 v/v, 30 mL), KOH (1.30 g, 23.1 mmol, 1.5 eq.) was added and the solution was stirred for 3.5 h at room temperature. The reaction mixture was extracted with DCM (3 x 50 mL), the aqueous phase was acidified with 1 M HCl to pH 2 and extracted once more with DCM (3 x 50 mL). The combined organic layers were dried over Na_2SO_4, filtered and the solvent removed *in vacuo* to yield 3.46 g (15.8 mmol, 42%) of the title compound.

^{1}H-NMR (600 MHz, $CDCl_3$): δ = 7.48 (s_{br}, 1H, N*H*), 3.89 (t, $^3J_{H,H}$ = 6.0 Hz, 2H, *H*-4), 2.51 (t, $^3J_{H,H}$ = 7.1 Hz, 2H, *H*-2), 1.95 (quint, $^3J_{H,H}$ = 7.1 Hz, 6.0 Hz, 2H, *H*-3), 1.48 (s, 9H, C$H_{3,t\mathrm{Bu}}$) ppm.

^{13}C-NMR (150 MHz, $CDCl_3$): δ = 178.8 (*C*O_2H), 157.4 (*C*$O_{carbamate}$), 82.1 ($C_{q,t\mathrm{Bu}}$), 75.6 (*C*-4), 30.7 (*C*-2), 28.3 (*C*$H_{3,t\mathrm{Bu}}$), 23.2 (*C*-3) ppm.

HR-MS (ESI+): calcd. for $[M+H]^+$: 220.1179; found: 220.1178.

Synthesis of thiazolidine 2-carboxylic acid (90)[212]

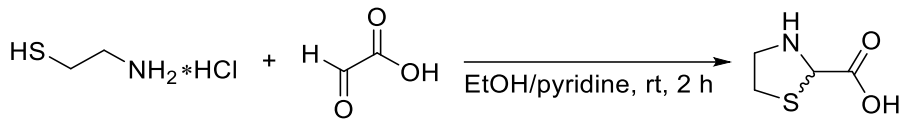

88 **89** **90**

Glyoxylic acid (50wt. % in H_2O, 6.52 g, 44.0 mmol, 1.0 eq.) was dissolved in EtOH (10 mL). A solution of 2-aminoethanethiol hydrochloride (5.00 g, 44.0 mmol, 1.0 eq) in EtOH/pyridine (5:2 (v/v), 28 mL) was added and the resulting mixture was stirred at room temperature for 2 h. The resulting precipitate was filtered, washed with EtOH and dried under reduced pressure to yield 4.48 g (33.6 mmol, 76%) of the title compound.

^{1}H-NMR (600 MHz, D_2O): δ = 5.18 (s, 1H, *H*-2), 3.82-3.76 (m, 1H, C*H*), 3.71-3.64 (m, 1H, C*H*), 3.27-3.24 (m, 2H, CH_2) ppm.

^{13}C-NMR (150 MHz, D_2O): δ = 171.7 (CO_2H), 62.3 (*C*-2), 49.3 (CH_2), 29.5 (CH_2) ppm.

HR-MS (ESI+): calcd. for $[M+H]^+$: 134.0270; found: 134.0271.

Synthesis of *N*-Boc-thiazolidine-2-carboxylic acid (91)[212]

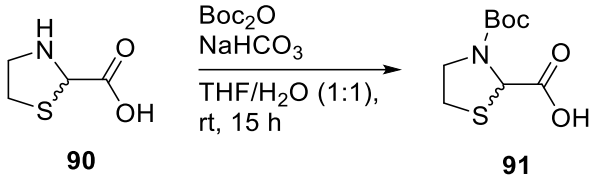

90 **91**

90 (4.47 g, 33.6 mmol, 1.0 eq.) was dissolved in THF (100 mL) and the solution was cooled to 0 °C. Di-*tert*-butyl dicarbonate (18.3 g, 83.9 mmol, 2.5 eq.) was added, followed by a solution of $NaHCO_3$ (16.6 g, 0.20 mol, 6.0 eq) in H_2O (100 mL). The mixture was allowed to warm to room temperature and was stirred for 15 h. The organic solvent was removed under reduced pressure, H_2O was added, and the aqueous phase was washed with Et_2O (3 x 75 mL). The aqueous phase was acidified with conc. HCl to pH 2 and extracted with DCM (3 x 75 mL). The combined organic phases were dried over Na_2SO_4, filtered and the solvent was removed under reduced pressure to yield 7.56 g (32.4 mmol, 96%) of the title compound.

^{1}H-NMR (600 MHz, $(CD_3)_2SO$): δ = 12.99 (s_{br}, 1H, CO_2H), 5.18 (s, 1H, *H*-2), 3.82-3.76 (m, 1H, CH_2), 3.71-3.64 (m, 1H, CH_2), 3.27-3.24 (m, 2H, CH_2) ppm.

^{13}C-NMR (150 MHz, $(CD_3)_2SO$): δ = 171.9 and 171.5 (CO_2H), 152.9 and 152.1 ($CO_{carbamate}$), 80.0 ($C_{q,tBu}$), 59.5 and 59.0 (*C*H), 49.6 and 49.3 (CH_2), 30.2 and 29.1 (CH_2), 27.8 ($CH_{3,tBu}$) ppm.

HR-MS (ESI+): calcd. for $[M+H]^+$: 234.0795; found: 234.0799.

Synthesis of 4-azidobutyric acid (113)[216]

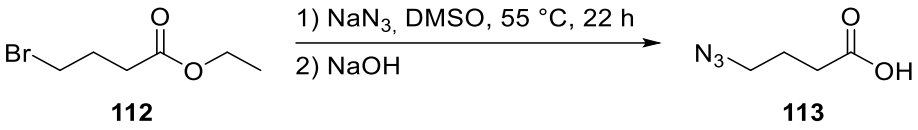

112 **113**

Ethyl 4-bromobutyrate (5.58 g, 4.29 mL, 30.0 mmol, 1.0 eq.) was dissolved in DMSO (25 mL) and sodium azide (2.92 g, 45.0 mmol, 1.5 eq.) was added. The resulting mixture was stirred at 55 °C for 20 h, before being allowed to cool to room temperature. H_2O (150 mL) was added and the solution was extracted with Et_2O (3 x 100 mL). The combined organic phases were washed with H_2O (150 mL) and brine (150 mL), dried over Na_2SO_4, filtered and the solvent was removed under reduced pressure. The crude intermediate was treated with 1 M NaOH (35 mL), MeOH (5 mL) was added and the solution was stirred at room temperature for 3 h. The organic solvent was removed under reduced pressure, the solution was diluted with H_2O (75 mL), acidified with conc. HCl to pH 1. The aqueous phase was extracted with Et_2O (3 x 75 mL) and the combined organic layers were dried over Na_2SO_4, filtered and the solvent was removed *in vacuo* to yield 3.71 g (28.7 mmol, 96%) of the title compound.

^{1}H-NMR (600 MHz, $CDCl_3$): δ = 10.53 (s_{br}, 1H, CO_2H), 3.36 (t, $^3J_{H,H}$ = 6.7 Hz, 2H, *H*-2), 2.46 (t, $^3J_{H,H}$ = 7.1 Hz, 2H, *H*-4), 1.90 (quint, $^3J_{H,H}$ = 7.1 Hz, 6.7 Hz, 2H, *H*-3) ppm.

^{13}C-NMR (150 MHz, $CDCl_3$): δ = 179.3 (CO_2H),50.5 (*C*-2), 31.0 (*C*-4), 23.9 (*C*-3) ppm.

HR-MS (ESI-): calcd. for $[M-H]^-$: 128.0466; found: 128.0469.

Synthesis of 1-(3-(trimethylammonium)propyl)-3-methylimidazole bromide (127)

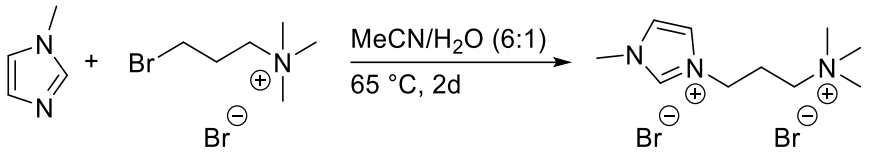

125 **126** **127**

N-Methylimidazole (0.82 g, 10.0 mmol, 3.3 eq.) was dissolved in MeCN (5 mL) and (3-bromopropyl)trimethylammonium bromide (0.78 g, 3.00 mmol, 1.0 eq.) as a solution in MeOH (30 mL) was added. The reaction mixture was stirred at 65 °C for two days and then allowed to cool to room temperature. The solvent was removed under reduced pressure and the residue was taken up in MeOH (5 mL). Upon addition of Et_2O (20 mL) a precipitate formed, which was filtered off and dried *in vacuo* to yield 0.25 g (0.72 mmol, 24%) of the title compound.

^{1}H-NMR (300 MHz, $(CD_3)_2SO$): δ = 9.30 (s, 1H, *H*-$2_{imidazole}$), 7.87 (m, 1H, *H*-$4_{imidazole}$), 7.77 (m, 1H, *H*-$5_{imidazole}$), 4.28 (t, $^3J_{H,H}$ = 6.9 Hz, 2H, NC*H*$_2$), 3.88 (s, 3H, NC*H*$_3$), 3.45-3.40 (m, 2H, $(CH_3)_3NCH_2$), 3.11 (s, 9H, $N(CH_3)_3$), 2.38-2.28 (m, 2H, C*H*$_2$) ppm.

^{13}C-NMR (75 MHz, $(CD_3)_2SO$): δ = 136.9 (C-$2_{imidazole}$), 123.7 (C-$4_{imidazole}$), 122.2 (C-$5_{imidazole}$), 61.9 ($(CH_3)_3NCH_2$), 52.4 ($N(CH_3)_3$), 45.9 (NCH_2), 35.9 (NCH_3), 23.1 (CH_2) ppm.

HR-MS (ESI+): calcd. for $[M\text{-}Br+H]^+$: 262.0913; found: 262.0911, calcd. for $[M\text{-}2Br+2H]^{2+}$: 91.59; found: 91.59.

6.4 Peptide synthesis and related reactions

Synthesis of PNA 1 (1)

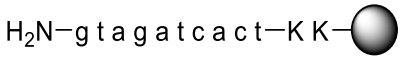

1

Coupling of the PNA sequence was performed following SOP 4 on a 25 µmol scale.
5 µmol of the peptide were cleaved from the resin following SOP 6 and purified by semi-preparative HPLC.
HPLC (column 4, gradient: 5-35% B in 30 min): t_R = 15.91 min.
UHPLC (gradient: 1-40% B in 20 min): t_R = 9.45 min.
HR-MS (ESI+): calcd. for $[M+2H]^{2+}$: 1492.1484; found: 1492.1497, calcd. for $[M+3H]^{3+}$: 995.1014; found: 995.1027, calcd. for $[M+4H]^{4+}$: 746.5779; found: 746.5792, calcd. for $[M+5H]^{5+}$: 597.4637; found: 597.4645, calcd. for $[M+6H]^{6+}$: 498.0543; found: 498.0548.

Synthesis of PNA 2 (4)

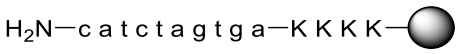

4

Coupling of the PNA sequence was performed following SOP 4 on a 25 µmol scale.
5 µmol of the peptide were cleaved from the resin following SOP 6 and purified by semi-preparative HPLC.
HPLC (column 4, gradient: 5-35% B in 30 min): t_R = 15.66 min.
UHPLC (gradient: 1-40% B in 20 min): t_R = 9.62 min.
HR-MS (ESI+): calcd. for $[M+3H]^{3+}$: 1080.4980; found: 1080.4986, calcd. for $[M+4H]^{4+}$: 810.6253; found: 810.6271, calcd. for $[M+5H]^{5+}$: 648.7017; found: 648.7027, calcd. for $[M+6H]^{6+}$: 540.7527; found: 540.7533, calcd. for $[M+7H]^{7+}$: 463.6462; found: 463.6465.

Synthesis of PNA 1' (2)

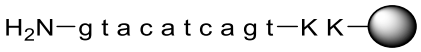

2

Coupling of the PNA sequence was performed following SOP 4 on a 25 µmol scale.
5 µmol of the peptide were cleaved from the resin following SOP 6 and purified by semi-preparative HPLC.
HPLC (column 4, gradient: 5-35% B in 30 min): t_R = 16.62 min.
UHPLC (gradient: 5-45% B in 20 min): t_R = 6.25 min.
HR-MS (ESI+): calcd. for $[M+2H]^{2+}$: 1492.1484; found: 1492.1494, calcd. for $[M+3H]^{3+}$: 995.1014; found: 995.1026, calcd. for $[M+4H]^{4+}$: 746.5779; found: 746.5793, calcd. for $[M+5H]^{5+}$: 597.4637; found: 597.4648, calcd. for $[M+6H]^{6+}$: 498.0543; found: 498.0546.

Synthesis of PNA 1'' (3)

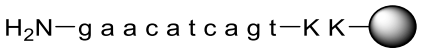

3

Coupling of the PNA sequence was performed following SOP 4 on a 25 µmol scale.
5 µmol of the peptide were cleaved from the resin following SOP 6 and purified by semi-preparative HPLC.
HPLC (column 4, gradient: 5-35% B in 30 min): t_R = 15.63 min.
UHPLC (gradient: 5-45% B in 20 min): t_R = 5.63 min.
HR-MS (ESI+): calcd. for $[M+2H]^{2+}$: 1496.6542; found: 1496.6530, calcd. for $[M+3H]^{3+}$: 998.1052; found: 998.1060, calcd. for $[M+4H]^{4+}$: 748.8307; found: 748.8311, calcd. for $[M+5H]^{5+}$: 599.2660; found: 599.2653, calcd. for $[M+6H]^{6+}$: 499.5563; found: 499.5550.

Synthesis of PNA 3 (5)

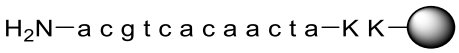

5

Coupling of the PNA sequence was performed following SOP 4 on a 25 µmol scale.
5 µmol of the peptide were cleaved from the resin following SOP 6 and purified by semi-preparative HPLC.
HPLC (column 4, gradient: 5-35% B in 30 min): t_R = 15.88 min.
UHPLC (gradient: 1-40% B in 20 min): t_R = 9.67 min.
HR-MS (ESI+): calcd. for $[M+3H]^{3+}$: 1160.1748; found: 1160.1753, calcd. for $[M+4H]^{4+}$: 870.3829; found: 870.3845, calcd. for $[M+5H]^{5+}$: 696.5078; found: 696.5088, calcd. for $[M+6H]^{6+}$: 580.5910; found: 580.5918, calcd. for $[M+7H]^{7+}$: 497.7934; found: 497.7937.

Synthesis of PNA 4 (6)

6

Coupling of the PNA sequence was performed following SOP 4 on a 25 µmol scale.
5 µmol of the peptide were cleaved from the resin following SOP 6 and purified by semi-preparative HPLC.
HPLC (column 4, gradient: 5-35% B in 30 min): t_R = 16.39 min.
UHPLC (gradient: 1-40% B in 20 min): t_R = 10.28 min.
HR-MS (ESI+): calcd. for $[M+3H]^{3+}$: 1276.9007; found: 1276.9010, calcd. for $[M+4H]^{4+}$: 957.9273; found: 957.9285, calcd. for $[M+5H]^{5+}$: 766.5433; found: 766.5442, calcd. for $[M+6H]^{6+}$: 638.9540; found: 638.9546, calcd. for $[M+7H]^{7+}$: 547.8187; found: 547.8196.

Synthesis of 44

44

Alkyne functionalization of **1** (15 µmol) was performed according to SOP 8. An analytical sample of the peptide was cleaved from the resin following SOP 6 and analyzed by HR-MS.

UHPLC (gradient: 1-40% B in 20 min): t_R = 8.87.

HR-MS (ESI+): calcd. for $[M+2H]^{2+}$: 1518.1459; found: 1518.1452, calcd. for $[M+3H]^{3+}$: 1012.4330; found: 1012.4336, calcd. for $[M+4H]^{4+}$: 759.5766; found: 759.5763, calcd. for $[M+5H]^{5+}$: 607.8627; found: 607.8603.

Synthesis of 18

18

Alkyne functionalization of **4** (15 µmol) was performed according to SOP 8. An analytical sample of the peptide was cleaved from the resin following SOP 6 and analyzed by UHPLC and HR-MS.

UHPLC (gradient: 1-40% B in 20 min): t_R = 10.12.

HR-MS (ESI+): calcd. for $[M+3H]^{3+}$: 1097.8297; found: 1097.8305, calcd. for $[M+4H]^{4+}$: 823.6241; found: 823. 6248.

Synthesis of 133

133

Alkyne functionalization of **5** (15 µmol) was performed according to SOP 8. An analytical sample of the peptide was cleaved from the resin following SOP 6 and analyzed by UHPLC and HR-MS.

UHPLC (gradient: 1-40% B in 20 min): t_R = 8.92.

HR-MS (ESI+): calcd. for $[M+3H]^{3+}$: 1177.5065; found: 1177.5076, calcd. for $[M+4H]^{4+}$: 883.3817; found: 883.3826, calcd. for $[M+5H]^{5+}$: 706.9068; found: 706.9066, calcd. for $[M+6H]^{6+}$: 589.2569; found: 589.2642.

Synthesis of 134

134

Alkyne functionalization of **6** (15 µmol) was performed according to SOP 8. An analytical sample of the peptide was cleaved from the resin following SOP 6 and analyzed by UHPLC and HR-MS.

UHPLC (gradient: 1-40% B in 20 min): t_R = 10.85.

HR-MS (ESI+): calcd. for $[M+3H]^{3+}$: 1294.2323; found: 1294.2320, calcd. for $[M+4H]^{4+}$: 970.9260; found: 970.9266, calcd. for $[M+5H]^{5+}$: 776.9423; found: 776. 9413.

Synthesis of 128

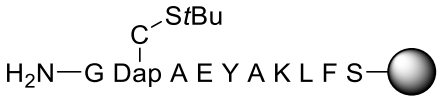

128

Synthesis of the peptide was performed according to SOP 1b at a 0.05 mmol scale on preloaded Wang resin (0.32 mmol/g). An analytical sample of the peptide was cleaved from the resin following SOP 6 and analyzed by UHPLC and HR-MS.

UHPLC (gradient: 10-60% B in 20 min): t_R = 11.26 min.

HR-MS (ESI+): calcd. for $[M+H]^+$: 1262.5908; found: 1262.5918, calcd. for $[M+2H]^{2+}$: 631.7990; found: 631.7998, calcd. for $[M+3H]^{3+}$: 421.5351; found: 421.5355.

Synthesis of 129

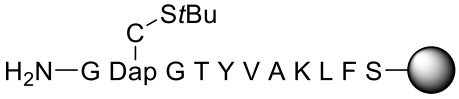

129

Synthesis of the peptide was performed according to SOP 1b at a 0.05 mmol scale on preloaded Wang resin (0.32 mmol/g). An analytical sample of the peptide was cleaved from the resin following SOP 6 and analyzed by UHPLC and HR-MS.

UHPLC (gradient: 10-60% B in 20 min): t_R = 12.78 min.

HR-MS (ESI+): calcd. for $[M+H]^+$: 1319.6468; found: 1319.6483, calcd. for $[M+2H]^{2+}$: 660.3280; found: 660.3280, calcd. for $[M+3H]^{3+}$: 440.5544; found: 440.5548.

Synthesis of 130

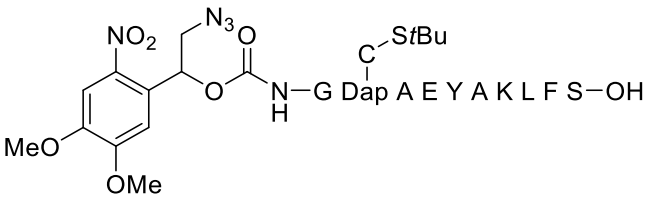

130

The photocleavable linker was attached to **128** according to SOP 7. The peptide was cleaved from the resin following SOP 6 and purified by preparative HPLC.

HPLC (column 1, gradient: 20-80% B in 30 min): t_R = 19.57 min.

UHPLC (gradient: 20-70% B in 20 min): t_R = 11.62 min.

HR-MS (ESI+): calcd. for $[M+H]^+$: 1556.6508; found: 1556.6498, calcd. for $[M+2H]^{2+}$: 778.8291; found: 778.8305.

Synthesis of 131

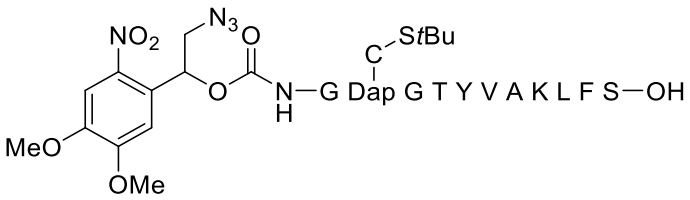

131

The photocleavable linker was attached to **129** according to SOP 7. The peptide was cleaved from the resin following SOP 6 and purified by preparative HPLC.

HPLC (column 1, gradient: 30-80% B in 30 min): t_R = 17.66 min.

UHPLC (gradient: 20-70% B in 20 min): t_R = 12.60 min.

HR-MS (ESI+): calcd. for $[M+H]^+$: 1613.7087; found: 1613.7078, calcd. for $[M+2H]^{2+}$: 807.3580; found: 807.3581.

Synthesis of 17

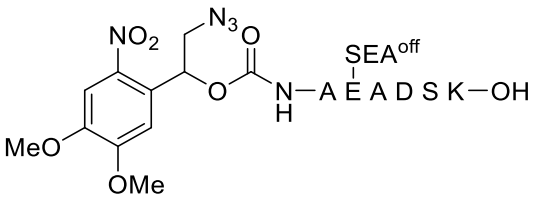

17

The peptide was coupled on a preloaded Wang resin (0.31 mmol/g) at a 0.1 mmol scale. Attachment of the photocleavable linker was performed according to SOP 7. The peptide was cleaved from the resin following SOP 6 and purified by preparative HPLC.

HPLC (column 1, gradient: 20-65% B in 30 min): t_R = 20.82 min.

UHPLC (gradient: 10-50% B in 20 min): t_R = 13.63 min.

HR-MS (ESI+): calcd. for $[M+H]^+$: 1031.3557; found: 1031.3562, calcd. for $[M+2H]^{2+}$: 516.1815; found: 516.1808.

Synthesis of 132

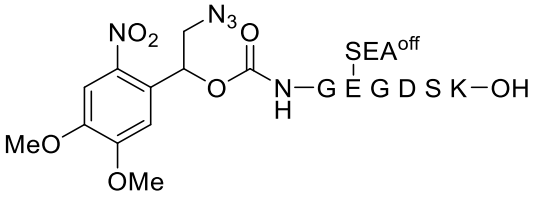

132

The peptide was coupled on a preloaded Wang resin (0.31 mmol/g) at a 0.1 mmol scale. Attachment of the photocleavable linker was performed according to SOP 7. The peptide was cleaved from the resin following SOP 6 and purified by preparative HPLC.

HPLC (column 1, gradient: 20-65% B in 30 min): t_R = 21.62 min.

UHPLC (gradient: 10-50% B in 20 min): t_R = 13.30 min.

HR-MS (ESI+): calcd. for $[M+H]^+$: 1003.3244; found: 1003.3243, calcd. for $[M+H+Na]^{2+}$: 513.1568; found: 513.1564.

Synthesis of 21

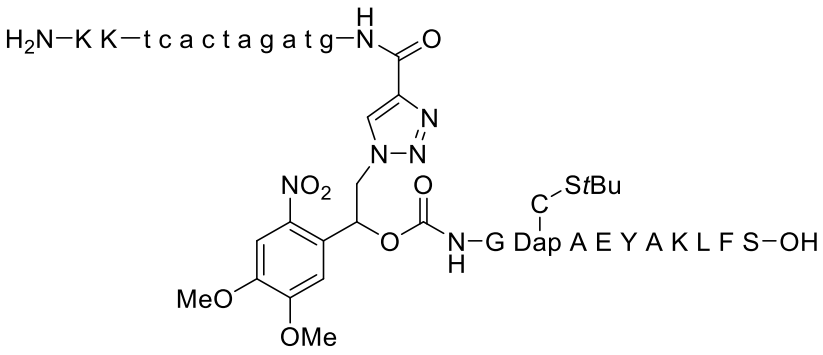

21

Generation of the PNA/peptide hybrid was achieved by CuAAc reaction following SOP 9 between **44** (10 µmol) and **130**. The peptide was cleaved from the resin following SOP 6 and purified by semi-preparative HPLC.

HPLC (column 4, gradient: 5-55% B in 30 min): t_R = 23.66 min.

UHPLC (gradient: 0-60% B in 20 min): t_R = 12.55.

HR-MS (ESI+): calcd. for $[M+4H]^{4+}$: 1148.7381; found: 1148.7320, calcd. for $[M+5H]^{5+}$: 919.1919; found: 919.1885, calcd. for $[M+6H]^{6+}$: 766.1611; found: 766.1604.

Synthesis of 19

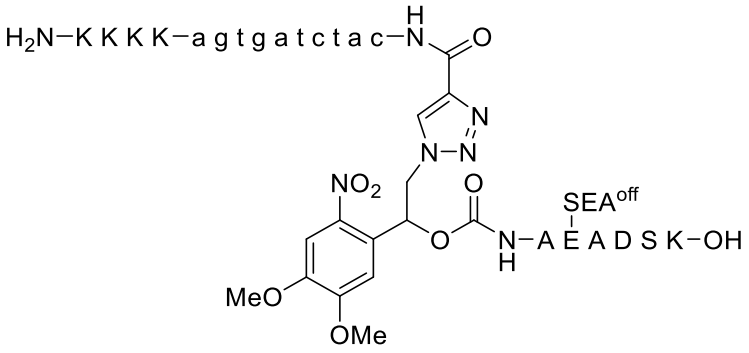

19

Generation of the PNA/peptide hybrid was achieved by CuAAc reaction following SOP 9 between **18** (10 µmol) and **17**. The peptide was cleaved from the resin following SOP 6 and purified by semi-preparative HPLC.

HPLC (column 4, gradient: 1-60% B in 30 min): t_R = 20.70 min.

UHPLC (gradient: 0-60% B in 20 min): t_R = 9.76.

HR-MS (ESI+): calcd. for $[M+3H]^{3+}$: 1441.6137; found: 1441.6124, calcd. for $[M+4H]^{4+}$: 1081.4621; found: 1081.4622, calcd. for $[M+5H]^{5+}$: 865.3712; found: 865.3710, calcd. for $[M+6H]^{6+}$: 721.3105; found: 721.3100, calcd. for $[M+7H]^{7+}$: 618.4100; found: 618.4087.

Synthesis of 22

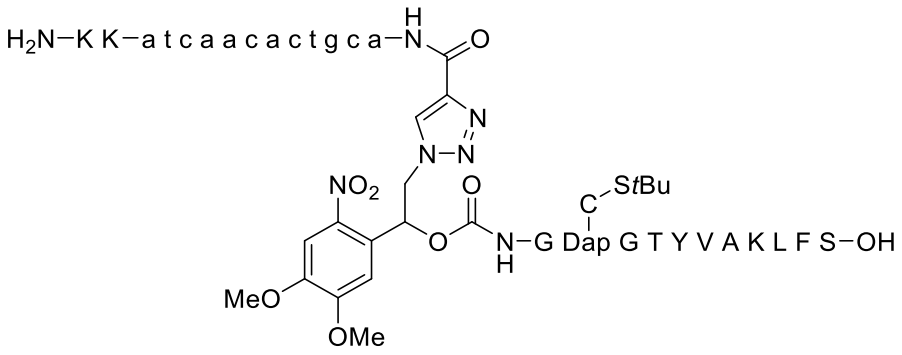

22

Generation of the PNA/peptide hybrid was achieved by CuAAc reaction following SOP 9 between **133** (10 µmol) and **131**. The peptide was cleaved from the resin following SOP 6 and purified by semi-preparative HPLC.

HPLC (column 4, gradient: 10-55% B in 30 min): t_R = 21.98 min.

UHPLC (gradient: 0-60% B in 20 min): t_R = 12.56.

HR-MS (ESI+): calcd. for $[M+3H]^{3+}$: 1715.7426; found: 1715.7397, calcd. for $[M+4H]^{4+}$: 1287.0588; found: 1287.0598, calcd. for $[M+5H]^{5+}$: 1029.8485; found: 1029.8487, calcd. for $[M+6H]^{6+}$: 858.3749; found: 858.3750, calcd. for $[M+7H]^{7+}$: 735.8938; found: 735.8936, calcd. for $[M+8H]^{8+}$: 644.0330; found: 644.0343.

Synthesis of BK135

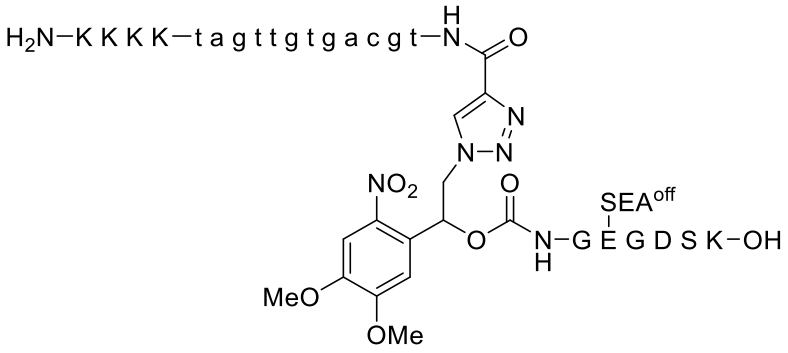

135

Generation of the PNA/peptide hybrid was achieved by CuAAc reaction following SOP 9 between **134** (10 µmol) and **132**. The peptide was cleaved from the resin following SOP 6 and purified by semi-preparative HPLC.

HPLC (column 4, gradient: 5-55% B in 30 min): t_R = 20.54 min.

UHPLC (gradient: 0-60% B in 20 min): t_R = 9.94.

HR-MS (ESI+): calcd. for $[M+3H]^{3+}$: 1628.3375; found: 1628.3385, calcd. for $[M+4H]^{4+}$: 1221.5050; found: 1221.5071, calcd. for $[M+5H]^{5+}$: 977.4054; found: 977.4069, calcd. for $[M+6H]^{6+}$: 814.6724; found: 814.6731, calcd. for $[M+7H]^{7+}$: 698.4345; found: 698.4339.

Synthesis of 20

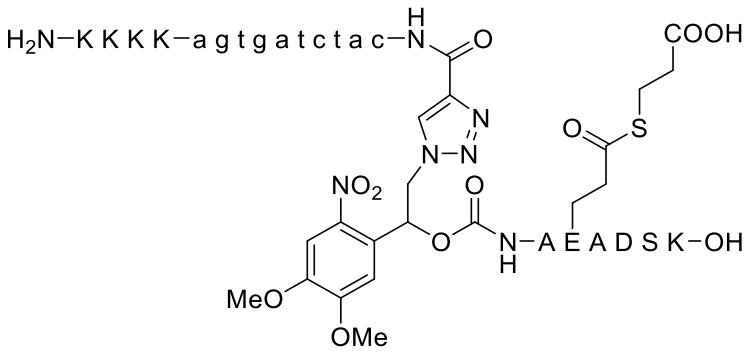

20

19 was dissolved in degassed buffer (1 mL; 10 mM NaH_2PO_4, 100 mM NaCl, 20 mM TCEP, 5% MPAA (v/v)). The pH was adjusted to 3 and the solution was stirred at 37 °C for 48 h. The reaction mixture was lyophilized and the crude product was purified by semi-preparative HPLC.

HPLC (column 4, gradient: 10-55% B in 30 min): t_R = 12.76 min.

UHPLC (gradient: 0-60% B in 20 min): t_R = 8.96.

HR-MS (ESI+): calcd. for $[M+3H]^{3+}$: 1431.9442; found: 1431.9424, calcd. for $[M+4H]^{4+}$: 1074.2099; found: 1074.2100, calcd. for $[M+5H]^{5+}$: 859.5694; found: 859.5694, calcd. for $[M+6H]^{6+}$: 716.4757; found: 716.4753, calcd. for $[M+7H]^{7+}$: 614.2659; found: 614.2650.

Synthesis of 23

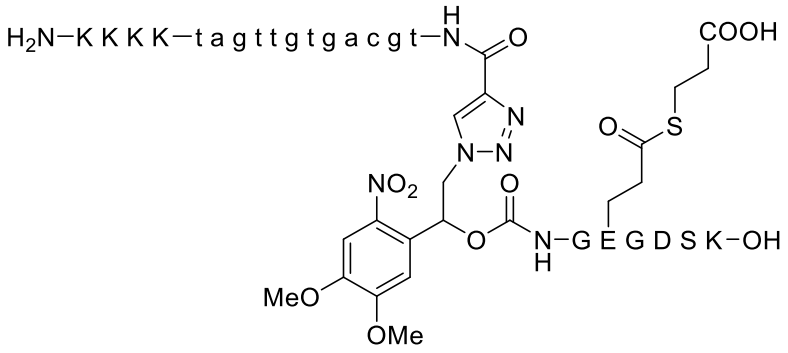

23

135 was dissolved in degassed buffer (1 mL; 10 mM NaH_2PO_4, 100 mM NaCl, 20 mM TCEP, 5% MPAA (v/v)). The pH was adjusted to 3 and the solution was stirred at 37 °C for 48 h. The reaction mixture was lyophilized and the crude product was purified by analytical HPLC.

HPLC (column 3, gradient: 10-55% B in 30 min): t_R = 12.88 min.

UHPLC (gradient: 0-60% B in 20 min): t_R = 9.20.

HR-MS (ESI+): calcd. for $[M+4H]^{4+}$: 1214.2528; found: 1214.2547, calcd. for $[M+5H]^{5+}$: 971.6037; found: 971.6052, calcd. for $[M+6H]^{6+}$: 809.8376; found: 809.8382, calcd. for $[M+7H]^{7+}$: 694.2904; found: 694.2914.

Synthesis of 26

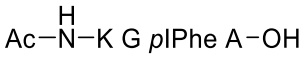

26

The peptide was synthesized according to SOP 2 at a 0.1 mmol scale on preloaded Wang resin (0.71 mmol/g). The peptide was cleaved from resin following SOP 6 and purified by preparative HPLC.

HPLC (column 1, gradient: 15-60% B in 30 min): t_R =16.55 min.

UHPLC (gradient: 5-90% B in 20 min): t_R = 7.45 min.

HR-MS (ESI+): calcd. for $[M+H]^+$: 590.1470; found: 590.1471.

Synthesis of 27

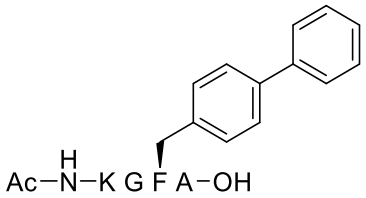

27

26 (10 mg, 17 µmol, 1.0 eq.), phenylboronic acid (5.17 mg, 42.4 µmol, 2.5 eq.) and K_2CO_3 (16.42 mg, 0.12 mmol, 7.0 eq.) were dissolved in 1 mL deionized H_2O. $Na_2[ADHP]_2{\cdot}Pd(OAc)_2$ (5 mol%) was added and the reaction mixture was agitated at 37 °C. Aliquots of 10 µL were taken after 0, 12, 24 and 36 h and diluted with 40 µL deionized H_2O for analysis by UPLC. The reaction was stopped by freezing the sample in liquid nitrogen, followed by lyophilization. The crude reaction mixture was purified by semi-preparative HPLC.

HPLC (column 2, gradient: 20-60% B in 30 min): t_R =22.19 min.

UHPLC (gradient: 15-60% B in 20 min): t_R = 10.23 min.

HR-MS (ESI+): calcd. for $[M+H]^+$: 540.2817; found: 540.2818.

Synthesis of 28

28

The peptide was synthesized following SOP 11 at a 0.15 mmol scale on preloaded Wang resin (0.71 mmol/g). The peptide was cleaved from resin following SOP 6 and purified by preparative HPLC.

HPLC (column 1, gradient: 10-45% B in 30 min): t_R =11.51 min.

UHPLC (gradient: 5-90% B in 20 min): t_R = 5.99 min.

HR-MS (ESI+): calcd. for $[M+H]^+$: 508.2577; found: 508.2562.

Synthesis of 29

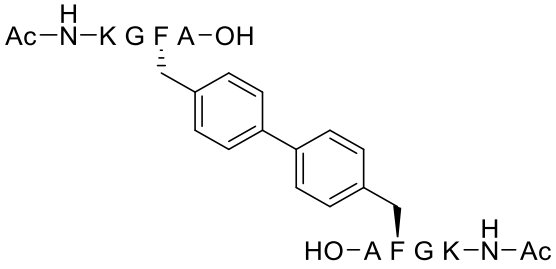

29

26 (10 mg, 17 µmol, 1.0 eq.), **28** (8.62 mg, 17 µmol, 1.0 eq.) and K_2CO_3 (16.42 mg, 0.12 mmol, 7.0 eq.) were dissolved in 1 mL deionized H_2O. $Na_2[ADHP]_2{\cdot}Pd(OAc)_2$ (5 mol%) was added and the reaction mixture was agitated at 37 °C. Aliquots of 10 µL were taken after 0, 12, 24, 36, 46, 60 and 84 h and diluted with 40 µL deionized H_2O for analysis by UPLC. The reaction was stopped by freezing the sample in liquid nitrogen, followed by lyophilization. The crude reaction mixture was purified by semi-preparative HPLC.

HPLC (column 2, gradient: 10-60% B in 30 min): t_R =16.47 min.

UHPLC (gradient: 5-90% B in 20 min): t_R = 7.91 min.

HR-MS (ESI+): calcd. for $[M+H]^+$: 925.4778; found: 925.4775.

Synthesis of 34

34

Synthesis of the peptide was performed according to SOP 2 at a 0.05 mmol scale on preloaded Wang resin (0.31 mmol/g). An analytical sample of the peptide was cleaved from the resin following SOP 6 and analyzed by UHPLC and HR-MS.

UHPLC (gradient: 5-90% B in 20 min): t_R = 11.60 min.

HR-MS (ESI+): calcd. for $[M+H]^+$: 422.2398; found: 422.2398.

Synthesis of 35

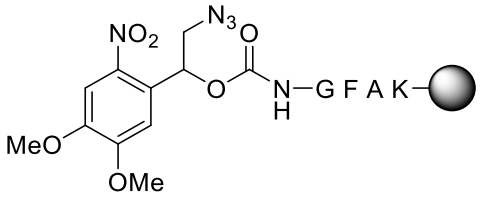

35

The photocleavable linker was attached to resin-bound **34** (25 µmol) according to SOP 7. An analytical sample of the peptide was cleaved from the resin following SOP 6 and analyzed by UHPLC and HR-MS.

UHPLC (gradient: 10-60% B in 20 min): t_R = 13.65 min.

HR-MS (ESI+): calcd. for $[M+H]^+$: 716.2998; found: 716.2992.

Synthesis of 36

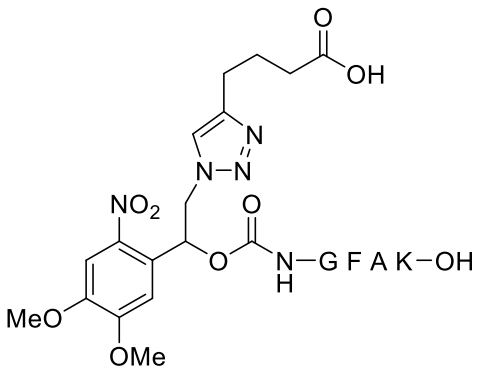

36

Generation of the peptide/cargo hybrid was achieved by CuAAc reaction following SOP 9 between resin-bound **35** (25 µmol) and 5-hexynoic acid. The peptide was cleaved from the resin following SOP 6 and purified by preparative HPLC.

HPLC (column 1, gradient: 10-60% B in 30 min): t_R = 20.96 min.

UHPLC (gradient: 10-60% B in 20 min): t_R = 11.14.

HR-MS (ESI+): calcd. for $[M+H]^+$: 828.3523; found: 828.3514.

Photolysis of 36

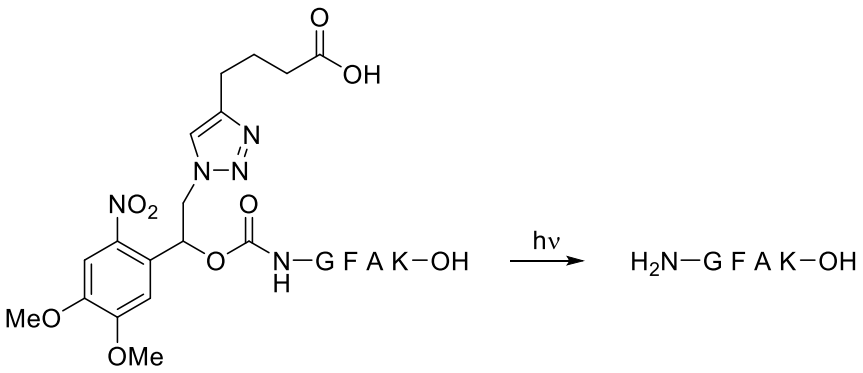

36 **34**

36 was dissolved in water (1 mL) to give a final concentration of 50 µM. The solution was irradiated at 347 nm (1000 W, lamp setup a) for 10 min. Samples were taken every 60 s and analyzed by UHPLC. Afterwards, the solution was frozen in liquid nitrogen, lyophilized and analyzed by HR-MS.

UHPLC (gradient: 5-90% B in 20 min): t_R = 4.75 min.

HR-MS (ESI+): calcd. for $[M+H]^+$: 422.2398; found: 422.2393.

Synthesis of 37

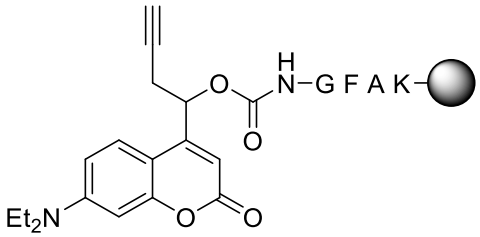

37

The photocleavable linker was attached to resin-bound **34** (25 µmol) according to SOP 7. An analytical sample of the peptide was cleaved from the resin following SOP 6 and analyzed by UHPLC and HR-MS.

UHPLC (gradient: 10-60% B in 20 min): t_R = 15.35 min.

HR-MS (ESI+): calcd. for $[M+H]^+$: 733.3556; found: 733.3541.

Synthesis of 38

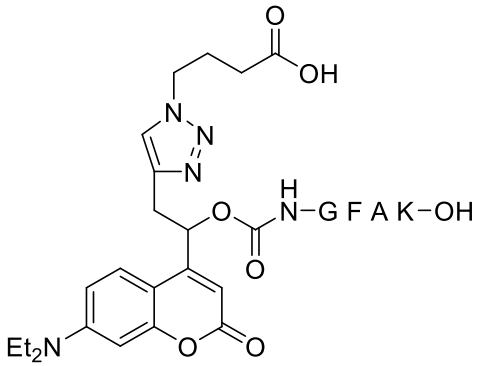

BKIG011

Generation of the peptide/cargo hybrid was achieved by CuAAc reaction following SOP 9 between resin-bound **37** (25 µmol) and 4-azidobutyric acid. The peptide was cleaved from the resin following SOP 6 and purified by preparative HPLC.

HPLC (column 1, gradient: 10-60% B in 30 min): t_R = 26.11 min.

UHPLC (gradient: 5-90% B in 20 min): t_R = 11.23.

HR-MS (ESI+): calcd. for $[M+H]^+$: 862.4094; found: 862.4093.

Photolysis of 38

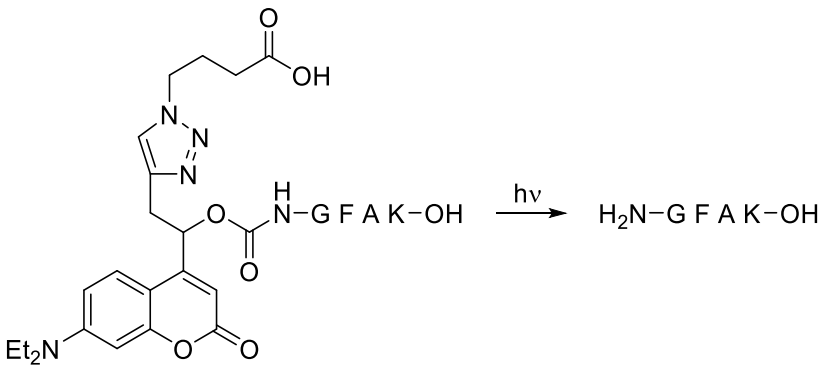

38 **34**

38 was dissolved in water (1 mL) to give a final concentration of 50 µM. The solution was irradiated at 405 nm (100 mW, lamp setup b) for 5 min. Samples were taken every 30 s and analyzed by UHPLC. Afterwards, the solution was frozen in liquid nitrogen, lyophilized and analyzed by HR-MS.

UHPLC (gradient: 5-90% B in 20 min): t_R = 4.76 min.

HR-MS (ESI+): calcd. for $[M+H]^+$: 422.2398; found: 422.2393.

Synthesis of 40

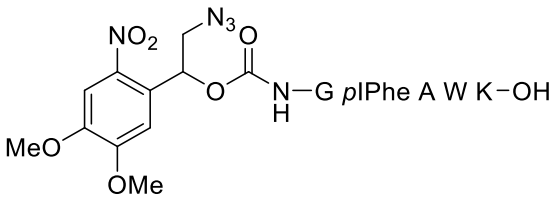

40

The peptide was synthesized on preloaded Wang resin (0.33 mmol/g) at a 0.1 mmol scale according to SOP 2. The photocleavable linker was attached according to SOP 7. The peptide was cleaved from the resin following SOP 6 and purified by semi-preparative HPLC.

HPLC (column 2, gradient: 45-80% B in 30 min): t_R = 16.20.

UHPLC (gradient 5-90% B in 20 min): t_R = 14.18 min.

HR-MS (ESI+): calcd. for $[M+H]^+$: 1028.2758; found: 1028.2751.

Synthesis of 43

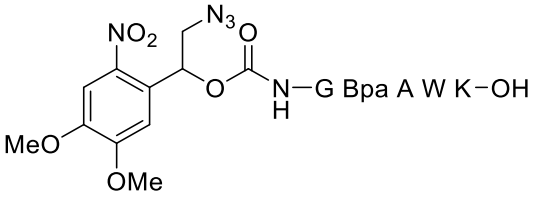

43

The peptide was synthesized following SOP 11 at a 25 µmol scale on preloaded Wang resin (0.33 mmol/g), with the last amino acid being Trt-Gly-OH. After Miyaura borylation, the *N*-terminal protecting group was removed by treatment with DCM/H_2O/TFA (98.8:1:0.2 (v/v), 0.5 mL/10 µmol) for 3 x 10 min, followed by washing five times each with DMF, 5% DIPEA in DCM, DCM and DMF (1 mL/10 µmol). The photocleavable linker was attached to **BK051** according to SOP 7, the peptide was cleaved from resin following SOP 6 and purified by preparative HPLC.

HPLC (column 1, gradient: 45-75% B in 30 min): t_R =9.13 min.

UHPLC (gradient: 5-90% B in 20 min): t_R = 12.16 min.

HR-MS (ESI+): calcd. for $[M+H]^+$: 946.3868; found: 946.3854.

Synthesis of 47

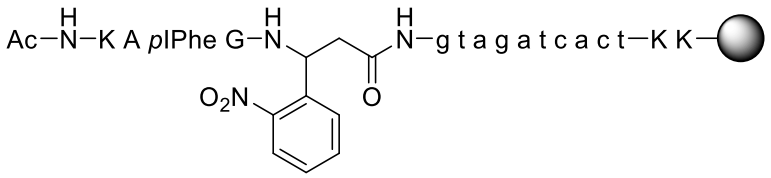

47

The PNA was synthesized following SOP 5. The dried resin (5 µmol) was suspended in DMF and chain elongation proceeded following SOP 2b. An analytical sample of the peptide was cleaved from the resin following SOP 6 and analyzed by UHPLC and HR-MS.
UHPLC (gradient: 5-60% B in 20 min): t_R = 10.28 min.
HR-MS (ESI+): calcd. for $[M+3H]^{3+}$: 1249.8302; found: 1249.8315, calcd. for $[M+4H]^{4+}$: 937.3735; found: 937.3748, calcd. for $[M+5H]^{5+}$: 750.3010; found: 750.3025.

Synthesis of 48

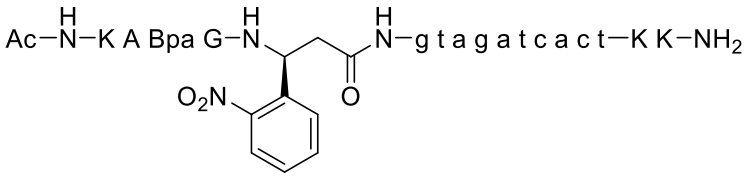

48

The PNA was synthesized following SOP 5. The dried resin (5 µmol) was suspended in DMF and chain elongation proceeded following SOP 2b. The peptide was cleaved from resin following SOP 6 and purified by semi-preparative HPLC.
HPLC (column 4, gradient 5-60% B in 30 min): t_R = 13.71 min.
UHPLC (gradient: 5-60% B in 20 min): t_R = 7.94 min.
HR-MS (ESI+): calcd. for $[M+3H]^{3+}$: 1222.1995; found: 1222.1988, calcd. for $[M+4H]^{4+}$: 916.9014; found: 916.9007, calcd. for $[M+5H]^{5+}$: 733.7226; found: 733.7210, calcd. for $[M+CH_2+3H]^{3+}$: 1226.8741; found: 1226.8713, calcd. for $[M+CH_2+4H]^{4+}$: 920.4035; found: 920.4050, calcd. for $[M+CH_2+5H]^{5+}$: 736.5257; found: 736.5249, calcd. for $[M+CH_2+6H]^{6+}$: 613.9393; found: 613.9381.

Synthesis of 49

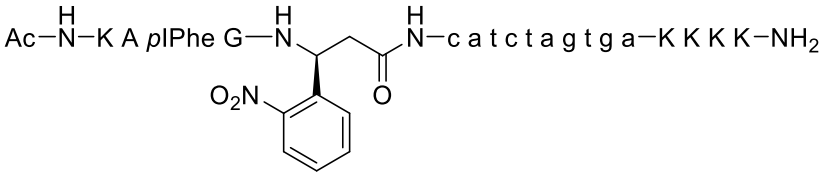

49

The PNA was synthesized following SOP 5. The dried resin (5 µmol) was suspended in DMF and chain elongation proceeded following SOP 2b. The peptide was cleaved from resin following SOP 6 and purified by semi-preparative HPLC.

HPLC (column 4, gradient 5-60% B in 30 min): t_R = 19.21 min.

UHPLC (gradient: 5-60% B in 20 min): t_R = 10.13 min.

HR-MS (ESI+): calcd. for $[M+3H]^{3+}$: 1335.2269; found: 1335.2253, calcd. for $[M+4H]^{4+}$: 1001.6720; found: 1001.6714, calcd. for $[M+5H]^{5+}$: 801.5390; found: 801.5384, calcd. for $[M+6H]^{6+}$: 668.1171; found: 668.1163, calcd. for $[M+7H]^{7+}$: 572.8157; found: 572.8144.

Synthesis of 136

136

The PNA was synthesized following SOP 4, cleaved from resin following SOP 6 and purified by semi-preparative HPLC.

HPLC (column 4, gradient 5-60% B in 30 min): t_R = 12.95 min.

UHPLC (gradient: 1-40% B in 20 min): t_R = 9.15 min.

HR-MS (ESI+): calcd. for $[M+3H]^{3+}$: 1094.5016; found: 1094.5056, calcd. for $[M+4H]^{4+}$: 821.1280; found: 821.1308, calcd. for $[M+5H]^{5+}$: 657.1038; found: 657.1059, calcd. for $[M+6H]^{6+}$: 547.7544; found: 547.7561.

Synthesis of 56

56

The peptide was synthesized following SOP 1 at a 0.1 mmol scale on H-Rink amide ChemMatrix® resin (0.41 mmol/g). An analytical sample of the peptide was cleaved from the resin following SOP 6 and analyzed by UHPLC and HR-MS.

UHPLC (gradient: 20-80% B in 15 min): t_R = 8.67 min.

HR-MS (ESI+): calcd. for $[M+2H]^{2+}$: 1199.1587; found: 1199.1574, calcd. for $[M+3H]^{3+}$: 799.7749; found: 799.7747.

Synthesis of 57

57

The peptide was synthesized following SOP 1 at a 0.1 mmol scale on H-Rink amide ChemMatrix® resin (0.41 mmol/g). An analytical sample of the peptide was cleaved from the resin following SOP 6 and analyzed by UHPLC and HR-MS.

UHPLC (gradient: 20-80% B in 15 min): t_R = 5.53 min.

HR-MS (ESI+): calcd. for $[M+3H]^{3+}$: 798.5114; found: 798.5107, calcd. for $[M+4H]^{4+}$: 599.1353; found: 599.1362, calcd. for $[M+5H]^{5+}$: 479.5097; found: 479.5090.

Synthesis of 58

58

10 µmol of resin-bound **56** were elongated following SOP 2c. The peptide was cleaved from resin following SOP 6 and purified by semi-preparative HPLC.

HPLC (column 5, gradient 20-80% B in 30 min): t_R = 21.40 min.

UHPLC (gradient: 20-80% B in 15 min): t_R = 10.47 min.

HR-MS (ESI+): calcd. for $[M+H+Na]^{2+}$: 1291.1746; found: 1291.1728, calcd. for $[M+2H+Na]^{3+}$: 861.1188; found: 861.1192.

Synthesis of 59

59

10 µmol of resin-bound **57** were elongated following SOP 2c. The peptide was cleaved from resin following SOP 6 and purified by semi-preparative HPLC.

HPLC (column 5, gradient 20-80% B in 30 min): t_R = 14.66 min.

UHPLC (gradient: 20-80% B in 15 min): t_R = 7.54 min.

HR-MS (ESI+): calcd. for $[M+3H]^{3+}$: 903.5032; found: 903.5029, calcd. for $[M+4H]^{4+}$: 677.8793; found: 677.8805, calcd. for $[M+5H]^{5+}$: 542.5049; found; 542.5042.

Synthesis of 61

61

10 µmol of resin-bound **56** were elongated following SOP 2c. The peptide was cleaved from resin following SOP 6 and purified by semi-preparative HPLC.

HPLC (column 5, gradient 20-80% B in 30 min): t_R = 20.78 min.

UHPLC (gradient: 20-80% B in 15 min): t_R = 10.53 min.

HR-MS (ESI+): calcd. for $[M+CH_2+2H]^{2+}$: 1308.6944; found: 1308.6933, calcd. for $[M+CH_2+2H+Na]^{3+}$: 880.1260; found: 880.1258.

Synthesis of 62

62

10 µmol of resin-bound **57** were elongated following SOP 2c. The peptide was cleaved from resin following SOP 6 and purified by semi-preparative HPLC.

HPLC (column 5, gradient 20-80% B in 30 min): t_R = 14.89 min.

UHPLC (gradient: 20-80% B in 15 min): t_R = 7.37 min.

HR-MS (ESI+): calcd. for $[M+2H]^{2+}$: 1340.7356; found: 1340.7339, calcd. for $[M+3H]^{3+}$: 894.1595; found: 894.1596, calcd. for $[M+4H]^{4+}$: 670.8714; found: 670.8728, calcd. for $[M+5H]^{5+}$: 536.8986; found; 539.8988.

Synthesis of 63

63

10 µmol of resin-bound **57** were elongated following SOP 2c. The peptide was cleaved from resin following SOP 6 and purified by semi-preparative HPLC.

HPLC (column 5, gradient 20-80% B in 30 min): t_R = 15.04 min.

UHPLC (gradient: 20-80% B in 15 min): t_R = 7.53 min.

HR-MS (ESI+): calcd. for $[M+2H]^{2+}$: 1369.2463; found: 1369.2454, calcd. for $[M+3H]^{3+}$: 913.1666; found: 913.1665, calcd. for $[M+4H]^{4+}$: 685.1268; found: 685.1282, calcd. for $[M+5H]^{5+}$: 548.3029; found; 548.3028.

Synthesis of 64

64

10 µmol of resin-bound **57** were elongated following SOP 2c. The peptide was cleaved from resin following SOP 6 and purified by semi-preparative HPLC.

HPLC (column 5, gradient 20-80% B in 30 min): t_R = 15.07 min.

UHPLC (gradient: 20-80% B in 15 min): t_R = 7.62 min.

HR-MS (ESI+): calcd. for $[M+2H]^{2+}$: 1376.2541; found: 1376.2527, calcd. for $[M+3H]^{3+}$: 917.8385; found: 917.8391, calcd. for $[M+4H]^{4+}$: 688.6307; found: 688.6321, calcd. for $[M+5H]^{5+}$: 551.1060; found; 551.1063, calcd. for $[M+6H]^{6+}$: 459.4229; found: 459.4223.

Synthesis of 65

65

10 µmol of resin-bound **57** were elongated following SOP 2c. The peptide was cleaved from resin following SOP 6 and purified by semi-preparative HPLC.

HPLC (column 5, gradient 20-80% B in 30 min): t_R = 13.96 min.

UHPLC (gradient: 20-80% B in 15 min): t_R = 7.43 min.

HR-MS (ESI+): calcd. for $[M+2H]^{2+}$: 1383.2620; found: 1383.2605, calcd. for $[M+3H]^{3+}$: 922.5104; found: 922.5107, calcd. for $[M+4H]^{4+}$: 692.1346; found: 692.1354, calcd. for $[M+5H]^{5+}$: 553.9091; found; 553.9086.

Synthesis of 70

70

The peptide was synthesized following SOP 1 at a 0.1 mmol scale on H-Rink amide ChemMatrix® resin (0.41 mmol/g). An analytical sample of the peptide was cleaved from the resin following SOP 6 and analyzed by UHPLC and HR-MS.

UHPLC (gradient: 20-60% B in 15 min): t_R = 6.31 min.

HR-MS (ESI+): calcd. for $[M+2H]^{2+}$: 1228.1306; found: 1228.1300, calcd. for $[M+3H]^{3+}$: 819.0895; found: 819.0879.

Synthesis of 71

71

The peptide was synthesized following SOP 1 at a 0.1 mmol scale on H-Rink amide ChemMatrix® resin (0.41 mmol/g). An analytical sample of the peptide was cleaved from the resin following SOP 6 and analyzed by UHPLC and HR-MS.

UHPLC (gradient: 10-50% B in 15 min): t_R = 7.73 min.

HR-MS (ESI+): calcd. for $[M+2H]^{2+}$: 1225.2877; found: 1225.2861, calcd. for $[M+3H]^{3+}$: 817.1942; found: 817.1947, calcd. for $[M+4H]^{4+}$: 613.1475; found: 613.1488, calcd. for $[M+5H]^{5+}$: 490.7195; found: 490.7192.

Synthesis of 75

75

15 µmol of resin-bound **70** were elongated following SOP 2c. The peptide was cleaved from resin following SOP 6 and purified by semi-preparative HPLC.

HPLC (column 5, gradient 10-70% B in 30 min): t_R = 21.27 min.

UHPLC (gradient: 20-80% B in 15 min): t_R = 7.47 min.

HR-MS (ESI+): calcd. for $[M+2H]^{2+}$: 1302.1477; found: 1302.1478, calcd. for $[M+3H]^{3+}$: 868.4343; found: 868.4330.

Synthesis of 76

76

5 µmol of resin-bound **71** were elongated following SOP 2c. The peptide was cleaved from resin following SOP 6 and purified by semi-preparative HPLC.

HPLC (column 5, gradient 20-80% B in 30 min): t_R = 12.05 min.

UHPLC (gradient: 10-50% B in 15 min): t_R = 10.36 min.

HR-MS (ESI+): calcd. for $[M+3H]^{3+}$: 922.1861; found: 922.1855, calcd. for $[M+4H]^{4+}$: 691.8914; found: 691.8922, calcd. for $[M+5H]^{5+}$: 533.7146; found: 533.7158, calcd. for $[M+6H]^{6+}$: 461.5967; found: 461.5961.

Synthesis of 77

77

3.3 µmol of resin-bound **71** were elongated following SOP 2c. The peptide was cleaved from resin following SOP 6 and purified by semi-preparative HPLC.

HPLC (column 5, gradient 20-80% B in 30 min): t_R = 11.32 min.

UHPLC (gradient: 20-80% B in 15 min): t_R = 5.27 min.

HR-MS (ESI+): calcd. for $[M+2H]^{2+}$: 1446.8048; found: 1446.8038, calcd. for $[M+3H]^{3+}$: 964.8723; found: 964.8721, calcd. for $[M+4H]^{4+}$: 723.9061; found: 723.9069, calcd. for $[M+5H]^{5+}$: 579.3263; found: 579.3281, calcd. for $[M+6H]^{6+}$: 482.9398, found: 482.9409.

Synthesis of 78

78

3.3 µmol of resin-bound **71** were elongated following SOP 2c. The peptide was cleaved from resin following SOP 6 and purified by semi-preparative HPLC.

HPLC (column 5, gradient 20-60% B in 30 min): t_R = 10.54 min.

UHPLC (gradient: 20-80% B in 15 min): t_R = 4.93 min.

HR-MS (ESI+): calcd. for $[M+3H]^{3+}$: 1007.5706; found: 1007.5698, calcd. for $[M+4H]^{4+}$: 755.9298; found: 755.9299, calcd. for $[M+5H]^{5+}$: 604.9453; found: 604.9462, calcd. for $[M+6H]^{6+}$: 504.2890; found: 540.2902, calcd. for $[M+7H]^{7+}$: 432.3916; found: 432.3919.

Synthesis of 79

79

3.3 µmol of resin-bound **71** were elongated following SOP 2c. The peptide was cleaved from resin following SOP 6 and purified by semi-preparative HPLC.

HPLC (column 5, gradient 20-80% B in 30 min): t_R = 11.64 min.

UHPLC (gradient: 20-80% B in 15 min): t_R = 5.50 min.

HR-MS (ESI+): calcd. for $[M+3H]^{3+}$: 1045.2653; found: 1045.2646, calcd. for $[M+4H]^{4+}$: 784.2008; found: 784.2012, calcd. for $[M+5H]^{5+}$: 627.5621; found: 627.5630, calcd. for $[M+6H]^{6+}$: 523.1363; found: 523.1373, calcd. for $[M+7H]^{7+}$: 448.5464; found: 448.5470.

Synthesis of 87

87

5 µmol of resin-bound **70** were elongated with **86** following SOP 2c. The peptide was cleaved from resin following SOP 6 and purified by semi-preparative HPLC.

HPLC (column 5, 5-65% B in 30 min): t_R = 21.13 min.

UHPLC (gradient: 5-65% B in 15 min): t_R = 10.45 min.

HR-MS (ESI+): calcd. for $[M+2H]^{2+}$: 1278.6545; found: 1278.6558, calcd. for $[M+3H]^{3+}$: 852.7721; found: 852.7722.

Synthesis of 92

92

5 µmol of resin-bound **71** were elongated with **91** following SOP 2c. The peptide was cleaved from resin following SOP 6 and an analytical sample was analyzed by UHPLC and HR-MS.

UHPLC (gradient: 5-65% B in 15 min): t_R = 7.63 min.

HR-MS (ESI+): calcd. for $[M+2H]^{2+}$: 1282.7923; found: 1282.7919, calcd. for $[M+3H]^{3+}$: 855.5306; found: 855.5304, calcd. for $[M+4H]^{4+}$: 641.8998; found: 641.9005, calcd. for $[M+5H]^{5+}$: 513.7213; found: 513.7216, calcd. for $[M+6H]^{6+}$: 428.2690; found: 428.2691.

Synthesis of 94

94

Introduction of the peptide aldehyde was performed according to SOP 13b on 5 µmol of resin-bound **70**. The crude peptide was purified by semi-preparative HPLC.

HPLC (column 5, 10-70% B in 30 min): t_R = 21.73 min.

UHPLC (gradient: 5-65% B in 15 min): t_R = 11.13 min.

HR-MS (ESI+): calcd. for $[M+2H]^{2+}$: 1256.8116; found: 1256.1220, calcd. for $[M+3H]^{3+}$: 837.7528; found: 837.7505.

Synthesis of 95

95

5 µmol of resin-bound **71** were elongated with **86** following SOP 2c. The peptide was cleaved from resin following SOP 6 and purified by semi-preparative HPLC.

HPLC (column 5, 5-65% B in 30 min): t_R = 14.39 min.

UHPLC (gradient: 5-65% B in 15 min): t_R = 7.46 min.

HR-MS (ESI+): calcd. for $[M+2H]^{2+}$: 1275.8116; found: 1275.8107, calcd. for $[M+3H]^{3+}$: 850.8768; found: 850.8761, calcd. for $[M+4H]^{4+}$: 638.4094; found: 638.4096, calcd. for $[M+5H]^{5+}$: 510.9290; found: 510.9294, calcd. for $[M+6H]^{6+}$: 425.9420; found: 452.9414.

Synthesis of 96

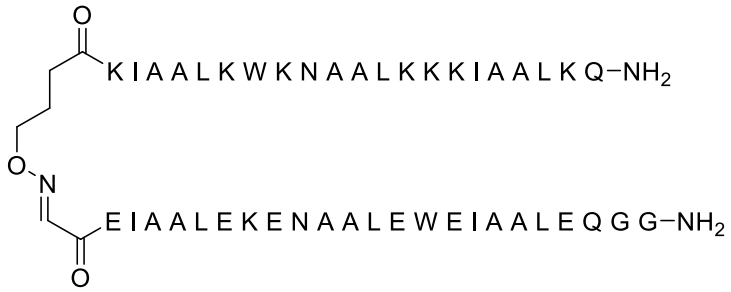

96

94 and **95** were ligated following SOP 14 with a strand concentration of 100 µM and a total volume of 400 µL. After 7 h, the reaction solution was frozen in liquid nitrogen and lyophilized.

UHPLC (gradient: 1-90% B in 15 min): t_R = 8.69 min.

HR-MS (ESI+): calcd. for $[M\text{-}H_2O+5H]^{5+}$: 1005.7721; found: 1005.7732, calcd. for $[M\text{-}H_2O+6H]^{6+}$: 838.3113; found: 838.3120.

Synthesis of 97

97

The peptide was synthesized following SOP 1 at a 0.1 mmol scale on H-Rink amide ChemMatrix® resin (0.41 mmol/g). An analytical sample of the peptide was cleaved from the resin following SOP 6 and analyzed by UHPLC and HR-MS.

UHPLC (gradient: 10-50% B in 15 min): t_R = 11.64 min.

HR-MS (ESI+): calcd. for $[M+2H]^{2+}$: 1256.6414; found: 1256.6422, calcd. for $[M+3H]^{3+}$: 838.0967; found: 838.0970.

Synthesis of 98

98

The peptide was synthesized following SOP 1 at a 0.1 mmol scale on H-Rink amide ChemMatrix® resin (0.41 mmol/g). An analytical sample of the peptide was cleaved from the resin following SOP 6 and analyzed by UHPLC and HR-MS.

UHPLC (gradient: 10-50% B in 15 min): t_R = 6.84 min.

HR-MS (ESI+): calcd. for $[M+2H]^{2+}$: 1242.2905; found: 1242.2883, calcd. for $[M+3H]^{3+}$: 828.5294; found: 828.5290, calcd. for $[M+4H]^{4+}$: 621.6489; found: 621.6490, calcd. for $[M+5H]^{5+}$: 497.5205; found: 497.5205.

Synthesis of 99

99

The peptide was synthesized following SOP 1 at a 0.1 mmol scale on H-Rink amide ChemMatrix® resin (0.41 mmol/g). An analytical sample of the peptide was cleaved from the resin following SOP 6 and analyzed by UHPLC and HR-MS.

UHPLC (gradient: 20-80% B in 15 min): t_R = 9.85 min.

HR-MS (ESI+): calcd. for $[M+2H]^{2+}$: 1473.7335; found: 1473.7343, calcd. for $[M+3H]^{3+}$: 982.8247; found: 982.8260.

Synthesis of 100

100

The peptide was synthesized following SOP 1 at a 0.1 mmol scale on H-Rink amide ChemMatrix® resin (0.41 mmol/g). An analytical sample of the peptide was cleaved from the resin following SOP 6 and analyzed by UHPLC and HR-MS.

UHPLC (gradient: 20-80% B in 15 min): t_R = 5.90 min.

HR-MS (ESI+): calcd. for $[M+2H]^{2+}$: 1459.3826; found: 1459.3797, calcd. for $[M+3H]^{3+}$: 973.2575; found: 973.2564, calcd. for $[M+4H]^{4+}$: 730.1949; found: 730.1952, calcd. for $[M+5H]^{5+}$: 584.3574; found: 584.3577, calcd. for $[M+6H]^{6+}$: 487.1324; calcd: 487.1315.

Synthesis of 101

101

The peptide was synthesized following SOP 1 at a 0.1 mmol scale on H-Rink amide ChemMatrix® resin (0.41 mmol/g). An analytical sample of the peptide was cleaved from the resin following SOP 6 and analyzed by UHPLC and HR-MS.

UHPLC (gradient: 5-65% B in 15 min): t_R = 8.81 min.

HR-MS (ESI+): calcd. for $[M+H]^{+}$: 1585.8122; found: 1585.8092, calcd. for $[M+2H]^{2+}$: 793.4097; found: 793.4093, calcd. for $[M+3H]^{3+}$ 529.2756; found: 529.2758.

Synthesis of 102

102

The peptide aldehyde was introduced to 5 µmol of **97** following SOP 13 and purified by semi-preparative HPLC.

HPLC (column 5, gradient: 10-70% B in 30 min): t_R = 18.89 min.

UHPLC (gradient: 20-80% B in 15 min): t_R = 7.00 min.

HR-MS (ESI+): calcd. for $[M+H_2O+2H]^{2+}$: 1293.6416; found: 1293.6409, calcd. for $[M+H_2O+3H]^{3+}$ 862.7635; found: 862.7632.

Synthesis of 103

103

10 µmol of resin-bound **100** were elongated with **86** following SOP 2c. The alloc protecting group of the *C*-terminal lysine was removed following SOP 15 and FITC was introduced following SOP 2c using only DIPEA as an additive. The peptide was cleaved from resin following SOP 6 and purified by semi-preparative HPLC.

HPLC (column 5, gradient: 5-65% B in 30 min): t_R = 18.58 min.

UHPLC (gradient: 5-65% B in 15 min): t_R = 8.26 min.

HR-MS (ESI+): calcd. for $[M+3H]^{3+}$: 1034.5889; found: 1034.5880, calcd. for $[M+4H]^{4+}$: 776.1935; found: 776.1937, calcd. for $[M+5H]^{5+}$ 621.1562; found: 621.1564, calcd. for $[M+6H]^{6+}$: 517.7981; found: 517.7979.

Synthesis of 104

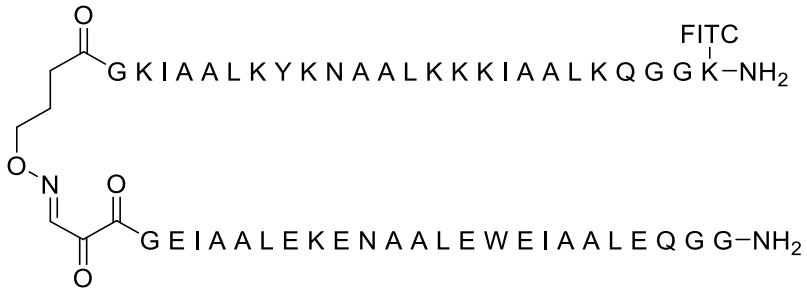

104

102 and **103** were ligated following SOP 14 with a strand concentration of 100 µM and a total volume of 1000 µL. Aliquots of the reaction mixture were taken after 5, 20, 45 and 60 min, and after 2, 4, 6, 10 and 20 h and analyzed by UHPLC. After 20 h, the reaction solution was frozen in liquid nitrogen, lyophilized and subsequently purified by analytical HPLC.

HPLC (column 6, gradient: 20-80% B in 30 min): t_R = 14.55 min.

UHPLC (gradient: 5-95% B in 15 min): t_R = 7.93 min.

HR-MS (ESI+): calcd. for $[M+4H]^{4+}$: 1413.7563; found: 1413.7578, calcd. for $[M+5H]^{5+}$: 1131.2065; found: 1131.2078, calcd. for $[M+6H]^{6+}$ 942.8400; found: 942.8416, calcd. for $[M+7H]^{7+}$: 808.2925; found: 808.2936, calcd. for $[M+8H]^{8+}$: 707.3818; found: 707.3827.

Synthesis of 105

105

The peptide aldehyde was introduced to 5 µmol of **101** following SOP 13 and purified by semi-preparative HPLC.

HPLC (column 5, gradient: 5-65% B in 30 min): t_R = 21.44 min.

UHPLC (gradient: 20-80% B in 15 min): t_R = 5.88 min.

HR-MS (ESI+): calcd. for $[M+H]^+$: 1641.8020; found: 1641.7999, calcd. for $[M+2H]^{2+}$: 821.4046; found: 821.4033, calcd. for $[M+3H]^{3+}$ 547.9388; found: 547.9380.

calcd. for $[M+H_2O+H]^+$: 1659.88125; found: 1659.8103, calcd. for $[M+H_2O+2H]^{2+}$: 830.4099; found: 830.4105, calcd. for $[M+3H]^{3+}$ 553.9424; found: 553.9416.

Synthesis of 106

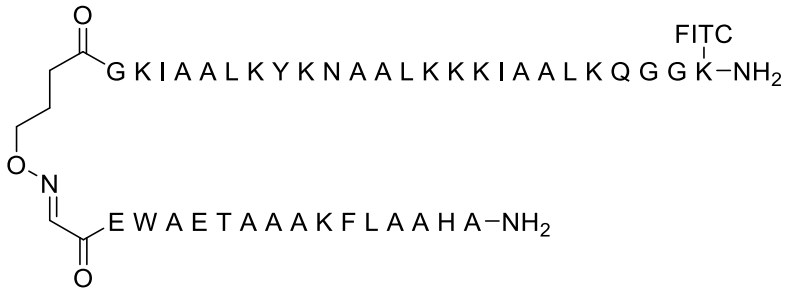

106

103 and **105** were ligated following SOP 14 with a strand concentration of 100 µM and a total volume of 1000 µL. Aliquots of the reaction mixture were taken after 5, 20, 45 and 60 min, and after 2, 4 and 8 h and analyzed by UHPLC. After 8 h, the reaction solution was frozen in liquid nitrogen, lyophilized and subsequently purified by analytical HPLC.

HPLC (column 6, gradient: 20-80% B in 30 min): t_R = 15.44 min.

UHPLC (gradient: 5-95% B in 15 min): t_R = 7.60 min.

HR-MS (ESI+): calcd. for $[M+3H]^{3+}$: 1575.8512; found: 1575.8518, calcd. for $[M+4H]^{4+}$: 1182.1402; found: 1182.1412, calcd. for $[M+5H]^{5+}$: 945.9136; found: 945.9143, calcd. for $[M+6H]^{6+}$ 788.4292; found: 788.4297, calcd. for $[M+7H]^{7+}$: 675.9404; found: 675.9409, calcd. for $[M+8H]^{8+}$: 591.5737; found: 591.5741, calcd. for $[M+9H]^{9+}$: 525.9552; found: 525.9551.

Synthesis of 107

107

5 µmol of resin-bound **97** were elongated with chloroacetic acid following SOP 2c. The peptide was cleaved from resin following SOP 6 and purified by semi-preparative HPLC.

HPLC (column 5, 10-70% B in 30 min): t_R = 21.90 min.

UHPLC (gradient: 5-65% B in 15 min): t_R = 11.40 min.

HR-MS (ESI+): calcd. for $[M+2H]^{2+}$: 1294.6272; found: 1294.6266, calcd. for $[M+3H]^{3+}$: 863.4205; found: 863.4203, calcd. for $[M+3H+Na]^{4+}$: 653.3127; found: 653.3114.

Synthesis of 108

108

5 µmol of resin-bound **100** were elongated with Fmoc-Cys(Trt)-OH following SOP 2c. After removal of the temporary protecting group and subsequent acetylation of the *N*-terminus, the alloc protecting group of the *C*-terminal lysine was removed following SOP 15 and FITC was introduced following SOP 2c using only DIPEA as an additive. The peptide was cleaved from resin following SOP 6 and purified by semi-preparative HPLC.

HPLC (column 5, gradient: 5-65% B in 30 min): t_R = 20.70 min.

UHPLC (gradient: 10-70% B in 15 min): t_R = 7.35 min.

HR-MS (ESI+): calcd. for $[M+3H]^{3+}$: 1049.2462; found: 1049.2460, calcd. for $[M+4H]^{4+}$: 787.1865; found: 787.1882, calcd. for $[M+5H]^{5+}$: 629.9507; found: 629.9494, calcd. for $[M+6H]^{6+}$: 525.1268; found: 525.1279.

Synthesis of 110

110

5 µmol of resin-bound **101** were elongated with chloroacetic acid following SOP 2c. The peptide was cleased from resin following SOP 6 and purified by semi-preparative HPLC.

HPLC (column 5, 20-80% B in 30 min): t_R = 17.29 min.

UHPLC (gradient: 20-80% B in 15 min): t_R = 6.98 min.

HR-MS (ESI+): calcd. for $[M+2H]^{2+}$: 831.3955; found: 831.3953, calcd. for $[M+3H]^{3+}$: 554.5994; found: 554.5993.

Synthesis of 111

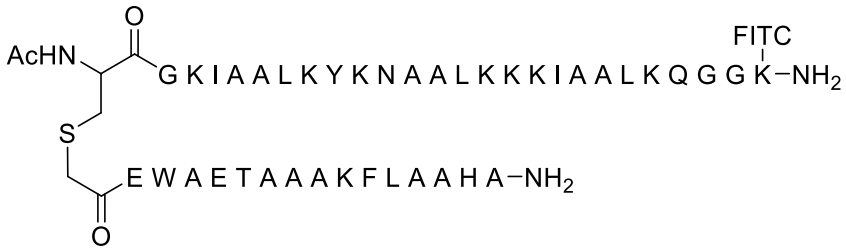

111

Ligation was performed between **108** and **110** according to SOP with a strand concentration of 100 µM and a total volume of 1000 µL. Aliquots of the reaction mixture were taken after 5, 40 and 75 min, and after 3.25, 4, 6 and 8 h and analyzed by UHPLC. After 8 h, the reaction solution was frozen in liquid nitrogen, lyophilized and subsequently purified by analytical HPLC.

HPLC (column 6, gradient: 10-70% B in 30 min): t_R = 20.31 min.

UHPLC (gradient: 5-95% B in 15 min): t_R = 7.21 min.

HR-MS (ESI+): calcd. for $[M+3H]^{3+}$: 1591.1804; found: 1591.1790, calcd. for $[M+4H]^{4+}$: 1193.6371; found: 1193.6362, calcd. for $[M+5H]^{5+}$: 955.1111; found: 955.1103, calcd. for $[M+6H]^{6+}$: 796.0938; found: 796.0931, calcd. for $[M+7H]^{7+}$: 682.5100; found: 682.5094, calcd. for $[M+8H]^{8+}$: 597.3222; found: 597.3217.

Synthesis of 114

114

5 µmol of resin-bound **99** were elongated with **113** following SOP 2c. The alloc protecting group of the *C*-terminal lysine was removed following SOP 15 and FITC was introduced following SOP 2c using only DIPEA as an additive. The peptide was cleaved from resin following SOP 6 and purified by semi-preparative HPLC.

HPLC (column 5, gradient: 20-80% B in 30 min): t_R = 19.08 min.

UHPLC (gradient: 20-80% B in 15 min): t_R = 8.43 min.

HR-MS (ESI+): calcd. for $[M+2H]^{2+}$: 1570.7284; found: 1570.7285, calcd. for $[M+3H]^{3+}$: 1047.4880; found: 1047.4889, calcd. for $[M+4H]^{4+}$: 785.8678; found: 785.8676.

Synthesis of 115

115

5 µmol of resin-bound **98** were elongated with DBCO acid following SOP 2c. Deviating from the SOP, 3.0 eq. of the building block were used in the coupling step and activation was performed with 3.0 eq. HOAt, 2.9 eq. HATU and 6.0 eq. DIPEA. The peptide was cleaved from resin following SOP 6 and purified by semi-preparative HPLC.

HPLC (column 5, gradient: 10-70% B in 30 min): t_R = 18.74 min.

UHPLC (gradient: 20-80% B in 15 min): t_R = 6.00 min.

HR-MS (ESI+): calcd. for $[M+2H]^{2+}$: 1399.8535; found: 1399.8524, calcd. for $[M+3H]^{3+}$: 933.5714; found: 933.5702, calcd. for $[M+4H]^{4+}$: 700.4304; found: 700.4307, calcd. for $[M+5H]^{5+}$ 560.5457; found: 560.5466, calcd. for $[M+6H]^{6+}$: 467.2893; found: 467.2897.

Synthesis of 119

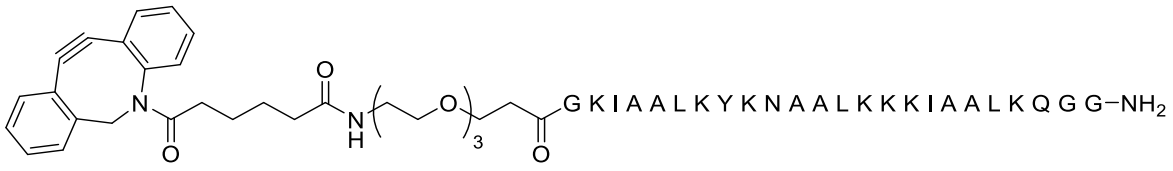

119

5 µmol of resin-bound **98** were elongated with Fmoc-NH-PEG(3)-OH and DBCO acid following SOP 2c. Coupling of the latter was performed deviating from the SOP, 3.0 eq. of the building block were used in the coupling step and activation was performed with 3.0 eq. HOAt, 2.9 eq. HATU and 6.0 eq. DIPEA. The peptide was cleaved from resin following SOP 6 and purified by semi-preparative HPLC.

HPLC (column 5, gradient: 10-70% B in 30 min): t_R = 21.19 min.

UHPLC (gradient: 20-80% B in 15 min): t_R = 5.98 min.

HR-MS (ESI+): calcd. for $[M+3H]^{3+}$: 1001.2767; found: 1001.2788, calcd. for $[M+4H]^{4+}$: 751.2093; found: 751.2077, calcd. for $[M+5H]^{5+}$ 601.1689; found: 601.1686, calcd. for $[M+6H]^{6+}$: 501.1420; found: 501.1426.

Synthesis of 117

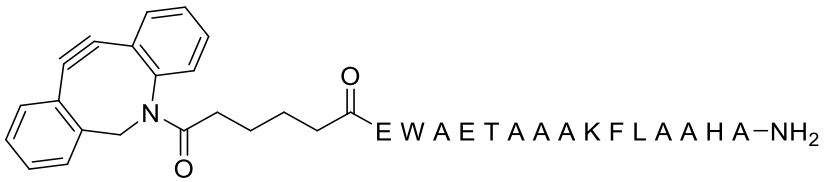

117

5 µmol of resin-bound **101** were elongated with DBCO acid following SOP 2c. Deviating from the SOP, 3.0 eq. of the building block were used in the coupling step and activation was performed with 3.0 eq. HOAt, 2.9 eq. HATU and 6.0 eq. DIPEA. The peptide was cleaved from resin following SOP 6 and purified by semi-preparative HPLC.

HPLC (column 5, gradient: 20-80% B in 30 min): t_R = 24.52 min.

UHPLC (gradient: 20-80% B in 15 min): t_R = 10.24 min.

HR-MS (ESI+): calcd. for $[M+2H]^{2+}$: 951.4742; found: 951.4740, calcd. for $[M+3H]^{3+}$: 634.6519; found: 634.6516.

Synthesis of 121

121

5 µmol of resin-bound **98** were elongated with Fmoc-D-β-Phe(2-NO_2)-OH and **86** following SOP 2c. The peptide was cleaved from resin following SOP 6 and purified by semi-preparative HPLC.

HPLC (column 5, gradient: 5-65% B in 30 min): t_R = 17.37 min.

UHPLC (gradient: 5-65% B in 15 min): t_R = 7.69 min.

HR-MS (ESI+): calcd. for $[M+2H]^{2+}$: 1388.8410; found: 1388.8374, calcd. for $[M+3H]^{3+}$: 926.2298; found: 926.2275, calcd. for $[M+4H]^{4+}$: 694.9242; found: 694.9238, calcd. for $[M+5H]^{5+}$: 556.1408; found: 556.1417, calcd. for $[M+6H]^{6+}$: 463.6185; found: 463.6184.

Synthesis of 122

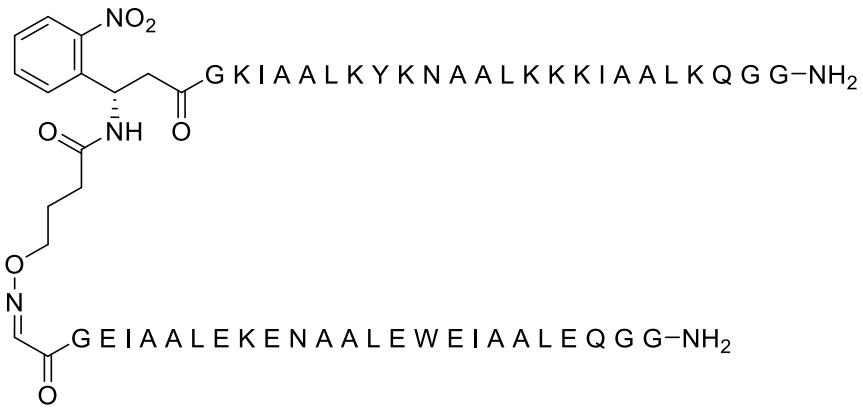

122

102 and **121** were ligated following SOP 14 with a strand concentration of 100 µM and a total volume of 1000 µL. Aliquots of the reaction mixture were taken after 0, 4 and 17.5 h and analyzed by UHPLC. After 18 h, the reaction solution was frozen in liquid nitrogen, lyophilized and subsequently purified by analytical HPLC.

HPLC (column 6, gradient: 10-70% B in 30 min): t_R = 19.31 min.

UHPLC (gradient: 5-95% B in 15 min): t_R = 7.86 min.

HR-MS (ESI+): calcd. for $[M+4H]^{4+}$: 1332.4870; found: 1332.4850, calcd. for $[M+5H]^{5+}$: 1066.1911; found: 1066.1896, calcd. for $[M+6H]^{6+}$ 888.6604; found: 888.6589, calcd. for $[M+7H]^{7+}$: 761.8528; found: 761.8518.

Photolysis of 122

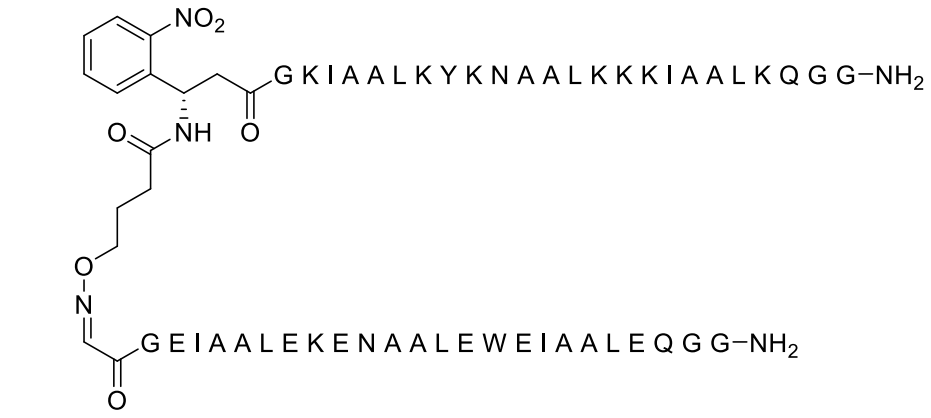

122

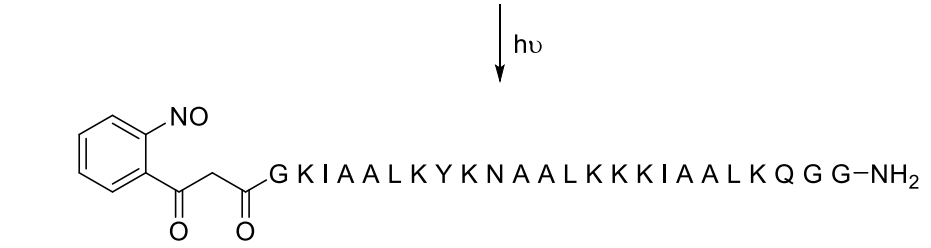

123

+

124

122 was dissolved in phosphate buffer (250 µL, 50 mM, pH 7.0) to give a concentration of 25 µM. The solution was irradiated at 600 W (lamp setup a) for 40 min without using the cut-on filter. The reaction solution was analyzed by LC-MS.

LC-MS (gradient: 10-100% B in 15 min): t_R (**123**) = 5.05 – 5.35 min, t_R (**124**) = 12.02 – 12.25 min.

HR-MS (ESI+): calcd. for [**123**+3H]$^{3+}$: 886.8719; found: 886.8717, calcd. for [**123**+4H]$^{4+}$: 665.4057; found: 665.4054, calcd. for [**123**+5H]$^{5+}$: 532.5260; found: 532.5257.

HR-MS (ESI+): calcd. for [**124**+2H]$^{2+}$: 1334.6683; found: 1334.6681, calcd. for [**124**+3H]$^{3+}$: 890.1147; found: 890.1146.

7 Appendix

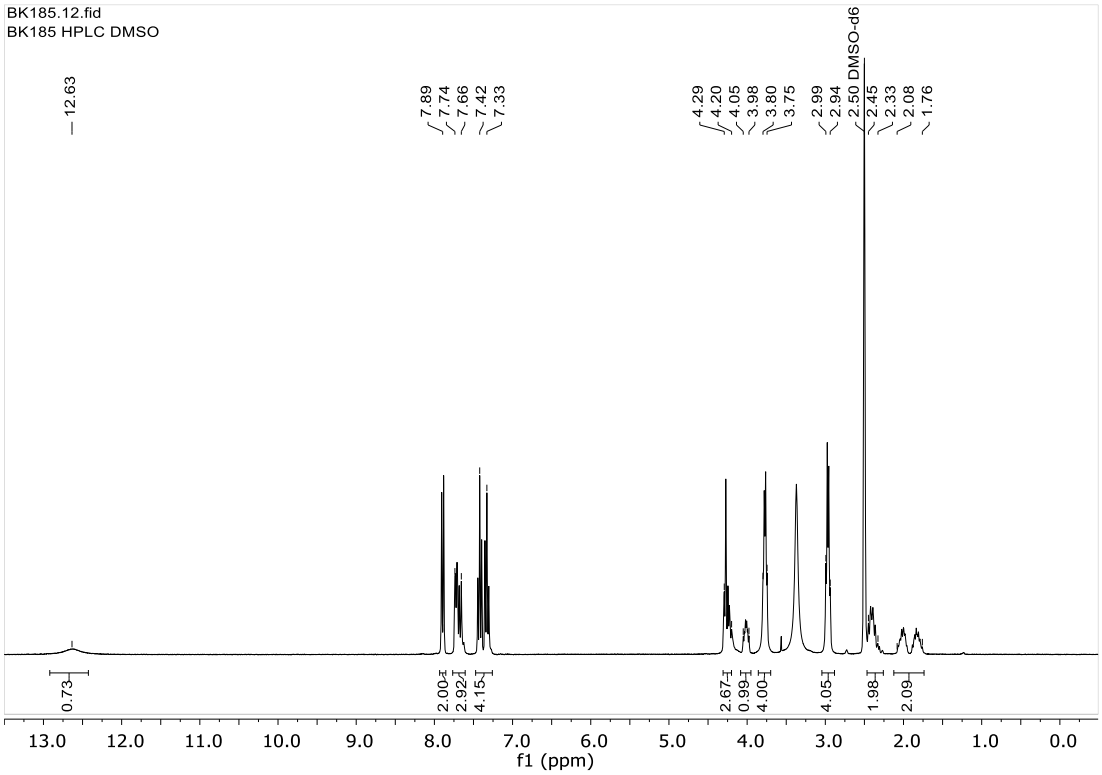

Figure A 1: ^{1}H-NMR spectrum of Fmoc-Glu(SEA^{off})-OH (**11**).

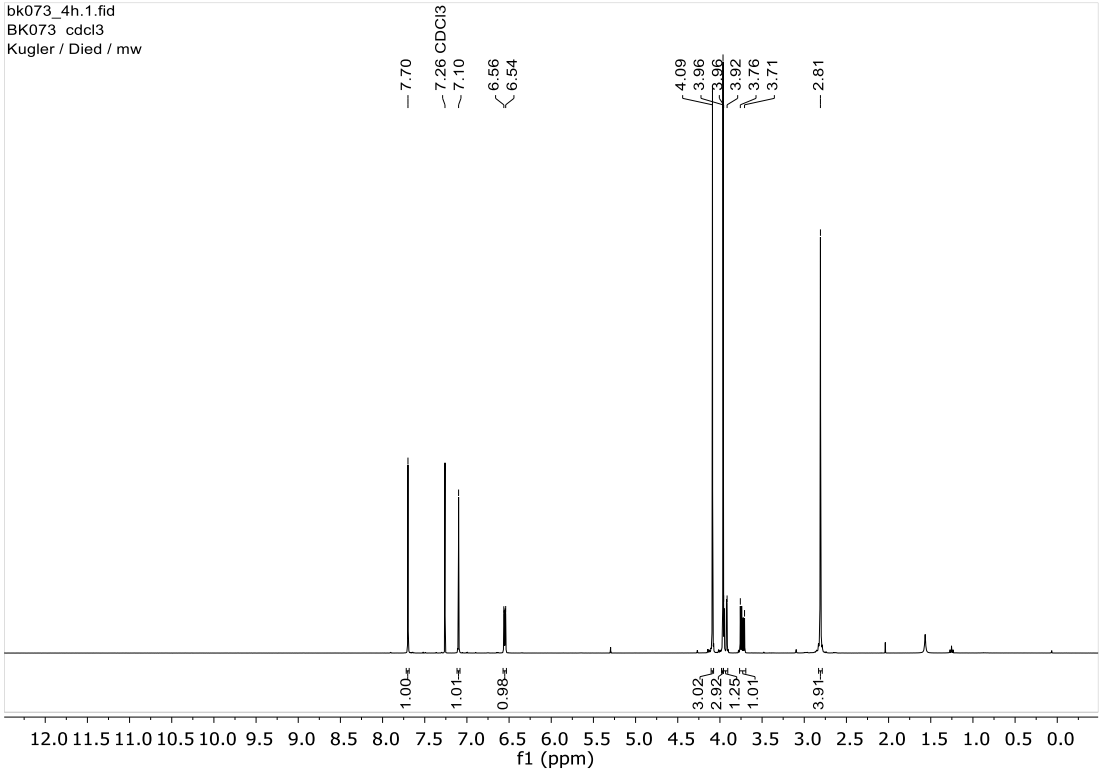

Figure A 2: ^{1}H-NMR spectrum of 2-azido-1-(4,5-dimethoxy-2-nitrophenyl)ethyl *N*-succinimidyl carbonate (**15**).

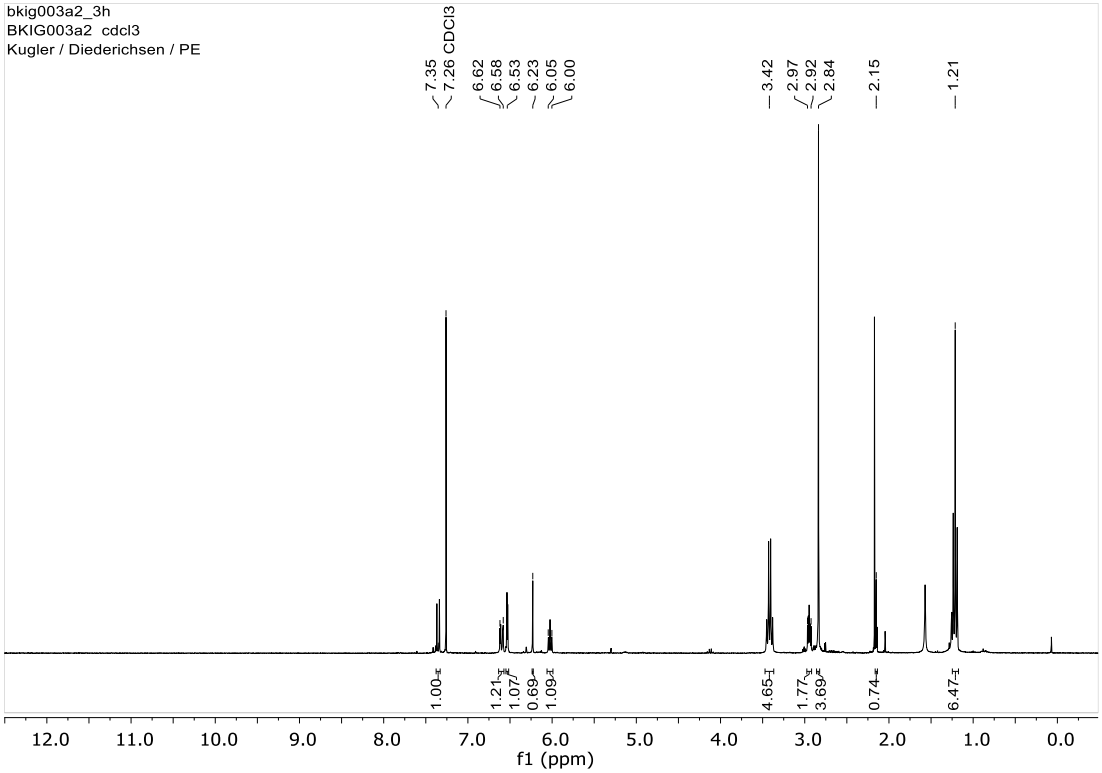

Figure A 3: ^{1}H-NMR spectrum of 1-(7-diethylamino-coumarinyl)-3-butynyl *N*-succinimidyl carbonate (**33**).

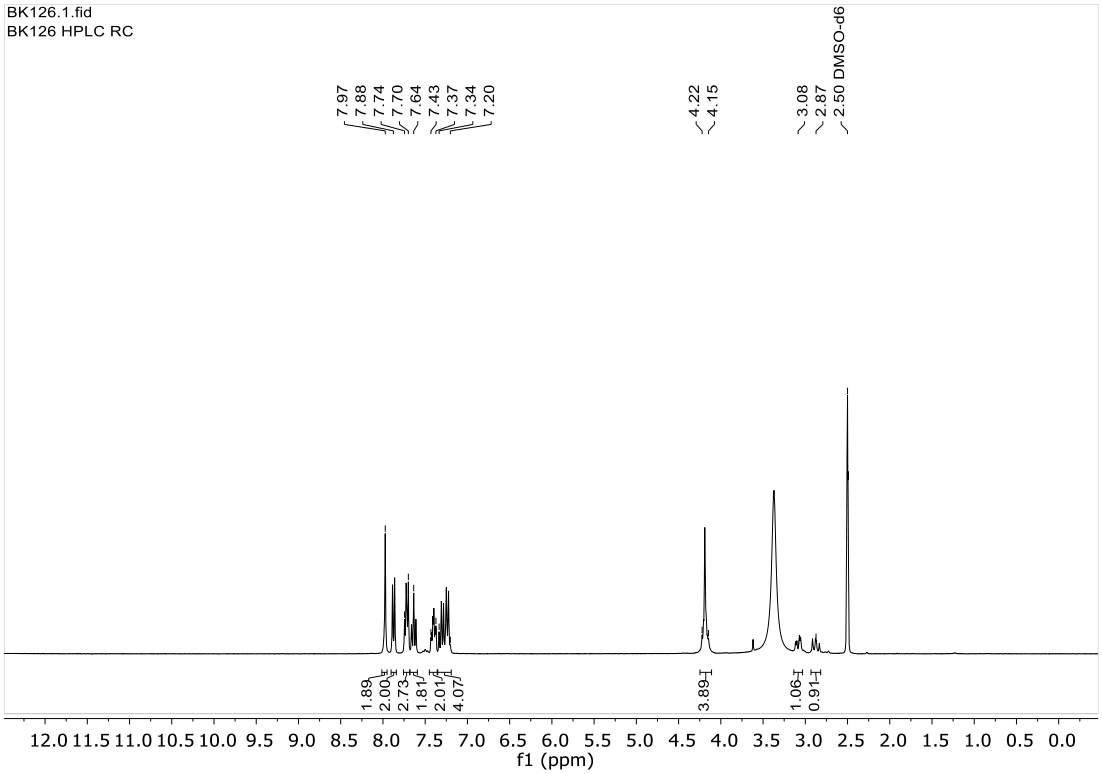

Figure A 4: ^{1}H-NMR spectrum of Fmoc-Bpa (**53**).

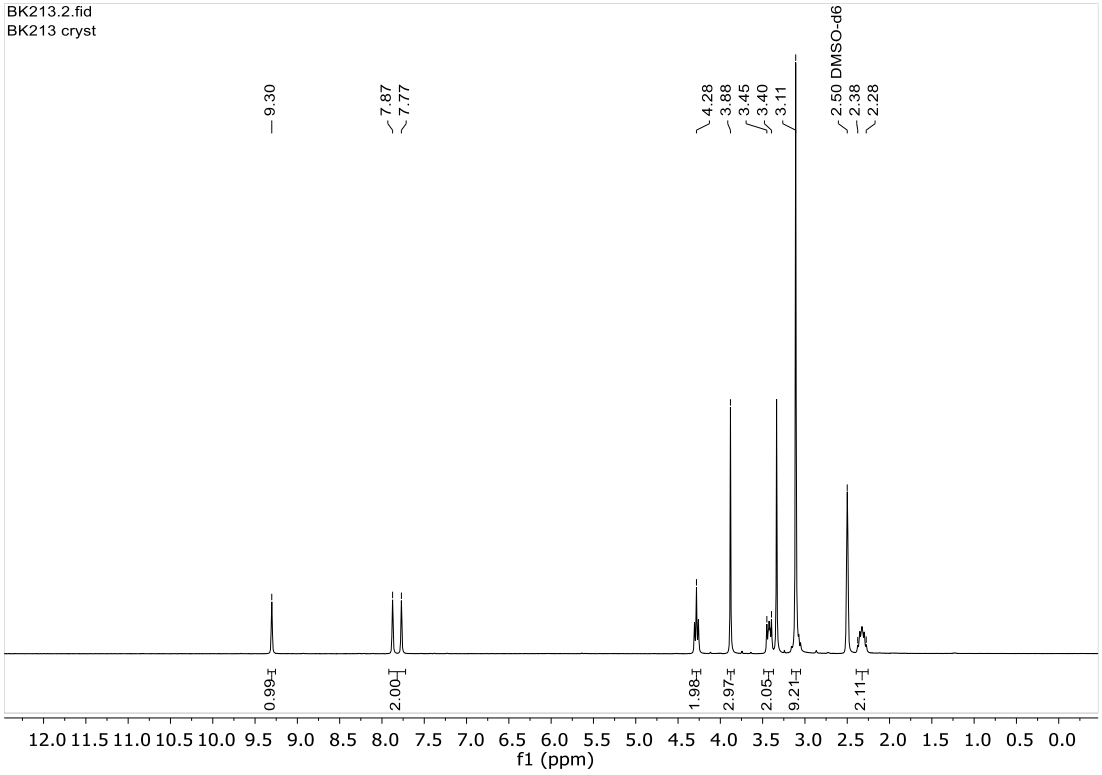

Figure A 5: ^{1}H-NMR spectrum of 1-(3-(trimethylammonium)propyl)-3-methylimidazole bromide (**127**).

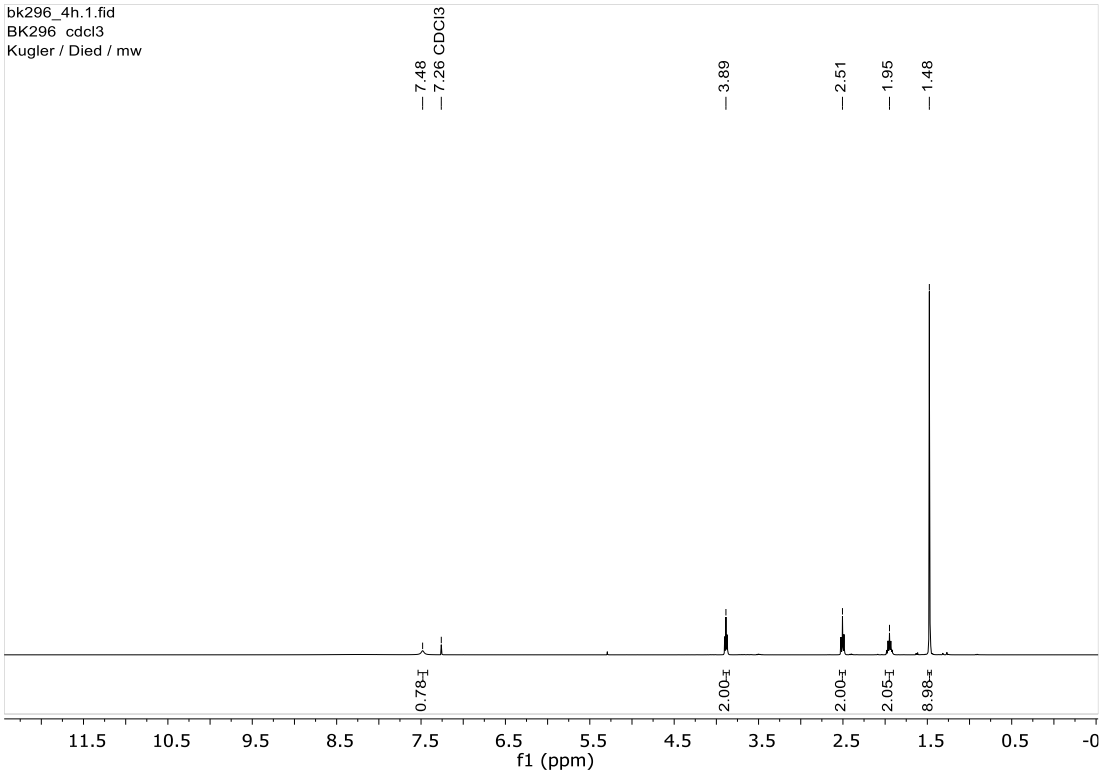

Figure A 6: ^{1}H-NMR spectrum of *N*-Boc-4-(aminooxy)butanoic acid (**86**).

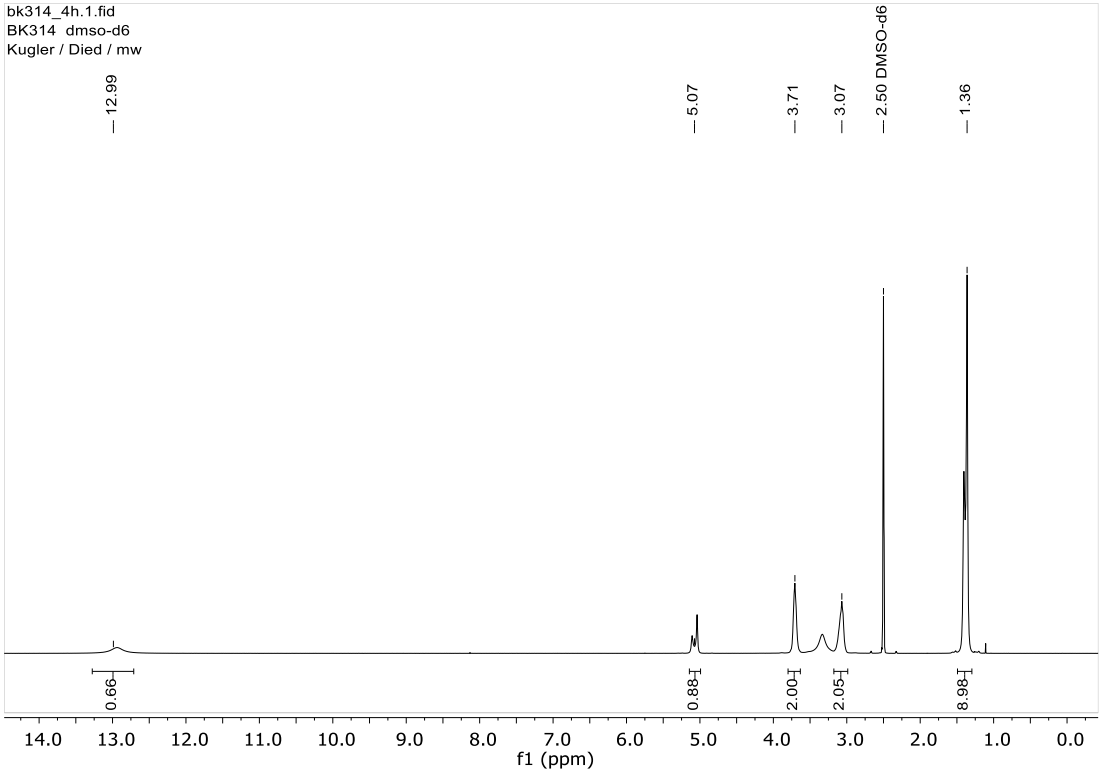

Figure A 7: ^{1}H-NMR spectrum of *N*-Boc-thiazolidine-2-carboxylic acid (**91**).

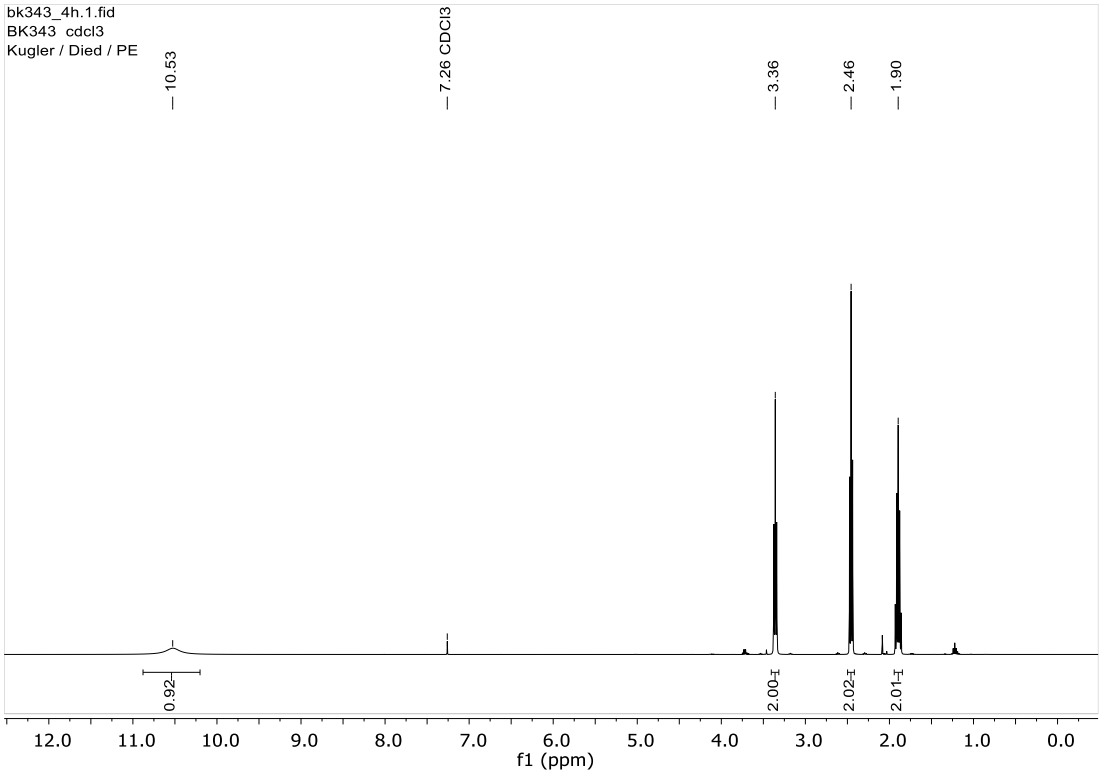

Figure A 8: ^{1}H-NMR spectrum of 4-azidobutyric acid (**113**).

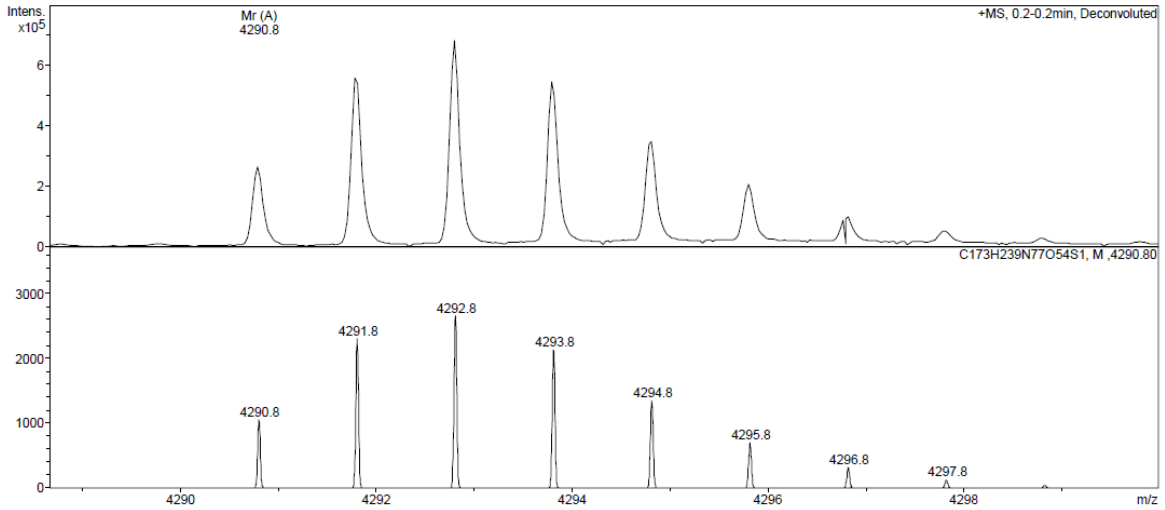

Figure A 9: Deconvoluted ESI (+) mass spectrum of **20**.

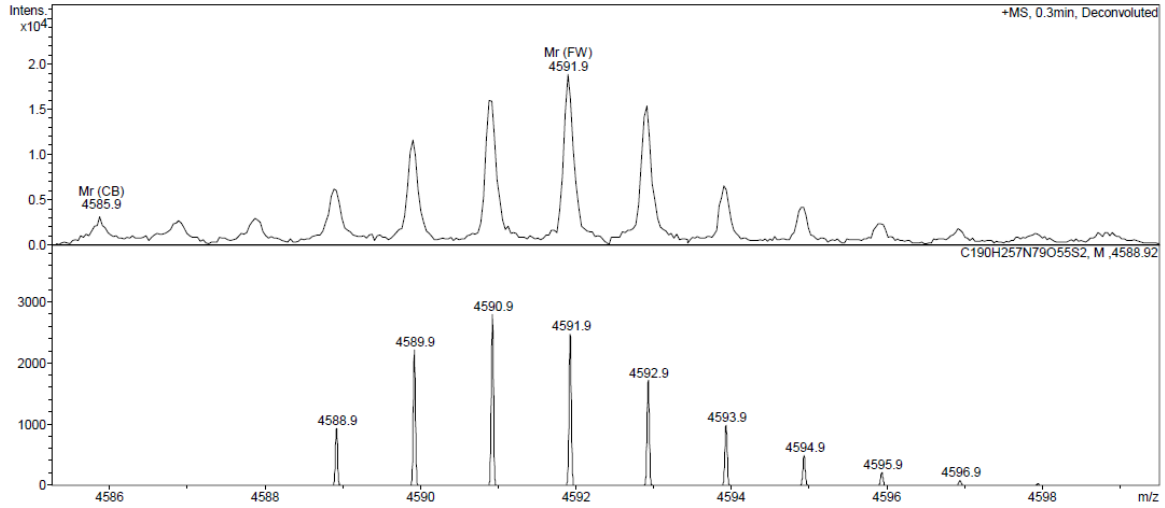

Figure A 10: Deconvoluted ESI (+) mass spectrum of **21**.

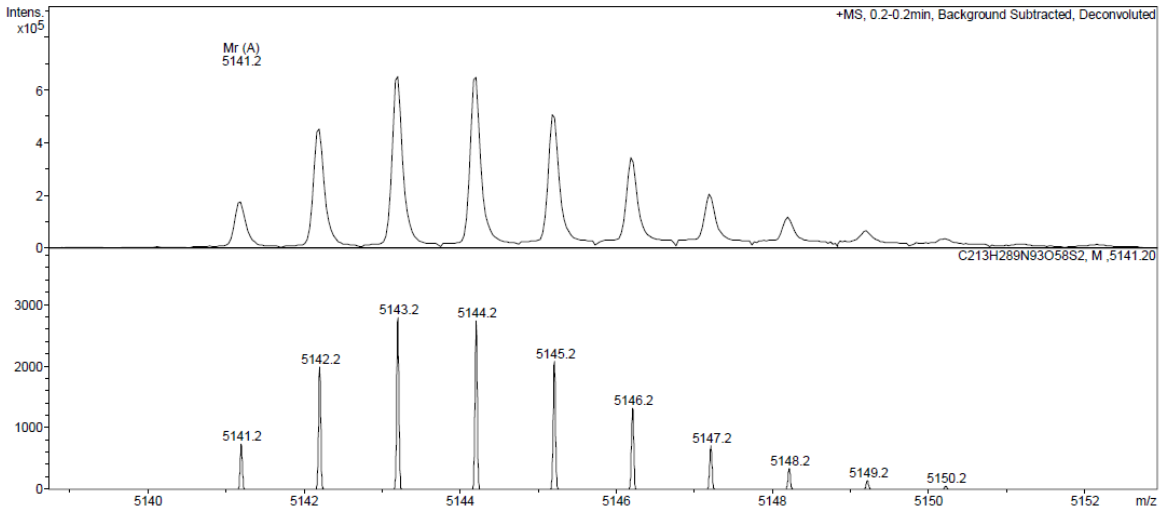

Figure A 11: Deconvoluted ESI (+) mass spectrum of **22**.

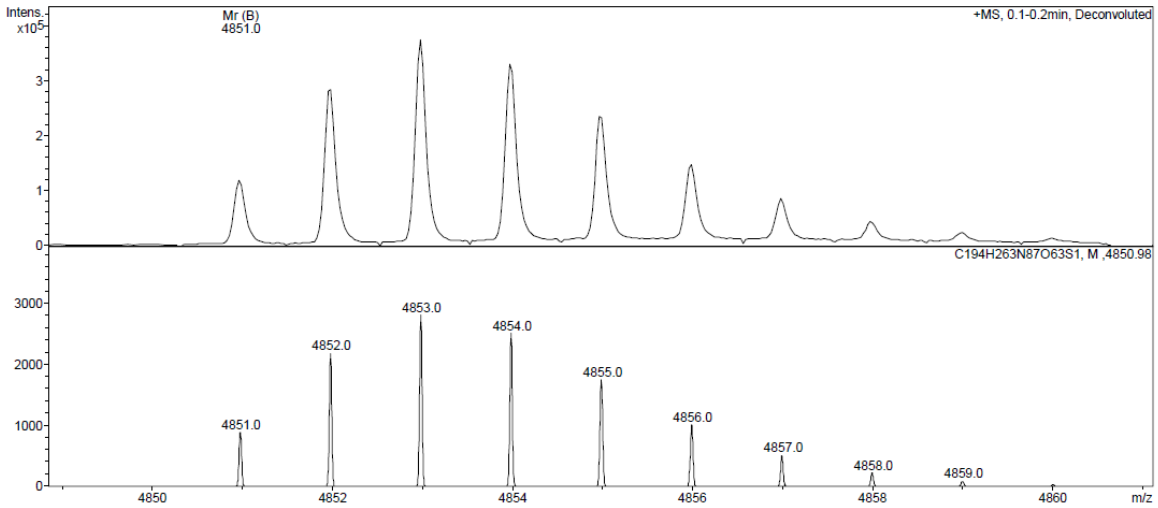

Figure A 12: Deconvoluted ESI (+) mass spectrum of **23**.

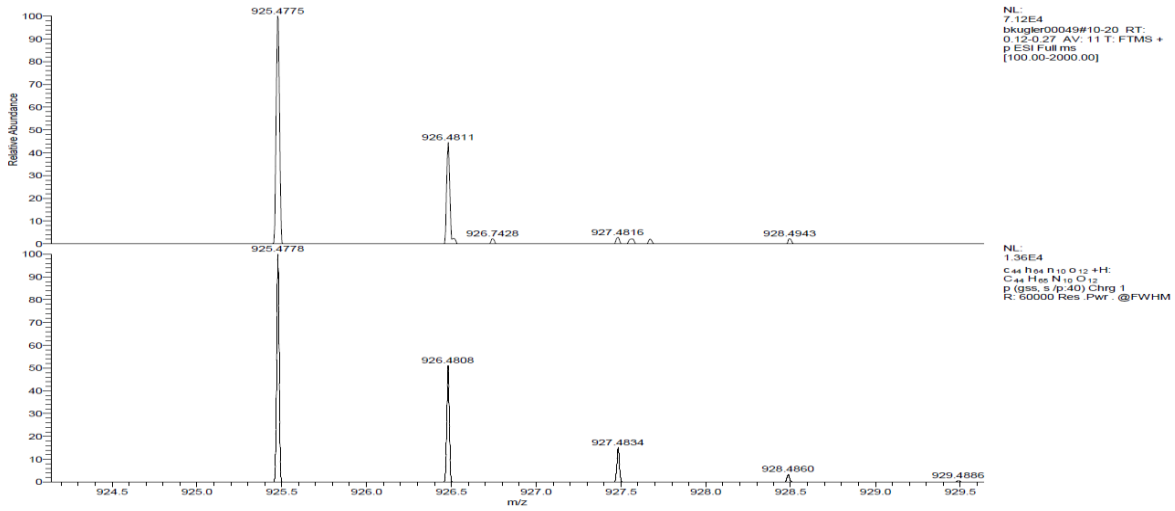

Figure A 13: High-resolution ESI (+) mass spectrum of **29**.

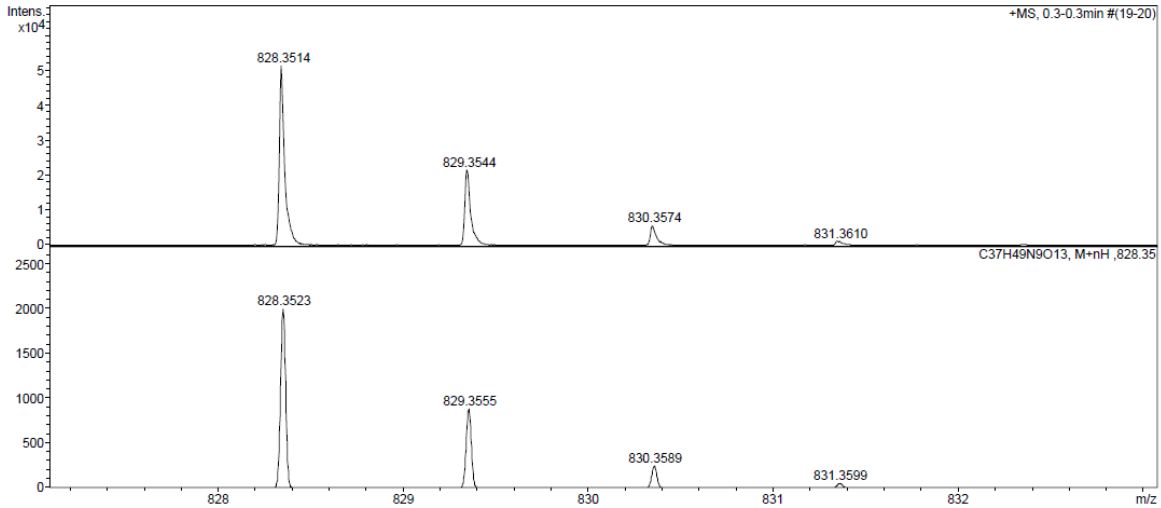

Figure A 14: High-resolution ESI (+) mass spectrum of **36**.

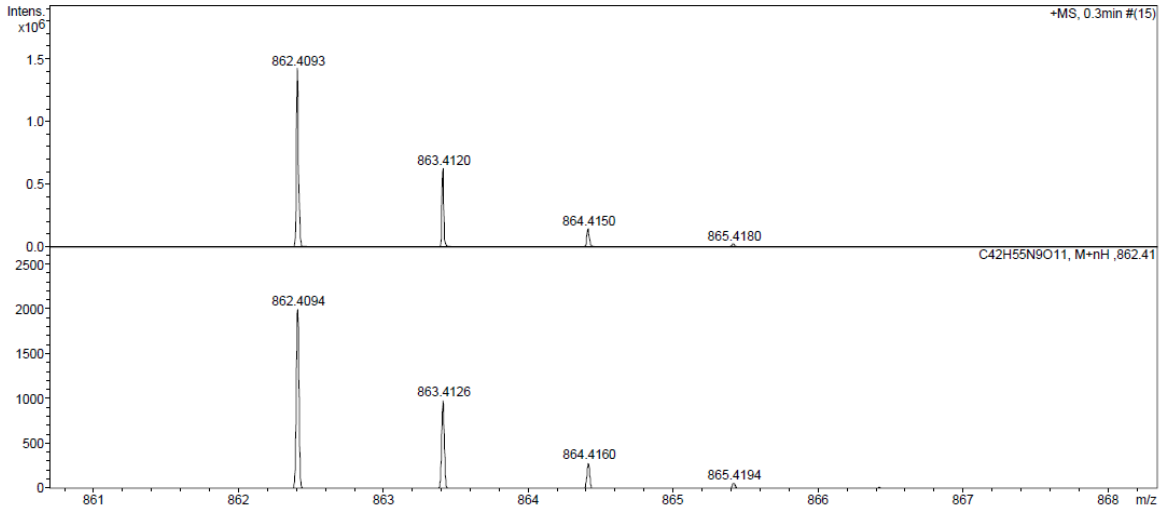

Figure A 15: High-resolution ESI (+) mass spectrum of **38**.

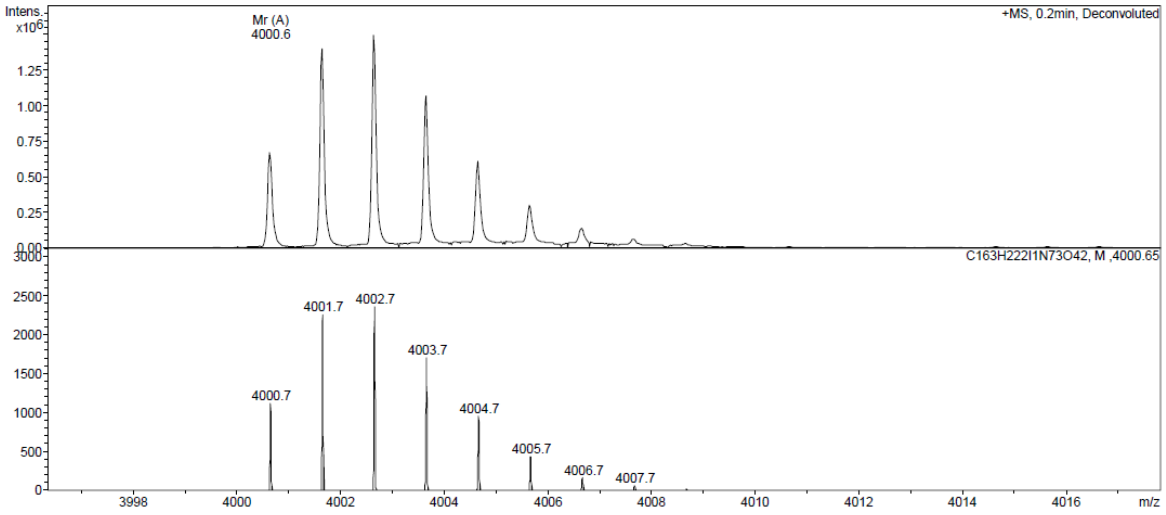

Figure A 16: Deconvoluted ESI (+) mass spectrum of **48**.

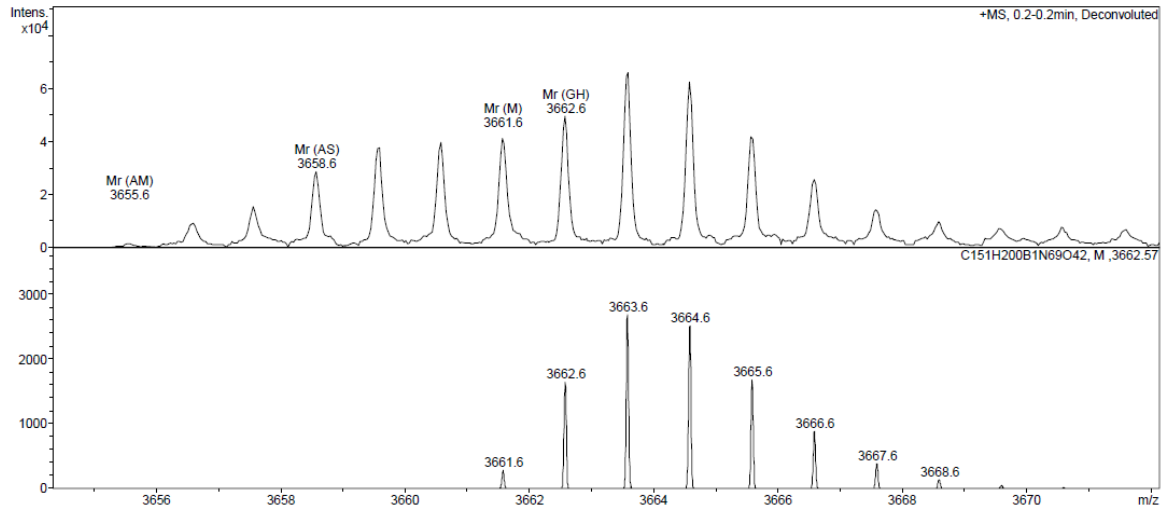

Figure A 17: Deconvoluted ESI (+) mass spectrum of **49**.

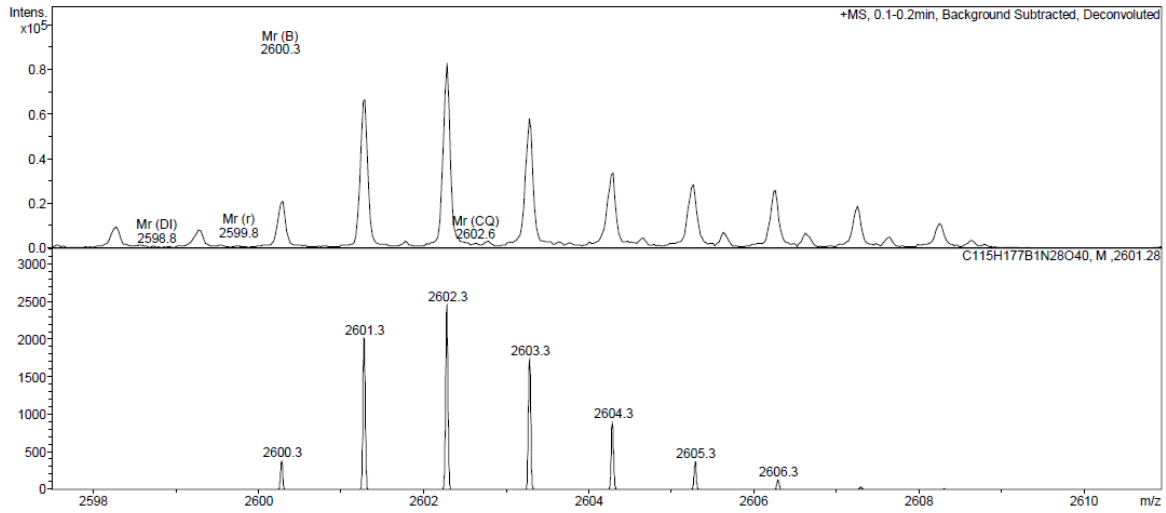

Figure A 18: Deconvoluted ESI (+) mass spectrum of **75**.

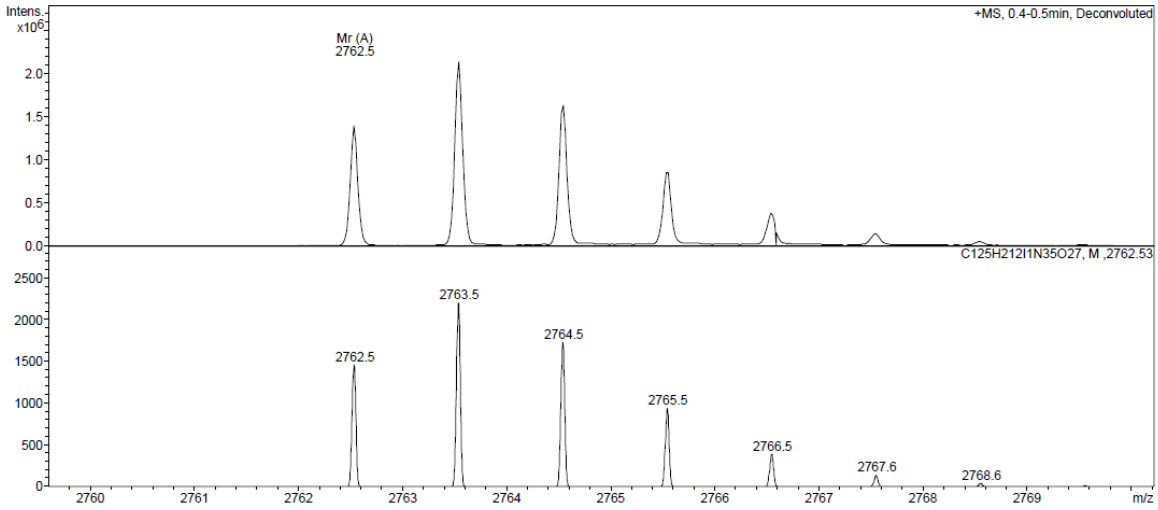

Figure A 19: Deconvoluted ESI (+) mass spectrum of **76**.

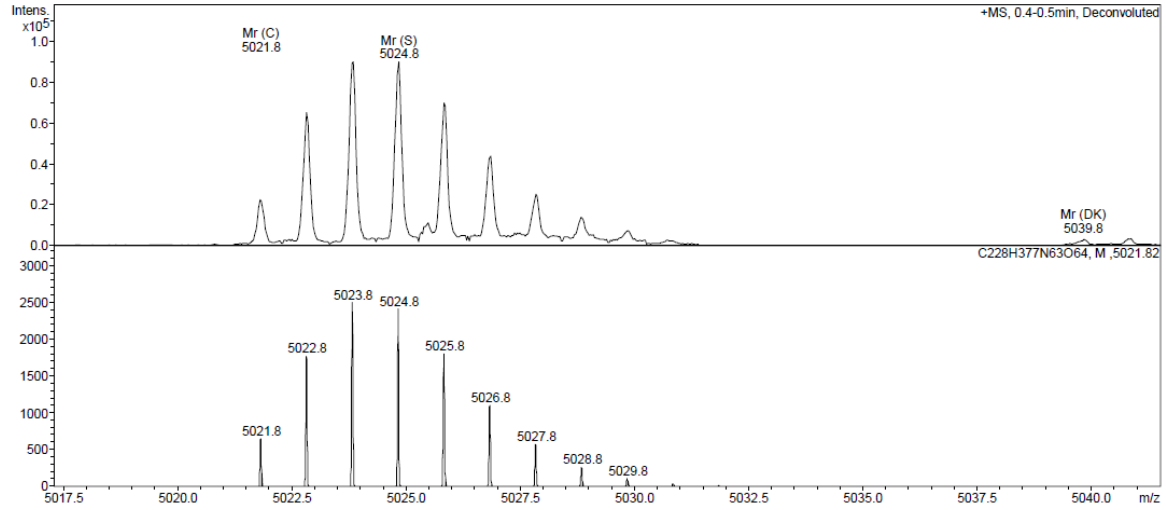

Figure A 20: Deconvoluted ESI (+) mass spectrum of **96** (-H_2O).

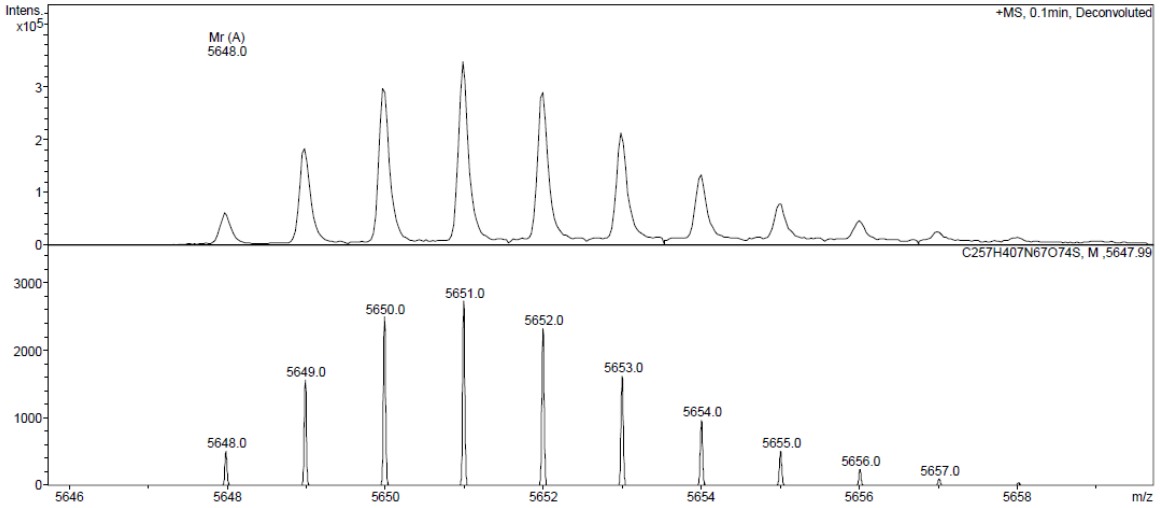

Figure A 21: Deconvoluted ESI (+) mass spectrum of **104**.

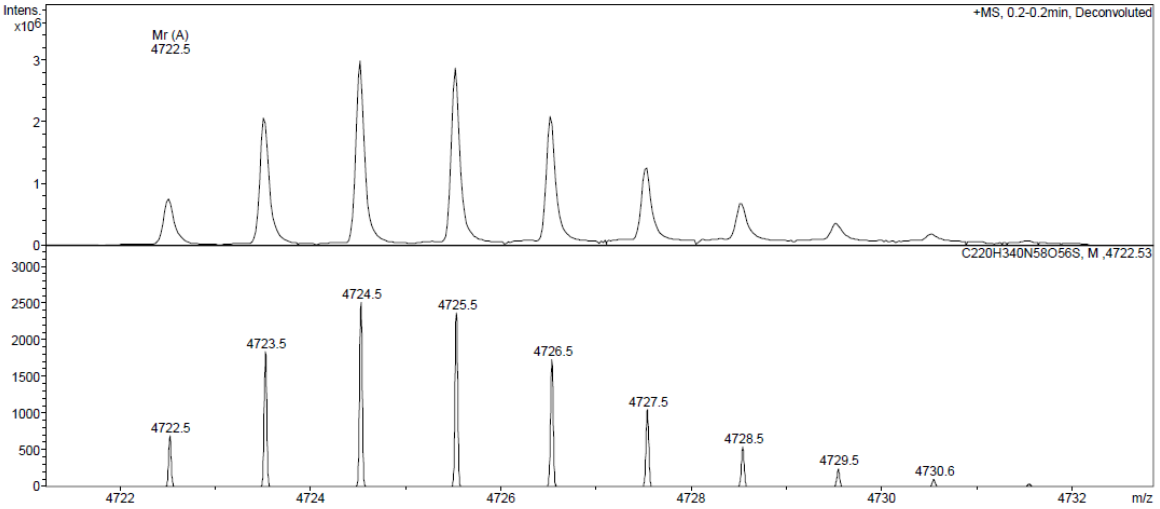

Figure A 22: Deconvoluted ESI (+) mass spectrum of **106**.

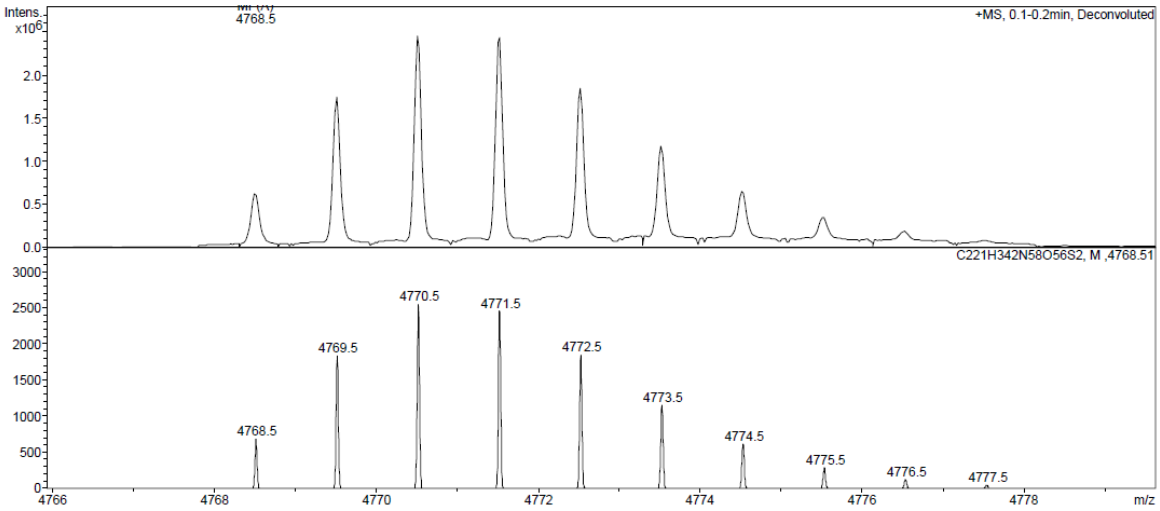

Figure A 23: Deconvoluted ESI (+) mass spectrum of **111**.

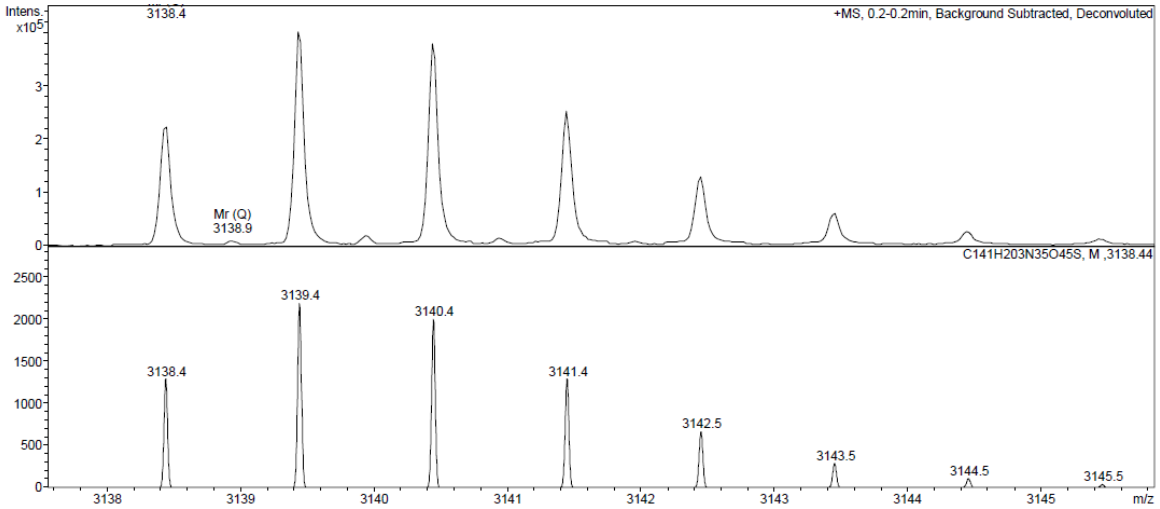

Figure A 24: Deconvoluted ESI (+) mass spectrum of **114**.

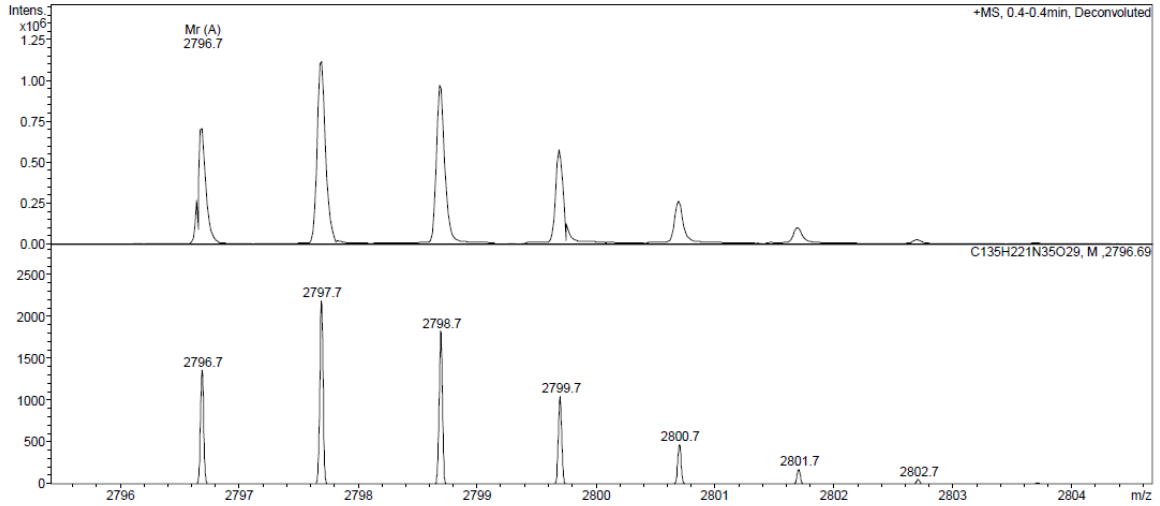

Figure A 25: Deconvoluted ESI (+) mass spectrum of **115**.

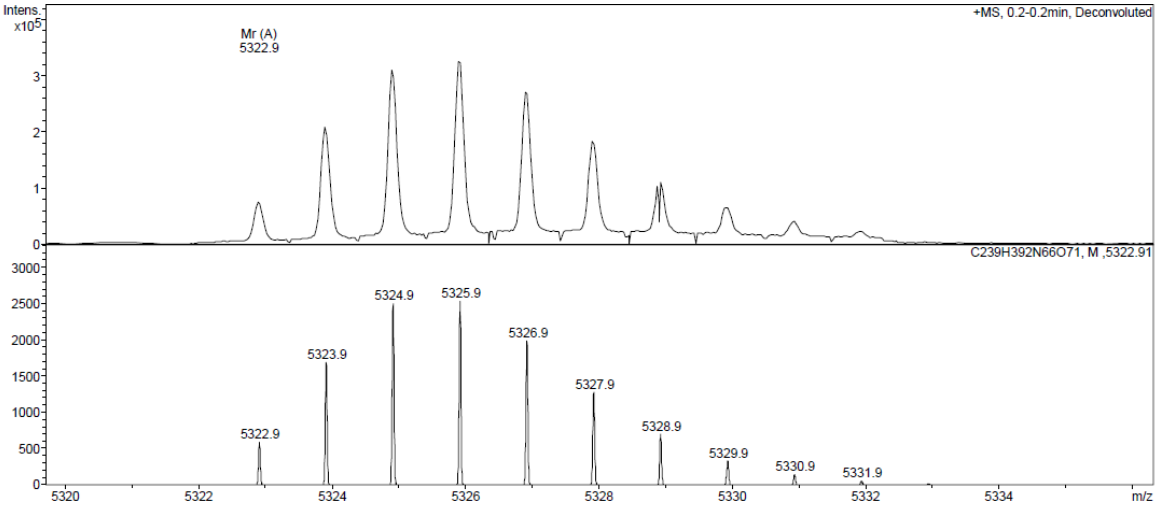

Figure A 26: Deconvoluted ESI (+) mass spectrum of **122**.

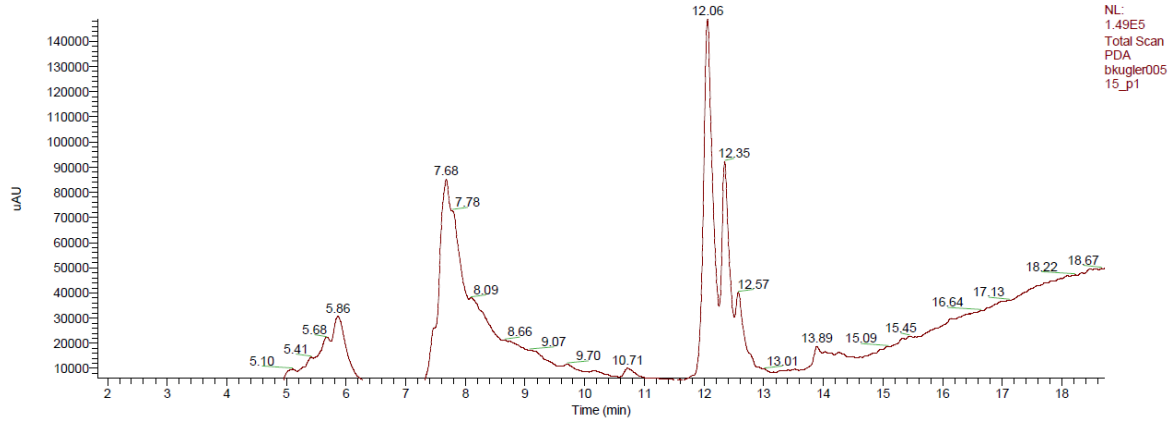

Figure A 27: HPLC Chromatogram of the photolysis of **122**.

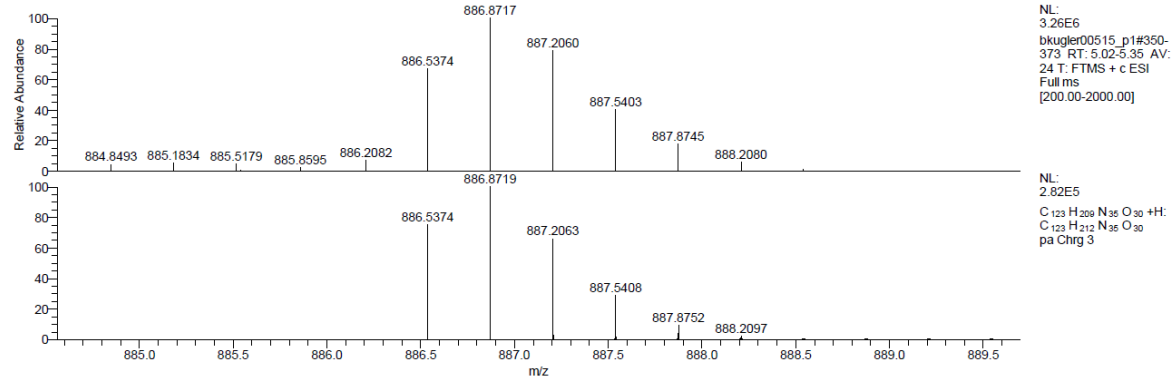

Figure A 28: High-resolution ESI (+) mass spectrum of **123**.

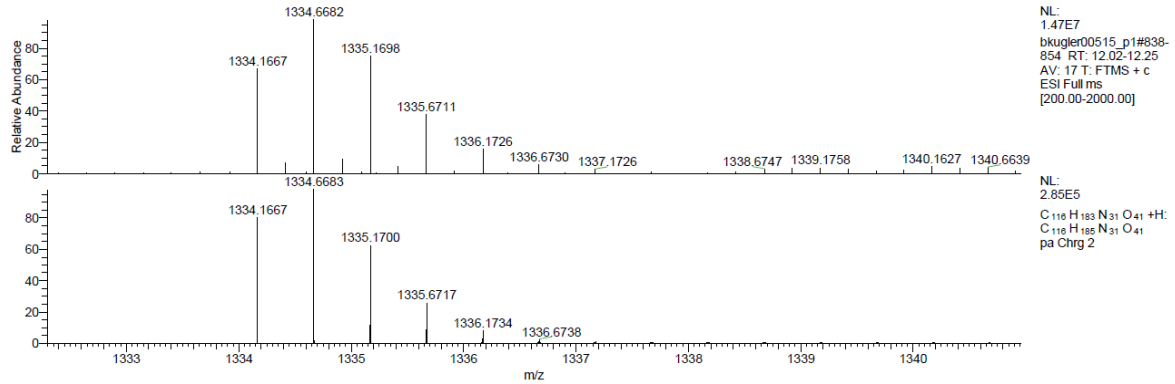

Figure A 29: High-resolution ESI (+) mass spectrum of **124**.

8 List of abbreviations

Standard α-amino acids were abbreviated using one- or three-letter code. Single nucleobases were abbreviated using capital letters (A, C, G, T), while PNA sequences were written in lower case.

A	absorbance
AA	amino acid
abs	absorption
Ac	acetylated
Ac_2O	acetic anhydride
ADC	antibody-drug conjugate
ADHP	2-amino-4,6-dihydroxy-pyrimidine
aeg	*N*-2-(aminoethyl)-glycine
AF	Alexa Fluor (dye)
Ahc	*S*-allylhomocysteine
alloc	allyloxycarbonyl
AO	aminooxy
ar	aromatic
B_2pin_2	bis(pinacolato)diboron
BARAC	biarylazacyclooctyne
BD syringe	syringe supplied by *Becton Dickinson*
Bhoc	benzhydryloxycarbonyl
Boc	*tert*-butyloxycarbonyl
Boc_2O	di-*tert*-butyl dicarbonate
BODIPY	dipyrromethene boron difluoride
bp	base pair
Bpa	4-borono-L-phenylalanine
br	broad
BSA	bovine serum albumin
BSL	*Bacillus lentus*
BTTES	3-(4-((bis((1-(*tert*-butyl)-1*H*-1,2,3-triazol-4-yl)methyl)amino) methyl)-1*H*-1,2,3-triazol-1-yl)propane-1-sulfonic acid
bZip	basic leucine zipper
C. elegans	*Caenorhabditis elegans*
calcd.	calculated

CC	coiled-coil
CD	circular dichroism
CHO	chinese hamster ovary
ClAc	chloroacetic acid
CM	cross-metathesis
CM	coumarin
CPMV	cowpea mosaic virus
cPNA	complementary peptide nucleic acid
CuAAC	Cu(I)-catalyzed azide-alkyne cycloaddition
Cy	cyanine (dye)
Da	Dalton
Dap	2,3-diaminopropionic acid
DBCO	dibenzocyclooctyne
DBU	1,8-diazabicyclo[5.4.0]undec-7-ene
DCM	dichloromethane
deac	deactivation
DEACM	7-diethylamino-4-methylcoumarin
decarb	decarboxylation
DIBO	4-dibenzocyclooctynol
DIC	*N*,*N'*-diisopropylcarbodiimide
DIFO	difluorinated cyclooctyne
DIMAC	aza-dimethoxycyclooctyne
DIPEA	*N*,*N*-diisopropylethylamine
DMF	*N*,*N*-dimethylformamide
DMNB	4,5-dimethoxy-2-nitrobenzyl
DMSO	dimethyl sulfoxide
DNA	deoxyribonucleic acid
DOTA	1,4,7,10-tetracyclododecane-1,4,7,10-tetraacetic acid
dppf	1,1'-bis(diphenylphosphino)ferrocene
ds	double stranded
DSC	*N*,*N'*-disuccinimidyl carbonate
DTPS	DNA-templated protein conjugation
DTS	DNA-templated organic synthesis
E. coli	*Escherichia coli*
EEDQ	*N*-ethoxycarbonyl-2-ethoxy-1,2-dihydroquinoline
EGFR	epidermal growth factor

eq.	equivalents
esc	escape
ESI	electrospray ionization
Et_2O	diethyl ether
Et_3N	triethylamine
EtOAc	ethyl acetate
EtOH	ethanol
ex	excitation
Fab	fragment antigen binding
FBS	fetal bovine serum
FG	functional group
FITC	fluorescein isothiocyanate
FLAG	protein tag with sequence DYKDDDDK
Fmoc	fluorenylmethoxycarbonyl
FRET	Förster resonance energy transfer
FA	formic acid
GABA	γ-aminobutyric acid
GFP	green fluorescent protein
GLP	glucagon-like peptide
GPCR	G protein-coupled receptor
GST	glutathione *S*-transferase
GYG	glycosyltransferase enzyme
H	hyperchromicity
HAT	*H*-atom transfer
HATU	1-[bis(dimethylamino)methylene]-1*H*-1,2,3-triazolo[4,5-b] pyridinium 3-oxide hexafluorophosphate
HBSS	Hanks' balanced salt solution
hDR	human dopamine receptor
HEPES	4-(2-hydroxyethyl)-1-piperazineethanesulfonic acid
Her	human epirdermal growth factor receptor
HFIP	1,1,1,3,3,3-hexafluoro-propan-2-ol
HIV	human immunodeficiency virus
hNPFFR	human neuropeptide FF receptor
HOAc	acetic acid
HOAt	1-hydroxy-7-azabenzotriazole
HOBt	hydroxybenzotriazole

hpf	hours post fertilization
HPG	homopropargylglycine
HPLC	high-performance liquid chromatography
HR-MS	high-resolution mass spectrometry
hyd	hydration
hYR	human neuropeptide Y receptor
IEDDA	inverse electron demand Diels-Alder
IgG	immunoglobulin G
*i*PrOH	propan-2-ol
J	coupling constant
k	rate constant
K_a	acid dissociation constant
KAHA	ketoacid-hydroxylamine
KAT	potassium acyltrifluoroborate
K_D	dissociation constant
LC-MS	liquid chromatography-mass spectrometry
m/z	mass-to-charge ratio
mAb	monoclonal antibody
MBP	maltose binding protein
*m*CPBA	*meta*-chloroperoxybenzoic acid
Me_3SI	trimethylsilyl iodide
MeCN	acetonitrile
MeOH	methanol
MHz	megahertz
Mmt	(4-methoxyphenyl)diphenylmethyl
mol%	mole percentage
MPA	3-mercaptopropanoic acid
MPAA	4-mercaptophenylacetic acid
MRW	mean residue molecular weight
MS	mass spectrometry
NaAsc	sodium ascorbate
NB	nitrobenzyl
NCL	native chemical ligation
NHC	*N*-heterocyclic carbene
NHS	*N*-hydroxysuccinimide
NIR	near-infrared

NMP	*N*-methyl-2-pyrrolidone
NMR	nuclear magnetic resonance
OAc	acetate
OMe	methoxy
OmpC	outer membrane porin protein C
ON	oligonucleotide
OSu	*O*-succinimide
Oxyma	ethyl cyanohydroxyiminoacetate
PBS	phosphate buffered saline
PCL	photocleavable linker
PEG	polyethylene glycol
Ph	phenyl
PIC	*p*-iodobenzyl cysteine
*p*IPhe	*p*-iodophenylalanine
PNA	peptide nucleic acid
pNPY	porcine neuropeptide Y
POI	protein of interest
PPG	photocleavable protecting group
PPh_3	triphenylphosphine
PS	polystyrene
PTM	post-translational modification
PyBOP	benzotriazol-1-yloxytripyrrolidinophosphonium hexafluorophosphate
PyBrOP	bromo-tris-pyrrolidino-phosphonium hexafluorophosphate
q	quaternary
QTOF	quadrupole time-of-flight
Ras	rat sarcoma
RNA	ribonucleic acid
rt	room temperature
SCO	strained cyclooctyne
SEA	bis(2-sulfanylethyl)amido
S_N	nucleophilic substitution
SNARE	soluble *N*-ethylmaleimide-sensitive factor attachment protein receptor
SOP	standard operating procedure
SPAAC	strain-promoted azide-alkyne cycloaddition

SPECT	single photon emission computed tomography
SPPS	solid phase peptide synthesis
TAMRA	carboxytetramethylrhodamine
TBTA	tris((1-benzyl-4-triazoyl)methyl)amine
*t*Bu	*tert*-butyl
*t*BuOH	*tert*-butyl alcohol
TCEP	tris(2-carboxyethyl)phosphine
TCO	*trans*-cyclooctene
TEV	tobacco etch virus
TFA	trifluoroacetic acid
THF	tetrahydrofuran
THPTA	tris(3-hydroxypropyltriazoylmethyl)amine
Thz	2-carboxy thiazolidine
TIS	triisopropylsilane
TLC	thin-layer chromatography
T_m	melting temperature
TMG	1,1,3,3-tetramethylguanidine
TMP-tag	trimethoprim-based tag
TOF	time-of-flight
TPPTS	trisodium 3,3',3-phosphinetriyltribenzenesulfonate
t_R	retention time
Tris	tris(hydroxymethyl)aminomethane
Trt	trityl
Trx	thioredoxin
Tz	tetrazine
UAA	unnatural amino acid
Ub	ubiquitin
UHPLC	ultra high performance liquid chromatography
UV	ultraviolet
v/*v*	volume-to-volume ratio
vis	visible
WT	wild type
wt.%	percentage by weight
YFP	yellow fluorescent protein
δ	chemical shift
ε	extinction coefficient

θ	molar elipticity
λ	wavelength
Φ	quantum yield

9 Bibliography

[1] G. L. Rosano, E. A. Ceccarelli, *Front. Microbiol.* **2014**, *5*, 172.

[2] C. T. Walsh, S. Garneau-Tsodikova, G. J. Gatto, *Angew. Chem. Int. Ed.* **2005**, *44*, 7342–7372.

[3] C. J. Noren, S. J. Anthony-Cahill, M. C. Griffith, P. G. Schultz, *Science* **1989**, *244*, 182–188.

[4] L. Wang, A. Brock, B. Herberich, P. G. Schultz, *Science* **2001**, *292*, 498–500.

[5] T. S. Young, P. G. Schultz, *J. Biol. Chem.* **2010**, *285*, 11039–11044.

[6] C. P. Toseland, *J. Chem. Biol.* **2013**, *6*, 85–95.

[7] M. Chalfie, Y. Tu, G. Euskirchen, W. W. Ward, D. C. Prasher, *Science* **1994**, *263*, 802–805.

[8] C. Freidel, S. Kaloyanova, K. Peneva, *Amino acids* **2016**, *48*, 1357–1372.

[9] C. D. Spicer, B. G. Davis, *Nat. Commun.* **2014**, *5*, 4740.

[10] N. Krall, F. P. Da Cruz, O. Boutureira, G. J. L. Bernardes, *Nat. Chem.* **2016**, *8*, 103–113.

[11] J. A. Shadish, C. A. DeForest, *Matter* **2020**, *2*, 50–77.

[12] S. Middel, C. H. Panse, S. Nawratil, U. Diederichsen, *ChemBioChem* **2017**, *18*, 2328–2332.

[13] H. P. Hemantha, S. N. Bavikar, Y. Herman-Bachinsky, N. Haj-Yahya, S. Bondalapati, A. Ciechanover, A. Brik, *J. Am. Chem. Soc.* **2014**, *136*, 2665–2673.

[14] S. Massa, C. Xavier, J. de Vos, V. Caveliers, T. Lahoutte, S. Muyldermans, N. Devoogdt, *Bioconjugate Chem.* **2014**, *25*, 979–988.

[15] J. Morales-Sanfrutos, J. Lopez-Jaramillo, M. Ortega-Muñoz, A. Megia-Fernandez, F. Perez-Balderas, F. Hernandez-Mateo, F. Santoyo-Gonzalez, *Org. Biomol. Chem.* **2010**, *8*, 667–675.

[16] X. Chen, K. Muthoosamy, A. Pfisterer, B. Neumann, T. Weil, *Bioconjugate Chem.* **2012**, *23*, 500–508.

[17] P. Rosa-Neto, B. Wängler, L. Iovkova, G. Boening, A. Reader, K. Jurkschat, E. Schirrmacher, *ChemBioChem* **2009**, *10*, 1321–1324.

[18] A. Moosmann, J. Blath, R. Lindner, E. Müller, H. Böttinger, *Bioconjugate Chem.* **2011**, *22*, 1545–1558.

[19] P. E. Dawson, T. W. Muir, I. Clark-Lewis, S. B. Kent, *Science* **1994**, *266*, 776–779.

[20] P. E. Dawson, S. B. Kent, *Annu. Rev. Biochem.* **2000**, *69*, 923–960.

[21] V. Y. Torbeev, S. B. H. Kent, *Angew. Chem. Int. Ed.* **2007**, *46*, 1667–1670.

[22] M. N. Fodje, S. Al-Karadaghi, *Protein Eng., Des. Sel.* **2002**, *15*, 353–358.

[23] L. Z. Yan, P. E. Dawson, *J. Am. Chem. Soc.* **2001**, *123*, 526–533.

[24] P. E. Dawson, *Isr. J. Chem.* **2011**, *51*, 862–867.

[25] L. R. Malins, R. J. Payne, *Aust. J. Chem.* **2015**, *68*, 521.

[26] D. S. Y. Yeo, R. Srinivasan, M. Uttamchandani, G. Y. J. Chen, Q. Zhu, S. Q. Yao, *Chem. Commun.* **2003**, 2870–2871.

[27] J. A. Prescher, C. R. Bertozzi, *Nat. Chem. Biol.* **2005**, *1*, 13–21.

[28] V. Mäde, S. Els-Heindl, A. G. Beck-Sickinger, *Beilstein J. Org. Chem.* **2014**, *10*, 1197–1212.

[29] H. C. Hang, C. Yu, D. L. Kato, C. R. Bertozzi, *Proc. Natl. Acad. Sci. USA* **2003**, *100*, 14846–14851.

[30] E. M. Sletten, C. R. Bertozzi, *Acc. Chem. Res.* **2011**, *44*, 666–676.

[31] L. Wang, Z. Zhang, A. Brock, P. G. Schultz, *Proc. Natl. Acad. Sci. USA* **2003**, *100*, 56–61.

[32] A. Dirksen, T. M. Hackeng, P. E. Dawson, *Angew. Chem. Int. Ed.* **2006**, *45*, 7581–7584.

[33] J. Y. Axup, K. M. Bajjuri, M. Ritland, B. M. Hutchins, C. H. Kim, S. A. Kazane, R. Halder, J. S. Forsyth, A. F. Santidrian, K. Stafin et al., *Proc. Natl. Acad. Sci. USA* **2012**, *109*, 16101–16106.

[34] A. Dirksen, P. E. Dawson, *Bioconjugate Chem.* **2008**, *19*, 2543–2548.

[35] Y. Zeng, T. N. C. Ramya, A. Dirksen, P. E. Dawson, J. C. Paulson, *Nat. Methods* **2009**, *6*, 207–209.

[36] Q. A. E. Guthrie, C. Proulx, *Org. Lett.* **2018**, *20*, 2564–2567.

[37] Q. A. E. Guthrie, H. A. Young, C. Proulx, *Chem. Sci.* **2019**, *10*, 9506–9512.

[38] Y. Xu, L. Xu, Y. Xia, C.-J. Guan, Q.-X. Guo, Y. Fu, C. Wang, Y.-M. Li, *Chem. Commun.* **2015**, *51*, 13189–13192.

[39] Y. Xu, Y. Wang, P. Liu, G.-C. Chu, H. Xu, Y.-M. Li, J. Wang, J. Shi, *Org. Biomol. Chem.* **2018**, *16*, 7036–7040.

[40] J. W. Bode, R. M. Fox, K. D. Baucom, *Angew. Chem. Int. Ed.* **2006**, *45*, 1248–1252.

[41] I. Pusterla, J. W. Bode, *Angew. Chem. Int. Ed.* **2012**, *51*, 513–516.

[42] T. G. Wucherpfennig, F. Rohrbacher, V. R. Pattabiraman, J. W. Bode, *Angew. Chem. Int. Ed.* **2014**, *53*, 12244–12247.

[43] L. Ju, J. W. Bode, *Org. Biomol. Chem.* **2009**, *7*, 2259–2264.

[44] V. R. Pattabiraman, A. O. Ogunkoya, J. W. Bode, *Angew. Chem. Int. Ed.* **2012**, *51*, 5114–5118.

[45] A. O. Ogunkoya, V. R. Pattabiraman, J. W. Bode, *Angew. Chem. Int. Ed.* **2012**, *51*, 9693–9697.

[46] S. Baldauf, A. O. Ogunkoya, G. N. Boross, J. W. Bode, *J. Org. Chem.* **2020**, *85*, 1352–1364.

[47] S. Baldauf, D. Schauenburg, J. W. Bode, *Angew. Chem. Int. Ed.* **2019**, *58*, 12599–12603.

[48] I. Pusterla, J. W. Bode, *Nat. Chem.* **2015**, *7*, 668–672.

[49] F. Rohrbacher, G. Deniau, A. Luther, J. W. Bode, *Chem. Sci.* **2015**, *6*, 4889–4896.

[50] F. Rohrbacher, A. Zwicky, J. W. Bode, *Chem. Sci.* **2017**, *8*, 4051–4055.

[51] C. He, S. S. Kulkarni, F. Thuaud, J. W. Bode, *Angew. Chem. Int. Ed.* **2015**, *54*, 12996–13001.

[52] A. M. Dumas, G. A. Molander, J. W. Bode, *Angew. Chem. Int. Ed.* **2012**, *51*, 5683–5686.

[53] H. Noda, G. Erős, J. W. Bode, *J. Am. Chem. Soc.* **2014**, *136*, 5611–5614.

[54] F. Saito, H. Noda, J. W. Bode, *ACS Chem. Biol.* **2015**, *10*, 1026–1033.

[55] S. M. Liu, D. Mazunin, V. R. Pattabiraman, J. W. Bode, *Org. Lett.* **2016**, *18*, 5336–5339.

[56] D. Mazunin, J. W. Bode, *Helv. Chim. Acta* **2017**, *100*, e1600311.

[57] H. Staudinger, J. Meyer, *Helv. Chim. Acta* **1919**, *2*, 635–646.

[58] E. Saxon, C. R. Bertozzi, *Science* **2000**, *287*, 2007–2010.

[59] P. V. Chang, J. A. Prescher, M. J. Hangauer, C. R. Bertozzi, *J. Am. Chem. Soc.* **2007**, *129*, 8400–8401.

[60] M. J. Hangauer, C. R. Bertozzi, *Angew. Chem. Int. Ed.* **2008**, *47*, 2394–2397.

[61] A. S. Cohen, E. A. Dubikovskaya, J. S. Rush, C. R. Bertozzi, *J. Am. Chem. Soc.* **2010**, *132*, 8563–8565.

[62] B. L. Nilsson, L. L. Kiessling, R. T. Raines, *Org. Lett.* **2000**, *2*, 1939–1941.

[63] E. Saxon, J. I. Armstrong, C. R. Bertozzi, *Org. Lett.* **2000**, *2*, 2141–2143.

[64] B. L. Nilsson, R. J. Hondal, M. B. Soellner, R. T. Raines, *J. Am. Chem. Soc.* **2003**, *125*, 5268–5269.

[65] N. J. Agard, J. M. Baskin, J. A. Prescher, A. Lo, C. R. Bertozzi, *ACS Chem. Biol.* **2006**, *1*, 644–648.

[66] R. Serwa, I. Wilkening, G. Del Signore, M. Mühlberg, I. Claussnitzer, C. Weise, M. Gerrits, C. P. R. Hackenberger, *Angew. Chem. Int. Ed.* **2009**, *48*, 8234–8239.

[67] V. Böhrsch, R. Serwa, P. Majkut, E. Krause, C. P. R. Hackenberger, *Chem. Commun.* **2010**, *46*, 3176–3178.

[68] R. Serwa, P. Majkut, B. Horstmann, J.-M. Swiecicki, M. Gerrits, E. Krause, C. P. R. Hackenberger, *Chem. Sci.* **2010**, *1*, 596.

[69] R. Huisgen, *Angew. Chem. Int. Ed.* **1963**, *2*, 565–598.

[70] V. V. Rostovtsev, L. G. Green, V. V. Fokin, K. B. Sharpless, *Angew. Chem. Int. Ed.* **2002**, *41*, 2596–2599.

[71] C. W. Tornøe, C. Christensen, M. Meldal, *J. Org. Chem.* **2002**, *67*, 3057–3064.

[72] H. C. Kolb, M. G. Finn, K. B. Sharpless, *Angew. Chem. Int. Ed.* **2001**, *40*, 2004–2021.

[73] V. O. Rodionov, S. I. Presolski, D. D. Díaz, V. V. Fokin, M. G. Finn, *J. Am. Chem. Soc.* **2007**, *129*, 12705–12712.

[74] T. R. Chan, R. Hilgraf, K. B. Sharpless, V. V. Fokin, *Org. Lett.* **2004**, *6*, 2853–2855.

[75] D. Soriano Del Amo, W. Wang, H. Jiang, C. Besanceney, A. C. Yan, M. Levy, Y. Liu, F. L. Marlow, P. Wu, *J. Am. Chem. Soc.* **2010**, *132*, 16893–16899.

[76] Q. Wang, T. R. Chan, R. Hilgraf, V. V. Fokin, K. B. Sharpless, M. G. Finn, *J. Am. Chem. Soc.* **2003**, *125*, 3192–3193.

[77] P. V. Chang, X. Chen, C. Smyrniotis, A. Xenakis, T. Hu, C. R. Bertozzi, P. Wu, *Angew. Chem. Int. Ed.* **2009**, *48*, 4030–4033.

[78] C. Uttamapinant, A. Tangpeerachaikul, S. Grecian, S. Clarke, U. Singh, P. Slade, K. R. Gee, A. Y. Ting, *Angew. Chem. Int. Ed.* **2012**, *51*, 5852–5856.

[79] C. Kofoed, S. Riesenberg, J. Šmolíková, M. Meldal, S. Schoffelen, *Bioconjugate Chem.* **2019**, *30*, 1169–1174.

[80] N. J. Agard, J. A. Prescher, C. R. Bertozzi, *J. Am. Chem. Soc.* **2004**, *126*, 15046–15047.

[81] J. M. Baskin, J. A. Prescher, S. T. Laughlin, N. J. Agard, P. V. Chang, I. A. Miller, A. Lo, J. A. Codelli, C. R. Bertozzi, *Proc. Natl. Acad. Sci. USA* **2007**, *104*, 16793–16797.

[82] X. Ning, J. Guo, M. A. Wolfert, G.-J. Boons, *Angew. Chem. Int. Ed.* **2008**, *47*, 2253–2255.

[83] J. C. Jewett, E. M. Sletten, C. R. Bertozzi, *J. Am. Chem. Soc.* **2010**, *132*, 3688–3690.

[84] S. T. Laughlin, J. M. Baskin, S. L. Amacher, C. R. Bertozzi, *Science* **2008**, *320*, 664–667.

[85] S. T. Laughlin, C. R. Bertozzi, *ACS Chem. Biol.* **2009**, *4*, 1068–1072.

[86] J. M. Baskin, K. W. Dehnert, S. T. Laughlin, S. L. Amacher, C. R. Bertozzi, *Proc. Natl. Acad. Sci. USA* **2010**, *107*, 10360–10365.

[87] P. V. Chang, J. A. Prescher, E. M. Sletten, J. M. Baskin, I. A. Miller, N. J. Agard, A. Lo, C. R. Bertozzi, *Proc. Natl. Acad. Sci. USA* **2010**, *107*, 1821–1826.

[88] F. Thalhammer, U. Wallfahrer, J. Sauer, *Tetrahedron Lett.* **1990**, *31*, 6851–6854.

[89] M. L. Blackman, M. Royzen, J. M. Fox, *J. Am. Chem. Soc.* **2008**, *130*, 13518–13519.

[90] N. K. Devaraj, R. Weissleder, S. A. Hilderbrand, *Bioconjugate Chem.* **2008**, *19*, 2297–2299.

[91] D. Hunter, D. G. Neilson, T. J. R. Weakley, *J. Chem. Soc., Perkin Trans. 1* **1985**, 2709.

[92] R. Rossin, P. R. Verkerk, S. M. van den Bosch, R. C. M. Vulders, I. Verel, J. Lub, M. S. Robillard, *Angew. Chem. Int. Ed.* **2010**, *49*, 3375–3378.

[93] J. Yang, J. Šečkutė, C. M. Cole, N. K. Devaraj, *Angew. Chem. Int. Ed.* **2012**, *51*, 7476–7479.

[94] D. M. Patterson, L. A. Nazarova, B. Xie, D. N. Kamber, J. A. Prescher, *J. Am. Chem. Soc.* **2012**, *134*, 18638–18643.

[95] I. Nikić, T. Plass, O. Schraidt, J. Szymański, J. A. G. Briggs, C. Schultz, E. A. Lemke, *Angew. Chem. Int. Ed.* **2014**, *53*, 2245–2249.

[96] P. G. Isenegger, B. G. Davis, *J. Am. Chem. Soc.* **2019**, *141*, 8005–8013.

[97] K. Kodama, S. Fukuzawa, H. Nakayama, T. Kigawa, K. Sakamoto, T. Yabuki, N. Matsuda, M. Shirouzu, K. Takio, K. Tachibana et al., *ChemBioChem* **2006**, *7*, 134–139.

[98] J. M. Chalker, C. S. C. Wood, B. G. Davis, *J. Am. Chem. Soc.* **2009**, *131*, 16346–16347.

[99] C. D. Spicer, T. Triemer, B. G. Davis, *J. Am. Chem. Soc.* **2012**, *134*, 800–803.

[100] C. D. Spicer, B. G. Davis, *Chem. Commun.* **2013**, *49*, 2747–2749.

[101] M. K. Bilyard, H. J. Bailey, L. Raich, M. A. Gafitescu, T. Machida, J. Iglésias-Fernández, S. S. Lee, C. D. Spicer, C. Rovira, W. W. Yue et al., *Nature* **2018**, *563*, 235–240.

[102] N. Li, R. K. V. Lim, S. Edwardraja, Q. Lin, *J. Am. Chem. Soc.* **2011**, *133*, 15316–15319.

[103] A. Dumas, C. D. Spicer, Z. Gao, T. Takehana, Y. A. Lin, T. Yasukohchi, B. G. Davis, *Angew. Chem. Int. Ed.* **2013**, *52*, 3916–3921.

[104] J. Li, S. Lin, J. Wang, S. Jia, M. Yang, Z. Hao, X. Zhang, P. R. Chen, *J. Am. Chem. Soc.* **2013**, *135*, 7330–7338.

[105] X. Ma, H. Wang, W. Chen, *J. Org. Chem.* **2014**, *79*, 8652–8658.

[106] B. Bhushan, Y. A. Lin, M. Bak, A. Phanumartwiwath, N. Yang, M. K. Bilyard, T. Tanaka, K. L. Hudson, L. Lercher, M. Stegmann et al., *J. Am. Chem. Soc.* **2018**, *140*, 14599–14603.

[107] J. L. Seitchik, J. C. Peeler, M. T. Taylor, M. L. Blackman, T. W. Rhoads, R. B. Cooley, C. Refakis, J. M. Fox, R. A. Mehl, *J. Am. Chem. Soc.* **2012**, *134*, 2898–2901.

[108] X. Chen, Y.-W. Wu, *Org. Biomol. Chem.* **2016**, *14*, 5417–5439.

[109] X. Li, D. R. Liu, *Angew. Chem. Int. Ed.* **2004**, *43*, 4848–4870.

[110] A. A. Brakhage, *Microbiol. Mol. Biol. Rev.* **1998**, *62*, 547–585.

[111] A. Keppler, S. Gendreizig, T. Gronemeyer, H. Pick, H. Vogel, K. Johnsson, *Nat. Biotechnol.* **2003**, *21*, 86–89.

[112] A. Gautier, A. Juillerat, C. Heinis, I. R. Corrêa, M. Kindermann, F. Beaufils, K. Johnsson, *Cell Chem. Biol.* **2008**, *15*, 128–136.

[113] G. V. Los, L. P. Encell, M. G. McDougall, D. D. Hartzell, N. Karassina, C. Zimprich, M. G. Wood, R. Learish, R. F. Ohana, M. Urh et al., *ACS Chem. Biol.* **2008**, *3*, 373–382.

[114] C. Jing, V. W. Cornish, *ACS Chem. Biol.* **2013**, *8*, 1704–1712.

[115] M. W. Popp, J. M. Antos, G. M. Grotenbreg, E. Spooner, H. L. Ploegh, *Nat. Chem. Biol.* **2007**, *3*, 707–708.

[116] I. Chen, M. Howarth, W. Lin, A. Y. Ting, *Nat. Methods* **2005**, *2*, 99–104.

[117] C.-W. Lin, A. Y. Ting, *J. Am. Chem. Soc.* **2006**, *128*, 4542–4543.

[118] Z. J. Gartner, D. R. Liu, *J. Am. Chem. Soc.* **2001**, *123*, 6961–6963.

[119] Z. J. Gartner, M. W. Kanan, D. R. Liu, *Angew. Chem. Int. Ed.* **2002**, *41*, 1796–1800.

[120] Z. J. Gartner, R. Grubina, C. T. Calderone, D. R. Liu, *Angew. Chem. Int. Ed.* **2003**, *42*, 1370–1375.

[121] C. T. Calderone, J. W. Puckett, Z. J. Gartner, D. R. Liu, *Angew. Chem. Int. Ed.* **2002**, *41*, 4104–4108.

[122] S. Ficht, A. Mattes, O. Seitz, *J. Am. Chem. Soc.* **2004**, *126*, 9970–9981.

[123] S. Ficht, C. Dose, O. Seitz, *ChemBioChem* **2005**, *6*, 2098–2103.

[124] G. Hayashi, M. Yanase, Y. Nakatsuka, A. Okamoto, *Biomacromolecules* **2019**, *20*, 1246–1253.

[125] C. B. Rosen, A. L. B. Kodal, J. S. Nielsen, D. H. Schaffert, C. Scavenius, A. H. Okholm, N. V. Voigt, J. J. Enghild, J. Kjems, T. Tørring et al., *Nat. Chem.* **2014**, *6*, 804–809.

[126] A. L. B. Kodal, C. B. Rosen, M. R. Mortensen, T. Tørring, K. V. Gothelf, *ChemBioChem* **2016**, *17*, 1338–1342.

[127] T. Liu, P. Song, A. Märcher, J. Kjems, C. Yang, K. V. Gothelf, *ChemBioChem* **2019**, *20*, 1014–1018.

[128] T. B. Nielsen, R. P. Thomsen, M. R. Mortensen, J. Kjems, P. F. Nielsen, T. E. Nielsen, A. L. B. Kodal, E. Cló, K. V. Gothelf, *Angew. Chem. Int. Ed.* **2019**, *58*, 9068–9072.

[129] D. H. Lee, J. R. Granja, J. A. Martinez, K. Severin, M. R. Ghadiri, *Nature* **1996**, *382*, 525–528.

[130] A. J. Kennan, V. Haridas, K. Severin, D. H. Lee, M. R. Ghadiri, *J. Am. Chem. Soc.* **2001**, *123*, 1797–1803.

[131] W. Nomura, T. Mino, T. Narumi, N. Ohashi, A. Masuda, C. Hashimoto, H. Tsutsumi, H. Tamamura, *Pept. Sci.* **2010**, *94*, 843–852.

[132] D. N. Woolfson in *Subcellular Biochemistry*, Vol. 82 (Eds.: D. A. D. Parry, J. M. Squire), Springer International Publishing, Basel, **2017**, 35–61.

[133] J. R. Litowski, R. S. Hodges, *J. Biol. Chem.* **2002**, *277*, 37272–37279.

[134] U. Reinhardt, J. Lotze, S. Zernia, K. Mörl, A. G. Beck-Sickinger, O. Seitz, *Angew. Chem. Int. Ed.* **2014**, *53*, 10237–10241.

[135] U. Reinhardt, J. Lotze, K. Mörl, A. G. Beck-Sickinger, O. Seitz, *Bioconjugate Chem.* **2015**, *26*, 2106–2117.

[136] J. Lotze, P. Wolf, U. Reinhardt, O. Seitz, K. Mörl, A. G. Beck-Sickinger, *ACS Chem. Biol.* **2018**, *13*, 618–627.

[137] J. Wang, Y. Yu, J. Xia, *Bioconjugate Chem.* **2014**, *25*, 178–187.

[138] Y. Yano, N. Furukawa, S. Ono, Y. Takeda, K. Matsuzaki, *Pept. Sci.* **2016**, *106*, 484–490.

[139] B. V. Popp, Z. T. Ball, *J. Am. Chem. Soc.* **2010**, *132*, 6660–6662.

[140] B. V. Popp, Z. T. Ball, *Chem. Sci.* **2011**, *2*, 690.

[141] Z. Chen, B. V. Popp, C. L. Bovet, Z. T. Ball, *ACS Chem. Biol.* **2011**, *6*, 920–925.

[142] Z. Chen, F. Vohidov, J. M. Coughlin, L. J. Stagg, S. T. Arold, J. E. Ladbury, Z. T. Ball, *J. Am. Chem. Soc.* **2012**, *134*, 10138–10145.

[143] P. Wittung, P. E. Nielsen, O. Buchardt, M. Egholm, B. Nordén, *Nature* **1994**, *368*, 561–563.

[144] T. Ratilainen, A. Holmén, E. Tuite, P. E. Nielsen, B. Nordén, *Biochemistry* **2000**, *39*, 7781–7791.

[145] D. R. M. Smith, T. Willemse, D. S. Gkotsi, W. Schepens, B. U. W. Maes, S. Ballet, R. J. M. Goss, *Org. Lett.* **2014**, *16*, 2622–2625.

[146] A. D. Roy, R. J. M. Goss, G. K. Wagner, M. Winn, *Chem. Commun.* **2008**, 4831–4833.

[147] P. Klán, T. Šolomek, C. G. Bochet, A. Blanc, R. Givens, M. Rubina, V. Popik, A. Kostikov, J. Wirz, *Chem. Rev.* **2013**, *113*, 119–191.

[148] V. Hagen, S. Frings, B. Wiesner, S. Helm, U. B. Kaupp, J. Bendig, *ChemBioChem* **2003**, *4*, 434–442.

[149] V. R. Shembekar, Y. Chen, B. K. Carpenter, G. P. Hess, *Biochemistry* **2007**, *46*, 5479–5484.

[150] L. J. G. W. van Wilderen, C. Neumann, A. Rodrigues-Correia, D. Kern-Michler, N. Mielke, M. Reinfelds, A. Heckel, J. Bredenbeck, *Phys. Chem. Chem. Phys.* **2017**, *19*, 6487–6496.

[151] L.-M. Herzig, I. Elamri, H. Schwalbe, J. Wachtveitl, *Phys. Chem. Chem. Phys.* **2017**, *19*, 14835–14844.

[152] P. Seyfried, L. Eiden, N. Grebenovsky, G. Mayer, A. Heckel, *Angew. Chem. Int. Ed.* **2017**, *56*, 359–363.

[153] W. M. Rink, F. Thomas, *Chem. Eur. J.* **2019**, *25*, 1665–1677.

[154] S. Middel, *PhD thesis*, Georg-August-Universität Göttingen, Germany, **2016**.

[155] E. Boll, J. Dheur, H. Drobecq, O. Melnyk, *Org. Lett.* **2012**, *14*, 2222–2225.

[156] P. E. Nielsen, M. Egholm, O. Buchardt, *Bioconjugate Chem.* **1994**, *5*, 3–7.

[157] M. Eriksson, P. E. Nielsen, *Nat. Struct. Biol.* **1996**, *3*, 410–413.

[158] S. C. Brown, S. A. Thomson, J. M. Veal, D. G. Davis, *Science* **1994**, *265*, 777–780.

[159] M. Egholm, O. Buchardt, L. Christensen, C. Behrens, S. M. Freier, D. A. Driver, R. H. Berg, S. K. Kim, B. Norden, P. E. Nielsen, *Nature* **1993**, *365*, 566–568.

[160] H. Rasmussen, J. S. Kastrup, J. N. Nielsen, J. M. Nielsen, P. E. Nielsen, *Nat. Struct. Biol.* **1997**, *4*, 98–101.

[161] K. K. Jensen, H. Orum, P. E. Nielsen, B. Nordén, *Biochemistry* **1997**, *36*, 5072–5077.

[162] G. L. Igloi, *Proceedings of the National Academy of Sciences of the United States of America* **1998**, *95*, 8562–8567.

[163] I. Sacui, W.-C. Hsieh, A. Manna, B. Sahu, D. H. Ly, *J. Am. Chem. Soc.* **2015**, *137*, 8603–8610.

[164] G. Höger, *PhD thesis*, Georg-August-Universität Göttingen, Germany, **2019**.

[165] CEM Bioscience Division, *Liberty Demonstration PNA 10-mer*, https://cem.com/media/contenttype/media/literature/PNA-10mer-Synthesis_Report.pdf, **2016**, last accessed: 17.12.2020.

[166] CEM Corporation, *Liberty Blue User Guide*, http://cem.com/media/contenttype/media/literature/525_User_Guide_LibBlue_600329.pdf, **2016**, last accessed: 17.12.2020.

[167] J. Weiler, H. Gausepohl, N. Hauser, O. N. Jensen, J. D. Hoheisel, *Nucleic acids research* **1997**, *25*, 2792–2799.

[168] N. Ollivier, J. Dheur, R. Mhidia, A. Blanpain, O. Melnyk, *Org. Lett.* **2010**, *12*, 5238–5241.

[169] S. Nawratil, *PhD thesis*, Georg-August-Universität Göttingen, Germany, **2017**.

[170] C. D. Spicer, B. G. Davis in *Encyclopedia of Metalloproteins (Eds.:* R. H. Kretsinger, V. N. Uversky, E. A. Permyakov), Springer, New York, NY, **2013**.

[171] A. Afonso, C. Rosés, M. Planas, L. Feliu, *Eur. J. Org. Chem.* **2010**, *2010*, 1461–1468.

[172] D. Duran, N. Wu, B. Mao, J. Xu, *J. Liq. Chromatogr. Relat. Technol.* **2006**, *29*, 661–672.

[173] I. Gavrilova, *Bachelor thesis*, Georg-August-Universität Göttingen, Germany, **2018**.

[174] A. Patchornik, B. Amit, R. B. Woodward, *J. Am. Chem. Soc.* **1970**, *92*, 6333–6335.

[175] T. Furuta, S. S. Wang, J. L. Dantzker, T. M. Dore, W. J. Bybee, E. M. Callaway, W. Denk, R. Y. Tsien, *Proc. Natl. Acad. Sci. USA* **1999**, *96*, 1193–1200.

[176] T. Solomek, S. Mercier, T. Bally, C. G. Bochet, *Photochem. Photobiol. Sci.* **2012**, *11*, 548–555.

[177] A. V. Pinheiro, P. Baptista, J. C. Lima, *Nucleic Acids Res.* **2008**, *36*, e90.

[178] R. O. Schönleber, J. Bendig, V. Hagen, B. Giese, *Bioorg. Med. Chem.* **2002**, *10*, 97–101.

[179] V. R. Shembekar, Y. Chen, B. K. Carpenter, G. P. Hess, *Biochemistry* **2005**, *44*, 7107–7114.

[180] S. Sakamoto, M. Terauchi, Y. Araki, T. Wada, *Biopolymers* **2013**, *100*, 773–779.

[181] T. Watanabe, T. Hoshida, J. Sakyo, M. Kishi, S. Tanabe, J. Matsuura, S. Akiyama, M. Nakata, Y. Tanabe, A. Z. Suzuki et al., *Org. Biomol. Chem.* **2014**, *12*, 5089–5093.

[182] A. Taniguchi, M. Skwarczynski, Y. Sohma, T. Okada, K. Ikeda, H. Prakash, H. Mukai, Y. Hayashi, T. Kimura, S. Hirota et al., *ChemBioChem* **2008**, *9*, 3055–3065.

[183] M. Skwarczynski, M. Noguchi, S. Hirota, Y. Sohma, T. Kimura, Y. Hayashi, Y. Kiso, *Bioorg. Med. Chem. Lett.* **2006**, *16*, 4492–4496.

[184] A. Z. Suzuki, T. Watanabe, M. Kawamoto, K. Nishiyama, H. Yamashita, M. Ishii, M. Iwamura, T. Furuta, *Org. Lett.* **2003**, *5*, 4867–4870.

[185] M. M. Mahmoodi, S. A. Fisher, R. Y. Tam, P. C. Goff, R. B. Anderson, J. E. Wissinger, D. A. Blank, M. S. Shoichet, M. D. Distefano, *Org. Biomol. Chem.* **2016**, *14*, 8289–8300.

[186] J. Liu, J. Hemphill, S. Samanta, M. Tsang, A. Deiters, *J. Am. Chem. Soc.* **2017**, *139*, 9100–9103.

[187] S. Yamazoe, Q. Liu, L. E. McQuade, A. Deiters, J. K. Chen, *Angew. Chem. Int. Ed.* **2014**, *53*, 10114–10118.

[188] J. Luo, R. Uprety, Y. Naro, C. Chou, D. P. Nguyen, J. W. Chin, A. Deiters, *J. Am. Chem. Soc.* **2014**, *136*, 15551–15558.

[189] B. Schade, V. Hagen, R. Schmidt, R. Herbrich, E. Krause, T. Eckardt, J. Bendig, *J. Org. Chem.* **1999**, *64*, 9109–9117.

[190] R. Schmidt, D. Geissler, V. Hagen, J. Bendig, *J. Phys. Chem. A* **2007**, *111*, 5768–5774.

[191] C. Malan, C. Morin, *J. Org. Chem.* **1998**, *63*, 8019–8020.

[192] R. T. Raines, G. Ellis, M. Palte, WO 2013/110005 Al, **2013**.

[193] T. Willemse, K. Van Imp, R. J. M. Goss, H. W. T. Van Vlijmen, W. Schepens, B. U. W. Maes, S. Ballet, *ChemCatChem* **2015**, *7*, 2055–2070.

[194] Z. Gao, V. Gouverneur, B. G. Davis, *J. Am. Chem. Soc.* **2013**, *135*, 13612–13615.

[195] B. Lippert, *Coord. Chem. Rev.* **2000**, *200-202*, 487–516.

[196] G. L. Eichhorn, Y. A. Shin, *J. Am. Chem. Soc.* **1968**, *90*, 7323–7328.

[197] A. M. Pyle, J. P. Rehmann, R. Meshoyrer, C. V. Kumar, N. J. Turro, J. K. Barton, *J. Am. Chem. Soc.* **1989**, *111*, 3051–3058.

[198] D. N. Woolfson in *Advances in Protein Chemistry*, Vol. 70 (Eds.: D. A. D. Parry, J. M. Squire), Academic Press, Cambridge, MA, **2005**.

[199] A. N. Lupas, J. Bassler, S. Dunin-Horkawicz in *Subcellular Biochemistry*, Vol. 82 (Eds.: D. A. D. Parry, J. M. Squire), Springer International Publishing, Basel, **2017**, 35–61.

[200] E. H. C. Bromley, R. B. Sessions, A. R. Thomson, D. N. Woolfson, *J. Am. Chem. Soc.* **2009**, *131*, 928–930.

[201] H. Gradišar, R. Jerala, *J. Pept. Sci.* **2011**, 100–106.

[202] T. Lebar, D. Lainšček, E. Merljak, J. Aupič, R. Jerala, *Nat. Chem. Biol.* **2020**, 513–519.

[203] S. M. Kelly, T. J. Jess, N. C. Price, *Biochim. Biophys. Acta* **2005**, *1751*, 119–139.

[204] N. J. Greenfield, *Nat. Protoc.* **2006**, *1*, 2876–2890.

[205] P. López-García, M. Goktas, A. E. Bergues-Pupo, B. Koksch, D. Varón Silva, K. G. Blank, *Phys. Chem. Chem. Phys.* **2019**, *21*, 9145–9149.

[206] B. Apostolovic, H.-A. Klok, *Biomacromolecules* **2008**, *9*, 3173–3180.

[207] J. Yang, C. Xu, C. Wang, J. Kopecek, *Biomacromolecules* **2006**, *7*, 1187–1195.

[208] F. Thomas, A. L. Boyle, A. J. Burton, D. N. Woolfson, *J. Am. Chem. Soc.* **2013**, *135*, 5161–5166.

[209] S. M. Agten, P. E. Dawson, T. M. Hackeng, *J. Pept. Sci.* **2016**, *22*, 271–279.

[210] J. Huang, H. Qin, Z. Sun, G. Huang, J. Mao, K. Cheng, Z. Zhang, H. Wan, Y. Yao, J. Dong et al., *Sci. Rep.* **2015**, *5*, 10164.

[211] S. Duflocq, J. Zhou, F. Huguenot, M. Vidal, W.-Q. Liu, *RSC Adv.* **2020**, *10*, 17681–17685.

[212] R. L. Brabham, R. J. Spears, J. Walton, S. Tyagi, E. A. Lemke, M. A. Fascione, *Chem. Commun.* **2018**, *54*, 1501–1504.

[213] C. E. Schafmeister, J. Po, G. L. Verdine, *J. Am. Chem. Soc.* **2000**, *122*, 5891–5892.

[214] D. Chelius, T. A. Shaler, *Bioconjugate Chem.* **2003**, *14*, 205–211.

[215] C. Mueller, T. N. Grossmann, *Angew. Chem. Int. Ed.* **2018**, *57*, 17079–17083.

[216] G. von Maltzahn, Y. Ren, J.-H. Park, D.-H. Min, V. R. Kotamraju, J. Jayakumar, V. Fogal, M. J. Sailor, E. Ruoslahti, S. N. Bhatia, *Bioconjugate Chem.* **2008**, *19*, 1570–1578.

[217] B. E. Hubrich, P. M. Menzel, B. Kugler, U. Diederichsen in *Methods in Molecular Biology*, Vol. 2105 (Ed.: P. E. Nielsen), Springer US, New York, NY, **2020**.

[218] H. E. Gottlieb, V. Kotlyar, A. Nudelman, *J. Org. Chem.* **1997**, *62*, 7512–7515.

[219] S. C. Gill, P. H. von Hippel, *Anal. Biochem.* **1989**, *182*, 319–326.

[220] L. Goltermann, P. E. Nielsen in *Methods in Molecular Biology*, Vol. 2105 (Ed.: P. E. Nielsen), Springer US, New York, NY, **2020**.

[221] T. J. Measey, F. Gai, *Langmuir* **2012**, *28*, 12588–12592.

[222] H. M. Berman, J. Westbrook, Z. Feng, G. Gilliland, T. N. Bhat, H. Weissig, I. N. Shindyalov, P. E. Bourne, *Nucleic Acids Res.* **2000**, *28*, 235–242.

[223] E. F. Pettersen, T. D. Goddard, C. C. Huang, G. S. Couch, D. M. Greenblatt, E. C. Meng, T. E. Ferrin, *J. Comput. Chem.* **2004**, *25*, 1605–1612.

[224] M. A. Avery, M. S. Verlander, M. Goodman, *J. Org. Chem.* **1980**, *45*, 2750–2753.

[225] X. Zhang, W. Xi, C. Wang, M. Podgórski, C. N. Bowman, *ACS Macro Lett.* **2016**, *5*, 229–233.

10 Acknowledgements

First of all, I would like to thank Prof. Dr. Ulf Diederichsen for the opportunity to work on this project, his support and the scientific freedom granted to pursue my own ideals.
I am thankful to Prof. Dr. Manuel Alcarazo for assuming the position of my second supervisor, for the helpful discussions and for providing a different viewpoint on my experiments.
Moreover, I would like to express my thanks to Prof. Dr. Marina Bennati, Prof. Dr. Kai Tittmann, Dr. Holm Frauendorf and Dr. Michael John for their willingness to be members of my examination board.
I would like to thank the MS and NMR departments headed by Dr. Holm Frauendorf and Dr. Michael John for the measurement of countless samples.
In addition, a big thank you goes to Angela Heinemann for her assistance regarding all organizational concerns.
I would further like to extend my gratitude to Prof. Dr. Harald Kolmar and Bastian Becker for the fruitful cooperation as part of the priority program 1623.
I am deeply grateful to Jun.-Prof. Dr. Franziska Thomas for the training I have received in her lab during my master thesis, the ongoing support, guidance, and discussions, especially when sharing her expertise on coiled-coil peptides.
Thank you to Ulrike Rost, Anastasiya Schirmacher and especially Mathis Rink for sharing their expertise, providing counsel, and discussing my work with me.
For their experimental contributions to my work I would like to extend my gratitude to “my” students Ivana Gavrilova and Valentina Kallina.
To my proofreaders Mike Groth, Viktoria Mrđen Debono, Anastasiya Schirmacher and Tobias Schmidt: Thank you for the helpful suggestions, for putting the finishing touches on this work and in the case of Tobias for suffering through yet another experimental section.
I would also like to express my appreciation to the past and present members of Lab 109, Geralin Höger, Anastasiya Schirmacher, Tobias Schmidt, Pirajeev Selvachandran, Clara Bosbach and Luisa Bachmann for the joyful, cooperative working atmosphere and fun extracurricular activities. A special thank you to Geralin and Anastasiya for welcoming me into “their” lab, helping me get started in the field of peptide chemistry and including me in their activities in and around the lab. I will always fondly remember the coffee breaks and evenings spent together. Anastasiya, thank you in addition for your continuous support, your willingness to listen and your providing of different perspectives on and off work. I’m grateful for your encouragement to broaden my horizon and improving my work-life balance by jointly engaging in sports, cookouts, and other activities.

Thank you to the members of the Diederichsen and Thomas group for the enjoyable working atmosphere, fun group trips, celebrations and distractions on the foosball table.
Thank you as well to my friends for supporting me throughout my studies and providing relief on particularly stressful days, especially to Chris and Laura for the considerate, enjoyable, and necessary distractions.
Last but not least, I would like to thank my family for their well-meant advice and continuous emotional and financial support during my time at university. A special thank you to my brother Felix for always listening to and supporting me.